Multi-Objective Methods for History Matching, Uncertainty Prediction and Optimisation in Reservoir Modelling

Junko Jhonson Juntianus Hutahaean

Submitted for the degree of Doctor of Philosophy

Institute of Petroleum Engineering

School of Energy, Geoscience, Infrastructure and Society

Heriot-Watt University

April 2017

Abstract

Robust decision-making and reliable forecasting uncertainty are the two key factors to the success of modern reservoir development and management. The reason is straightforward: significant capital investments are involved (i.e. hundreds of millions of dollars or more) by an incomplete understanding of the oil and gas reservoirs developed. Hence, well-informed decision-making with a good knowledge of the reservoir has always been a critical component in the risk-based oil and gas industry.

The research in this thesis focuses on developing solutions for robust decision-making and reliable forecasting using multi-objective methods to history matching and reservoir development optimisation within a Bayesian approach for uncertainty quantification. The multi-objective approach on history matching can find an ensemble of diverse set and good matched models. This diverse set of good matched models is essential for reliable and yet realistic uncertainty prediction of future field behaviours. Additionally, the models from multi-objective history matching also can be used in the reservoir development optimisation to obtain robust decision under uncertainty.

Several challenges in the framework of multi-objective history matching, uncertainty quantification and optimisation have been identified and investigated in this thesis. These challenges include: (1) impact of the uncertainty in the model parameterisation on the forecast reliability; (2) history matching efficiency in case of many matched-criteria and the way they can be grouped into multiple objectives; (3) the problem with a high number of objectives; and (4) reservoir development optimisation under uncertainty.

The thesis proposes solutions for each of the challenges mentioned above through extensive studies on both synthetic and real field cases supported by rigour statistical evaluations. The opportunity offered by multi-objective to generate an ensemble of a diverse set of good matched models has been explored to handle the first challenge. A novel technique on how to group and select the objective grouping properly for multi-objective history matching has been proposed to address the second challenge. A recently proposed many-objective optimisation algorithm has been applied to cope with the third challenge. Finally, a new workflow for reservoir development optimisation under uncertainty to obtain robust and reliable uncertainty estimation in the optimisation forecast is proposed.

To my Mother and Father,

a woman of prayer and a man of wisdom.

Prediction is very difficult, especially about the future.

(Niels Bohr, 1885–1962)

Acknowledgements

Completing the requirements to receive a Doctor of Philosophy (PhD) degree strongly reminds me of completing a marathon. It has demanded a great deal of time, dedication, preparation, training, and the proper equipment. It has required an internal drive and desire to see the race through. Like a marathon, it has also benefited from support along the course.

Although too many to mention by name you know who you are. Past lecturers, co-workers, classmates, officemates, friends and families — you have all had an impact on me, some even positive! Your investment in me is partly responsible for this success. However, certain individuals were absolutely key to completing this marathon.

My sincerest gratitude to Dr Vasily Demyanov and Prof Mike Christie who have provided me with the opportunity to work on this PhD. Both of you have guided, coaxed, criticised, supported, humoured, and continually motivated me for three and quarter years. Your guidances have led me towards excellence. Your encouragement, coaching style and immense knowledge have left me deep impressions. I feel fortunate to have both of you as my coaches and friends.

Prof Amilcar Soares and Prof David Corne, my thesis examiners, for your invaluable comments and feedbacks that have improved the quality of the thesis.

Dr Dan Arnold and the best magician Jack Talbot, key members of uncertainty quantification group at Heriot-Watt, for your help, feedback and support.

Computer support team for making any computer-related things smoother; the administration and purchase teams for your cooperative efforts.

My gratitude is extended to the sponsors of the Heriot-Watt University Uncertainty Quantification JIP Phase IV: BG Group, E.ON, JOGMEC, and Rock Flow Dynamics for funding my PhD study. Special thanks go to Rock Flow Dynamics for the real field data used in this thesis. Schlumberger-GeoQuest for the ECLIPSE™ simulator, Rock Flow Dynamics for the tNavigator™ simulator, and Epistemy for the Raven™ software.

I would like to thank also several funding bodies and organisations for supporting my PhD study and research dissemination. The Adrian Todd Golden Key Student Support Fund (thanks to Prof (retired) Adrian Todd and Prof Patrick Corbett). The IEEE Computational Intelligence Society Travel Grant and SPE Aberdeen Bursaries. Special thanks to the SPE STAR Fellowships for the North Sea Region for its continuous financial support during my PhD years of study (and for this particular fellowships I thank Dr Andy Gardiner for the supportive reference letter.)

My wife Grace for your endless patience, continuous support and willingness to do the "hard" work at home. Thank you so much for letting me do this PhD, and especially for keeping things straight on the home front. My lovely daughter Giannabel for always making me smile and laugh. You have had a hard go of it as I have been constantly locked up in the study and research for the past three and quarter years. I am glad three of us are travelling together through this journey called life!

Finally, I would like to express my heartfelt gratitude to my Mother and Father — both of you have always set an example I would do well to emulate. Your prayer and wisdom that something good would finally come to me appear to be giving fruit. Thanks for teaching me to do a good job for the first time, to appreciate the value of education and hard work, and especially for never giving up! I dedicate this thesis for both of you.

Edinburgh, April 2017

Junko J.J. Hutahaean

Contents

List of Figures

List of Tables

List of Publications

1. **J. Hutahaean**, V. Demyanov, and M. Christie, "On Optimal Selection of Objective Grouping for Multi-Objective History Matching," *SPE Journal*, SPE-185957-PA, 2017, accepted/InPress.

2. **J. Hutahaean**, V. Demyanov, and M. Christie, "Many-Objective Optimization Algorithm applied to History Matching," in *2016 IEEE Symposium Series on Computational Intelligence (SSCI)*, 2016, pp. 1–8.

3. **J. Hutahaean**, V. Demyanow, and M. Christie, "Impact of Model Parameterisation and Objective Choices on Assisted History Matching and Reservoir Forecasting," in *2015 Asia Pacific Oil and Gas Conference and Exhibition (APOGCE)*, SPE-176389-MS, 2015, pp. 1-20.

4. **J. Hutahaean**, V. Demyanov, and M. Christie, "Reservoir Development Optimisation under Uncertainty for Infill Well Placement," *SPE Journal*, to be submitted.

5. **J. Hutahaean**, V. Demyanov, and M. Christie, "3R: Rapid, Robust and Reliable History Matching and Uncertainty Quantification Framework," in progress to submit for a journal.

Chapter 1

Introduction

1.1 Background and Motivation

The exploration and production of oil and gas reservoirs (usually termed the *upstream* sector in the petroleum industry) plays an important role in world economy. BP Outlook predicts that oil and gas remain the key sources of energy powering the global economy and together with coal, they provide around 60% of today's energy demand and will account for more than 75% of total energy supplies by 2035 [1].

The upstream sector includes activities to recover oil and gas from underground to surface for commercial use. It involves finding subsurface oil and gas reservoirs (exploration stage), appraising the economic viability of the field to be developed (appraisal stage), developing the reservoir based on one or more development plans (development stage), and producing oil and gas at the surface through production wells (production stage).

A central tool for the decision-making in upstream oil and gas activities is the reservoir model [2]. It provides a digital numerical representation of the subsurface derived from available subsurface data and knowledge from different subsurface disciplines (i.e. petrophysics, geology, geophysics, reservoir engineering, production technology, statistics, and computer sciences). The goal is to establish a successful model(s) that is (are) useful to support in decision-making.

In practice, we typically distinguish between *static reservoir models* and *dynamic reservoir models* [2]. The static reservoir model describes the initial state of the reservoir before any production of oil or gas has taken place. Its primary purpose is for oil- or gas-in-place volume calculations and often becomes the most critical tool in the exploration stage of the upstream activities.

A dynamic reservoir model is constructed dependent on the framework and spatial distribution of reservoir properties from the static reservoir model. Equations governing fluid flow in porous media are applied to simulate the movement of reservoir fluids as a function of production and injection. Different data types relevant to flow simulation, such as relative permeability, capillary pressure and compressibility are also incorporated in the model. The primary purposes of a dynamic reservoir model are calculating recoverable oil or gas volumes, establishing production profiles, optimising the depletion plan for a field, understanding the reservoir dynamics and well placement planning. These objectives are the priorities in the appraisal, development, and production stages in the upstream activities.

Static models are in the hands of geologists, petrophysicists, and geophysicists, whereas the dynamic models are the daily job of the reservoir engineers and are the focus of this thesis. Therefore, from this point forward throughout the thesis, the term reservoir model refers to dynamic reservoir model.

A key part of reservoir modelling related to decision-making is the uncertainty handling. Because data about reservoirs almost always lack a degree of detail and accuracy, it is important to recognise the effects of this limitation on the model uncertainty and to know to what extent it may affect the response of reservoir models, and consequently, propagate through to the decision-making. Moreover, as our understanding of the reservoir evolves through the life of a field, it is essential to update our models to reproduce similar responses to the observations made from the field, and consequently, reduce the uncertainty.

1.1.1 Thesis Map

Figure 1.1 shows a map of this thesis in a high-level perspective that is described below (i.e. *"the criterion or the expected outcome"* of a process; *"the what"* is the task; and *"the how"* to do the task).

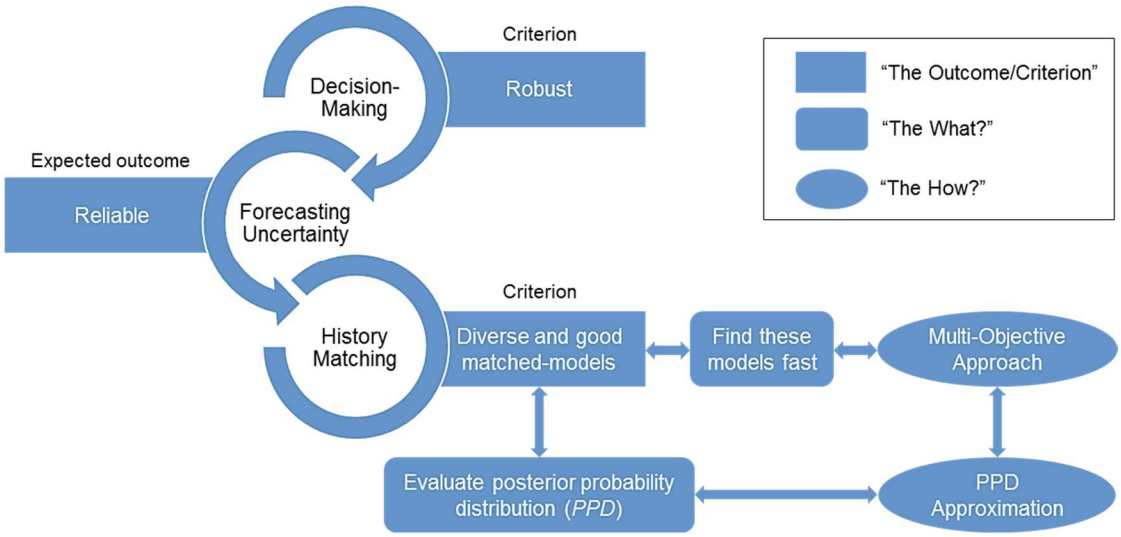

Figure 1.1—The map of the thesis.

Robust decision-making is essential to reservoir development and management practices in the upstream sector. Robust decisions are ones that should hold under uncertainty to avoid any disappointment. The reason is straightforward: significant capital investments are involved (i.e. hundreds of millions of dollars or more) by an incomplete understanding of the oil and gas reservoirs developed. Hence, well-informed decision-making with a good knowledge of the reservoir has always been a critical component in the risk-based oil and gas industry.

Reliable forecasting uncertainty is expected to support robust decision-making. Reliable uncertainty predictions provide a confidence interval that encapsulates the real observations obtained from the future field performance. The main idea behind a confidence interval is to represent the uncertainty of the model forecast. Typically, this confidence interval is represented by probabilistic predictions such as the 10-th, 50-th and 90-th quantile of the cumulative distribution function, known as *P90*, *P50* and *P10* respectively.

Forecasting of a reservoir performance based on reservoir model simulations is typically based on multiple history-matched models. These models are obtained by fitting the response of the model to the available observed data. The fitting is done by adjusting the properties of a reservoir model iteratively until a reasonable match is obtained. Afterwards, the confidence interval is derived based on the responses of these multiple matched models.

A diverse set of good history-matched models is important for reliable and yet realistic forecasting uncertainty of future field behaviour. The diversity of models may be represented by different reservoir properties such as permeability and porosity that may provide equally good history matches [3,4]. This plausibility is due to the characteristic of history matching as an *ill-posed* inverse problem with non-unique solutions [5,6]. Such a diverse set of good history-matched models is required to capture the range of uncertainty as the models are likely to produce different future field behaviours [7–10].

It is important to find this diverse set of good history-matched models fast. This is due to the limited resource allocation for decisions to be made based on reservoir model simulation. However, it is difficult to find these models due to the nature of the history matching problem that is a complex and nonlinear problem. It is a complex problem due to its high dimensionality, i.e. it involves many model parameters. It is a nonlinear problem due to the strong nonlinearity between reservoir properties and observed production data. Due to these difficulties, history matching has always been one of the most challenging and resource-intensive stages in reservoir management. Therefore, methods that can handle these difficulties and obtain a diverse and good set of history-matched models in a timely manner are needed.

The multi-objective approach on history matching can find an ensemble of diverse set of good matched models. Thus, in the past few years, there has been a renewed interest in multi-objective history matching [7–10]. In the multi-objective approach, objective components (usually groups of them) guide the algorithm to different areas of objective space for tradeoffs between objectives and should lead to a diverse set of good matched models [7–10]. Moreover, the multi-objective approach can accommodate the nature of history matching as a multivariate calibration problem. In this sense, the mechanism of

multi-objective to find optimal solutions that balance between match criteria, called Pareto solutions [11], reflects the multivariate calibration.

The probability for each history-matched model is required to compute the confidence interval of reservoir forecasting based on many history-matched models. Assuming that all history-matched models are equally probable is not a plausible assumption. Hence, methods to estimate the probability of each matched model given the data, so-called *posterior probability distribution* (PPD) [5,6], are needed. However, a practical issue that has dominated the predictions under uncertainty is an accurate PPD evaluation of the history-matched models [6]. This issue is due to the computational cost as many thousands of flow simulations are required to perform such an evaluation. The classical approach to address this problem consists of using the Monte Carlo method that requires a high number of flow simulations to propagate uncertainty [6].

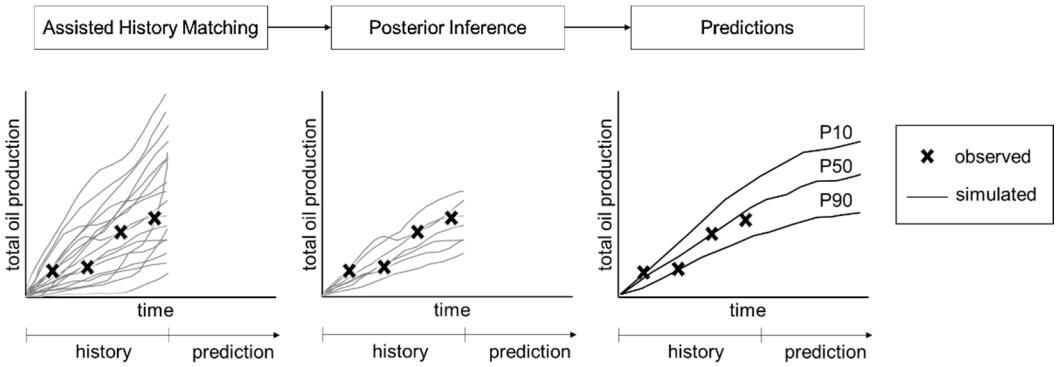

Figure 1.2—The Bayesian framework for uncertainty quantification.

Therefore, over the past few years, there has been significant research dealing with the PPD approximation [5,12,13] enabling us to perform uncertainty predictions at minor computational costs in terms of flow simulations, as shown in Figure 1.2. Figure 1.2 shows a general workflow in uncertainty predictions from the ensemble of history-matched models. The PPD is approximated on the ensemble of history-matched models, and the resulting ensemble contains only the likely models, referred to as the *inference models* that are used for uncertainty predictions. However, as the number of inference models can also be large, the computational cost remains an issue if these models are used for optimisation under geological uncertainty. The fact that the Pareto solutions

from multi-objective history matching are diverse and good [7–10], means that these models can be potentially used to capture the uncertainty prediction on the optimisation with a manageable computational cost. This is investigated in this thesis.

1.1.2 Research Focus

In this thesis, the research focuses on developing solutions for robust decision-making and reliable forecasting using a multi-objective approach to history matching and reservoir development optimisation within a Bayesian approach to uncertainty quantification. The general framework of multi-objective history matching implemented in the thesis is illustrated in Figure 1.3.

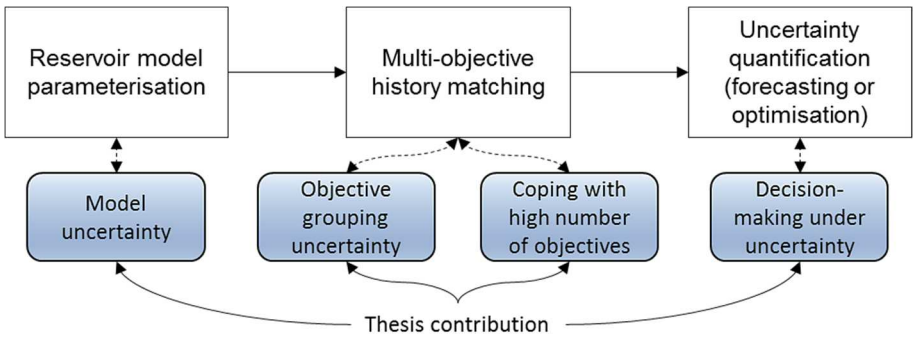

Figure 1.3—Thesis contribution to the identified challenges related to the reservoir model simulation.

We describe each step of the diagram blocks shown in Figure 1.3.

Reservoir model parameterisation in the assisted history matching framework is the process of describing possible variations of a reservoir system that may exist in a reservoir through a limited number of parameters [14]. In the parameterisation, we assume that a given set of model parameters will contain a combination of parameter values that accurately represents the reservoir. We quantify our initial state of knowledge of the uncertainty in the reservoir by describing the probabilistic distributions of these model parameters.

The nature of reservoir history matching is multi-objective because the match criteria are usually related to multiple wells and production variables, such as rates and pressures

in wells and regions in the field. In many cases, these match criteria are conflicting, and no feasible solution optimises all of them simultaneously. For instance, an improvement in oil rate match in one well causes a deterioration of the gas rate in another well. Therefore, the multi-objective algorithm is used to effectively handle multiple and conflicting objectives in the reservoir history matching.

Finally, an ensemble-based reservoir prediction and optimisation is performed to capture uncertainty that requires multiple flow simulation models.

1.1.3 Identified Challenges

We identified several challenges in the framework of multi-objective history matching and uncertainty quantification, as shown in Figure 1.3, and briefly describe the solution to address each of these challenges.

The first identified challenge is related to the impact of model parameterisation uncertainty on the quality of history-matched models and the reliability of the forecast. The issue with the uncertainty in the model parameterisation is the risk of underestimating the uncertainty of forecasts when different alternatives are possible. Therefore, it is necessary to have a method that can robustly and reliably generate a forecast under different model parameterisations.

The second identified challenge is the *curse of dimensionality* in the objective space in the multi-objective history matching, as the reservoir may feature far too many match criteria. This issue often leads to the inability of optimisation algorithms to produce a representative ensemble of history-matched models for reliable uncertainty prediction. Even though some multi-objective algorithms perform well in two or three objectives, their performances deteriorate (i.e. slow convergence) in a high number of objectives, i.e. problems with four or more objectives [15–17]. Therefore, it is necessary to have an algorithm that can cope with a high number of objectives. This challenge is tackled in two ways in this thesis: (i) reduction of the number of objectives by grouping into a lower dimension and selection of proper groupings; (ii) application of a novel multi-

objective algorithm that has been recently developed for handling many-objective problems (i.e. problems with more than three objectives).

The third identified challenge focuses on a practical approach for reservoir optimisation across multiple models that represent uncertainty to achieve a robust decision. Even though attempts at this task have been conducted in the literature [18–22], the computational cost involved and the proper estimation of uncertainty remains an issue. Therefore, it is necessary to have a practical workflow in the reservoir optimisation under uncertainty that can reliably estimate the range of uncertainty and yet, with a manageable computational cost. Reliable estimation of uncertainty includes the development of a novel technique to approximate the posterior probability of the ensemble of history-matched models for optimisation that is computationally efficient with a manageable number of flow simulations.

1.2 Research Objectives

The research objectives driven by several identified challenges mentioned above are as follows:

- How to properly account for the uncertainty in the model parameterisation in history matching?
- How to manage the uncertainty arising from the different choice of misfit definitions (objective grouping choices) in multi-objective history matching?
- How to cope with the high number of objectives in multi-objective history matching?
- How to account for the geological uncertainty in the field development optimisation in regards to decision-making on infill well placement?

The work carried out in the thesis contributes to the research of methods for the multi-objective history matching and uncertainty quantification in the forecast and field development optimisation. We investigated the impact of different model parameterisations on the history matching and consequently on reservoir forecasting by a multi-objective approach in contrast to classical single-objective history matching. We

developed a new technique to group and select optimally objective components for an improved multi-objective history matching. We implemented one of the recent many-objective optimisation algorithms (the term for a problem with more than three objectives), namely the reference vector guided evolutionary algorithm, to history matching. Finally, we developed a new workflow for robust and reliable reservoir development optimisation under uncertainty and applied them to decision-making on infill well placement.

1.3 Structure of the Thesis

The thesis is organised as follows:

Chapter 2 presents a literature review of the fundamental knowledge on different modelling techniques for reservoir performance prediction, history matching, uncertainty quantification, and multi-objective optimisation. This chapter also reviews stochastic sampling algorithms used in the thesis, such as the neighbourhood algorithm (NA), particle swarm optimisation (PSO) and its multi-objective variant i.e. multi-objective particle swarm optimisation (MOPSO), genetic algorithm (GA) and its multi-objective variant i.e. the elitist nondominated sorting genetic algorithm (NSGA-II). Finally, the chapter discusses the identified challenges based on the reviewed literature.

Chapter 3 investigates the impact of different geological model parameterisations on history matching and reservoir forecasting by single-objective and multi-objective approaches. The strategy for the comparative study is described. The comparative analysis is presented on a synthetic PUNQ-S3 reservoir model based on a real field.

Chapter 4 introduces a novel technique to group and select optimal objective groupings for multi-objective history matching. The key challenge of the multi-objective algorithm is demonstrated. The nonparametric-conflict-based objective grouping is proposed. The descriptions of performance measures and statistical-significance tests are presented. The proposed technique is applied to two case studies, PUNQ-S3 and Zagadka, and the results are analysed with rigorous statistical tests.

Chapter 5 introduces one of the recent many-objective optimisation algorithm, a reference vector guided evolutionary algorithm (RVEA), to solve one of the challenges in multi-objective history matching with a high number of objective. The description of the main components of the algorithm is presented to serve as the foundation for understanding the technique. The method is applied to standard benchmark mathematical test functions, DTLZ1-4 and scaled DTLZ1 and 3, and history matching of two reservoir model case studies, PUNQ-S3 and Zagadka. Comparative studies with the current state-of-the-art multi-objective algorithm in history matching, namely MOPSO and NSGA-II, are performed for both mathematical test functions and reservoir model history matching.

Chapter 6 introduces a new workflow for reservoir development optimisation under model uncertainty with application to the decision-making on infill well placement. A brief review of the current state of knowledge on well placement optimisation is presented followed by the description of the proposed workflow that includes the approximation of PPD for the selected models for optimisation, the extended nominal optimisation and robust optimisation frameworks. Finally, the proposed workflow are applied to the PUNQ-S3 reservoir model with various tests to place infill well(s).

Chapter 7 concludes the thesis with a summary of the chapters, major contributions, and key findings. It also discusses some recommendations for future work.

Chapter 2

Literature Review

2.1 Introduction

In reservoir studies, planning a realistic modelling workflow and correctly estimating resources may become a difficult exercise. Project managers experience the challenge of justifying to management on the unexpected delays in the results or disconcert of asking for more time and more financial support to complete an ongoing study. Reservoir project managers are not worse than others managers. However, their planning task is more difficult due to some particular characteristics that differentiate it from other types of projects [23]:

- **Every study is different from all others**. In reservoir studies, we can expect a different composition of work activities depending on the amount of time, some technical and costs constraints. Previous experience is useful, but the variables involved are too many and, consequently, the range of unexpected outcomes is too broad to be considered properly.
- **There is an underlying technical uncertainty in most phases of the study**. Different scale of data in each phase can cause this challenge. For instance, in the well log data acquisition stage. In the beginning, it was planned only to acquire resistivity data by a standard logging tool. However, it is found later that the data acquired are not conclusive hence, need to get more data with more advanced logging tool such as an imaging tool. The impact of this uncertainty

can be appreciated to the resource allocation at the beginning of the project to the expected range of accuracy for decision support.

The number of work phases to be performed in a typical reservoir study and their duration depend on the reservoir and the available resources. However, it is possibly useful to have a glance at the individual activities in a typical reservoir study even though this would preclude any generalisation. For instance, we can see to typical activities on an oil reservoir development with a significant degree of geological heterogeneity as illustrated in Table 2.1.

Phase	Individual Tasks	Duration (weeks)	Duration (%)
Data collection	Raw seismic, log and core data collection Water and oil PVT analysis data Well testing data Pressure data Field production and injection data Existing studies and reports for collection Database construction	9 to 20	6 to 14
Data preprocessing	Log data correction and normalisation Core-log depth matching Pressure data correction and cleaning Production data validation Seismic processing	3 to 6	2 to 4
Well data analysis	Petrophysical interpretation Synthetic seismograms generation Facies analysis and classification Production log analysis Well tests interpretation PVT study	20 to 28	14 to 18
Spatial distribution analysis and geomodelling	Sedimentological study Seismic interpretation and modelling Geological correlation Facies distribution analysis Petrophysical distribution study Pressure analysis Water/gas advance with time	30 to 44	20 to 28
Production analysis	Production/injection performance analysis Material balance	9 to 12	6 to 8
Simulation model	Model building History match Production forecast	40 to 60	30 to 40
Final report	Report writing and editing	6 to 9	4 to 6
Total (average)		**148 weeks**	**100%**

Table 2.1—Typical phases and duration of a reservoir study with the activities related to simulation model are highlighted (after [23]).

The amount of time allocated for the activities related to reservoir simulation model is the largest amongst others as highlighted in Table 2.1. Table 2.1 illustrates the activities that could be foreseen and their individual duration on the basis of total man-weeks for a reservoir with high heterogeneity, 30 to 50 producers, few injections and been produced for 20 to 30 years [23]. The total man-weeks can be expressed in percentage of the total study duration. These estimations are subject to significant variations depending on the particular project (see [23] for detail).

Having allocated the largest time-resource, the efforts to speed up the process and activities related to reservoir model simulation should contribute significantly to the project flawlessness. These efforts include the application of other fields such as mathematics, statistics, and computer sciences. The goal is a *fit for purpose* reservoir model with realistic tolerance for imprecision and uncertainty in the production forecasting that affects many important decisions.

In general, there are three activities in the simulation model phase: (i) simulation model building; (ii) history matching and; (iii) production forecast. After a simulation model has been constructed, the model upscaling may be performed for the efficiency of the model flow simulation time. If the production or other dynamic data such as well test data are available, history matching is then conducted. History matching is calibration of a reservoir model to historical production or dynamic data and essential to make the model consistent with the observed data. It is well-known to be a time-consuming and non-unique task. Hence, quantifying the uncertainty in production forecast from the history-matched models as the next step is also imperative to manage the risk in decision-making.

This chapter provides a literature review on reservoir modelling and simulation, history matching, and uncertainty quantification. Following that, recent progress on multi-objective approach in history matching is presented with the description of two state-of-the-art multi-objective algorithms in history matching used in the thesis. Finally, the chapter discusses some identified critical challenges and issues from the literature and briefly directs the reader to the corresponding chapters regarding the solutions proposed from the thesis.

2.2 Reservoir Modelling and Simulation

In 1956, Uren [24] defined a petroleum reservoir as follows:

" … a body of porous and permeable rock containing oil and gas through which fluids may move towards recovery openings under the pressure existing or that may be applied. All communicating pore space within the productive formation is properly a part of the rock, which may include several or many individual rock strata and may encompass bodies of impermeable and barren shale. The lateral extent of such a reservoir is contingent only upon the continuity of pore space and the ability of the fluids to move through the rock pores under the pressure available."

This fine example of old fashioned literature is not easy to the contemporary ear, but in fact, it does "say it all". This prose is precisely what the present day reservoir simulation engineer must model. At its most complex form, our task is to incorporate all the data we have in a model to predict the reservoir performance.

A reservoir model should be built dependent on its purpose for decision support. We should ask ourselves about the decision we are trying to make and to what extent the level of modelling and simulation (or which tool we can use) that allows us to make a decision adequately. Keith Coats in 1969 [25] put well this matter, who said: *"The tools of reservoir simulation range from the intuition and judgement of the engineer to complex mathematical models requiring the use of digital computers. The question is not whether to simulate, but rather which tool or method to use."* Therefore, we may choose a simple model of the reservoir or one that is quite complex depending on the question we are asking or the decision which we have to make.

In the following sections, we briefly review different model types and their ranges of complexities.

2.2.1 Analytical Methods

Traditionally, the reservoir performance prediction (e.g. recovery estimates and oil rate) can be calculated using numerous analytical models and techniques. These techniques include material balance equations [26], fractional flow curve techniques (such as the Buckley-Leverett one-dimensional displacement technique [27], the Dietz technique for inclined structures and segregated flow [28]), sweep efficiency estimation method for waterflood [29,30], and decline curve analysis [31]. Next, we briefly describe the two most common analytical methods for reservoir performance prediction: material balance and decline curve analysis.

In essence, the ***material balance*** equation expresses a simple concept. It states that, for a given pressure drop, the volume of fluids produced must equal to the total expansion of the reservoir system plus any natural fluid influx. The description of the material balance expressed in reservoir conditions is given in Dake [32] as follows:

$$\begin{aligned} \text{withdrawal} &= \text{expansion of oil and solution gas left in the reservoir} \\ &+ \text{expansion of the gas cap} \\ &+ \text{reduction in pore volume due to rock compressibility} \\ &+ \text{reduction in hydrocarbon pore volume due to connate water expansion} \\ &+ \text{aquifer influx} \end{aligned} \tag{2.1}$$

In its application, material balance use pressure data, reservoir and Pressure Volume Temperature (termed as PVT) properties to calculate the expected reservoir performance in terms of fluid withdrawal. There is no assumption to be made as far as the geometry of the system is concerned, thus providing an independent assessment of the classical geological estimates. Moreover, material balance gives an insight into the reservoir drive mechanisms, while providing in most cases a reliable quantification of the reservoir energy sources.

Decline curve analysis is a graphical technique for estimating the reservoir performance by fitting a curve on the available production data. The last day of production plateau is usually used as the starting point of the curve and then extrapolated to the end point

using the equation of a curve to predict the future performance. In its practical application, the plot of production rate (or the logarithm of production rate) against the cumulative production is used in the decline curve analysis. A curve is then fitted to this data based on of three models: harmonic, hyperbolic, and exponential [31].

Material balance and decline curve analysis were developed long time ago and are used even in the present high-performance computing era. They are well-known for their inexpensive computation due to simple homogenous reservoir description. These techniques are used as a screening or preliminary evaluation tools and suitable for potential assets evaluation when the data are limited and the time is critical. Moreover, in a large reservoir study, these techniques often to be performed and included in the final report of a reservoir study.

Even though analytical techniques are typically numerically fast and sufficiently reliable, they generally cannot possibly capture all the details and alterations of the given reservoir or process. For instance, in decline curve analysis, as predictions are based on fitting to the production data rather than modelling the subsurface physics, this technique will become inaccurate if the field development strategy is changed. Moreover, no pressure data is included in the decline curve analysis. Thus, only future production can be extrapolated from this technique. In the material balance, the reservoir is considered to be a single tank, i.e. homogenous and reacts immediately and equally throughout its entire volume. The drawback to such technique is that in reality the reservoir is never homogenous, and as such, any prediction on the effect of a new development scheme is unlikely to be accurate.

2.2.2 Numerical Reservoir Model Simulation

A more complex and robust technique for predicting reservoir performance is a numerical reservoir simulation model which is based on the discretisation of the reservoir in space and time. It consists of grid blocks, where each block represents a local part of the reservoir with uniform properties (such as porosity, permeability and relative permeability). Grid blocks are connected to neighbouring blocks so fluid may flow in a block-to-block manner. The model incorporates a variety of data, such as

reservoir fluid (PVT data), reservoir description (e.g. geological concepts), rock properties (e.g. porosity and permeability) and their spatial distribution, dynamic data and production/injection stage and controls.

Simulation of petroleum reservoir performance is attributed to a model construction and operation whose behaviour assumes the representation of actual reservoir behaviour. A model can be either physical (i.e. a laboratory sand pack) or mathematical. A mathematical model itself is a set of equations that describes the physical processes in the reservoir subject to certain assumptions. The behaviour of a valid model, assuming a simplified description of a reservoir, simulates the actual reservoir even though the model itself obviously lacks the realistic detail of the reservoir. The ultimate purpose of the model simulation is reservoir performance prediction (e.g. oil recovery) under one or more producing schemes to aid on the decision-making of reservoir management.

Numerical reservoir model simulation has been practised since the beginning of the 1960's and is closely related to the availability of fast digital computing machines and the parallel evolution of numerical techniques. This evolution allows for the solution of the large-scale finite-difference equations, describing 2D and 3D multi-phase flow in porous and heterogeneous media. New developments are ongoing especially in the parallel computer hardware and software domain to speed up the simulations time and model larger models. Thus, large-scale simulations are becoming increasingly common [33–36].

Nowadays, numerical reservoir model simulation is an everyday practice in oil and gas companies and is handled by most reservoir engineers. The most important reason is perhaps from a commercial perspective where the ability of a reservoir simulation to generate oil production profiles under various exploitation and production options that lead to different cash flow predictions. In general, all commercial simulators are provided with well-management routines that allow a reservoir engineer to set operating conditions at the levels of producing interval in a well, well, well group, reservoir and field. These operating conditions may include specified rates and pressures to the wells, shut-in or work over a well to optimise an individual well production to match facilities

capacity or injection rates. For these reasons, reservoir simulation is considered as the best technique for reservoir management.

2.2.2.1 Reservoir Model Simulation Fundamentals

Numerical reservoir model simulation requires two parts: (1) a reservoir model which includes a set of input data, and (2) a mathematical model in the form of a simulator that will make computations and predictions of the reservoir performance.

Symbol	Property	Source
	Geometry	
D	Structural top map	Seismic, pressure transient tests, material balance calculation, regional exploration studies, analogue studies.
h_g	Gross formation thickness for each reservoir layer	
h_n	Net formation thickness for each reservoir layer	
NTG	Net-to-Gross ratio	
n/a	Fault, boundaries	
n/a	Aquifers	
	Rock Properties	
ϕ	Porosity	Core analyses, well logs, pressure transient tests, correlation, well performance, interference tests, seismic.
k	Absolute permeability	
c	Rock compressibility	
n/a	Fracture spacing, orientation, connectivity	
	Fluid Properties	
B_o, B_w, B_g	Oil, water, and gas formation volume factor	Laboratory analyses of reservoir fluid samples, downhole formation testing.
ρ_o, ρ_w, ρ_g	Oil, water, and gas density	
R_s	Gas in solution	
μ_o, μ_w, μ_g	Oil, water, and gas viscosity	
c_o, c_g	Oil and gas compressibility	
	Saturation Functions	
Pc_{wo} vs. Sw	Water-oil capillary pressure (drainage and imbibition)	Laboratory core flow tests, well logs, core analyses, pressure cores, single-well tracer tests.
Pc_{go} vs. Sg	Gas-oil capillary pressure (drainage and imbibition)	
Kr_o, Kr_w vs.Sw	Oil and water relative permeability functions (drainage and imbibition)	
Kr_o, Kr_g vs. So	Oil and water relative permeability functions (drainage and imbibition)	
Kr_o, Kr_g, Kr_w	Three phase oil, gas, and water relative permeability functions	
	Production and Completion Data	
n/a	Rate and pressure data	Field performance history, workover data.
n/a	Completion data	

Table 2.2—Data required for a simulation study and their sources (after [23], [37]).

The summary of input data required in a simulation model and their sources are summarised in Table 2.2 [23,37]. The input data and their sources can be divided into

five categories: reservoir geometry, rock properties, fluid properties, saturation functions, and production and completion data. Some of the key parameters used in a reservoir model are the porosity (ϕ), absolute (k) and relative (k_r) permeabilities, the fluid saturations, and water-oil capillary pressure (P_c), which are briefly described as below.

Porosity is defined as the ratio of the pore space volume to the bulk volume of the reservoir rock. It is a dimensionless parameter and can be expressed in a percentage or a fraction. Despite such simple definition, porosity can be a difficult parameter to quantify, because the pore volume of a reservoir rock is often a complex network of spaces of different shapes, dimensions, and origins.

Permeability is defined as the ability of rock to conduct fluids. It is measured in Darcies or more commonly milliDarcies (mD), and is often highly *anisotropic* throughout the entire reservoir. The anisotropic properties of permeability are often related to the heterogeneity of the reservoir rocks and is represented in the model as permeability vectors k_x, k_y, and k_z. Permeability is the most important petrophysical property of a reservoir due to its direct impact on fluid flow and its scale that is used to define the economics of a development project. For instance, 0.1–10 mD reservoir is less attractive compared to 50–500 mD reservoir given the same amount of oil and gas in the reservoir.

Fluid saturations are fractional values representing the ratio of oil (S_o), water (S_w), or gas (S_g) in the fluid-filled pore space in a reservoir rock. The determination of the fluid saturations in a reservoir is one of the most important task in a reservoir model simulation as it affects the calculation of the hydrocarbon in place and the fluid mechanics, and consequently the expected production performance of a field.

Relative permeability is included in a reservoir model to account for *immiscible* (fluid do not mix) multi-phase flow combinations that may exist in the reservoir, such as oil-water, oil-gas, and oil-water-gas. In essence, relative permeability curves model the drop in permeability due to the presence of another fluid. It is encapsulated in a curve of fractional values plotted against water or oil saturations. Relative permeability curves

define flow mechanisms such as imbibition or drainage and fluid wettability. Curves for each phase are used to calculate an *effective permeability* (k_e) where $k_e = k_r \times k$.

Capillary pressure occurs whenever two fluids coexist in the pore space of a reservoir rock, and it is defined as the difference in the pressure measurable in the two phases. Capillary pressure data are included in a reservoir model to define the initial fluid contacts, transition zones, and to control the flow of fluid between the fracture and rock matrix in fractured reservoir models. The relationship between capillary pressure and height is used to build the initial transition zone in the reservoir.

Numerical reservoir model simulation is performed by large-scale finite volume or finite element method simulators which are mathematically modelled. Like most of the computational fluid dynamics (CFD), numerical reservoir model simulators discretise conservation of mass, momentum, and energy on a computational grid.

For the flow of oil, conservation of momentum is replaced by a slow flow approximation called Darcy's law, as in Equation (2.2), where the fluid flow rate is directly proportional to pressure gradient (see [38] for detail). For simulation, a more useful version of the Darcy equation is by the partial differential form for u termed as Darcy velocity, as in Equation (2.3).

$$q = \frac{kA}{\mu}\frac{\Delta P}{L} \tag{2.2}$$

$$u = -\frac{k}{\mu}\frac{\partial P}{\partial x} \tag{2.3}$$

where q is the volumetric flow rate, A is the cross-sectional area over which flow is occurring, ΔP and k is the pressure differential and homogeneous permeability over a distance L, μ is the fluid viscosity, and u is the Darcy velocity.

Conceptually, the simulation equations are the volumetric material balance equation written for each phase of each grid block, and the fluid flow rates between each grid block and its adjacent blocks are formulated by Darcy's law [39] as illustrated in Figure 2.1. The derivation of the equations is performed to relate the pressure and saturation

changes with time throughout the reservoir. These equations are complicated nonlinear partial differential equations (PDEs) that are difficult or impossible to solve analytically. Hence, numerical methods are used, including spatial discretisation of PDEs, PDEs linearisation by the implicit or explicit scheme, and the use of appropriate boundary and initial conditions. Finally, the linear equations system is solved by a direct or an iterative process.

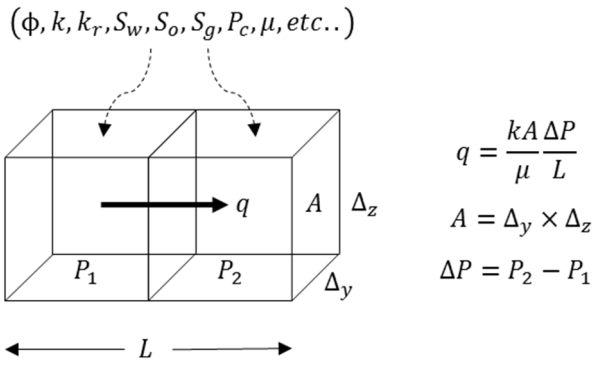

Figure 2.1—Reservoir model simulation technique.

2.2.2.2 Main Steps in a Reservoir Simulation Study

The key steps in a reservoir simulation study are: (1) reservoir model building; (2) history matching when production data are available; and then (3) perform production forecasting with uncertainty quantification and prepare a reservoir management plan [40], as shown in Figure 2.2. We describe the first step in this section and the next two steps are described in Section 2.3 and Section 2.6, respectively.

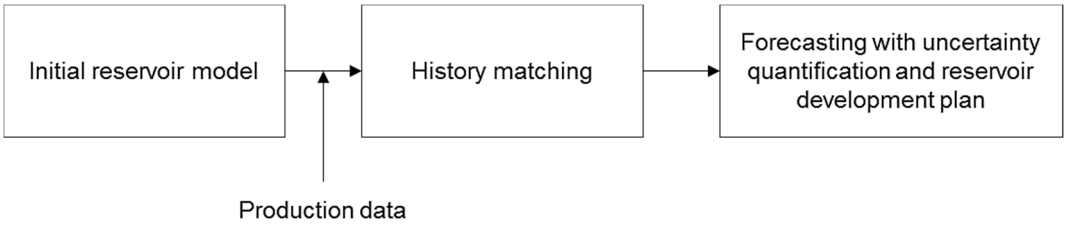

Figure 2.2—Main steps in a reservoir simulation study.

The steps to build an initial reservoir model are outlined as below [23]:

- Data collection — to collect input data mentioned above in Table 2.2 and perform quality control on the collected data.
- Designing the simulation model — to select the type of model geometry to use whether 1D, 2D, 3D, or radial and the simulator type to use whether a black-oil, a compositional, thermal or chemical.
- Building the simulation grid — as far as the type of grid is concerned, two basic geometries are used, the Cartesian and the Corner Point. For finite element method simulator, more grid types can be used such as an unstructured grid, distorted grid, and perpendicular bisector grid.
- Assigning the input parameters — to assign all the input parameters (geometry-related, rock and fluid properties, and the saturation functions as in Table 2.2) to the reservoir model grid. Model upscaling is required to reduce the simulation time.
- Set up the production schedule — to define production and injection scenarios, field and well controls such as bottom hole pressure, oil production and water injection rates.
- Model initialisation — to establish the initial pressure and saturation (equilibrium) conditions, which requires oil reference pressure at a datum depth and fluid contacts.
- Define outputs — to define the output variables such as average field pressure, grid blocks pressure and saturation, fluid (oil, water, and gas) production rates from the field and wells, and their frequency in the form of *timesteps* and visualisations (map, plot, 1D, 2D, or 3D visualisations).

The validity and reliability of the output from a reservoir model simulation are paramount for decision support in a reservoir management. It is vital for multi-billion-dollar investment and making sound operational decisions in reservoir management.

Initially, a reservoir model validation can be done in the initialisation phase of reservoir model building. In this phase, the calculation of the original-oil-in-place (OOIP) in the model can be conducted, which is then compared with the available volumetric figures. The differences between these two estimates may span from negligible fractions to significant percentages and are related to many factors such as capillary function used, fault

description or static property assignment in the grids. Even though the global estimate of the OOIP from a reservoir model agrees with the volumetric figure, there is no certainty that the geometry, petrophysical, and saturation estimates are precisely correct.

Once the field has been on production, the dynamic data become available, and a model validation or calibration to the dynamic production data (termed as *history matching* in the oil and gas industry) can be conducted. Afterwards, the history-matched models can be used to predict the future performance of the reservoir. The next section describes the history matching process and discusses the current techniques used in reservoir model history matching.

2.3 History Matching as an Inverse Problem

History matching is the process of modifying a reservoir model to obtain an acceptable match between the simulated model response and the observed dynamic data from the fields, regions or wells by adjusting uncertain model parameters. The dynamic data can be production data, pressure data from the well test and formation tester, tracer observations, well testing, and time-lapse seismic data which have been included as well in more recent history matching studies [41–46]. The most widely used dynamic data for history matching are well production data. Well production data are time series of measurements of pressure, flow rate, water cut or ratios of flow rate, made in producing or injecting wells. Model parameters that may be modified include but are not limited to rock properties (porosity, horizontal and vertical permeability), fluid properties (compressibility, oil and water relative permeability, capillary pressure), fluid contacts, and geological properties (net-to-gross, fault transmissibility, fracture data, aquifer volume and strength).

History matching is a complex inverse problem with ill-posed and underconstrained characteristics. The complexity is related to the nonlinearity of the dynamics and the nonlinearity induced by the relationship between data and model parameters. Moreover, even though the observation data are frequently repeated and the amount of the production data can be quite large, the information content is often relatively low due to redundancy.

History matching has been strongly influenced by the geophysicists' approach to parameter estimation or *inverse problem* as opposed to that of mathematicians [47]. Geophysicists made advances towards the understanding of the inverse problem since the beginning of the 1970s, when they spent most of their time trying to infer the properties of planetary interiors using only data acquired at the surface. Even though the modern theory was initiated by geophysicists, the inverse problem can be applied in all the field of physics [48]. For example, using data on the two-dimensional brightness observed on the sky sphere, astronomers infer the three-dimensional luminosity density of the Milky Way [48].

The inverse problem is the reciprocal of the *forward problem*. Using a physical theory in the form of a model for predicting the results of observations corresponds to solving the forward problem. On the contrary, in the inverse problem, the observations ($\mathbf{d}_{\mathrm{obs}}$) are used to determine the model parameters (**m)** that describe the reservoir model ($\mathbf{g}(\mathbf{m})$), where $\mathbf{g}(\cdot)$ is the forward model that predicts reservoir behaviour. Real observations are often with errors ($\boldsymbol{\epsilon}$) and assume to have Gaussian distribution with mean zero and standard deviation [5]. Therefore, the inverse problem is to solve the set of equations $\mathbf{d}_{\mathrm{obs}} = \mathbf{g}(\mathbf{m}) + \boldsymbol{\epsilon}$, for the model parameters $\mathbf{m}$ with the aim of making accurate predictions of future performance [5].

History matching is an *ill-posed* problem as it has no unique solution, i.e. plausible reservoir models can demonstrate similar simulation response that matches observation data (see [49] for a clear demonstration). As referenced from [13], Hadamard [50] introduced the mathematical term *well-posed* whose definition states that, if the mathematical models of physical phenomena have the properties that: (1) a solution exists; (2) the solution is unique; and (3) the solution depends continuously on the data over the range of parameter space, then the problem is well-posed. The problems that do not satisfy at least one of these conditions are called ill-posed problems (in this case, history matching does not meet condition 2).

History matching is an *underconstrained* problem as it has more possible solutions than the data that are available to constrain, though it is not completely unconstrained as there are some data available. This problem is due to a large number of parameters involved

(conceptually infinite), whereas the number of data is always finite [5]. Tarantola viewed this problem to that of *finding a needle in a haystack that has hundreds of dimensions* [48]. Nonetheless, in practice we adopt the philosophy by Oliver *et al.* 2008 [5] to approach the history matching problem by limiting the number of model parameters to solve the forward problem and setting the expectation that it is impossible to correctly estimate all the parameters of a model from inaccurate, insufficient, and inconsistent data [47].

2.3.1 Manual History Matching

Traditionally, history matching is accomplished by a repetitive manual trial-and-error process in which an engineer carries out a sequence of model simulations with different input model parameters to improve the match with the observed data. The engineer then performs a visual assessment on the matching curves, or he/she can quantify the mismatch by some mathematical formulation separated from the process. This exercise is time-consuming, requires engineer's experience, knowledge, and engineering judgement, and is often frustrating.

A structured approach in manual history matching of a reservoir model to improve the efficiency of reservoir management is reported in the literature. Amongst several guidelines in the literature [37,53,54], Williams *et al.* 1997 [51] provided a stratigraphic method to perform a manual history matching of a complex and multi-layered reservoir model which is now the reference for many history matching studies. The approach was developed over ten years in various reservoir studies and had been used successfully on highly complex reservoirs (more than 1,700 wells and over 50 years of production history), including more recent application in Tenqiz super-giant carbonate oil field in the Caspian Sea of the Republic of Kazakhstan [55].

In the stratigraphic method, the simulation model is adjusted at three levels: global or field wide, flow units or layer groups, and individual wells. The history matching is approached in two phases: pressure match and saturation match. Furthermore, the stratigraphic method starts the history matching with a bottom-up approach from the

deepest zone as the water moves from the bottom; and top-down approach if there is free gas movement as the gas moves from the top.

1	**Gather data**	Formation testing measurements Bottom hole pressure data Allocated production and injection data Well test data Tracer data Interference test data 4D seismic
2	**Quality control**	Errors from tubing communication Data reallocation errors Metering errors
3	**Prepare tools**	Prepare analysis tools Observation plots Observation maps
4	**Identify key wells**	Wells completed in only one flow unit Wells have formation testing data for pressure match Wells with pulsed neutron logs Newer wells with open hole logs for water match
5	**Interpret reservoir**	RFT and spatial pressure gradient maps for pressure match Waterfront maps and water occurrence coming from vertical rise Lateral fingering, coning for water match
6	**Repeat matching**	Until acceptable model matched to history is achieved
	6.1 Run the model	Initially controlled by total reservoir voidage for pressure match After that controlled by oil rate for saturation match (validation) Constrained by minimum BHP and maximum fluid and gas rates
	6.2 Compare model	Compare model results to observed and interpreted data
	6.3 Adjust the model	Adjust the model parameter (see Table 2.4)

Table 2.3—The manual history-matching procedure (after [51] as referenced to [52]).

Table 2.3 summarises the steps in manual history matching following the stratigraphic method, [51] as referenced to [52]. Some key notes on the steps of stratigraphic method are that, understanding the individual flow units and dealing with them individually are the key to making an effective history match as this approach is based on reservoir stratigraphy; the stratigraphic method provides a structured analysis tools for understanding reservoir behaviour and achieving a controlled history match; an organised history match plan by the stratigraphic method can provide an effective engineering and geologic control.

Table 2.4 summarises its history matching phases by the stratigraphic method of adjusting model parameters to match pressure and saturation, [51] as referenced to [52]. Model parameters adjustment depends on the degree of variation in a reservoir defined by the level of heterogeneity. As suggested by Kelkar 2002 [56], the level of heterogeneity

ranges from pore, core, grid and reservoir levels dependent on their scale. The different level has a different kind of measurements and its impact on the reservoir performance, for instance, in the core level we can get both porosity and permeability measurements that affect sweep efficiency (bypassed oil).

1. Match Pressure	Where	How
1.1 Global	Field	Adjust pore volumes, aquifer strength, permeability, fault transmissibility, WOC, rock compressibility (not adjusted if free gas is available).
1.2 Regional	Flow units, layer groups, and individual layers	Adjust lateral permeability, vertical transmissibility (start with the deepest zones, bottom-up, in water-drive and top-down for free gas reservoirs).
1.3 Individual Wells	Well cell or surrounding cells	Change layer allocations (well conductivity).
2. Match Saturation		
2.1 Global	Field	Water cut only if all wells or flow units are experiencing similar behaviour: change relative permeability, inter-sector connections, WOC, fault transmissibility, vertical transmissibility, and layer PI.
2.2 Regional	Flow units, layer groups, and individual layers	Water cut (if different water breakthrough times is seen from different zones): adjust relative permeability, layer or zone separation based on facies variation.
2.3 Individual Wells	Well cell or surrounding cells	Water cut (adjust layers' fluid allocations, PI, may ruin pressure match! Change inter-sector connections, WOC, relative permeability). GOR (significant measurement inaccuracies and inclusion of gas-lift gas in reported gas).

Table 2.4—Two phases history matching by the stratigraphic method (after [51] as referenced to [52]).

Additional guidance on adjusting the model parameters is based on the common sources of uncertainty for each data type given in [56]. For instance, for adjusting pore volumes, we may change either volume, net-to-gross or porosity data; for adjusting fault-related data type, we may change fault location and transmissibility. Combining this two information, data scale and type, we may proceed with the two phases of history matching by the stratigraphic method as in Table 2.4.

Nonetheless, manual history matching can be a hugely time-consuming process even though with a structured approach described above. For instance, in large fields, it may take many months of work to produce even one matched model that is acceptable. The

produced matched model also may be impractical and inconsistent with the geologic interpretation due to merely the engineers have to generate the best practical model given the project allocation time. Furthermore, Tavassoli et al [49] clearly demonstrated that even the best matched model failed to predict the production reliably. Therefore, a single history-matched prediction is no way defines the true extent of the reservoir uncertainty.

2.3.2 Assisted History Matching

Nowadays, history matching is often done automatically through optimisation techniques, although it is not fully automated yet, as speculated by Watts in 1997 [57]. Therefore, this technique is also well-known as assisted history matching (note the word 'assisted' is used instead of 'automatic'), and will be used throughout the rest of thesis interchangeably with history matching. Although it is computationally more intense than manual history matching, the assisted history matching was significantly favoured due to the vast improvement of computer capacities (in terms of processing speed and memory) as well as the development of advanced optimisation methods. Moreover, this technique is able to generate many more history-matched models and provide as good as or better matches than manual history matching (see [58,59]).

Diverse and good set of history-matched models are important factors for a reliable and yet realistic forecasting uncertainty of the future field behaviour. The diversity of models is represented by different reservoir properties such as permeability and porosity that may provide equally good history matches. This diversity is due to the characteristic of history matching as an *ill-posed* inverse problem with non-unique solutions.

It is important to find diverse and good history-matched models fast given the time allocation in a project. In manual history matching, a reservoir engineer can control the diversity of the model by starting the history matching with different model properties. However, it is difficult to get multiple good history-matched models fast by manual approach. In this sense, an assisted history matching is more favoured than manual history matching. However, in assisted history matching the algorithm is in control on the diversity of the history-matched models. Therefore, it is necessary to have a method that

can find these diverse and good set of models from assisted history matching, such as multi-objective approach as further described in Section 2.5 [7–10].

Figure 2.3 shows the typical assisted history matching workflow. It involves the determination of lower and upper bounds for the uncertain model parameter values (uncertainty parameterisation), the formulation of a scalar performance criterion (objective function) that measures the discrepancy between simulated responses and observed data (refers to as the *misfit* throughout the thesis), and the selection of a searching procedure (algorithm) to optimise the parameters with respect to the aforementioned criterion.

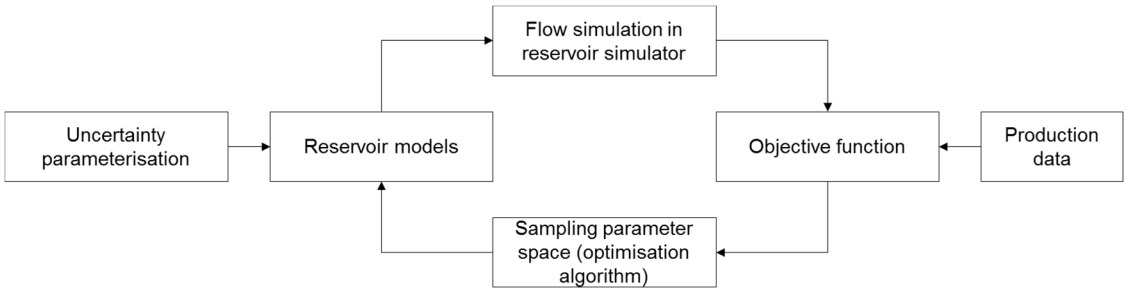

Figure 2.3—Typical workflow in assisted history matching using optimisation technique.

2.3.2.1 Uncertainty Parameterisation

Uncertainty in petroleum reservoirs is a result of the reservoir heterogeneity, the sparsity and limited accuracy of measurements. The main sources of the uncertainty are the reservoir geometry and structure, the spatial distribution of rock properties (e.g. porosity and permeability), and the reservoir fluid. Although one can argue that the fluid properties can be determined with a reasonable accuracy, the fluid flow in the reservoir is controlled by the poorly known rock properties (i.e. porosity and permeability) and reservoir structure (i.e. fault and top structure).

The data are commonly measured by taking samples at wells, which represent only a tiny fraction of the total reservoir leading to significant uncertainties. A good analogy of these uncertainties is pointed out by Christie *et al.* [60] by '*drawing a street map of*

London and then predicting traffic flow based on what you see from twelve street corners in a thick fog!'.

In the uncertainty parameterisation, we (1) determine the uncertain model parameters; (2) assign their uncertainty range distribution based on our prior knowledge (i.e. exponential, Gaussian, lognormal, triangular, truncated, uniform or discrete uniform) or based on informative priors (see [61] for detail). As the number of grid blocks in a reservoir simulation model can be quite large, the number of uncertain model parameters can be several orders magnitude greater than the number of independent data and constraints that are available if we want to estimate properties for each grid block. Thus, the necessity arises to reduce the number of model parameters through *parameterisation* methods. Uncertainty parameterisation through dimension reduction is quite intuitive for reservoir models because of spatial correlation of geological properties and redundancy in the reservoir description options related to geological continuity. Oliver *et al*. [5] stated that it is sometimes advantageous to adjust the number of uncertain model parameters in a much lower dimensional. This is due to the low content of information in most sets of production data as they were collected from a limited number of observation locations and because of the diffusive nature of the flow.

Uncertainty parameterisation in history matching is typically based on geological and engineering knowledge of the reservoir. The most common way of doing a geological parameterisation in history matching is through zonation. This approach assigns constant properties such as porosity and permeability over a domain that is larger than a single grid block based on some geological and engineering prior knowledge (see [62–64] for some pioneer works on the zonation approach in history matching). Based on the engineering knowledge, the parameterisation in history matching is typically related to the fluid properties such as relative permeability curve and capillary pressure. Assigning zonation approach in the engineering parameterisation is also a typical approach, for instance, to assign different fluid saturation table on different geological layer or zonation.

In practice, choosing which model parameterisation method to use is not straightforward as the selection of model parameters to be estimated and the determination of an optimal

number of model parameters can be difficult. Nonetheless, we can adopt the top-down reservoir modelling (TDRM) philosophy [65] which is developed by BP, to choose and design the model parameterisation. In essence, the TDRM philosophy is *'to start investigations with the simplest possible model and simulator appropriate for the business decision'* [65]. Christie *et al.* [9] have applied the TDRM approach in history matching of a real field and successfully obtained significantly good history matches.

2.3.2.2 Objective Function for History Matching

The objective function is a scalar performance criterion in an assisted history matching. It measures the discrepancy between simulated responses and observed data. It is also well-known as a misfit in history matching of petroleum reservoirs, and we aim to minimise its value (abbreviated as M throughout the thesis). As referenced to [48], some scientists (Boscovich and Laplace) were minimising the sum of the absolute value of the misfits, as in Equation (2.4) (so-called the least-absolute-values method), whereas other scientists (Legendre and Gauss) were minimising the sum of the squared values of the misfits, as in Equation (2.5) (so-called the least-squares method).

$$M = \sum_{i=1}^{N} |obs_i - sim_i| \tag{2.4}$$

$$M = \sum_{i=1}^{N} w_i (obs_i - sim_i)^2 \tag{2.5}$$

where obs and sim are the observed data and simulated response at data point i, respectively, N is the number of data points, and w_i is the weight factor at data point i to emphasise the importance of data point.

The popularity of the least-squares method over the least-absolute-values procedure in the oil industry is due to its simplicity, even though the least-absolute-values method is more robust to outliers than the least-squares method. It only involves the use of simple linear algebra in solving a least-squares problem, whereas in solving a least-absolute-values problem requires more complex computation such as linear programming (e.g. simplex method).

Some literatures have studied these different misfit definitions on history matching problems. Thomas *et al.* [66] used the least-squares method in Equation (2.5) for the misfit definition, which improved the results of history matching carried out by Coats *et al.* [67] that used the least-absolute-values method in Equation (2.4). Thomas *et al.* [66] demonstrated that the least-squares method led to fewer simulation runs than the least-absolute-values method for the same accuracy. A more recent history matching study by Bertolini and Schiozer in 2011 [68] on eight different objective functions (including the least-absolute-values and the least-squares method) confirmed these results. In their study on a synthetic reservoir model, a smaller number of simulations was achieved with the least-squares method (termed as the square error in their paper) than the least-absolute-values method (termed as the simple error in their paper) for the same match quality.

A more general form of the least-squares method in misfit definition is given in Equation (2.6) which includes a scaling factor.

$$M = \sum_{i} w_i \sum_{t} w_{i,t} \left(\frac{obs_{i,t} - sim_{i,t}}{scale_i} \right)^2 \tag{2.6}$$

where i is the data type, t is time, w_i is the weight for the i-th data, $w_{i,t}$ is the weight for the i-th data at the time t, obs and sim are the observed and simulated data respectively, and $scale_i$ is the scale factor for the i-th data type. A scaling factor is used to consider data with different absolute value ranges. A common choice is to use the noise standard deviation of the observed data (σ) as a scaling factor. Therefore, in its simplified version, the least-squares method with scaling factor can be defined as in Equation (2.7).

$$M = \sum_{i=1}^{N} \frac{(obs_i - sim_i)^2}{2\sigma^2} \tag{2.7}$$

where obs and sim are the observed data and simulated response at data point i, respectively, and N is the number of data points.

The misfit value based on Equation (2.7) will increase as the number of wells and data measured at those wells increases. This is due to the use of the noise variance (σ^2) to

weigh the squared data mismatch. As will be seen in the subsequent chapters, the misfit value obtained for synthetic models containing lower number of wells is significantly less than that of the real field case where there are many wells and observed data for each well. Nonetheless, the visual assessment of the match will appear similar on both cases.

The more generalised form of misfit value as the objective function in the history matching includes a regularisation term to account for prior geological knowledge regarding the spatial distribution of rock properties, as defined in Equation (2.8) [5].

$$\begin{aligned} M = \quad & \frac{1}{2}\left(\mathbf{m} - \mathbf{m}_{\text{prior}}\right)^T C_m^{-1}\left(\mathbf{m} - \mathbf{m}_{\text{prior}}\right) \\ & + \frac{1}{2}(\mathbf{obs} - \mathbf{sim})^T C_d^{-1}(\mathbf{obs} - \mathbf{sim}) \end{aligned} \tag{2.8}$$

where $\mathbf{m}$ is the vector of model, $\mathbf{m}_{\text{prior}}$ is the mean of prior geological model, C_m represents the prior covariance matrix, **obs** and **sim** denote the vectors of observed production data and simulated responses of dimension N (number of data points), and C_d is the $N \times N$ covariance matrix for the measurement error in production data. Assuming there is no simulation error and Gaussian distribution for the error data, the covariance C_d is equal to a $N \times N$ diagonal matrix, as defined in Equation (2.9), and the generalised form of misfit value in Equation (2.8) becomes Equation (2.7).

$$C_d = \begin{pmatrix} \sigma_1^2 & \cdots & 0 \\ \vdots & \ddots & \vdots \\ 0 & \cdots & \sigma_N^2 \end{pmatrix} \tag{2.9}$$

The least-squares method defined in Equation (2.7) does not take into account of time-dependent noise variance that may exist in the data as it uses a single value for noise variance (σ^2). A time-dependent misfit definition can be employed by using a covariance matrix to describe measurement errors, as described in Equation (2.9) (see [69] for example). Nonetheless, the least-squares method is adopted throughout the thesis due to its simplicity to implement on reservoir studies.

2.3.2.3 Optimisation Algorithms

Optimisation algorithms that are widely used for assisted history matching in the industry nowadays broadly fall into three categories: (i) gradient-based, (ii) data assimilation and (iii) stochastic sampler methods.

Gradient-based Methods

Gradient-based methods were the earliest optimisation techniques used in the assisted history matching [64,66,67,70,71]. These methods, such as such as Gauss-Newton, Levenberg-Marquardt, and steepest descent, work by calculating the derivative of the objective function with respect to the model parameters as either gradients or sensitivity coefficients.

The gradients are obtained by perturbing each parameter value independently and evaluating the sensitivity of the model to that parameter from the full simulation run of each case. This gradients computation is not practical for a large number of parameters as it requires a correspondingly large number of simulation runs. However, in [72], Li *et al.* suggested a solution to solving gradients computation for a large number of parameters by an *adjoint method* to calculate the sensitivity coefficients. The formulation given in [72] allows the construction of adjoint equations directly from information computed in solving the finite-difference equations. The advantage of this method is that the number of matrix solutions required to calculate the sensitivity coefficients is independent of the number of reservoir model parameters to be estimated.

Despite their fast convergence rates near minimum, gradient-based methods have several disadvantages. These methods can potentially get trapped in a local minimum as they try to find a single good solution. They may be relatively efficient for a single history match, but cannot be used for uncertainty assessment which requires multiple history matches. Moreover, the gradient-based methods require continuous objective functions (for gradient calculations) which inhibit their use on discrete variables. As pointed out by Oliver *et al.* [73], the gradient-based methods are also difficult to adapt to multi-phase flow simulators.

Data Assimilation Methods

The other category in assisted history matching is *data assimilation methods*. In these methods, depends on which approach, i.e. ensemble smoother or ensemble Kalman filter (EnKF), the model parameters are calibrated sequentially to the observed data over the space and/or time domain before the next simulation is run. In EnKF the global update of model parameters is done through recursive updates in the time domain, whereas in ensemble smoother the update is done in space-time domain. A comprehensive review on EnKF in reservoir engineering can be found in [74], whereas the comparative study between EnKF and ensemble smoother on assisted history matching of a reservoir model can be found in [75].

The main data assimilation method in history matching based on the number of published works is the EnKF [76–78]. EnKF has several advantages and disadvantages. Oliver *et al.* [73] pointed out that the EnKF has similar advantages with stochastic methods (i.e. highly parallelisable, suitable for large parameters and easily adaptable to different simulators). The disadvantages of the EnKF are it generally underestimates uncertainty (unless there is an additional perturbation), it requires additional parameterisation to adapt to a discrete variable and is not well-suited for parameters with multi-modal distributions.

Stochastic Methods

Stochastic methods refer to the optimisation of an objective function in the presence of randomness in the optimisation process. This randomness is useful in preventing entrapment in local minima. Stochastic methods are suitable for both continuous and discrete parameters, easily adaptable to various simulators and suitable for highly non-Gaussian distributions. Although there is no guarantee that the best solutions can always be found, stochastic methods are to perform robustly on a variety of complex real-world problems.

Stochastic methods usually do not require gradient information in their searching process, and their convergence rate is typically slower than gradient-based methods. However, several attempts have been reported in the literature that combines stochastic algorithm with gradient search to speed up the misfit convergence in history matching.

For instance, in [79], Valjak coupled the NA with gradients and demonstrated that the low misfit models are obtained faster than when alone. In [80], Mohamed *et al.* implemented Hamiltonian Monte Carlo (HMC) which uses gradient information to guide the stochastic sampling (by PSO or NA) towards the higher probability regions in parameter space. The HMC provides more explorative behaviour towards different areas in the parameter space and able to capture the "truth" case value. Moreover, HMC provides more models with low misfit value than the PSO or NA alone.

Stochastic optimisation algorithms have been growing rapidly in popularity over the last two decades, with some methods now becoming industry-standard approach for solving challenging history matching problems. These methods provide means of coping with inherent noise in the system and coping with models that are highly nonlinear, high-dimensional, or otherwise inappropriate for classical gradient-based methods (i.e. high number of parameters and continuous parameter values).

Key amongst these algorithms that have been applied to history matching are mostly in the class of *nature-inspired optimisation algorithms*. The motivation behind these algorithms is to take advantages of natural mechanisms or phenomena for solving optimisation problems. Amongst these algorithms that have been applied for history matching are: simulated annealing (SA) [81], evolutionary algorithms (EAs) which includes genetic algorithm (GA) and evolutionary strategy (ES) [13,82–86], NA [13,14,79,87], differential evolution (DE) [88], ant colony optimisation (ACO) [89], and PSO [90]. Even though estimation of distribution algorithm (EDA) [91] and Bayesian optimisation algorithm (BOA) [92] are not inspired by anything, the mechanisms in both algorithms are closely related to the GA or EA that are inspired by the theory of evolution and natural selections. Further development of these algorithms by hybridising amongst algorithms, parallelisation of algorithms processes, and making an adaptive search have also been applied to improve the performance of history matching, such as parallel GA-EDA [93], parallel BOA-PSO [94], and a more recently hybrid DE [95].

In this thesis, optimisation algorithms used for history matching and optimisation are in the class of stochastic methods. PSO and GA or EA variants are used for history

matching and optimisation, whereas NA is used as part of resampling in the forecasting that is described in the following sections.

2.4 Stochastic Sampling Algorithms

As discussed earlier, various stochastic sampling algorithms have been used in last two decades for assisted history matching. Amongst them, GA, NA, and PSO are the ones that have been applied to the real field case study and reported in the literature [9,13,79,96]. In this section, we will describe those three algorithms. The description of NA serves for the fundamental knowledge on the Bayesian uncertainty quantification that will be used throughout the thesis (as will be described in Section 2.6). The PSO algorithm is used for history matching study in Chapter 3. The description of GA serves for the fundamental knowledge on the nondominated sorting genetic algorithm II (as will be explained in Section 2.5.7) that is used for history matching study in Chapter 6.

2.4.1 Glossary for Stochastic Sampling Algorithms

Regardless of different search procedures, between stochastic sampling algorithms have some common terminologies due to the nature of optimisation process involved. Before giving an overview of the algorithms, a glossary of some the stochastic sampling algorithms used in the thesis is provided in this section.

Parameter (or search) space refers to a hypothetical space that contains all possible solutions of the problem. Its dimension is usually determined by the number of parameters. A vector of parameter values defines the location of any solution in the space.

Individual refers to a possible solution of the problem, e.g. in a history matching problem, a set of model parameters in a reservoir model corresponds to an individual. The term *individual* is the same to the term *particle* in PSO algorithm.

Population refers to a group of individuals at any timestep or iteration in the evolution. The population size determines the number of individuals in a population. The term *population* is the same to the term *swarm* in PSO algorithm.

Generation (or iteration) refers to one timestep of the evolution.

Fitness (objective function or misfit) value is the value of objective function measuring the fitness of an individual or particle to the specific problem objective. The fitness is either to be minimised or maximised depend on the specific problem, e.g. to be minimised in history matching or to be maximised in oil recovery optimisation.

Fitness (objective function or misfit) landscape refers to the changes in the fitness values over parameter space. In a minimisation problem, valleys are the (local and global) optima of the problem. A plateau or flat landscape indicates that the fitness value is not sensitive to that parameter.

2.4.2 The Neighbourhood Algorithm

The NA is a stochastic sampling algorithm developed by Sambridge [97] and has been used for history matching [14,84,87,98] as well as solving geophysical inverse problems [97]. It is a gradient-free method to find an ensemble of acceptable models rather than seeking a single optimal solution. The algorithm works by making use of Voronoi cells in a high-dimensional parameter space to tessellate the ensemble of misfits and locate good-fitting regions of the parameter space (see Voronoi [99] and Okabe *et al.* [100], as referenced to Sambridge [97] for formal definitions and further details on spatial tessellation concepts of Voronoi cells).

As excerpted from Erbas [13] and Sambridge [97], Figure 2.4 shows the workflow for the NA and is summarised in Algorithm 2.1. An example of the Voronoi diagram and the evolution of a 2D parameter space throughout the parameter search is shown beside the workflow in Figure 2.4. Note that for any distribution and density of samples, the Voronoi cells are always unique, space filling and have size inversely proportional to the sampling density.

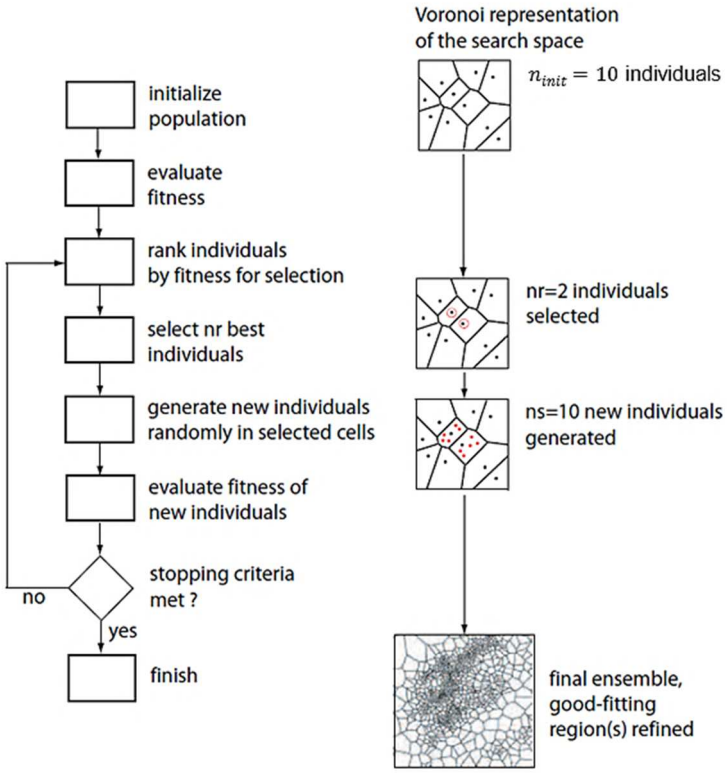

Figure 2.4—The NA workflow as referred to Algorithm 2.1 and an example of Voronoi representation of the search space with $n_s/n_r = 2$ (modified after Erbas [13]).

Algorithm 2.1—The Neighbourhood Algorithm [97].	
Step 1	(Initialisation) Generate an initial set of n_{init} models in parameter space;
Step 2	Calculate the misfit function for the most recently generated set of n_s models, construct Voronoi cells, and determine the n_r models with the lowest misfit of all models generated so far;
Step 3	Generate n_s new models using a Gibbs sampler in the Voronoi cell of each the n_r chosen models (i.e. n_s/n_r samples in each cell);
Step 4	Go to Step 2 and repeat the process until stopping criterion n_{iter} is met;

Thus, a total of $N = n_{init} + n_s \times n_{iter}$ models is generated by the algorithm.

The NA requires only two tuning parameters (n_s and n_r) which controls the behaviour of search in the parameter space. The lowest value of $n_s/n_r = 1$ emphasises the parameter space exploration (i.e. more explorative in nature) and as the value of n_s/n_r ratio is increased, the algorithm tends to improve the matches and the sampling should be more localised (i.e. more exploitative in nature).

The diversity of model solutions in the parameter space from NA is controlled by the n_s/n_r ratio. The lower the n_s/n_r ratio the more diverse the solutions, and vice versa the higher the n_s/n_r ratio the less diverse the solutions found by NA. As referenced to Christie *et al.* [101], the ratio of $n_s/n_r = 2$ can be used as starting point to obtain a balance between exploration and exploitation of search in the parameter space.

2.4.3 Particle Swarm Optimisation

PSO algorithm is originally proposed by Kennedy and Eberhart in 1995 [102]. It is a population-based stochastic search algorithm inspired by the simulation of the social behaviour of a flock of birds. It is originally adopted to balance the weights in neural networks [103], which soon became popular as global optimiser, mainly in problems with real numbers parameters [104,105]. PSO is relatively straightforward and easy to implement, computationally efficient, and has been found to be effective in a wide range variety of applications [106]. In petroleum industry, PSO has been applied to history matching [90,96,107–113], well placement optimisation [114], and drilling [115,116].

In PSO algorithm, a particle is 'flown' through multi-dimensional parameter space affected by its own experience and that of its neighbours. These neighbours are the ones that are close to each other based on the neighbourhood topology that defines the social structure of the swarm (see [106] for detail). The balance between exploration and exploitation in search for multiple optima is maintained by updating the particle's motion iteratively. The best solution the particle has seen, and the best solution across the whole population are used to update the velocity of each particle, and consequently its position. The main workflow of PSO is shown in Figure 2.5 and described in Algorithm 2.2, as excerpted from [102,108].

There are a number of variants of the PSO algorithm. Variants include the use of velocity clamping [117], an inertia weight [118] as described above, the cognition only PSO [119], the flexi PSO [120], and the more recent parallel BOA-PSO hybrid [94] which has been applied to history matching. Detailed comparisons of PSO variants and several sensitivity studies on different PSO parameter settings in history matching problem are given by Kathrada [120] and Mohamed [3].

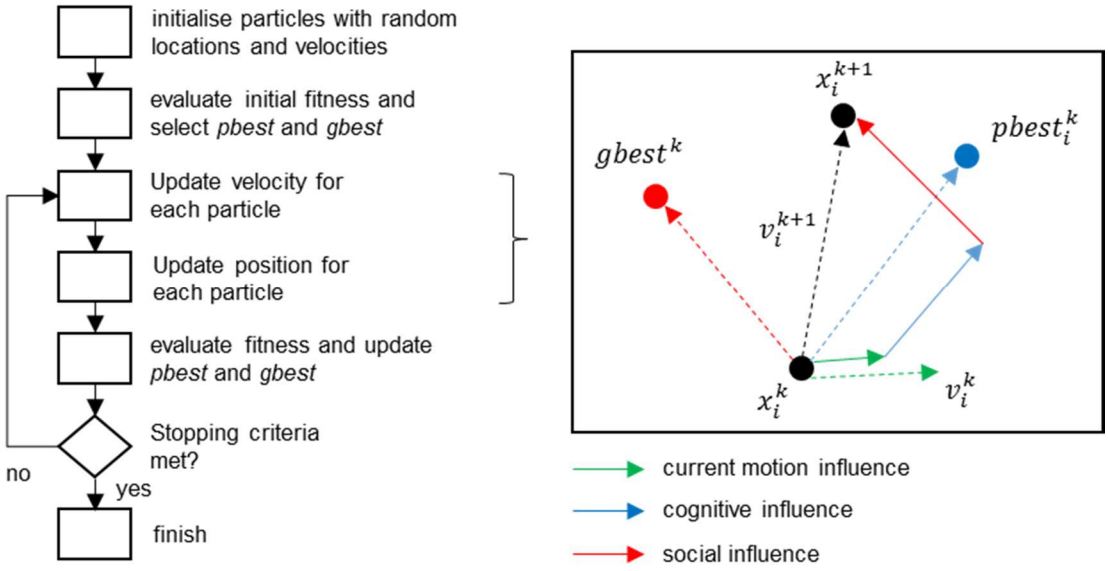

Figure 2.5—PSO workflow and graphical representation of a particle update in a parameter space.

Other variants of PSO algorithm is based on the particles update (position and velocity) during the search process, which are the originally synchronous update and the asynchronous update. In a synchronous update, the whole swarm fitness is evaluated first before particle update process is conducted. Whereas in an asynchronous update a particle can update its velocity and position after its fitness is evaluated. It is noted in the literature that asynchronous update provides faster convergence and diverse solutions than synchronous update [121,122].

Throughout the thesis, we use the standard PSO parameter settings following Trelea Set Type I' [123] in which $c_1 = c_2 = 1.494$, $w = 0.729$ for history matching studies. The PSO algorithm itself is already implemented in Raven™ of Epistemy (www.epistemy.com), which is one of the spin-out company from the research within Uncertainty Quantification Research Group at Heriot-Watt University.

2.4.4 Evolutionary and Genetic Algorithms

EAs are widely used optimisation and search algorithms in evolutionary computing, which is a rapidly growing area of artificial intelligence. EAs work based on Darwin's natural selection theory of evolution, where a population is progressively improved by

Algorithm 2.2—PSO Algorithm (taken from [102]).

Step 1 (Initialisation) Generate an initial set of n_{init} models (or particles) at random location ($x_i^{k=0}$) in parameter space and with an assigned random velocity ($v_i^{k=0}$) to each particle;

Step 2 Calculate the misfit value for each model (or particle);

Step 3 For each particle i, update the position and value of $pbest$ (*personal best*, the best solution the particle has seen). If current fitness value of one particle is better than its $pbest$ value, then its $pbest$ value and the corresponding position are replaced by the current fitness value and position, respectively;

Step 4 Find the $gbest$ (*global best*) fitness value and the corresponding best position of the entire population of $pbest$, and update if required;

Step 5 Update the velocity for each particle, as in Equation (2.10). The updated velocity is determined by the previous iteration velocity and the distance of the respective particle from the *pbest* and *gbest* location; Initially, the velocity is randomly generated with $v_i^{k=0} \in [-v_{max}, v_{max}]$. If a particle violates the velocity limit v_{max}, its velocity will be set back to the limit.

$$v_i^{k+1} = wv_i^k + c_1 r_1 \times \left(pbest_i^k - x_i^k\right) + c_2 r_2 \times \left(gbest^k - x_i^k\right) \tag{2.10}$$

where:

v_i^k is the velocity of particle i at iteration k;

x_i^k is the position of particle i at iteration k;

c_1 is the weighting factor, termed as cognitive component that represents the acceleration constant that changes the velocity of the particle towards $pbest_i^k$;

c_2 is the weighting factor, termed as the social component that represents the acceleration constant that changes the velocity of the particle towards $gbest^k$;

r_1 and r_2 are two random vectors with each component corresponding to a uniform random number between 0 and 1;

$pbest_i^k$ is the $pbest$ of particle i at iteration k;

$gbest^k$ is the global best of the entire swarm at iteration k;

and w is an inertia weight that determines the tendency of a particle to continue in the same direction it has been moving.

Step 6 Update the position of each particle, as in Equation (2.11);

$$x_i^{k+1} = x_i^k + v_i^{k+1} \tag{2.11}$$

Step 7 Repeat steps 2 to 6 until maximum iteration is reached;

selectively discarding the weaker ones and breeding new children from the stronger ones, also known as the "survival of the fittest" strategy.

There have been three main independent implementations of EAs [124]: GAs, developed by John Holland [125] and thoroughly reviewed by Goldberg [126]; ES, developed by Rechenberg [127] and Schwefel [128]; and evolutionary programming, originally developed by L.J. Fogel *et al.* [129] and refined by D. B. Fogel [130] as referenced to [131]. Each of these three algorithms has been proved capable of obtaining approximately optimal solutions given complex, multi-modal, non-differential, discontinuous parameter space, noisy and time-dependent problems (see [124,130,132]). Since 1992 we saw an explosion in the number of seemingly intractable problems to which EAs have been successfully applied [131].

GAs have been widely used as search and optimisation tools in various problems in petroleum industry domain such as history matching [65,82,84,133], well placement optimisation [134,135], production optimisation [136], and well-workover scheduling [137]. The primary reasons for their success are their broad applicability, ease of use and global perspective (i.e. finding global optima solution) [126].

GAs have five stages to be specified in their implementation: genetic encoding (*genotype*), evaluation, selection, reproduction, and replacement, as summarised in Figure 2.6. In the literature, we may also find the term *phenotype* specification as a preliminary stage for GAs. The phenotype stage is similar to the parameterisation in history matching where we define the parameter space of the problem (i.e. parameters, their ranges and prior distributions). A more comprehensive description of GAs, along with other EAs can be found in the compiled 'Handbook on Evolutionary Computation' [138].

Genetic encoding (genotype) defines how a solution in the population is represented. Binary, grey coding, real-value, and tree encodings are some of the most encoding schemes used in GAs. We used real-value encoding (see for example [139]) for history matching and field development optimisation application as it is the most suitable one for applications whose representation requires an array of real number parameters.

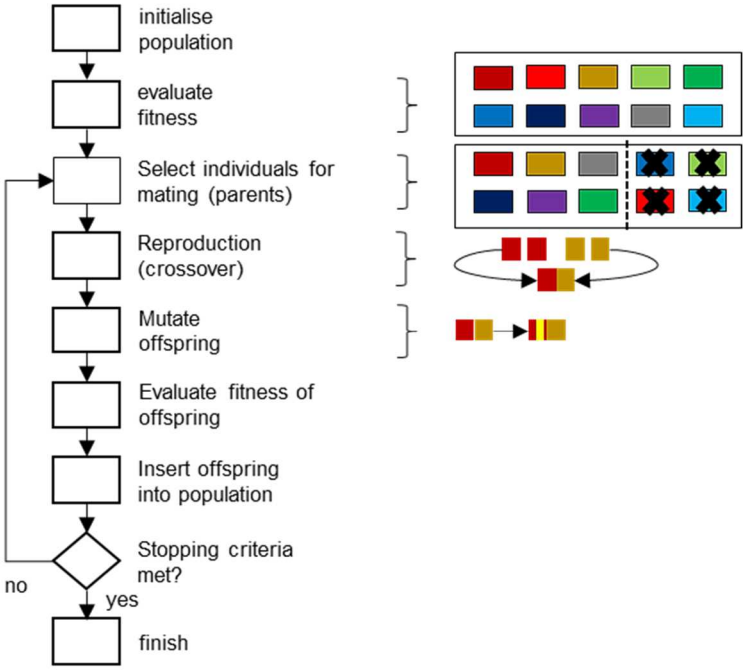

Figure 2.6—GA workflow and a graphical representation of individual selection, crossover, and mutation (modified after [13]).

Evaluation refers to the fitness evaluation of the solutions and can be obtained by measuring the goodness of fit as defined in the objective function.

In **selection** stage, the algorithm chooses the individuals in the population that will create offspring for the next generation, and determine how many offspring each will create. The selection stage aims to emphasise the fitter individuals in the population in hopes that their offspring will, in turn, have even higher fitness. Fitness proportionate selection with either Roulette Wheel or Stochastic Universal Samplings, sigma scaling, elitism, Boltzmann, rank, tournament, and steady state selections are amongst the most used selection methods. In the thesis, we used the tournament selection method as the original implementation of the algorithms used in Chapter 5. Nonetheless, for more thorough comparisons of different selection methods, see [140–143].

Reproduction involves mating the selected individuals (parents) and generating the offspring (children) by genetic operators (*crossover* and *mutation*). Crossover provides means for information exchange with the hope that new individuals will contain good parts of old ones, thereby making the new individuals more successful. Single-point,

two-point, blend, and simulated binary crossovers are amongst the most used for crossover operator. Mutation introduces variety into the population and generally helps the GA out if the search falls into local extremes. Gaussian and polynomial mutations are the two common methods for mutation operator. Two parameters can be used to tune the algorithm that controls the probability of crossover and mutation operations (P_c and P_m respectively).

In the thesis, we used the simulated binary crossover (SBX) [144] and polynomial mutation [145] genetic operators in the elitist nondominated sorting genetic algorithm (NSGA-II) (described in Section 2.5.7).

Replacement determines how the new offspring (children) are inserted into the population. Simple and steady state GAs are amongst the most used replacement strategies. Simple GAs replaces the entire population by a new population, whereas steady state GAs replaces only a certain proportion of the population in each generation. Another term related to the replacement is *elitism,* which means that the best individual from each generation is kept for the next generation.

2.5 Multi-Objective Optimisation

Most real-world search and optimisation problems naturally involve multiple objectives. For instance: in a product manufacturing process optimisation scenario engineers aim for the best performance of their design while the business owner seeks for the lowest cost required to implement the design; in decision-making of buying a car scenario a consumer look for the most comfortable car while limited for a certain amount of budget; in finance where a company desires to have the maximum revenue while look for the minimum risk as possible. Without exaggeration, multi-objective optimisation problems are everywhere.

Multi-objective optimisation is defined as a task of finding one or more optimum solutions when an optimisation problem involves more than one objective function [11]. It is also known as multiple criterion decision-making in the view of management as the

decision-maker, or also recognised as *vector optimisation* as it involves vector of objectives in the search and optimisation process instead of a single scalar objective.

Multi-objective optimisation has been favoured over single-objective optimisation. This is due to the adaptability of multi-objective optimisation on problem or objective function formulation that suits with the real-life optimisation problem.

In single-objective optimisation, the objectives in the optimisation problem is transformed into a single-objective problem. This approach has several challenges such as different units between objectives to optimise. For instance, in the production facility optimisation where the decision-maker wants to maximise profit (in monetary units) and to minimise production water cut (in fraction unit). Another challenge in single-objective is where the ranges of objective values between objectives that can be different (i.e. in the order of more than one or two magnitudes). As an example, in the well placement optimisation to maximise oil recovery with the objective values of millions barrel of oil whereas the other objective is to minimise the water production rate with the objective values of hundreds or thousands barrel per day of water.

On the contrary, these challenges in single-objective optimisation can be rectified by multi-objective optimisation in that the optimisation is performed simultaneously over several objectives or criteria. Instead of a single best solution, multi-objective optimisation results in several optimal solutions that is the set of tradeoff solutions and no solution from this set makes all objectives look better than any other solution from the set. Without any further information, no solution from the set of optimal solution can be said to be better than any other. In a multi-objective optimisation problem, many such (tradeoff) optimal solutions are important because a number of solutions are important. Afterwards, decision-maker can choose which optimal solution(s) to pick based on his/her preference.

In history matching problem, the superiority of multi-objective is demonstrated in several studies that are able to speed up the misfit convergence and obtain a diverse set of solutions [7,8,10]. The applications of multi-objective in petroleum industry are reviewed in Section 2.5.3.

Both approaches, single and multi-objective optimisation, are further described in the following two subsections.

2.5.1 Classical Methods

There are a few commonly used classical methods for handling multi-objective optimisation. The most widely used method is the weighted-sum approach where a set of objectives are scalarised into a single-objective by premultiplying each objective with a user-supplied weight. Faced with multiple objectives, this method is the most convenient one that comes to mind.

Although there exist ways to quantify the weights based on the objective's relative importance in the problem, the weighted-sum approach requires a precise value of the weight for each objective ([146] as referenced to [11]). Setting up an appropriate weight vector also depends on the scaling of each objective function as an inappropriate scaling result in extremely rough response surface of objective functions (see [147] for an example in history matching with different weight can results in different area of objective functions).

Another classical methods exists which basically appear to alleviate the difficulties and challenges faced from the other methods, such as ϵ-constraint, weighted Tchebycheff metric, Benson's, value function, goal programming, and interactive methods (see [11] for details). Nonetheless, these classical methods suggest a way to convert a multi-objective optimisation problem into a single-objective optimisation problem.

2.5.2 Multi-Objective Approach

In many cases, the objectives in multi-objective problems are conflicting and no possible solution optimises all of them simultaneously. This means that an improvement or better fitness in one objective may cause a deterioration or worse fitness in another objective. In these problems, multi-objective optimisation approach is useful as it aims to find good compromises or *tradeoffs* between those conflicting objectives. Therefore, in problems with more than one conflicting objective, there exist a number of solutions which are all optimal, and thus there is no single optimum solution. This tradeoff concept was first

introduced by Anglo-Irish philosopher and political economist Francis Ysidro Edgeworth in 1881 and later was generalised by an Italian economist Vilfredo Federico Pareto in 1896.

Figure 2.7 illustrates examples of multi-objective schemes on hypothetical history matching and well placement optimisation problems with two conflicting objectives. For the hypothetical history matching problem, there are two match criteria to minimise (oil rate and water rate matches), whereas on the hypothetical well placement optimisation problem there is one objective to maximise (oil recovery) and another one to minimise (cost). In history matching problem, as shown in Figure 2.7 (a) for two extreme hypothetical solutions 1 and 2, better match quality on oil rate cause a deterioration in match quality on water rate, i.e. solution 1 has better match on oil rate than solution 2, but this come at the cost of worse match on water rate in solution 2 compared to solution 1. In well placement optimisation as in Figure 2.7 (b), for two extreme hypothetical solutions 1 and 2, higher oil recovery can be achieved but with higher cost, i.e. solution 1 can be selected if the cost is the only objective in decision-making or if budget permits, solution 2 can be chosen to get the highest oil recovery.

Nonetheless, in these two examples, there are also many other solutions where a tradeoff between objectives exists, i.e. solutions A, B, and C. Thus, between any two such solutions, one is better in one objective, but this betterment comes only from a sacrifice on the other objective.

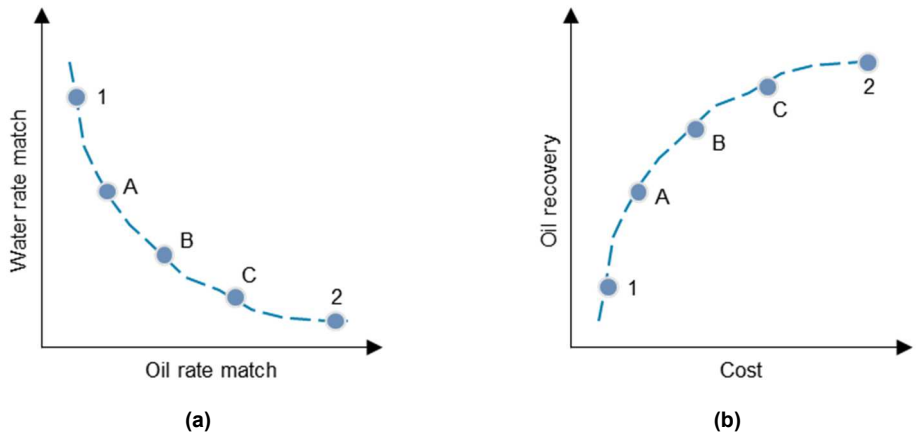

Figure 2.7—Hypothetical tradeoff solutions for multi-objective schemes on (a) History matching and (b) Well placement optimisation problems.

2.5.3 Applications of Multi-Objective Optimisation in Petroleum Industry

Multi-objective optimisation has been used on a wide range of real-world applications, in areas ranging from engineering design, hydrology, medical treatments, water resources, economics and finances. Stewart *et al.* [148] provide an excellent brief on the broad range of multi-objective optimisation applications in real-world problems. They classified applications based on the number of objectives involved (i.e. few, moderate, and large) and the level of interaction with decision makers (i.e. low, moderate, and intensive). Efstratiadis and Koutsoyiannis [149] provides an excellent review of the multi-objective optimisation approach for the hydrological modelling and calibration, an area that often shares common knowledge and practice to the reservoir history matching. In their review, the early attempt of multi-objective optimisation in hydrology was found in the work of Harlin in 1991 [150], who formulated an iterative procedure that focuses on different process descriptions and associated performance measures. However, the use of automatic routines employing multi-objective optimisation concept was only established in 1998 after the pioneering work by Yapo *et al.* [151], whereas in water resources technology, multi-objective optimisation appeared a few years earlier [152–154].

In the petroleum literature, the concept of multi-objective was firstly applied by Harrison and Tweedie in 1981 [155]. They constructed a mathematical model, called MULTIPOL, for economic analysis of oilfield production policy in a typical North Sea project. In the model, they applied a multi-objective optimisation to find a compromise in the production policy to avoid the project abandonment. Four objectives included in the model are internal rate of return, operator net present value (NPV_o), NPV_o per unit investment (NPV_o /I), and government net present value (NPV_g).

In 2000, Saputelli *et al.* [156] introduced the technology of integrated computer-aided design and operations to petroleum production that triggers the application of multi-objective optimisation in petroleum industry. In their paper, the authors emphasised the integration of multi-objective optimisation and stochastic optimiser in the surface production facility optimisation that can bring the success to the project. Since then, multi-

objective optimisation had enjoyed its popularity in the petroleum industry as indicated by an increasing trend in the number of published paper related to multi-objective optimisation, as shown in Figure 2.8.

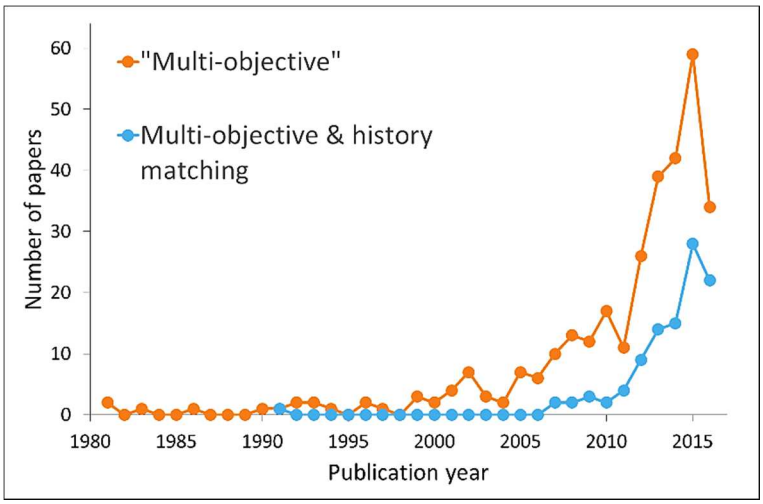

Figure 2.8—Number of published papers in OnePetro library (www.onepetro.org) over the years from 1981 to 2016 that are related to multi-objective optimisation and history matching.

Figure 2.8, indicated by the orange line, shows the number of published papers in the OnePetro library (www.onepetro.org) related to multi-objective optimisation concept in their methodologies and applications. Papers are searched with keyword "multi-objective" and filtered by screening the abstracts which are using multi-objective in their main methods and applications. The topics of their implementations are ranged from facility and manufacture design related to petroleum industry [157–166], reservoir and well optimisation [167–174], and petroleum economics [164,175–178]. The slight reduction in the number of studies in 2016 shown in this figure is most likely to result from the non-availability of some material to the author until after the date of publication of this thesis.

A number of multi-objective optimisation application for history matching have been reported in the literature over the years and indicated as the blue line in Figure 2.8, where published papers are searched with keyword "multi-objective" and "history matching." Early work of Chung and Kravaris in 1991 [179] marked a conceptual use of multi-

objective optimisation as a method to incorporate *a priori* information in history matching problem. In their work, Chung and Kravaris presented a stepwise procedure to determine optimal values for the weights as a tradeoff amongst multiple criteria.

One and a half decade later, it was Schulze-Riegert *et al.* in 2007 [180] who implemented the first application of assisted multi-objective history matching using strength Pareto evolutionary algorithm 2 (SPEA2). Since then, multi-objective history matching with various optimisation algorithms have gained popularity. For example, Ferraro and Verga in 2009 [181] applied the multi-objective genetic algorithm and multi-objective evolution strategies (MOGA and MOES, respectively) for history matching and uncertainty quantification of the PUNQ-S3 synthetic case. In another application, Hajizadeh *et al.* (2011) [8] implemented multi-objective DE based on MOGA Pareto Ranking (DEMOPR) for history matching of the PUNQ-S3 synthetic case. Mohamed *et al.* (2011) [7] used multi-objective particle swarm optimisation (MOPSO) for history matching of the IC (stands for Imperial College) Fault model. Stephen (2013) [41] implemented multi-objective neighbourhood algorithm (MONA) and included seismic data in the history matching. Watanabe *et al.* (2013) [182] applied NSGA-II to the history matching of The Norne Field. Min *et al.* (2014) [183] combined dynamic goal programming (DGP) and successive linear objective reduction (SLOR) with MOGA, called DS-MOGA, for history matching of a heavy oil reservoir. Olalotiti-Lawal and Datta-Gupta (2015) [184] implemented multi-objective Markov chain Monte Carlo (MOMCMC) for history matching of a synthetic model. More recently, Huguet *et al.* (2016) [185] combined self-organising map (SOM) and multi-objective covariance matrix adaptation evolution strategy (MO-CMA-ES) for history matching of a model called the Chemery PREPRE.

Out of 102 published papers in total that are related to multi-objective optimisation and history matching as indicated in Figure 2.8, 19 are selected based on the algorithms used and summarised in Table 2.5 with their problem formulations. In general, these 19 selected studies fall into four categories based on the objective and type of the study, as described below:

a. Handling conflicting objective, where multi-objective optimisation was used to handle conflicting match criteria in the history matching studies;
b. Misfit convergence, where the study evaluated and compared the misfit convergence performance between multi-objective and single-objective optimisations;
c. Forecast evaluation, where the multi-objective optimisation was used to estimate the future production performance in reservoir management;
d. Objective definition, where the concept of multi-objective optimisation was used in the objective definition of history matching studies.

Related to the objective grouping, Hutahaean *et al.* [10] initiated a comparative study between three different objective grouping schemes in two-objective history matching on PUNQ-S3 reservoir model. We demonstrated that different objective groupings could lead to the different performance of history matching. Even though the geoengineering knowledge-based grouping, as shown in that paper, may improve the misfit convergence and match quality in multi-objective history matching, the grouping method can be difficult to use consistently in more complex reservoir. Hence, it is essential to have a formal approach or guideline to help reservoir engineers on how to group the objectives more consistently to improve the history-matching performance.

Several history matching studies have dealt with the objectives more than three (called many-objective problems), as shown in Table 2.5. Han *et al.* [186] used multi-objective evolutionary algorithm (MOEA) for history matching with four objective functions. Niri and Lumley [189] applied NSGA-II for history matching with four objective functions to measure the mismatch of the geological and seismic data. Min *et al.* [183] developed an algorithm called DS-MOGA combining DGP and SLOR with NSGA-II to deal with history matching with eight objective functions. However, there is no published work so far that evaluates the performances of history matching under increasing number of objectives which may affect the performance of history matching, i.e. misfit convergence and match quality. This type of study is important for practical reason where reservoir engineers are not aware about the limitation some multi-objective algorithms on a high number of objectives.

Several attempts on using the multi-objective formalism on uncertainty prediction have demonstrated in the literature. In [7,8,10], the authors combined the multi-objective history matching with the Bayesian framework for forecasting uncertainty. In other work, Park *et al.* [147] picked the centroids of optimal solutions for predictions. Finally, in [184], Olalotiti-Lawal and Datta-Gupta used the MOMCMC algorithm that allows for quantifying uncertainties in the process. However, in these noted studies there is no such a structured way of approximating the PPD within the multi-objective formalism that is required for accurate uncertainty predictions and yet manageable computational cost. Hence, in this thesis we propose a methodology on how to approximate PPD from multi-objective history matching that are used for uncertainty prediction in the optimisation.

Reference	Type of study[a, b, c, or d], model, number of wells	Problem formulation (parameters and objectives)	Algorithms
Schulze-Riegert *et al.* (2007) [180][1]	Handling conflicting objective[a]. The synthetic 3D model derived from North Sea reservoir model. 4 wells.	9 parameters and 4 objectives. Production data mismatch.	SPEA2
Ferraro and Verga (2009) [181]	Misfit convergence[b]. PUNQ-S3. 6 wells.	12 parameters and 3 objectives. Production data mismatch.	MOGA and MOES
Han *et al.* (2010) [186]	Forecast evaluation[c]. Synthetic 2D model. 4 wells.	Unknown parameters and 4 objectives. Production data mismatch for waterflood performance estimation.	MOEA
Hajizadeh *et al.* (2011) [8]	Misfit convergence[a]. PUNQ-S3. 6 wells.	45 parameters and 2 objectives. Production data mismatch.	DEMOPR
Mohamed *et al.* (2011) [7]	Misfit convergence and forecast[a,b]. IC Fault model. 2 wells.	3 parameters and 2 objectives. Production data mismatch.	MOPSO
Sayyafzadeh *et al.* (2012) [187]	Objective definition[d]. Synthetic 3D model. 9 wells.	51 parameters and 2 objectives. Prior and likelihood as the objectives.	MOGA
Christie *et al.* (2013) [9][2]	Misfit convergence[b]. Zagadka, 100 wells.	19 parameters (TDRM) and 3 objectives. Production data mismatch.	MOPSO
Stephen (2013) [41][3]	Objective definition[d]. Synthetics 3D model analogue to a sector of the Schiehallion field. 2 wells.	4 parameters and 2 objectives. Production data mismatch with the inclusion of seismic data.	MONA
Watanabe *et al.* (2013) [182]	Objective definition[d]. The Norne Field. 36 wells.	420 coefficients of Grid Connectivity Transform (GCT) and 3 objectives. Production data mismatch with the inclusion of 4D seismic data.	NSGA-II
Verga *et al.* (2013) [188]	Misfit convergence[b]. Synthetic 3D model. 2 wells.	10 parameters and 2 objectives. Production data mismatch.	SPEA2

[1] The first application of multi-objective in history matching
[2] The first application of multi-objective in real field
[3] The first inclusion of seismic data to the multi-objective history matching

Park *et al.* (2013) [147]	Handling conflicting objective[a]. Brugge model. 30 wells.	20 coefficients (GCT) and 3 objectives. Production data mismatch with the inclusion of seismic data.	NSGA-II
Kato *et al.* (2014) [96]	Handling conflicting objective[a]. Real field. 6 wells.	6 parameters and 2 objectives. Production data mismatch.	MOPSO
Niri and Lumley (2014) [189]	Objective definition[d]. The Stybarrow field. 4 wells.	3 parameters and 4 objectives. Seismic and geological data mismatch.	NSGA-II
Min *et al.* (2014) [183]	Objective definition[d]. Heavy oil reservoir model. 5 wells.	7 parameters and 8 objectives. Production data mismatch.	DS-MOGA
Hutahaean *et al.* (2015) [10]	Misfit convergence, objective definition and forecasting[b,c,d]. PUNQ-S3. 6 wells.	24 and 38 parameters, and 2 objectives. Production data mismatch, objective grouping studies and forecast reliability.	MOPSO
Olalotiti-Lawal and Datta-Gupta (2015) [184]	Misfit convergence[b]. Synthetic 2D (9 wells) and Brugge (30 wells) models.	10 coefficients (GCT) and 2 objectives (for synthetic case), 32 coefficients (GCT) and 2 objectives (for Brugge)	MOMCMC
Kam *et al.* (2016) [190]	Objective definition[d]. The Norne Field. 36 wells.	440 coefficients (GCT) and 3 objectives. Production data mismatch.	MOGA
Huguet *et al.* (2016) [185]	Objective definition[d]. The Chemery PREPRE model. 67 wells.	29 parameters (SOM) and 3 objectives. Production data mismatch.	MO-CMA-ES
Kanfar and Clarkson (2016) [191]	Objective definition[d]. Model of liquid-rich shale well from Montney Formation.	22 parameters and 3 objectives. Production data mismatch.	NSGA-II

Table 2.5—Characteristic of applications of multi-objective reservoir model history matching.

In the next subsections, we describe key fundamental notions in multi-objective optimisation, a brief history of multi-objective algorithms followed by descriptions of two state-of-the-art multi-objective algorithms used in the thesis, namely MOPSO and NSGA-II, and the multi-objective optimisation paradigm in history matching.

2.5.4 Fundamental Notions in Multi-Objective Optimisation

In its general form, the multi-objective optimisation can be formally defined as:

$$\left.\begin{aligned} \text{Minimise/Maximise} \quad & f_m(\mathbf{x}), && m = 1,2,\dots,M; \\ \text{subject to} \quad & g_j(\mathbf{x}) \geq 0, && j = 1,2,\dots,J; \\ & h_k(\mathbf{x}) = 0, && k = 1,2,\dots,K; \\ & x_i^{(L)} \leq x_i \leq x_i^{(U)}, && i = 1,2,\dots,N; \end{aligned}\right\} \tag{2.12}$$

where $f_m(\mathbf{x}): \mathbb{R}^N \rightarrow \mathbb{R}^M$, $\mathbf{x} = \{x_1, x_2, \ldots, x_k, \ldots, x_N\}$ is the vector of the N parameters, M is the number of objective functions, g_j and h_k are the inequality and equality constraints, respectively, with J and K are the number of inequality and equality constraints, respectively, and the last set of constraints are the parameter bounds restricting each parameter x_i to take a value within a lower $x_i^{(L)}$ and an upper bound $x_i^{(U)}$.

Definition 2.1. (Feasible/infeasible solution or region). A solution **x** that does not satisfy *all* of the $(J + K)$ constraints and *all* of the parameter bounds stated above is called an *infeasible solution*. On the contrary, if any solution **x** satisfies *all* constraints and parameter bounds, it is known as a *feasible solution*. Accordingly, regions where all the infeasible or feasible solutions are located in parameter or objective spaces are called infeasible or feasible regions, respectively.

Multi-objective optimisation involves two search spaces: parameter space and objective space as illustrated in Figure 2.9 for two-objective optimisation problem with three parameters. Although these spaces are related by a unique mapping between them through the objective function definitions, often the mapping is nonlinear, and the properties of the two search spaces are not similar. For instance, a proximity of two solutions in one space does not mean a proximity in the other space.

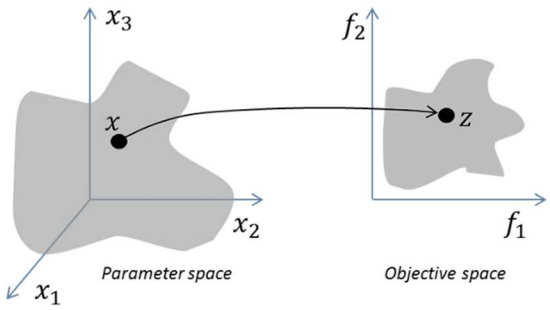

Figure 2.9—Representation of the parameter space and the corresponding objective space.

Most multi-objective optimisation algorithms use the concept of d*ominance* and *Pareto optimality* [11]. In these algorithms, two solutions are compared on the basis of whether one dominates the other solution or not. The dominance mechanism is an important

feature in a multi-objective algorithm as it determines which solutions to store in the archive that has influences on the fitness quality and diversity of solutions.

We describe dominance and Pareto optimality concepts in the following paragraph and use the operator $\lhd$ between two solutions i and j as $i \lhd j$ to denote the solution i is better than solution j on a particular objective, and vice versa $i \rhd j$ implies that solution i is worse than solution j for a particular objective. For instance, in minimisation problem, the operator $\lhd$ would mean the '$<$' operator, whereas in maximisation problem the operator $\lhd$ would mean the '$>$' operator. As an illustration, the definitions described below refer to the Figure 2.10 for a minimisation problem with two objectives.

Definition 2.2. **(Dominance)**. A solution $\mathbf{x}_1$ dominates a solution $\mathbf{x}_2$ (denoted $\mathbf{x}_1 \preceq \mathbf{x}_2$), if and only if the two conditions below are satisfied:

1. The solution $\mathbf{x}_1$ is no worse than $\mathbf{x}_2$ in all objectives, i.e. $f_m(\mathbf{x}_1) \not\rhd f_m(\mathbf{x}_2)$, $\forall m = 1, 2, \ldots, M$.
2. The solution $\mathbf{x}_1$ is strictly better than $\mathbf{x}_2$ in at least one objective, i.e. $\exists m = 1,2, \ldots, M$: $f_m(\mathbf{x}_1) \lhd f_m(\mathbf{x}_2)$.

As an example, the striped area in Figure 2.10 shows the dominance concept for a two-objective minimisation problem where solution $\mathbf{x}_2$ dominates solutions $\mathbf{x}_4$, $\mathbf{x}_5$, and $\mathbf{x}_6$.

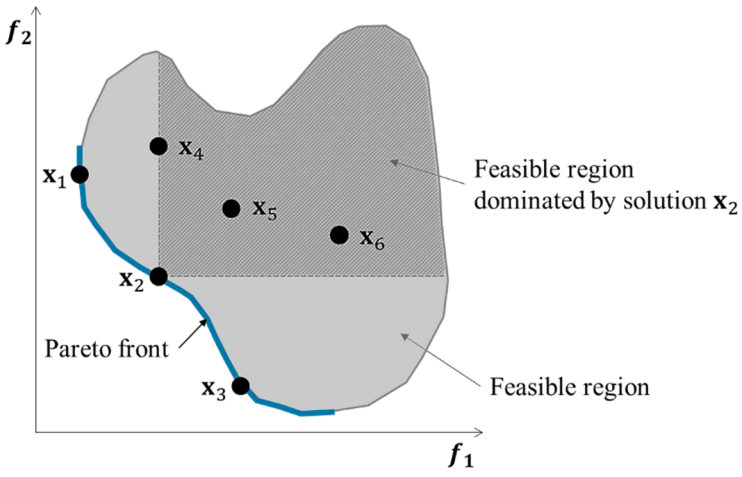

Figure 2.10—Pictorial view of Dominance and Pareto optimality in objective space of hypothetical two-objective minimisation problem. Striped area is the feasible region dominated by solution $\mathbf{x}_2$.

Definition 2.3. (Strong Dominance). A solution $\mathbf{x}_1$ strongly dominates a solution $\mathbf{x}_2$ (denoted $\mathbf{x}_1 \prec \mathbf{x}_2$), if solution $\mathbf{x}_1$ is strictly better than $\mathbf{x}_2$ in all M objectives.

As an example in Figure 2.10, solution $\mathbf{x}_2$ strongly dominates solutions $\mathbf{x}_5$ and $\mathbf{x}_6$ as it is better in all two objectives.

Definition 2.4. (Nondominated set/Pareto optimal set). Amongst a set of solutions P, the nondominated set of solutions P′ are those that are not dominated by any member of the set P. When the set P is the entire search space, the resulting nondominated set P′ is called the *Pareto optimal set*.

In the thesis, nondominated and Pareto optimal will be used interchangeably and refer to the similar meaning of Pareto optimal. As an example in Figure 2.10, solutions $\mathbf{x}_1$, $\mathbf{x}_2$, and $\mathbf{x}_3$ are the nondominated set of solutions.

Definition 2.5. (Weakly nondominated set). Amongst a set of solutions P, the weakly nondominated set of solutions P′ is those that are not strongly dominated by any member of the set P.

Definition 2.6. (Pareto optimal front). It is defined by the set that contains all the objective vectors corresponding to parameter vectors that are not dominated by any other parameter vector, i.e. the Pareto optimal front is the image of Pareto optimal set in the objective space.

Pareto optimal front, or often called Pareto front is depicted as the blue line in Figure 2.10. Depending on the type of optimisation (i.e. maximisation or minimisation), the location of the Pareto front can be in different areas in the objective space, as shown in Figure 2.11, which depicts four different scenarios for two objectives optimisation problems.

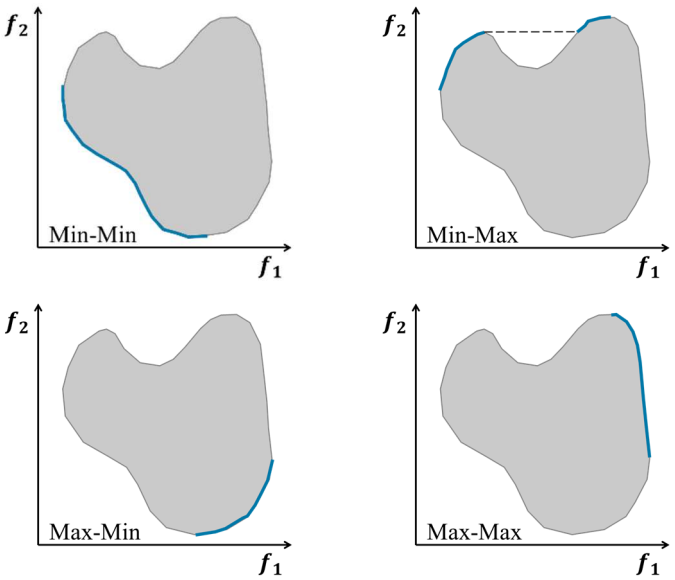

Figure 2.11—Pareto front (marked with blue curves) for four combinations of hypothetical two-objective problems (after [11]).

2.5.5 Goals in Multi-Objective Optimisation

There are two main goals in multi-objective optimisation as illustrated in Figure 2.12 (a). The first goal is to obtain the solutions as close as possible to the Pareto front, i.e. convergence performance of an algorithm to the Pareto front. The second goal is to obtain solutions as diverse as possible along the Pareto front, i.e. diversity or a variety of optimal solutions which trades off the objectives differently.

Figure 2.12 (b) illustrates the contrast of optimal solutions from multi-objective optimisation with the single-objective when plotted in the similar objective space. We can see from Figure 2.12 (b) that the optimal solutions from single-objective evolve to tight cluster on the Pareto front as the result of overrefinement, i.e. from the NA. Over-refined solutions are usually variants of the same solution with minimum alteration in parameters values [79]. Thus, they are not diverse solutions. Hence, it is necessary to perform multi-objective approach to ensure the diversity of the solutions.

An efficient multi-objective algorithm must work on satisfying both goals which are somewhat *orthogonal* to each other. The achievement of one goal does not necessarily achieve the other goal. Explicit or implicit mechanisms to emphasise convergence near

the Pareto front and the maintenance of a diverse set of solutions must be introduced in an algorithm.

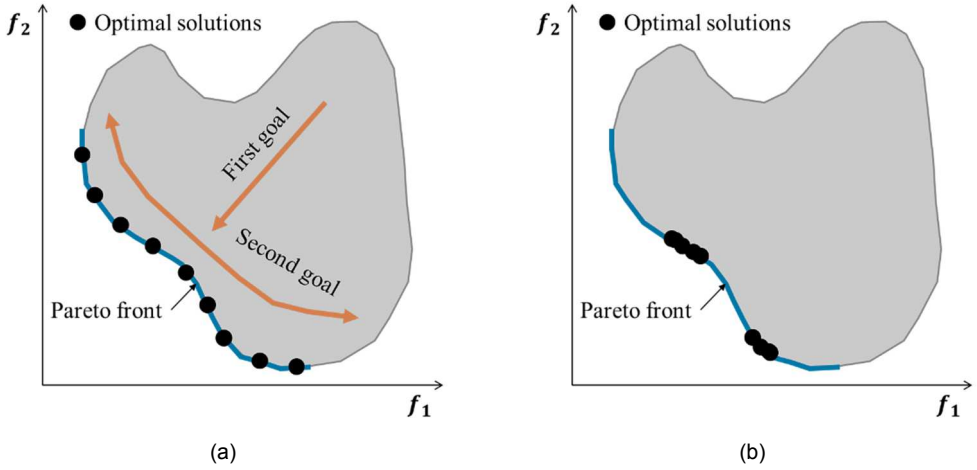

Figure 2.12—(a) Goals in multi-objective optimisation illustrated in a hypothetical two-objective minimisation problem, and (b) Contrast with the solutions from the single-objective that are tightly clustered on the Pareto front.

2.5.6 A Brief History of Multi-Objective Algorithms

Deb [11] classified MOEAs into two categories, namely non-elitist and elitist MOEAs based on the use of any *elite-preserving* operator. An elite-preserving operator favours the elites of a population (previously found optimum solutions) by giving them an opportunity to be directly carried over to the next generation. No matter how elitism is introduced, it makes sure that the fitness of the population best solution does not deteriorate. In this way, a good solution found early on in the run will never be lost unless a better solution is found.

Non-elitist MOEAs do not use any elite-preserving operator. Amongst these algorithms are the firstly MOEA by David Schaffer (1984) called vector-evaluated genetic algorithm (VEGA) [192], a 10-line sketch of nondominated sorting MOEA by Goldberg [126], Fonseca and Flemming's multi-objective GA (MOGA) [193], Srinivas and Deb's nondominated sorting GA (NSGA) [194], and Horn-Nafploits and Goldberg's niched Pareto-GA (NPGA) [195].

Elitist MOEAs use any elite-preserving operator. Amongst these algorithms are Zitzler,

Laumanns and Thiele's SPEA2 [196], Knowles and Corne's Pareto archived evolutionary strategy (PAES) [197], Osyczka and Kundu's distance-based Pareto genetic algorithm (DPGA) [198], thermodynamical genetic algorithm by Kita *et al.* [199], and multi-objective messy genetic algorithm by Veldhuizen [200]. Another popular elitist MOEA is the NSGA-II of Deb *et al.* [201], whose domination mechanism, so-called the *crowding distance*, is the most adopted technique in other multi-objective algorithms.

Zhou *et al.* [202] provides an excellent survey of the state-of-the-art on MOEAs with 310 lists of references, whereas an online repository of more than 5600 published papers on MOEAs can be found on the website maintained by Coello Coello at http://delta.cs.cinvestav.mx/~ccoello/EMOO/.

The advancement of the multi-objective optimisation algorithms in swarm intelligence such as PSO is also significant. Amongst those algorithms that extend PSO to solve multi-objective optimisation problems are aggregating function PSO [203], Fieldsend and Singh's PSO [204], nondominated sorting PSO (NSPSO) [205], and MOPSO [206]. Another popular multi-objective variant of PSO is Raquel and Naval's MOPSO with the NSGA-II's crowding distance (MOPSO-CD) [207], which was applied by Mohamed *et al.* [7] for history matching problem. In the rest of the thesis, MOPSO refers to the Raquel and Naval's MOPSO-CD. Reyes-Sierra and Coello Coello [208] provides an excellent survey of the state-of-the-art on MOPSO.

Amongst those algorithms mentioned above, NSGA-II and MOPSO are the two well-known multi-objective algorithms and have been applied successfully for history matching of a real field [9], [182] and will be described in the next sections.

2.5.7 Nondominated Sorting Genetic Algorithm II

In the following, we outline the NSGA-II algorithm as in Algorithm 2.3 and illustrate its procedure in Figure 2.13. Initially, a randomly generated population P_0 is sorted into different non-domination levels. A fitness equal to the domination level (1 is the best level) is assigned to each solution. Crowded tournament selection, recombination and mutation are performed to create an offspring population Q_0 of size N, and then the process is repeated until the termination criterion is met.

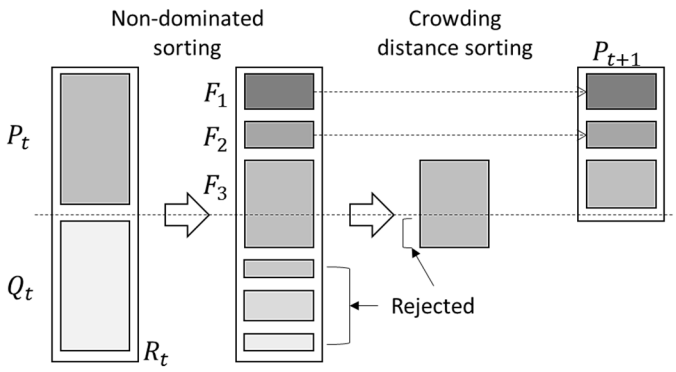

Figure 2.13—Schematic of the NSGA-II procedure (after [11]).

Algorithm 2.3—The Nondominated Sorting Genetic Algorithm II [11].	
Step 1	Combine parent and offspring populations and create $R_t = P_t \cup Q_t$. Perform a nondominated sorting to R_t and identify different fronts: F_i, $i = 1,2,$ ...,etc;
Step 2	Set new population $P_{t+1} = \emptyset$. Set a counter $i = 1$. Until $\lvert P_{t+1}\rvert + \lvert F_i\rvert < N$, perform $P_{t+1} = P_{t+1} \cup F_i$ and $i = i + 1$;
Step 3	Perform the crowding distance sorting procedure (described below) and include the most widely spread ($N - \lvert P_{t+1}\rvert$) solutions by using the crowding distance values in the sorted F_i to P_{t+1};
Step 4	Create offspring population Q_{t+1} from P_{t+1} by using the crowded tournament selection, simulated binary crossover and polynomial mutation operators;

2.5.7.1 Crowding Distance

The diversity of the solutions is also determined by the crowding distance mechanism. It is expected to obtain solutions with less crowded but spread out in the objective space than more crowded but clustered in particular area in the objective space.

The crowding distance value of a solution i provides an estimate of the density of solutions surrounding that solution in the population. It is computed by taking the average distance of two solutions on either side of solution i along each of the objectives. Figure 2.14 shows the crowding distance of the i-th solution in its front which is the average side-length of the cuboid (shown by a dashed box). Algorithm 2.4 is used to compute the crowding distance of each point in the set F.

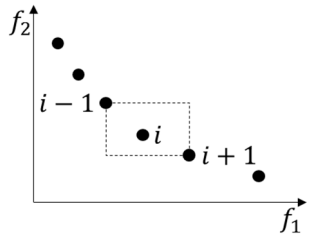

Figure 2.14—The crowding distance calculation (after [11]).

Algorithm 2.4—The Crowding Distance Sorting Procedure [11].

Step 1 Call the number of solutions in F as $l = |F|$. For each i in the set, first assign $d_i = 0$;

Step 2 For each objective function $m = 1,2, \dots M$, sort the set in worse order of f_m;

Step 3 For $m = 1,2, \dots, M$, assign a large distance to the boundary solution, i.e. $d_{I_1^m} = d_{I_l^m} = \infty$, and for all other solutions $j = 2$ to $(l-1)$, assign:

$$d_{I_j^m} = d_{I_j^m} + \frac{f_m^{(I_{j+1}^m)} - f_m^{(I_{j-1}^m)}}{f_m^{max} - f_m^{min}} \tag{2.13}$$

where I_j denotes the solution index of the j-th member in the sorted list, I_1 and I_l denote the lowest and highest objective function values for any objective, respectively.

2.5.7.2 Crowded Tournament Selection Operator

A solution i wins a tournament with another solution j if any of the following conditions are satisfied:

1. If solution i has a better non-domination rank, i.e. $r_i < r_j$;
2. If they have the same non-domination rank but solution i has a better crowding distance than solution j, i.e. $r_i = r_j$ and $d_i > d_j$.

The first condition makes sure that a better nondominated solution is always chosen and the second condition resolves the tie of condition one by selecting a solution with the less crowded area.

2.5.7.3 Simulated Binary Crossover Operator

Simulated binary crossover (SBX) operator works with two parent solutions and creates two offspring [144]. The procedure of producing the offspring $x_i^{(1,t+1)}$ and $x_i^{(2,t+1)}$ from the parent solutions $x_i^{(1,t)}$ and $x_i^{(2,t)}$ is described in Algorithm 2.5.

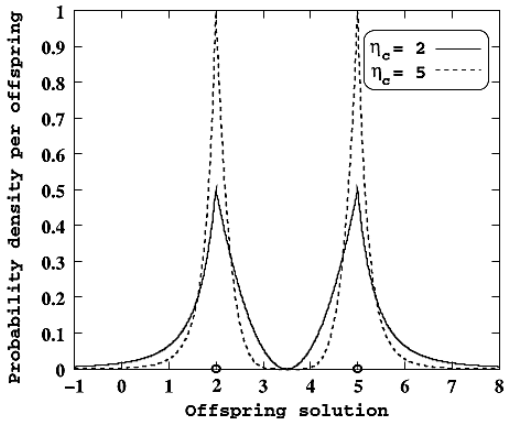

Figure 2.15—The probability density function for creating offspring under an SBX-η_c operator. Parents are marked with 'o', (taken from [11]).

Algorithm 2.5—Simulated Binary Crossover Operator Procedure [144].

Step 1 Simulate a shape of the probability distribution function according to Equation (2.14) (see Figure 2.15);

$$P(\beta_i) = \begin{cases} 0.5(\eta_c + 1)\beta_i^{\eta_c}, if\ \beta_i \leq 1; \\ 0.5(\eta_c + 1)\dfrac{1}{\beta_i^{\eta_{c+2}}}, otherwise. \end{cases} \tag{2.14}$$

where β_i is a spread factor, η_c is the distribution index which its value is any non-negative real number. A large value of η_c gives a higher probability for creating 'near-parent' solutions and a small value of η_c allows distant solutions of the offspring.

Step 2 Generate a random number $u_i \in [0,1]$;

Step 3 Calculate β_{qi} as in Equation (2.15), so that the area under the probability curve from 0 to β_{qi} is equal to the chosen random number u_i:

$$\beta_{qi} = \begin{cases} (2u_i)^{\frac{1}{\eta_c+1}}, if\ u_i \leq 0.5; \\ \left(\dfrac{1}{2(1-u_i)}\right)^{\frac{1}{\eta_c+1}}, otherwise. \end{cases} \tag{2.15}$$

Step 4 Compute the offspring by using Equations (2.16) and (2.17);

$$x_i^{(1,t+1)} = 0.5\left[(1+\beta_{qi})x_i^{(1,t)} + (1-\beta_{qi})x_i^{(2,t)}\right] \tag{2.16}$$

$$x_i^{(2,t+1)} = 0.5\left[(1-\beta_{qi})x_i^{(1,t)} + (1+\beta_{qi})x_i^{(2,t)}\right] \tag{2.17}$$

2.5.7.4 Polynomial Mutation Operator

Like in the SBX operator, the probability distribution can also be a polynomial function, as in Equation (2.18).

$$y_i^{(1,t+1)} = x_i^{(1,t+1)} + \left(x_i^{(U)} - x_i^{(L)}\right)\overline{\delta_i} \tag{2.18}$$

where y is the mutated parameter, $x_i^{(U)}$ and $x_i^{(L)}$ are upper and lower bound of the parameter, and $\overline{\delta_i}$ is computed from the polynomial probability distribution $P(\delta) = 0.5(\eta_m + 1)(1 - |\delta|)^{\eta_m}$, as in Equation (2.19).

$$\overline{\delta_i} = \begin{cases} (2r_i)^{\frac{1}{\eta_m+1}} - 1, if\ r_i < 0.5, \\ 1 - [2(1-r_i)]^{\frac{1}{\eta_m+1}}, if\ r_i \geq 0.5 \end{cases} \tag{2.19}$$

where r is the generated random number, and η_m is polynomial distribution index which its value is a non-negative real number. A large value of η_m gives a higher probability for creating 'near-parent' solutions and a small value of η_m allows distant solutions.

2.5.8 Multi-Objective Particle Swarm Optimisation

We describe one of the successful extension of PSO to multi-objective optimisation, called MOPSO, proposed by Raquel and Naval [207] which had been implemented and applied by Mohamed *et al.* [7] for history matching. The algorithm incorporates the crowding distance mechanism of NSGA-II for global leader selection and in the deletion method of the external archive of nondominated solutions. The diversity preservation is done by the crowding distance mechanism and mutation operator. The pseudo code of MOPSO is shown in Algorithm 2.6.

Leader Selection

Leader selection promotes both the convergence and the diversity of solutions in MOPSO as illustrated in Figure 2.12 (a) Section 2.5.5 for a general multi-objective algorithm. The leader is selected from an external archive which stores a number of nondominated solutions. The nondominated solutions are stored and sorted in decreased order based on the crowding distance computation. Then, the leader (global best, $gbest$) is selected randomly from a specified top portion (e.g. top 10%) of the sorted external archive.

Mutation

At the initial stage, a mutation operator acts on the entire swarm to facilitate the exploration of the algorithm and avoid the premature convergence as illustrated in Figure 2.12 (a) Section 2.5.5. Over time the mutation rate is decreased linearly to promote the convergence. This mechanism is adapted from the earlier version of MOPSO proposed by [206].

Random Replacement

Random replacement is used when the external archive is full by pruning the solutions with the more crowded area. For this, the crowding distance is used to select which solution to replace in the archive. This mechanism promotes the diversity of the solution as the solutions with most crowded areas most likely to be replaced by new solutions with the less crowded area.

Algorithm 2.6—General MOPSO algorithm pseudocode (taken from [3]).

```
Begin
    iter = 0
    Initialise the swarm
    Select leaders in an external archive
    Evaluate leader
    Repeat
        For each particle
            Select leader
            Update velocity
            Update position
            Mutation
            Evaluate misfit
            Update personal best pbest
        End for
        Update leaders in the external archive
        Random replacement when archive is full
        Evaluate leader
        Next iteration (iter++)
    Until stopping criterion is met
    Report results in the external archive
End
```

2.6 Uncertainty Quantification

The third stage in a reservoir simulation study is uncertainty quantification of the reservoir prediction from the ensemble of history-matched models, as shown in Figure 2.2 earlier. The non-uniqueness of the acceptable matched models from the history matching implies a range of uncertainty in the reservoir performance prediction that must be quantified as part of the decision-making in reservoir management. An

understanding of uncertainty and its consequences for decisions is a critical component of success in developing oil and gas fields.

Tarantola 2005 [6] postulates that the most general way to describe any state of information on a finite-dimensional parameter set Ψ (including both model parameters and data) is by defining a probability distribution (or, more generally a measure of distribution) over Ψ. Therefore, in essence, *uncertainty quantification* means describing the state of information we have by a probability distribution. Hence, in history matching case, the uncertainty of history-matched models is quantified with a probability of each model. Afterwards, the uncertainty in prediction can be described by a probability distribution based on the probability of multiple history-matched models.

2.6.1 Sources of Uncertainty

Uncertainty in a reservoir model simulation can come from various sources:

a) *Structure uncertainty*, as the model is an approximation of a complex physical system, there is uncertainty on what model structure should be used and how we specify our model to extrapolate or interpolate well.
b) *Parametric uncertainty* or *uncertainty in model parameters* that best explain the observed data. A large number of possible models might be able to explain a given dataset, in which case we might be uncertain on the model parameters to choose to estimate with.
c) *Condition uncertainty* which describes the uncertainty of the boundary conditions such as no flow boundary, initial conditions such as the equilibrium condition, and forcing conditions in the reservoir such as gravity, capillary and viscous forces.
d) *Solution uncertainty*, as the system equations can only be solved by some necessary level of approximation.
e) *Measurement uncertainty*, as the model is calibrated against system data all of which is measured with error.
f) *Multi-model uncertainty* due to there are many models related to the physical systems instead of one model.

g) *Methodological uncertainty*, which is related to the uncertainty on which methods or techniques to use better results within reservoir simulation studies, such as algorithms, common practices, or guidelines.

Uncertainty in reservoir prediction arises from a lack of knowledge due to a sparsity of data and errors in the models used to make predictions. Data sparsity is related to the limited number of measurement points made in the reservoir, i.e. through wells, compared to the scale of the field. We then infer the properties away from those well locations based on knowledge of how the reservoir was formed, on analogue outcrops where property variation can be measured, and on model calibration to observed data. This data sparsity leads to an incomplete understanding of the details of the oil and gas reservoirs.

The uncertainty contributed from the errors can be categorised as data measurements errors and simulation errors. Data measurement errors are attributed to: (1) the device or human errors when obtaining input data for simulation by direct measurements (e.g. core plug data from laboratory); (2) inherent errors in the data obtained by indirect measurements (e.g. well log data); and (3) errors in the measurement of dynamic data (e.g. production data). As stated by Christie et al 2005 [60], the main sources of simulation errors are: (1) input error which refers to the errors of the data used in the model (e.g. porosity and permeability) which are collected sparsely; (2) physics error which is induced by inadequate representation of the physical system (e.g. heterogeneity captured by the grid); and (3) solution errors which are due to the numerical solution errors such as truncation errors, numerical dispersion, assumptions and simplification of mathematical equations governing the fluid flow.

The error associated with the observations, i.e. production data, is typically incorporated in the objective function by a variance (see for example σ^2 term in the least-squares formulation given in Equation (2.7) Section 2.3.2.2). On the other hand, the simulation errors are usually not considered as they are difficult to estimate. Nonetheless, there have been efforts in the literature for modelling the simulation errors (see e.g. [60,209]).

2.6.2 Probabilistic Uncertainty Estimation

Baddeley *et al.* [210] distinguish probabilistic uncertainty estimation into *statistical* and *inductive* probabilities.

A statistical probability is "a limiting value of the relative frequency of an event over many trials", and as such, this branch of statistics is often termed *frequentist*. The uncertainty estimates are computed probabilistically based on its frequency of occurrence which can be tested by experiments and measurements. However, the frequentis approach is often a problem for reservoir simulation as it involves a high-cost subsurface data acquisitions and measurements.

Inductive probability, of which *Bayesian* statistic is the main method, describes a probability of a future event given on the present amount of data. This method allows us to quantify the uncertainty of a parameter given a limited knowledge of that parameter, as such Bayesian method provides a way for quantifying the uncertainty in the reservoir prediction when we have little knowledge of some reservoir parameters. Hence, this thesis uses the Bayesian method in the uncertainty quantification of reservoir performance prediction which is described below.

2.6.3 Bayesian Framework

Bayes Theorem is named after Rev. Thomas Bayes (1701–1761) and is stated mathematically in a simple form as follows:

$$P(A|B) = \frac{P(B|A)P(A)}{P(B)} \tag{2.20}$$

In essence, Bayes Theorem states that given an initial prior probability of event A, $P(A)$, we can compute its *posterior* probability, $P(A|B)$, based on the occurrence of event B based on the conditional probability $P(B|A)$ termed as the *likelihood* over evidence $P(B)$. In the history matching framework, Bayes Theorem can be used to answer a question of "how likely one set of model parameterisation A is given the historical observed data B?".

A further application of Bayes Theorem is *Bayesian inference* where we consistently update our knowledge on one or more unknown quantities of a physical system based on the observed data from the system. This technique can be applied on updating the initial reservoir model parameters probabilities based on observation data such as production rates. Started with a set of initial knowledge in the form of prior, we then sample a number of possible reservoir descriptions from the prior and examine how well the predictions made using these reservoir descriptions fit the data. The models that fit the data well are assigned higher probabilities, with the numerical values of the probabilities given by Bayes Theorem, as in Equation (2.21).

$$p(m|O) = \frac{p(O|m)p(m)}{\int p(O|m)p(m)dm} \tag{2.21}$$

where the prior probabilities $p(m)$ contains initial probabilities for the model parameters, $p(O|m)$ is the likelihood function that measures the degree of the observed and modelled data differ, and $p(m|O)$ is the new posterior probability of the model parameters based on observations O. The integral at the denominator of (2.21) is the evidence and acts as a normalisation constant, as such Bayes Theorem can be simply described as in Equation (2.22).

$$posterior \propto likelihood \times prior \tag{2.22}$$

2.6.3.1 Prior Information

Priors represent our knowledge of the unknown model parameters before seeing the observed data. The information contained in the priors can be based on previous knowledge of the problem or system (i.e. expert knowledge) or quantitative data from reliable sources (i.e. scientific publications, reports). Based on how much information we have, Gelman in [211] categorised three groups of prior distributions:

1. Non-informative prior distributions which are usually set as uniform distributions on one or many uncertainty parameters. This type of distributions assigns the same probability to occur at all values of the parameters ranges.

2. Highly informative prior distributions, which are used when a fair amount of information about the possible values of model parameters are available. Typically, this type of priors is represented by normal distributions defined by the mean and the standard deviation.
3. Moderately informative hierarchical prior distributions, which are used when limited information about the model parameters values are available.

Prior distributions that incorporate the available information about the parameters probabilities will improve the posterior probability estimates. In this sense, by having more information on the prior, the posterior probability estimates will be more constrained towards realistic values based on the prior knowledge.

Some studies on the use of informative priors exist in the literature. Arnold [14] introduced a technique of modelling geological prior information based on published equations that relate channel width and thickness. The study highlighted the impact of preserving realism of geological models in history matching. Rojas [61] constructed complex relationships on the geological feature by using machine learning technique (i.e. support vector machine) and built sedimentological intelligent priors. The inclusion of intelligent priors in this study resulted in more realistic history-matched models and the reduction of computational time of history matching.

However, throughout the thesis, the non-informative prior distributions are used in the whole of the history matching and uncertainty quantification studies for the sake of the thesis's focus.

2.6.3.2 Likelihood Definition

The likelihood of a reservoir model can be defined by comparing the simulation results with the observed data (i.e. to use the misfit value in a similar way to the objective function defined by Equation (2.7) in Section 2.3.2.2). For instance, if we are matching on oil rate, the likelihood $p(O|m)$ is the probability that the measured observation q_{obs} is equal to the simulated value q_{sim} given the reservoir model m. Assuming that the measurement errors at any time are Gaussian, independent, identically distributed (all

have the same variance) with zero mean error, and there are no simulation errors, the likelihood at timestep t can be defined as:

$$p(O_t|m) = \frac{1}{\sigma\sqrt{2\pi}} exp\left\{-\frac{1}{2}\frac{(q_{obs} - q_{sim})_t^2}{\sigma^2}\right\} \tag{2.23}$$

where σ is the standard deviation of the measurement error, q_{obs} and q_{sim} are the observed and simulated data, respectively.

As the measurement errors are assumed to be independent between timesteps, the joint probability density is calculated by the product of probabilities of each measurement for N data points, as given by Equation (2.24).

$$p(O|m) = \left(\frac{1}{\sigma\sqrt{2\pi}}\right)^N \prod_{t=1}^{N} exp\left\{-\frac{1}{2}\frac{(q_{obs} - q_{sim})_t^2}{\sigma^2}\right\} \tag{2.24}$$

As $\left(\frac{1}{\sigma\sqrt{2\pi}}\right)^N$ is a constant:

$$p(O|m) \propto \prod_{t=1}^{N} exp\left\{-\frac{1}{2}\frac{(q_{obs} - q_{sim})_t^2}{\sigma^2}\right\} \tag{2.25}$$

Hence, if we use misfit definition M in Equation (2.7), we can define the likelihood function as in Equation (2.26) so that by minimising the misfit M we maximise the likelihood [6].

$$p(O|m) \propto e^{-M} \tag{2.26}$$

2.6.3.3 Posterior Probability Distribution

Determining PPD function is probably the most important part of the inverse problem [6]. In general, an inverse problem can be stated as follows: given prior information on some model parameters, inexact measurements of some observable parameters, and an uncertain relation between the observed data and the model parameters, how should we modify the prior probability density function (PDF) to include the information provided

by the observed data? In this sense, the PPD refers to the modified PDF. Hence, the solution to the inverse problem is represented by the construction of the PPD estimate that afterwards the realisations of the model are constructed by sampling the PPD.

Many history-matched models, typically referred to as the *ensemble*, are required to estimate the PPD. This requirement is due to that a single history-matched models is usually not a good representative of the PPD. Then, the calculation of probability estimates on the reservoir prediction can be performed from the PPD estimation of each matched model.

Analogue to the frequentist's confidence interval, the probability estimates in the predictions is usually described by *credible interval* for Bayesian. First, the cumulative distribution function is constructed from the PPD for a particular production data. Then, the credible interval can be reported in different ways. For instance, 90% *maximum credible interval* (x, y) represents the largest interval whose probabilistic uncertainty estimation for that particular production data encapsulating the true is 0.9. We can define the other way by taking $x = 0$ and reporting y that corresponds to 0.9 quantile of the cumulative distribution function. In this case, the truth value is below the reported y value with probability of 0.9. In this thesis, the latter approach is used and 0.1, 0.5, 0.9 quantiles are reported as *P90*, P50, P10, respectively, as shown in Figure 2.16.

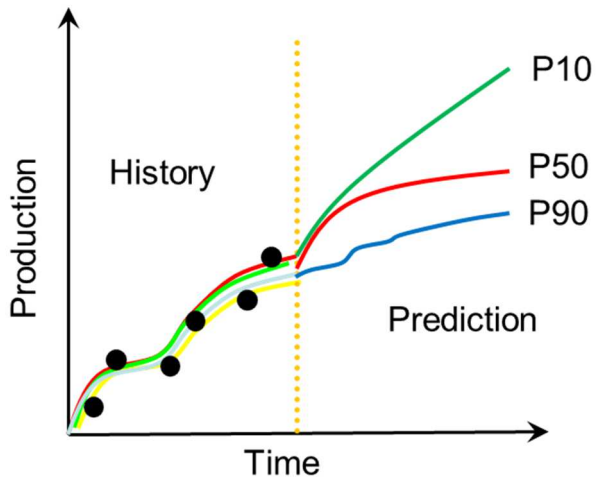

Figure 2.16—History matching and uncertainty quantification in the prediction period. Black dots show the observed data in the historical period; coloured lines show plausible fitting models. The history-matched models are used for making predictions, and the results are showed in typical *P10*, *P50*, and *P90* credible intervals.

Techniques for Determining Posterior Probability Distribution

There are many techniques for estimating a PPD and consequently quantifying the uncertainty for an ensemble of models. These techniques fall into two categories, *exact methods* and *approximate methods* [6].

In the exact method, a way of estimating PPD analytically was demonstrated in [6] for a known function. However, in real-world inverse problems such as history matching, the analytical method encounter difficulty due to the complex, nonlinear, high-dimensionality and ill-posedness characteristics of the history matching. Thus, it can be difficult to characterise the PPD analytically. Therefore, a numerical integration method to estimate the PPD is needed. A particularly common technique in this criterion is Monte Carlo sampling in which the parameter space sampling is done by Monte Carlo simulation runs, which are computationally expensive.

Another widely used techniques for uncertainty quantification are approximate methods which often provide better solutions than the exact method considering the quality of the approximation to the correct PPD. Included in these methods are experimental design and response surface method (see e.g. [212,213]). These statistical approaches firstly identify uncertain parameters that most affect the response variable in a limited number of simulations and then fit a surface, usually a linear or quadratic model, to the response variable. Afterwards, this surface is used as a proxy for the simulations runs when it is used in Monte Carlo sampling. The main issue with these methods is that the small number of samples will provide only an approximation of the true model response. Another issue is the use of proxy model instead of forward simulations may introduce significant modelling errors. Other limitations are the number of parameters that the method can handle and the difficulty to handle highly nonlinear surfaces. Nonetheless, such methods are useful for appraisal stage uncertainty analysis, where data is limited and no production data is available.

In the other literature, Erbas [13] distinguished three different types of method to estimate the PPD that are compared in [12] as below. Some terminologies are required. *Maximum likelihood* (ML) solution represents the best history-matched model in the ensemble. It is can also be called as *maximum a posteriori* (MAP) solution if the prior

term is incorporated. If the prior is uniform and wide enough to overlap the likelihood, ML and MAP solutions are the same.

1. Methods that characterise the PPD locally around the ML or MAP model.
   In this method, the PPD is determined by characterising the distribution around the ML or MAP model, and then used this information into the prediction. An extended version of this approach is by using more than one equally good solution, such as in the case of multi-modal objective function. In this case, the local characterisation is performed on the found multiple ML or MAP solutions. An example of this extension is linearisation about the MAP (LMAP) [5].

2. Methods that use only a subset of the ensemble generated.
   Randomised Maximum Likelihood (RML) and Pilot Point (PP) methods fall into this category. RML works by randomly sample initial models from the prior reservoir model and randomly sample the observed data. Then, both samples (model and data samples) are history-matched individually using an optimisation technique. The objective function includes both the misfit between the simulated response and data sample, and the discrepancy of the reservoir model from the initially sampled model. The approximation to RML is called the PP method, where the model parameters are only varied at particular locations (pilot points) in the parameter space.

3. Methods that sample from the complete PPD.
   Rejection Sampling (RS) and Markov chain Monte Carlo (MCMC) methods fall into this category. RS produces independent samples from an initial model distribution, and they are either accepted or rejected based on the acceptance function. In the MCMC method, a chain of randomly selected samples is produced by taking a random step along each parameter axis from the present location to a new model. Then the model is accepted or rejected based on the acceptance criteria. The most common method for this mechanism in MCMC is the *Metropolis-Hastings* sampler [214, Ch. 6].

   In both RS and MCMC, the acceptance criteria are defined in proportion to the likelihood of the models. Hence, it is expected that the PPD distribution can be represented after a long chain. However, the main problem of these methods is that

they require a large number of computationally expensive samples to be produced to determine the PPD accurately.

Liu *et al.* [12] considered that RS and MCMC methods as the correct sampling methods for PPD construction, whereas the others (i.e. LMAP, RML and PP) are only approximately correct. They evaluated all of these methods on a 1D simple reservoir case and found that LMAP failed to approximate match to the data, PP method overestimated the uncertainty, and the RML method provided an acceptable uncertainty estimation which can be an alternative to the MCMC.

NA-Bayes (NAB)

In this thesis, a methodology based on MCMC called NA-Bayes (NAB) [215] is used to estimate the PPD. The main difference between MCMC and NAB is that NAB resamples previously generated ensemble of models from a search algorithm (e.g. NA, GA or PSO), whereas MCMC require that after each new proposed state of the Markov Chain, a new forward simulation is carried out and the misfit calculated. NAB also infers the information from the complete ensemble, not only a subset of it and it requires no further solving the forward problem, but from the new 'resampled' ensemble.

NAB constructs Voronoi cells to represent the model parameter space and to interpolate the PPD of unknown points in the high-dimensional parameter space. The Voronoi interpolation is done by assigning a constant misfit value to the sample point in each cell. By means of this interpolation, NAB does not require any forward simulation during the posterior sampling. Then, NAB uses a *Gibbs sampler*, a special case of Metropolis-Hastings sampler, to resample the ensemble of models. In summary, two points can be highlighted on the use of NAB for posterior inference as follows:

1. All the models in the ensemble are used to infer the information and to evaluate the PPD for the credible interval in prediction.
2. There is no further forward reservoir simulation for all the models generated by the sampling algorithm, but only for the ones resampled by NAB. This helps to save computational time.

Figure 2.17 illustrates the working mechanism of Gibbs sampler in NAB resampling for a two-dimensional problem that is summarised in Algorithm 2.6.

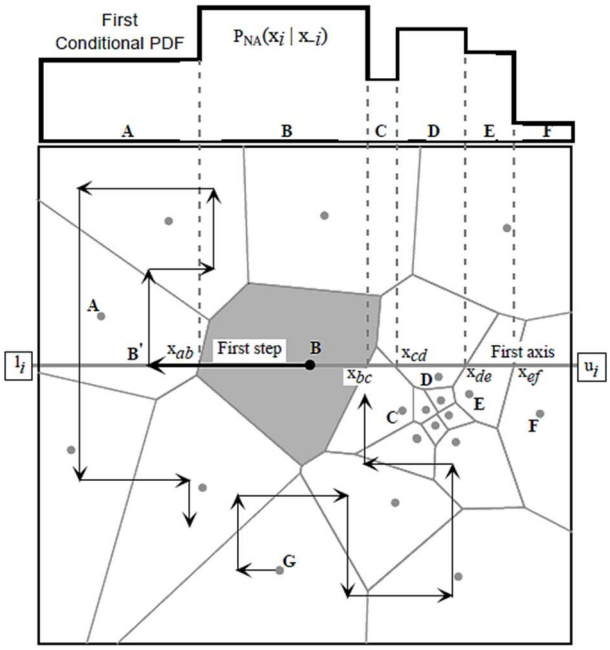

Figure 2.17—NAB resampling process showing two random walks of Gibbs sampler (taken from [215]).

The PPD for each model is determined by the sampling density for that particular model. The sampling density is affected by the size of the Voronoi cell for that particular model and the likelihood value of the sampled model. In [13, Fig. 2.23], Erbas demonstrated that the correlation between PPD of the resampled models with the likelihood L is lower than the correlation between PPD of the resampled models with likelihood "$L \times cell\ size$". Hence, in the PPD construction from NAB the sampling density is directly proportional to "$L \times cell\ size$".

The limitation of NAB is the assumption that all the models in one Voronoi cell have the same misfit value, and consequently the same likelihood. This assumption may lead to missing out some good matched models within a cell that are represented by a poorly matched model if the cell has not been refined. This problem could happen when the misfit surface has several steep minima, or in the higher dimensional problem.

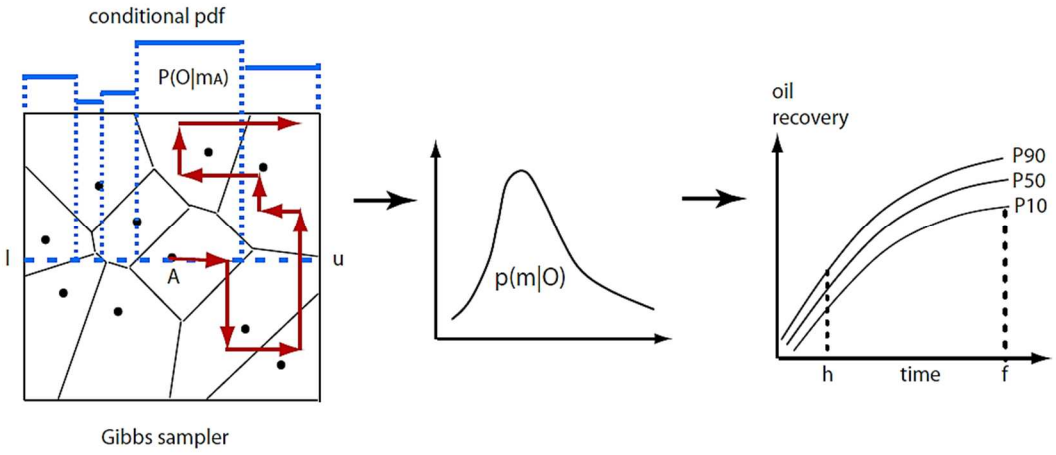

Figure 2.18—NAB workflow for uncertainty prediction (h=history; f=forecast; $p(m|O)$=posterior distribution) (taken from [13]).

Figure 2.18 illustrates how the results of NAB resampling are used to quantify the uncertainties in production forecasts. The number of resampled models is less than the input ensembles. The visit frequencies of these resampled models are counted and the posterior distribution, $p(m|O)$ is constructed. Then, forward simulations are performed on these resampled models for production forecasts. Note that the posterior inference is constructed from the complete ensemble, however we only need to run forward simulations of the resampled models for forecasting. The Bayesian credible intervals (*P10*, *P50* and *P90* values) are then computed individually at each timestep in prediction period and connected to construct the *P10*, *P50* and *P90* lines.

Several studies highlight the use of NAB as a method to estimate the PPD. Arnold [14, Fig. 3.9] provides an excellent summary and discussion of different methods for estimating PPD. In that, the NAB was chosen as it provides a robust method of producing probabilistic results with a greater accuracy (as it uses the entire ensemble) than LMAP, RML, and PP without the computational burden of using MCMC or RS. In other studies, NAB has been applied successfully on history matching and uncertainty quantification on reservoir simulation studies (see e.g. [84,87,88,92,108,216] for details).

Algorithm 2.6—Gibbs sampler in NAB resampling [215].

Step 1 A random walk starts at point B that can be a model from the input ensemble. A useful selection can be from the position of the better data fitting models;

Step 2 From this point, a series of steps or random walks is taken along each parameter axis in turn (i.e. two steps for the example in Figure 2.17);

Step 3 An interval (l_i to u_i in Figure 2.17) is defined for each axis covering the entire parameter space, in which a conditional probability is constructed by computing the intersection points of the interval with the ensemble's Voronoi cells. This results a PDF like $P_{NA}(x_i|x_{-i})$ shown in Figure 2.17. The random walks produce samples with a distribution that tends towards the approximate posterior distribution by taking the likelihood of the models (defined in (2.26)) as the probabilities that constructs the conditional PDF above;

Step 4 A new random step, x_i^p (point B'), is proposed by a uniform random deviate between the end points of the axis (i.e. in the interval l_i to u_i shown in Figure 2.17). The probability of proposing the B' in cell A is defined in Equation (2.27);

$$P(B' \in A) = \frac{cell\ size_A}{|u_i - l_i|} \tag{2.27}$$

where u_i and l_i are the upper and lower ranges of parameter respectively. The $cell\ size_A$ is the length of the length of the $l_i - u_i$ axis section passing through the *cell* A.

Step 5 This proposed step is accepted if a second random deviate, r, generated on the unit interval (0,1), satisfies Equation (2.28);

$$r \leq \frac{P_{NA}(x_i^p|x_{-i})}{P_{NA}(x_i^{max}|x_{-i})} \tag{2.28}$$

where $P_{NA}(x_i^{max}|x_{-i})$ is the maximum value of the conditional along the axis.

Step 6 If the proposed step is rejected, then the whole procedure is repeated until an accepted step is produced;

Step 7 The Gibbs sampler continues by generating the next step and cycles through each parameter axis in turn. An iteration is completed when all dimensions have been cycled through once;

Step 8 The constructed conditional PDF is believed to be a good approximation to the true posterior distribution after many independent walks starting from different locations [3], [4], [13], [108], [216].

The computational overhead for NAB depends on the setup of the algorithm. The user has to define the number of chains. The number of chains determines the number of independent random walks that starting from a different point in model parameter space. This will significantly reduce computation time as the calculations are performed simultaneously and improve the sampling of parameter space because each walk starts in a different place [13].

The user also has to define the *burn-in* period for NAB. The burn-in period is used to discard a number of steps at the beginning of each independent random walks on each chain. The motivation behind the use of burn-in is to improve the robustness of the results. The most commonly used method for determining burn-in period is by visual inspection of plots from the output as illustrated in Figure 2.19.

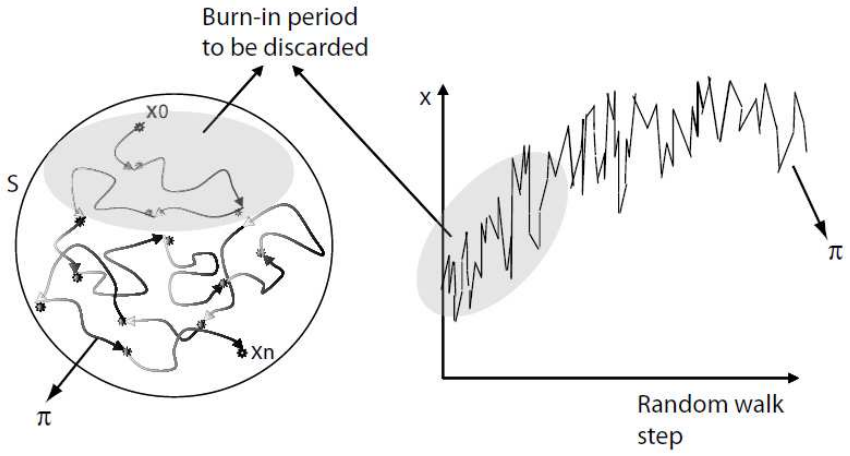

Figure 2.19—Schematic representation of a random walk and burn-in period. A number of iterations at the beginning of a random walk for each chain is discarded to ensure that the resulting target distribution π is independent of the starting point X_0. (taken from [13]).

The chain length determines the number of steps to be performed on each chain at a particular simulation case. This length is related to the convergence of the chain. Convergence is achieved when independent chains converge to the same distribution [13].

2.6.4 Bayesian Uncertainty Quantification Framework Used in the Thesis

In this thesis, we used the Bayesian framework shown in Figure 2.20 for uncertainty quantification of reservoir performance prediction [13]. The framework can be divided into two parts: (1) Sampling the parameter space, and (2) Posterior inference. In the first part, we used the stochastic optimisation algorithms, such as PSO and MOPSO to generate an ensemble of history-matched models. In the second part, we used NAB algorithm to estimate the PPD for uncertainty prediction.

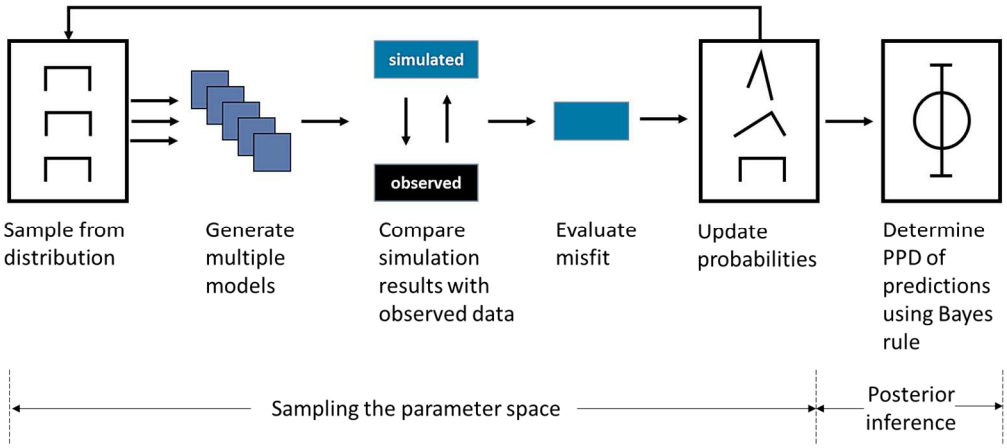

Figure 2.20—Bayesian uncertainty quantification framework used in the thesis (after [13]).

In the thesis, we also developed a way of approximating the PPD in multi-objective case. In Figure 2.20, the NAB is used to estimate the PPD of each history-matched model in the ensemble and resulted in inference models. The constructed PPD for each model is based on the total misfit values. In the multi-objective case, these misfit values are computed over all misfit components. Hence, it is necessary to approximate the PPD in the multi-objective case, i.e. when the parameter sampling is by the multi-objective approach. Therefore, we extended the PPD estimation by NAB to approximate the PPD for several selected models, i.e. Pareto models from multi-objective through clustering. These models are then can be used for optimisation of reservoir development under uncertainty. This proposed method is presented in Chapter 6 of the thesis.

2.7 Discussion

Even today, a common practice of history matching powered by optimisation algorithms is built on the hypothesis that a unique set of parameter values exists that ensures a global optimum fitting of the simulated model response to the observed data. In this sense, it is expected that the "best model" can be extracted from history matching process. Tarantola in his commentary [48] argued that the idea of using observation to infer one "best model" of the system is wrong. He stated that the observations could not produce models. Instead, they can only falsify models. He also suggested that after comparison between simulated and observed data, we use some criteria to decide if the match is acceptable or unacceptable, given the uncertainties in the observations. Based on this falsification and criteria we can either drop or keep the models as the solution. Hence, the notion of the "best model" is rather a relative terminology until a better model is found and does not refer to a model with its parameter set is the global optimum.

In general, terming "best model" for a reservoir is rather obscure, because there is no "best model" to be perfectly equivalent to the truth. In hydrological model calibration, similar area to petroleum reservoir history matching, the notion of the "best model" as referred to a unique set of model parameters as a global optimum have also been intensively disputed. This is in favour of the so-called *equifinality* concept [217,218], (similar to *equiprobable* term to some extent), where multiple models and parameter combination sets are considered as acceptable to represent the real-world system in some ways. Moreover, the fact that it is impossible to assign an appropriate formal error structure for the model misfits (i.e. discrepancy between model response and observed data) and detect a particular measure that is better suited for fitting model response to observations. This fact is based on the demonstrations of more than three decades of research in hydrology ([151,219,220] as referenced to [149]). This is due to the non-systematic interaction of uncertainties and errors in all modelling aspects that preclude defining a statistically proper fitting function and, consequently, making a statistically correct choice for the model parameters [221].

Accordingly, during the past years, much attention has been given to employing multi-objective optimisation search techniques in history matching. Multi-objective optimisation aims to find a diverse set of multiple optimum solutions across all of the objectives because all objectives are important. As opposed to multi-objective optimisation, in a single-objective optimisation there is one goal – the search for an optimum solution. Even when there exist a number of optimal solutions, most single-objective optimisation algorithms aim at finding one optimum solution. In that, as long as a new solution has a better objective function value than old solution, the new solution can be accepted. In this sense, the single-objective history matching adopts the idea of finding a global optimum of the model parameter set.

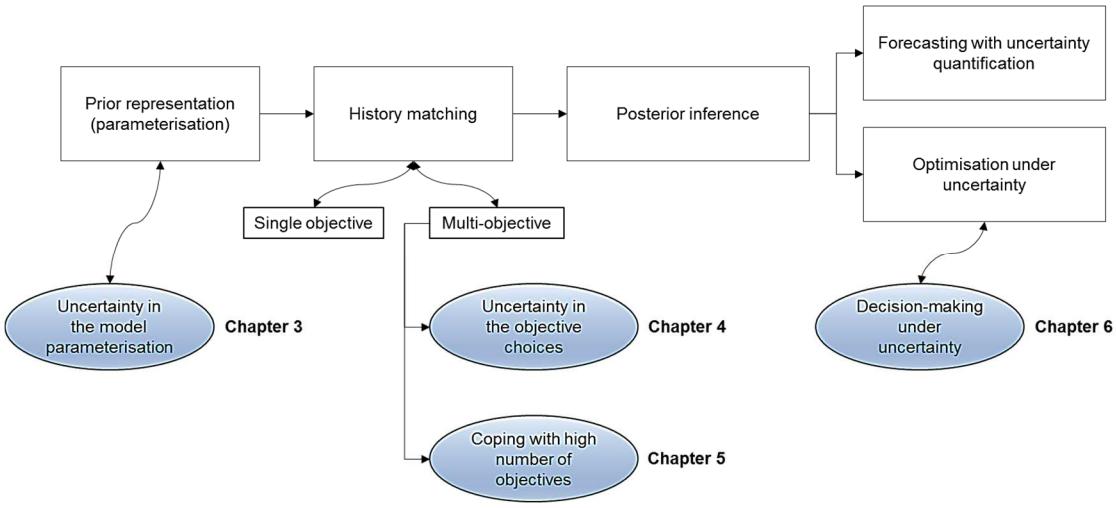

Figure 2.21—Thesis contribution into the overall uncertainty quantification research with the highlights on the identified challenges addressed in the respective chapters in the thesis.

In the thesis, we explore further multi-objective optimisation paradigm both in history matching, well placement optimisation and uncertainty quantification problems. We have identified several challenges and opportunities of the multi-objective optimisation in these problems as illustrated in Figure 2.21. We aim to address the challenges listed below and briefly describe those identified challenges and opportunities related to the multi-objective optimisation, and direct the reader to the corresponding chapters.

- How to properly account for the uncertainty on the model parameterisation in history matching?

- How to manage the uncertainty arising from the different choice of misfit definition (objective grouping choices) in multi-objective history matching?
- How to cope with the high number of objectives in multi-objective history matching?
- How to account the geological uncertainty in the field development optimisation in regards to decision-making on infill well placement?

2.7.1 Chapter 3: Dealing With Uncertainty in the Model Parameterisation

One of the obvious benefits of assisted history matching over the traditional manual history matching is that its ability to handle a large number of uncertain model parameters in the model parameterisation at the same time. In the manual history matching, it is difficult to calibrate a large number of model parameters at the same time due to the behaviour of the reservoir models and the extremely complex relations between parameters. On the other hand, the complexity of this problem is addressed by using stochastic search algorithms in assisted history matching.

However, in practice, this obvious advantage is not straightforward as there are two areas of concern related to the uncertainty in the model parameterisation. First, a number of possible geological models that are all plausible to some degree may represent the reality. The second is that the increasing number of unknown parameters may give a better fit to data, but may lead to a loss in predictive power if the model is over-fitted. Thus, it can be precarious when deciding which geological model, how many and which model parameters to calibrate at the same time, i.e. to find the optimal model parameterisation.

The objective of Chapter 3 is to investigate the impact of model parameterisation uncertainty on history-matching performance and prediction uncertainty quantification. The study examines and compares two approaches in history matching, single and multi-objective optimisation methods, on the performance of history matching and forecasting uncertainty quantification given two different set of model parameterisations. Both applications are illustrated with synthetic reservoir model based on a real field.

2.7.2 Chapter 4: Dealing With Uncertainty in the Objective Choices of Multi-Objective History Matching

In practice, any parameter estimation technique through data fitting is inherently multi-objective. Let $\boldsymbol{e}(\boldsymbol{\theta}) = \{e_1(\boldsymbol{\theta}), e_2(\boldsymbol{\theta}), \dots, e_M(\boldsymbol{\theta})\}$ describe the model misfits, i.e. the discrepancy between observed data from the simulated ones, where $\boldsymbol{\theta}$ is the vector of model parameters. We can define calibration as the simultaneous minimisation of the absolute discrepancies $|e_i(\boldsymbol{\theta})|$ with respect to $\boldsymbol{\theta}$ as:

$$minimise\ |\boldsymbol{e}(\boldsymbol{\theta})| = \{|e_1(\boldsymbol{\theta})|, |e_2(\boldsymbol{\theta})|, \dots, |e_M(\boldsymbol{\theta})|\}, \boldsymbol{\theta} \in \boldsymbol{\Theta} \tag{2.29}$$

where $\boldsymbol{\Theta}$ is the feasible parameter space, and M is the number of objectives. As the represented reservoir models are imperfect of complex natural systems, the vector optimisation problem above is ill-posed that inhibits the possibility of an ideal solution, namely a set of parameters that simultaneously minimised all misfits. However, we can locate a subset of the feasible parameter space, $\boldsymbol{\Theta}^* \in \boldsymbol{\Theta}$ that contains the nondominated solutions based on the Pareto optimality notion, that in turn provides acceptable tradeoffs between misfit components.

The formulation in (2.29) entails impractically a large number of separate minimisations of all model misfits. For instance, given a single observed production data to fit, e.g. oil production rate, the minimisation problem dimension is equal to the number of the timestep. Consequently, it is impossible to interpret the misfit tradeoffs as the Pareto front becomes too extended due to *the curse of dimensionality*, if not heading to cover the entire M-dimensional objective space [11].

Hence, the minimisation problem formulation in Equation (2.29) is reduced to as in Equation (2.30), that assumes a limited number of fitting criteria to account for representative aspects of the model performance about the behaviour of the reservoir system.

$$\text{minimise } \boldsymbol{g}[\boldsymbol{e}(\boldsymbol{\theta})] = \{g_1[\boldsymbol{e}(\boldsymbol{\theta})], g_2[\boldsymbol{e}(\boldsymbol{\theta})], \dots, g_m[\boldsymbol{e}(\boldsymbol{\theta})]\}, \boldsymbol{\theta} \in \boldsymbol{\Theta} \tag{2.30}$$

where $g_i[\boldsymbol{e}(\boldsymbol{\theta})]$ are scalar measures that ideally should be approximately uncorrelated and preserve the information contained in the observations, and m is the reduced dimension $m \ll M$. This problem can be handled by classical aggregation technique into a single-objective or a multi-objective, where the number of objectives is reduced to two or three. Even though single the objective is the most convenient way to use in practice, the multi-objective is more integrated as it allows for examining possible conflicts between the components of objective vectors. However, as the number of components increases, the number of possibilities to reduce the objective explodes due to combinatorics between components.

The aim of Chapter 4 is to develop a technique to group the objective components and select optimally the grouping that results in a better performance of multi-objective history matching. A novel technique based on the conflict information between objective components is proposed to group objective components into two objectives. Application of the proposed technique is demonstrated on both multi-objective history matching of a synthetic reservoir model and a real field.

2.7.3 Chapter 5: Dealing With High Number of Objectives

As the number of objective components increases (i.e. problems with more than three objectives), the performances of widely used and established multi-objective optimisation algorithms such as MOPSO and NSGA-II deteriorate (see e.g. Fig. 1 in [16] and Fig. 1 in [15]). In this problem, a Pareto-based multi-objective optimisation algorithm is no longer effective as the algorithm lose its selection pressure due to most or all of the solutions become nondominated.

In Chapter 5, we apply a recently proposed many-objective optimisation algorithm namely reference vector guided evolutionary algorithm (RVEA) to history matching problem. We compare the performance of many-objective history matching by using RVEA with both state-of-the-art multi-objective algorithms namely MOPSO and NSGA-II. The application and comparative study are illustrated in both a synthetic reservoir model and a real field case.

2.7.4 Chapter 6: Dealing With Decision-Making Under Uncertainty

One of the essential decisions from reservoir simulation studies is field development by optimally and robustly placing an infill well(s) to maximise recovery from the field and minimise operational expenditure. Robust optimal decisions are the ones that would hold in the presence of geological uncertainty, such as when a realisation of reservoir setting deviates from the base case. Would the decision optimised for the base case remain optimal for the updated reservoir condition? To answer this question, the optimisation across multiple realisations is required. Even though attempts on the optimisation across multiple realisations have been conducted in the literature, the computational cost involved in performing the task and resulting in the proper estimation of uncertainty remains a great challenge.

In Chapter 6, we introduce a new workflow for robust and reliable well placement optimisation. It accounts for geological uncertainty in choosing the optimal well location. The proposed workflow combines multi-objective history matching, Bayesian posterior inference based on PPD approximation of Pareto history-matched models and well placement optimisation across multiple geological models. The application and validation of the workflow are demonstrated on an industry-standard reservoir model case study.

Chapter 3

The Impact of Model Parameterisation in Reservoir History Matching and Forecasting

3.1 Introduction

A general workflow in the reservoir history matching and uncertainty quantification consists of three steps: (i) model parameterisation; (ii) history-matching process; and (iii) forecasting with uncertainty quantification, as shown in Figure 3.1. In the model parameterisation, we can assume that a limited number of model parameters will contain a combination of parameter values that accurately represents the reservoir. The choice of model parameterisation itself, either less or more detailed description, can be based on geological prior information, engineering knowledge, or a combination of both to represent uncertainty in the reservoir description. For instance, the model can be parameterised to different zones based on the geological interpretation of channel distribution in the reservoir, or it can be parameterised on the well drainage area and relative permeability curve based on the engineering knowledge.

In the history-matching process, powered by a stochastic optimisation algorithm, we can choose to use either single or multi-objective optimisation approach. Either way, the

ensemble of history-matched models is used for forecasting with uncertainty quantification. The uncertainty forecasting is done based on the posterior probability of each matched model that approximates the posterior probability distribution (PPD).

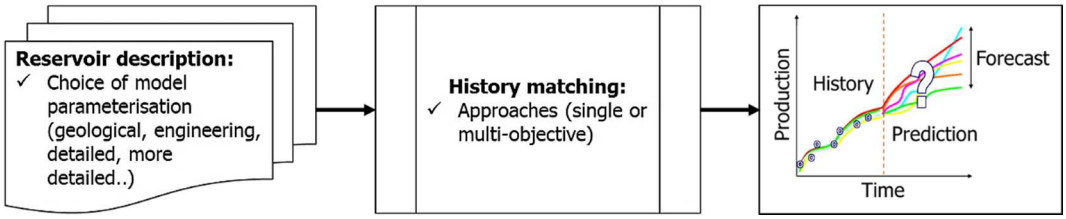

Figure 3.1—General workflow in the reservoir history matching and uncertainty quantification in forecasting.

Many techniques of model parameterisation have been developed in the literature to capture uncertainty in the geometry of the reservoir, the spatial distribution of rock properties, and reservoir fluid. In general, the aim of these techniques is to produce geologically realistic reservoir models that preserve spatial variability of reservoir properties inferred from the available static data for meaningful property estimates. These techniques include a gradual deformation method (GDM) [222], pilot point method (PPM) [223], gradual pilot point method (GPPM) [224], facies proportion calibration technique [225], coordinate-free approach called stochastic elliptic partial differential equations [226], and machine learning techniques including principal component analysis (PCA) [227], support vector machines (SVM) [228,229], and multiple kernel learning (MKL) [230,231]. A comprehensive description can be found in [232–234].

A common approach of model parameterisation in the petroleum engineering is the zonation or regionalisation technique [235] that is adopted from hydrology [236]. It has an extensive history of its application since the early history-matching studies of Jacquard and Jain in 1965 [237] and Jahns in 1966 [64]. The zonation technique involves dividing the reservoir model into a small number of zones or regions, in each of that the properties are treated as uniform. A modelling error is thus introduced through the assumption of uniform properties within each zone and the more or less arbitrary assignment of the zone boundaries. The modelling error increases as the number of zones are decreased [62].

Gavalas *et al.* [62] and Shah *et al.* [63] studied the use of zonation technique for history matching and concluded that zonation is preferable when the location of the zone boundaries is aligned with geological information. Both studies in [62] and [63] demonstrated that the zonation approach reaches the minimum modelling error at some intermediate level of parameterisation, i.e. at a particular number of zones, that can be regarded as the optimum level. Both studies [62,63] also suggested using prior geological information in the form of a prior probability density of the reservoir properties formulated in Bayesian estimation. The results of Bayesian estimation were found to be more accurate than those of zonation in a simulated case of a one-dimensional reservoir. The Bayesian formulation also resulted in improved convergence of the iterative minimisation algorithms.

The combination of zonation technique and prior geological information in the model parameterisation have been favoured by many researchers in the history-matching studies [7–9,92]. It offers a straightforward approach to reducing a large number of unknown parameters in the reservoir, and the problem becomes statistically better determined by using a prior statistical information on the unknown parameters. This technique has also managed to produce history-matched models with meaningful results. However, the choice of the model parameterisation based on this technique is also one of the sources of uncertainty in reservoir model simulation. More or less detailed zonation in the model parameterisation can be formed based on geological information and engineering knowledge that can vary subject to interpretation and data analysis.

When we come to model the parameterisation uncertainty in history matching, we encounter the situation where we can have different model parameterisations with different number of model parameters describing the reservoir system. These could be a simple “black box” models that are based on some simple physical theory or our best attempt at a “full” physics evaluation. Within each choice of model parameterisation, we could have a range of unknown parameters that we are trying to calibrate. Pickup *et al.* [238] examined two techniques to handle this problem. The first technique is based on Bayesian model comparison to choose the optimum number of parameters for a model. This technique includes the use of minimum description length (MDL) [239] and *Occam’s factor* [240]. The second technique applied the Bayesian model averaging that

combines two different model parameterisations with different level of parameterisation's complexity to improve the predictive capability compared to the use of individual models, which is also studied in [79].

In this chapter, contrast to the previous studies to handle the uncertainty on model parameterisation, we investigate the impact of different geological model parameterisations on history matching and uncertainty quantification in the forecasting. The parameterisations are based on zonation or regionalisation with prior geological information. We briefly discuss two different approaches in history-matching process powered by stochastic optimisation algorithm: single and multi-objective optimisation methods. The strategy for the comparison of the different approaches is then described. This is followed by a case study of PUNQ-S3 reservoir model to demonstrate the advantage of multi-objective approach over single-objective history matching in respect to forecasting with different model parameterisations. We describe two different model parameterisations and compare the results in history matching and uncertainty quantification in the forecasting between single and multi-objective optimisation approaches within the Bayesian framework. Finally, we discuss the verification of the possible improvement that the choice of history-matching approach can bring to the history matching and forecasting under model parameterisation uncertainty.

3.2 Methodology

3.2.1 Approaches in History Matching

History matching assisted by stochastic population-based sampling algorithms has been used widely to generate an ensemble of matched models. This assisted history-matching practice is significantly favoured by the vast improvement of computer capabilities, as well as by the development of advanced nonlinear optimisation algorithms.

In practice, history matching is multi-objective because there are multiple wells and match criteria in well and regions in the field. In many cases, these match criteria are conflicting, and no feasible solution optimises all of them simultaneously. For instance,

an improvement in oil rate match in one well causes a deterioration of the gas rate in another well.

3.2.1.1 Classical Approach Through Aggregating Scheme

History matching involving multiple and conflicting objectives has been traditionally handled by combining the objectives into a scalar function, usually referred to the weighted-sum approach, solving the equivalent single-objective to identify the best solution [82,88,90,92,181]. As an example, for a history matching with two objectives, the weighted-sum approach can be formulated as in Equation (3.1):

$$Obj_{Global} = (w_1 \times Obj_1) + (w_2 \times Obj_2) \tag{3.1}$$

where Obj_{Global} is the global objective function, w_1, w_2 are the weighting factors, Obj_1, Obj_2 are the two objective functions or misfit components.

This approach reduces the algorithm's sensitivity to variations in match quality within different parts of the reservoir and across various production data. Moreover, it is difficult to obtain the right set of weighting factor due to the behaviour of observed production data from different wells and regions can be strongly uncorrelated. Additionally, the weight also depends on the scaling of each objective that may have a different order of magnitude. The use of this single-objective approach without appropriate scaling results in extremely rough response surface of objective functions.

3.2.1.2 Multi-Objective Approach

The natural way to conduct history matching is the use of multi-objective approach that can effectively handle multiple match components in the reservoir characterised by multiple wells and many production data. This method works by splitting the objective function into several components, which are optimised simultaneously. In this case, we look for acceptable tradeoff rather than a unique solution, referred to as Pareto solutions. A set of feasible solution vectors is called Pareto optimal if there is no other feasible vector that would improve some criteria without causing a simultaneous deterioration of at least one other criteria. All Pareto optimal vectors are called nondominated, and the

image of these vectors in the objective space is called Pareto front [11]. More details of this approach are described in Chapter 2.

A number of multi-objective history matching have been reported in the literature with various optimisation algorithms. For example, Schulze-Riegert *et al.* [180] implement the first application of multi-objective history matching using strength Pareto evolutionary algorithm 2 (SPEA2). Ferraro and Verga [181] applied the multi-objective genetic algorithm and multi-objective evolution strategy (MOGA and MOES) for history matching and uncertainty quantification of the PUNQ-S3 synthetic case. In another application, Hajizadeh *et al.* [8] implemented differential evolution based on MOGA Pareto ranking (DEMOPR) for history matching of the PUNQ-S3 synthetic case. Mohamed *et al.* [7] used multi-objective particle swarm optimisation (MOPSO) based on the elitist nondominated sorting genetic algorithm II (NSGA-II) ranking technique for history matching of the IC Fault model. Park *et al.* [147] used multi-objective evolutionary algorithm (MOEA) on handling conflicting objectives. Finally, Christie *et al.* [9] used MOPSO in history matching of a real field case study.

In this chapter, we used PSO [90] and MOPSO [7] for single-objective and multi-objective history matching, respectively.

3.2.2 Strategy for Comparative Study

Maintaining a good balance between convergence and diversity is essential to the performance of stochastic population-based algorithms and approaches. In history matching, convergence is related to the misfit reduction rate over iterations, i.e. fast convergence is represented by high misfit reduction rate over iterations and vice versa. Diversity is related to the distribution of matched models towards different areas in the objective space, i.e. more diverse set of matched models is represented by more distributed of the models that are spread over in the objective space, whereas less diverse set of models are tightly clustered in particular area(s) in the objective space.

A history matching can be considered as successful if a balance performance of these two criteria is achieved in a timely manner. In extension to that, the uncertainty

quantification in the forecast period based on the ensemble of history-matched models should be reliable for an improved decision-making in reservoir management.

In this section, we evaluate the performance of history-matching approaches (single- and multi-objective) based on three measures: misfit value evaluation (i.e. convergence speed and match quality), diversity, and reliability in the forecasting. For each of these measures, we will use a related plot and score for the comparison study of different approaches under model parameterisation uncertainty.

3.2.2.1 Misfit Value Evaluation

We look at the minimum or *best-so-far* misfit value convergence plot over the history-matching iterations. The reason is that one of the goals in history matching assisted by optimisation algorithm is to obtain reservoir models with the lowest misfit value. This becomes the sum of the objective functions for the multi-objective approach. We repeat the experiments for 10 times and then compute the mean and standard deviation of the results to account for the stochastic nature of the algorithm used here (PSO and MOPSO). This strategy allows us to demonstrate the convergence speed and the match quality of history-matched models on average and check the robustness towards different stochastic seeds. Figure 3.2 shows an example of best-so-far misfit value over iterations from three trials of history-matching run.

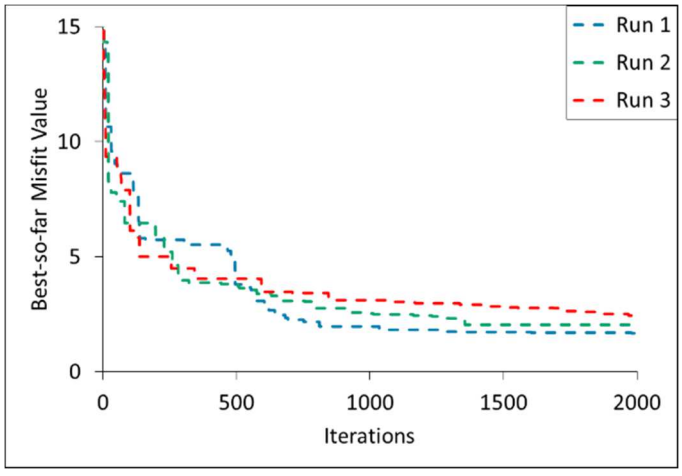

Figure 3.2—Best-so-far misfit value over iterations from three independent history-matching runs performed at a synthetic reservoir model.

3.2.2.2 Diversity

In this study, we evaluate the model diversity by visualising all the models in the objective space. Diversity can be defined as a measure that estimates the levels and types of variety of individuals in a population or solution space, i.e. objective space. The larger is the variety of individuals across the population in the objective space, the more diverse is the solutions. In other words, a more diverse set of models refers to a distribution of models across different areas in the objective space, whereas a less diverse set of models is shown by a refinement or clustering of models within one specific area in the objective space. It is worth pointing out that this measure indicates the diversity of all the models and match quality (objective function value) at the same time.

We also plot the Pareto front approximation from the history match runs to evaluate the diversity of high likelihood matched models. A high likelihood matched model is the one with the small total misfit value.

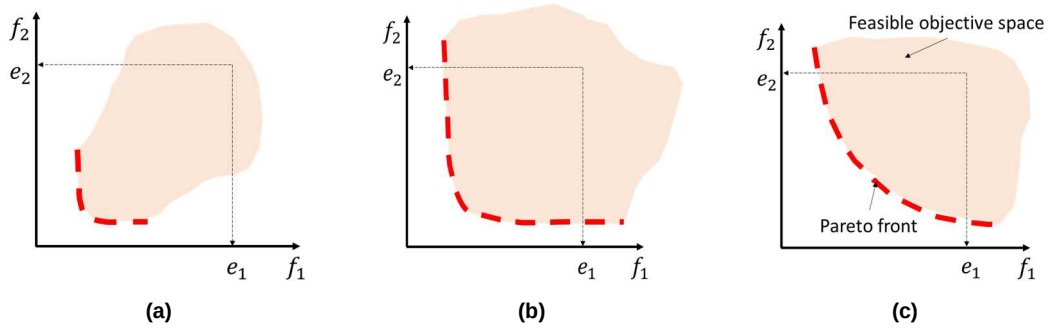

Figure 3.3—Graphical examples illustrating Pareto front for three hypothetical two-objective minimisation problems $[f_1, f_2]$ with (a) steep and less diverse; (b) steep and diverse; and (c) smooth and diverse tradeoffs. Vector $e = [e_1, e_2]$ indicates an arbitrary threshold for distinguishing low and high total misfit values.

Figure 3.3 illustrates three cases of Pareto front for three hypothetical problems in the objective space. Vector $\boldsymbol{e} = [e_1, e_2]$ indicates limits of acceptability, i.e. arbitrary thresholds for distinguishing high likelihood matched models (low total misfit values) and low likelihood matched models (high total misfit values). Diverse and smooth Pareto front shown in Figure 3.3 (c) is more preferable than less diverse and/or steep one shown in Figure 3.3 (a) and (b) [11]. Pareto front with smooth behaviour ensures that a small change in one objective does not prompt a large change in the other objective, whereas

a steep one indicates that a small change in one objective will change significantly in the other objective.

3.2.2.3 Forecasting Reliability

In this study, the NA-Bayes (NAB) algorithm [215] is used in uncertainty quantification of reservoir forecasting from the ensemble of history-matched models. NAB approximates PPD with Voronoi cells interpolation by a Gibbs sampler and saves computational costs, which allows getting inference with a limited number of flow simulations. The Voronoi interpolation is done simply by assigning the constant PPD value of each model inside the corresponding Voronoi cell. The Bayesian credible intervals (usually *P10, P50, P90* values) are calculated at each prediction timestep individually and then connected to construct the *P10, P50,* and *P90* lines. More details on this technique are described in Chapter 2.

Qualitatively, we evaluate the reliability in the forecast period based on the encapsulation of the "truth" case value within the probabilistic confidence interval. We used the Bayesian credible intervals of *P10* and *P90* lines as the confidence intervals. Specifically, we want to avoid the truth or simulated truth (known in the synthetic case study) being consistently outside these credible intervals.

However, in real life, we would not necessarily expect this result all the time as truth case value is represented by measurements and they may include measurement error. Therefore, a validation approach can be used to check the reliability in a real field case study [79]. Nonetheless, in general case, more reliable predictions are the ones that can be justified by more data or knowledge and lead to fewer contradictions.

Quantitatively, we evaluate the reliability of the forecast period by using modified Brier score (BS) [241]. In essence, BS evaluates the number of data points from the "truth" case that is inside the *P10* and *P90* credible intervals in the forecast period as given by Equation (3.2) and illustrated in Figure 3.4. We can see from Equation (3.2) and Figure 3.4 that the lower BS indicates more data points from the truth are encapsulated inside *P10* and *P90* credible intervals, whereas the higher BS indicates more data points from the truth are outside *P10* and *P90* credible intervals.

$$BS = \frac{1}{2}\left(\frac{1}{N}\sum_{i=1}^{N}(P10_i - 0.9)^2 + (P90_i - 0.9)^2\right) \tag{3.2}$$

where:

- BS is the *Brier* score
- N is the number of data points in the forecast period
- $P10_i = \begin{cases} 1, if\ p_i < P10_i \\ 0, if\ p_i > P10_i \end{cases}$
- $P90_i = \begin{cases} 1, if\ p_i > P90_i \\ 0, if\ p_i < P90_i \end{cases}$
- p_i is the truth value of data point i

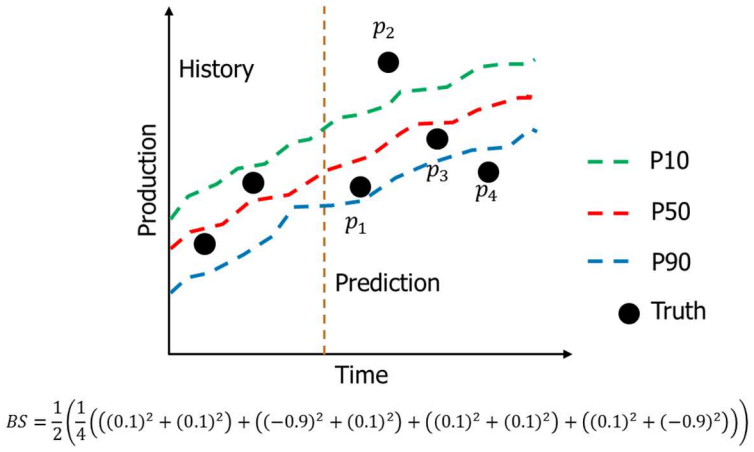

Figure 3.4—An example of BS calculation to quantify the forecast reliability. In this example, the BS is equal to 0.21 from four data points in the forecast.

3.3 Case Study: PUNQ-S3 Reservoir Model

3.3.1 Field and Production Overview

PUNQ-S3 (**P**roduction forecasting with **UN**certainty **Q**uantification variant 3) is a synthetic reservoir model based on a real field operated by Elf Exploration and Production [242]. It has five layers with a top depth of 2430 m, 1.5 degrees' dip angle and is bounded by a fault to the east and south and has a relatively strong aquifer on the north and west. The model has 19x28x5 grid blocks (2660 grid blocks), of which 1761 are active. The grid blocks have an equal side in the *x* and *y* directions of 180 m. It has been

modelled using corner point geometry and Carter-Tracey aquifer. The reservoir has a dome shape where initially there is a gas cap and oil rim at the centre of the structure. There are six production wells that are located near the initial gas-oil contact, as shown in Figure 3.5.

A brief of geological description and detailed petrophysical properties from each layer of the PUNQ-S3 reservoir model is shown in Table 3.1 and Table 3.2, respectively. A full description of the model can be found in [243,244].

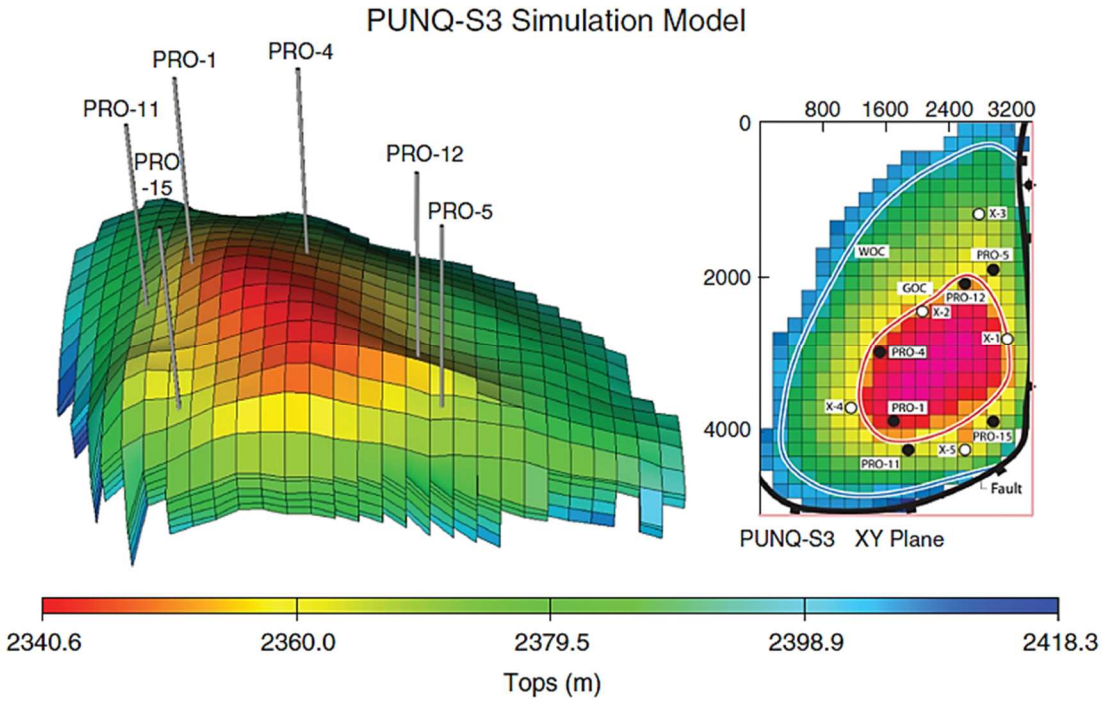

Figure 3.5—PUNQ-S3 reservoir model and location of wells in top structure map.

Layer	Facies	Width (m)	Spacing (km)	Flow Characteristics
1	Channel Fill	800	2–5	Good
2	Lagoonal Shale	–	–	Poor
3	Channel Fill	1,000	2–5	Good
4	Mouthbar	500–5,000	10	Intermediate
5	Channel Fill	2,000	4–10	Good

Table 3.1—Brief geological description of PUNQ-S3 reservoir including expected sedimentary facies with estimates of width and spacing of the main flow units for each layer [243].

Layer	Porosity, ϕ	Horizontal Permeability, k_h (mD)	Vertical Permeability, k_v (mD)
1	0.15–0.30	133–3,013	44–925
2	0.05–0.15	16–133	8–44
3	0.15–0.30	133–3,013	44–925
4	0.05–0.15	47–376	17–118
5	0.15–0.30	133–3,013	44–925

Table 3.2—Petrophysical properties of each of the five layers in PUNQ-S3 [243].

The field had been produced for 16.5 years from the six producer wells. Producers 1 (PRO1), 4 (PRO4) and 12 (PRO12) are perforated in Layers 4 and 5. Producers 5 (PRO5) and 11 (PRO11) are perforated in Layers 3 and 4, whereas producer 15 (PRO15) are completed only in Layer 4. The production schedule of PUNQ-S3 is summarised as follow:

- An extended well testing period (buildup test) during the first year.
- The shut-in period for the next three years.
- Production period for the next 12.5 years with fixed oil production rate at 150 SM^3/day and a bottom hole pressure (BHP) constraint of 120 bars with two weeks' periodic shut-in at the beginning of each year.

3.3.2 Truth Case and History-Matching Setup

The truth case was generated using Gaussian random fields for porosity and permeability properties [243]. Pressure, volume and temperature (PVT) data from the original model was used to complete the model. Reservoir simulation was then used to generate production data for 16.5 years, i.e. BHP, water cut (WCT), and gas-to-oil ratio (GOR), and the Gaussian noise was added to account for measurement error.

Eight years of production history data including BHP, WCT and GOR from all wells are used for the history matching and the rest of 8.5 years will be used to validate the forecasts based on the history-matched models. The data are assumed to be uncorrelated and following the original dataset [235]. The objective function, misfit M, to be minimised is defined as in Equation (3.3) [244]:

$$M = \frac{1}{n_w}\sum_i \frac{1}{n_p}\sum_j \frac{1}{n_t}\sum_k \left(w_{ijk}\frac{\left(obs_{ijk} - sim_{ijk}\right)}{\sigma_{ijk}} \right)^2 \tag{3.3}$$

where n_w is the number of evaluated wells with i runs over it, n_p is the number of observed production data with j runs over it, n_t is the number of timesteps for the j^{th} history data with k runs over it, obs is the observed history, sim is the simulated value, σ^2 is the variance of the measurement errors, and w is the weight factor, with runs over i, j and k. In PUNQ-S3, $n_w = 6$, $n_p = 3$, and the misfit for each production data will be lumped over all timesteps. Hence, we can see from Equation (3.3) that there are 18 misfit components in PUNQ-S3 which are the misfits from six wells with three production data (BHP, WCT, and GOR) from each well to minimise.

Objective Function Setup

We approach the history matching with both single and multi-objective optimisations. In single-objective approach, we sum up all the 18 misfit components into a single objective function with unity weight, as in Equation (3.4). In multi-objective approach, we group all the production data from wells PRO1, PRO4 and PRO12 into one objective function and all the production data from wells PRO5, PRO11 and PRO15 into another, making a two-objective history matching [10]. Similar to the single-objective approach, we use unity weight in the summation of all misfit components in each objective of multi-objective approach, as shown in Equation (3.5).

$$OF = M_{PRO1} + M_{PRO4} + M_{PRO5} + M_{PRO11} + M_{PRO12} + M_{PRO15} \tag{3.4}$$

$$\begin{aligned} OF_1 &= M_{PRO1} + M_{PRO4} + M_{PRO12} \\ OF_2 &= M_{PRO5} + M_{PRO11} + M_{PRO15} \end{aligned} \tag{3.5}$$

where OF is the objective function (only one in single-objective and two in multi-objective, i.e. OF_1 and OF_2), and M_{PROi} is the misfit at well PROi consists of three components from three production data in each well, where i = 1, 4, 5, 11, 12, and 15 and the production data are BHP, WCT, and GOR.

We describe the objective grouping process for multi-objective history matching on PUNQ-S3 reservoir model. In multi-objective approach, we group all the production data on the well basis with the geoengineering judgement in the reservoir model. Wells in the reservoir are grouped based on geological layer completed in each well and the connectivity between each layer through inflow/outflow to/from each layer.

Figure 3.6 shows the grouping process for multi-objective history matching on PUNQ-S3 reservoir model that is based on geoengineering judgement. First, wells are grouped based on the layer completed in the reservoir. Well PRO1, PRO4 and PRO12 are completed in Layers 4 and 5, and are grouped into one group. The same applies on well PRO5 and PRO11 which are completed in Layers 3 and 4 as one separate group. Well PRO15 is the only well completed in Layer 4 will be assigned as one group. We get three objectives by grouping through this well completion analysis as the basis for grouping (boxes with red, yellow and white colour in the middle top of Figure 3.6).

Next, we further analysed the grouping to make it into two-objective history matching. To do that, we add more intersection criterion that is the connectivity between each layer (as shown by curved arrow on the right of Figure 3.6). Layer 1 is connected to Layer 2, Layer 2 to Layer 3, Layer 3 to Layer 4, Layer 3 to Layer 1, and Layer 5 to Layer 4. As there is no direct connectivity between Layer 3 and Layer 5, we constrained the grouping so not to group the wells that are completed in Layer 3 or 5 into the same grouping. In this case, we do not group well PRO1, PRO4 and PRO12 which are completed in Layer 5 with group of well PRO5 and PRO11 which are completed in Layer 3. However, we can group well PRO15 that is completed in Layer 4 with group of well PRO5 and PRO11 that are completed in Layers 3 and 4 where there is connectivity between those layers.

The idea behind this grouping process is to assume if there is connectivity between each layer penetrated by the wells, production data from each respective well that connects to others will affects each other and can be grouped together.

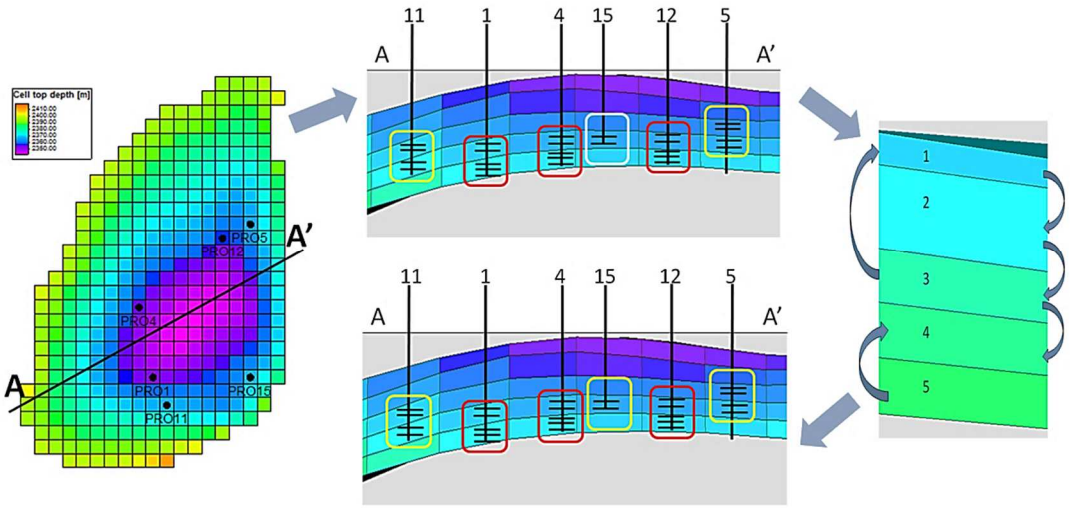

Figure 3.6—Geoengineering judgement as the basis for objective grouping in multi-objective history matching on PUNQ-S3 reservoir model.

3.3.3 Model Parameterisation

We have considered two sets of modelling type parameterisation based on geologically driven zonation approach and geological information: (1) less complex parameterisation with 24 parameters [245]; (2) more complex parameterisation with 38 parameters [52].

3.3.3.1 Set-1 Parameterisation

Set-1 parameterisation is based on the geological facies description of PUNQ-S3 to define the porosity range for each zone. The PUNQ-S3 reservoir model is described as a deltaic and coastal plain reservoir with good quality channel sands in Layers 1, 3 and 5. Three arbitrary channels of uniform thickness and spacing are placed in these layers and encased in a background floodplain. Layers 2 and 4 are interpreted as poor quality sand and shale classified in single facies respectively. This gives a total of 12 geological facies: nine sand channels (three channels each in Layers 1, 3, and 5), one floodplain, one homogeneous Layer 2, and one homogeneous Layer 4, as shown in Figure 3.7.

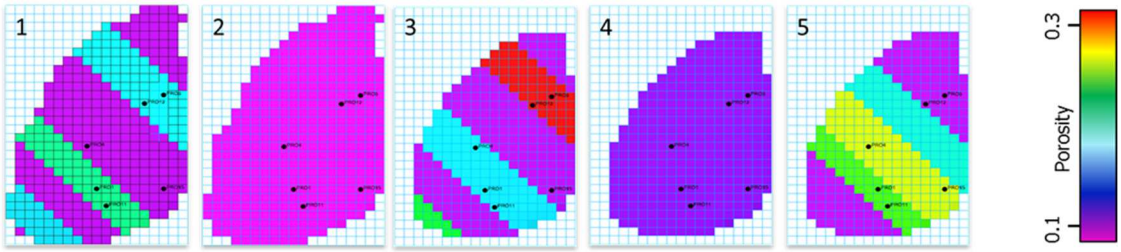

Figure 3.7—Porosity map of Set-1 model parameterisation in PUNQ-S3 for all five layers.

Equation (3.6) is used to correlate between horizontal permeability from porosity values based on least square fitting of well data cross plots [242]. Vertical permeability (k_v) is calculated from k_h, as in Equation (3.7).

$$\log(k_h) = \log(Mult) + (0.77 + 9.03\phi) \tag{3.6}$$

$$k_v = 3.124 + 0.306 k_h \tag{3.7}$$

Multipliers ($Mult$) are used to compensate for the error in the calculation of horizontal permeability (k_h) from porosity (ϕ) [245]. Multipliers are different for each facies in the model. Two orders of magnitude are decided the most suitable range for multiplier due to horizontal permeability being on a logarithmic scale [245]. In total, there are 24 parameters in Set-1 parameterisation: 12 for porosity (ϕ) and 12 for k_h multiplier ($Mult$). Table 3.3 shows the prior ranges of these parameters.

Parameter	Number	Range
Porosity for channels	9	0.15–0.30
Porosity for background floodplain	1	0.05–0.15
Porosity for Layers 2 and 4	2	0.05–0.15
Multiplier for channels	9	0.1–10
Multiplier for background floodplain	1	0.1–10
Multiplier for Layers 2 and 4	2	0.1–10

Table 3.3—Prior ranges of porosity and k_h multipliers for each facies in Set-1 parameterisation of PUNQ-S3.

3.3.3.2 Set-2 Parameterisation

The geological description in Set-2 parameterisation is more detail (34 different regions of facies) than in Set-1 parameterisation (12 different regions of facies). In Set-2 parameterisation, porosity in the reservoir model is parameterised by using eight homogeneous regions for each of Layers 1 and 2 and six homogeneous regions for each of Layers 3–5, making in total 34 porosity parameters. Layers 1 and 2 are characterised by more regions because of having a wider extension on the top structure map than the bottom three layers. The number of regions is determined based on the channels width (Table 3.1) and the size of the reservoir. Figure 3.8 shows the porosity map of Set-2 parameterisation in PUNQ-S3 for all layers.

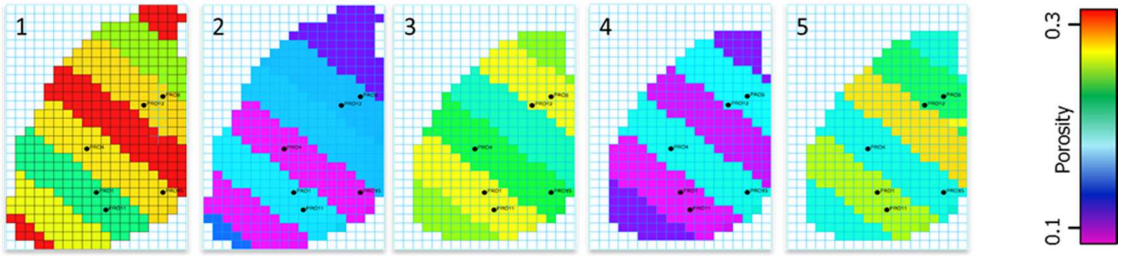

Figure 3.8—Porosity map of Set-2 model parameterisation in PUNQ-S3 for all five layers.

Equation (3.8) is used to correlate between horizontal permeability from porosity values based on least square fitting of well data cross plots [242]. Vertical permeability (k_v) is calculated from k_h, as in Equation (3.9).

$$\log(k_h) = a + b\phi \tag{3.8}$$

$$k_v = c + dk_h \tag{3.9}$$

Different from Set-1 parameterisation, Set-2 parameterisation uses variable values in both horizontal permeability against porosity and vertical permeability against horizontal permeability relations that also will be sampled in the history-matching process. These values are also parameterised because the cross plot in the original study [242] are generated only from well data, hence the permeability fields are unknown.

Therefore, two coefficients are taken for k_h vs. ϕ relation and another two coefficients for k_v vs. k_h relation. In total, there are 38 model parameters in Set-2 parameterisation: 34 for porosity and four for coefficient in the cross plot equations. Table 3.4 shows the prior ranges of these model parameters.

Parameter	Number	Range
Porosity Layer 1	8	0.15–0.30
Porosity Layer 2	8	0.05–0.15
Porosity Layer 3	6	0.15–0.30
Porosity Layer 4	6	0.05–0.15
Porosity Layer 5	6	0.15–0.30
a	1	0.5–1.0
b	1	6–12
c	1	1–5
d	1	0.1–0.4

Table 3.4—Prior ranges of model parameters in Set-2 parameterisation of PUNQ-S3.

3.3.4 Results

Repeated experiments with different stochastic seeds are required to account for the stochastic nature of the algorithm used here (PSO and MOPSO). We ran 10 trials of history matching with different seeds for both parameterisations. We performed history matching with single and multi-objective approaches using PSO [90] and MOPSO [7] algorithms, respectively. The parameters for the algorithm are as follows [123]:

- Number of particles : 20
- Inertia weight, w : 0.729
- Cognitive component, c_1 : 1.494
- Social component, c_2 : 1.494

We evaluated the results of the history matching based on three measures: misfit value evaluation (i.e. convergence speed and match quality), diversity, and forecasting reliability in the following sections.

3.3.4.1 Misfit Values Evaluation

Figure 3.9 shows the mean and the standard deviation (SD) of best-so-far misfit values evolutions through history-matching iterations from 10 runs of single and multi-objective approaches for both parameterisations. By looking at the slope angle of the mean of misfit convergence in both parameterisations, history matching with single and multi-objective approaches have the same misfit convergence on the first few (hundreds) of iterations, and afterwards, single-objective outweighs the multi-objective. In Set-1, the lower bound of best-so-far misfit values from multi-objective history matching is below the mean of single-objective up to around iteration 400, whereas in Set-2 it is up to around iteration 50. The upper bound of best-so-far misfit values from single-objective history matching is above the mean of multi-objective up to around iteration 400, whereas in Set-2 it is always below the mean of multi-objective history matching.

The mean best-so-far misfit values for the final iteration with Set-1 are lower than with Set-2 for both single and multi-objective approaches. In this case, more detailed parameterisation or more model parameters lead to lower match quality for both approaches. These results demonstrate that detailing the geological layers into more facies or regions does not guarantee the improvement of match quality from history matching. As suggested by Gavalas *et al.* [62] and Shah *et al.* [63], the zonation approach in the model parameterisation can reach an optimum level of modelling error at an intermediate level of parameterisation, i.e. at a particular number of zones. Any parameterisation that is over or under this number may deteriorate the quality of history-matched models.

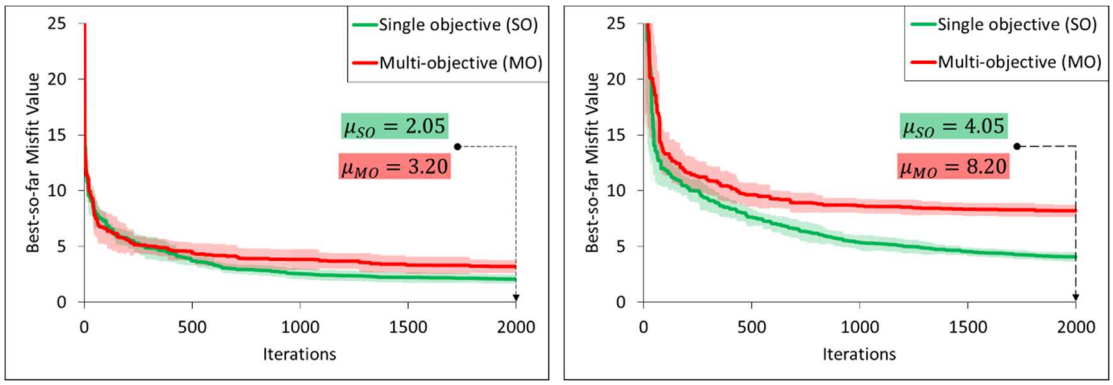

(a) Set-1 **(b) Set-2**

Figure 3.9—Mean and SD of best-so-far misfit values over iterations from 10 trials of single and multi-objective history matching for (a) Set-1 and (b) Set-2 parameterisations of PUNQ-S3.

Nonetheless, these results demonstrate that the exploitative capability of single-objective approach to minimise one objective contribute to faster misfit convergence and lower best-so-far misfit values. On the contrary, explorative capability by the multi-objective approach to trade off between objectives in minimisation contributes to slower misfit convergence and higher best-so-far misfit values.

3.3.4.2 Diversity

We looked at the diversity of the history-matched models from a single run with single- and multi-objective approaches for both parameterisations, as shown in Figure 3.10. We can see that multi-objective history matching resulted in the wider spread of models along the Pareto front than single-objective approach under different model parameterisation. These results imply that multi-objective approach in history matching obtains more diverse matched models than single-objective. This is because of the optimisation process in multi-objective approach is designed to trade off between two or more objectives, whereas in the single-objective approach converge to a single global optimum.

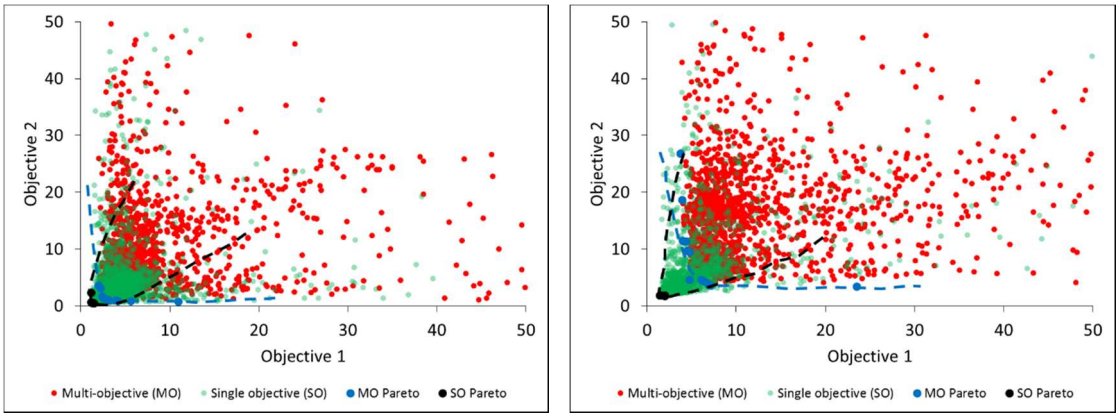

(a) Set-1 **(b) Set-2**

Figure 3.10—Diversity of history-matched models in the objective space from one run of both single- and multi-objective approaches for (a) Set-1 and (b) Set-2 parameterisations of PUNQ-S3.

We evaluated the Pareto front of the history-matched models from all 10 runs of single- and multi-objective approaches for both parameterisations, as shown in Figure 3.11. In both model parameterisations, the Pareto fronts of history-matched models from multi-objective approach are smoother and more diverse than the ones from single-objective history matching. These results are due to optimisation algorithm is more exploitative in

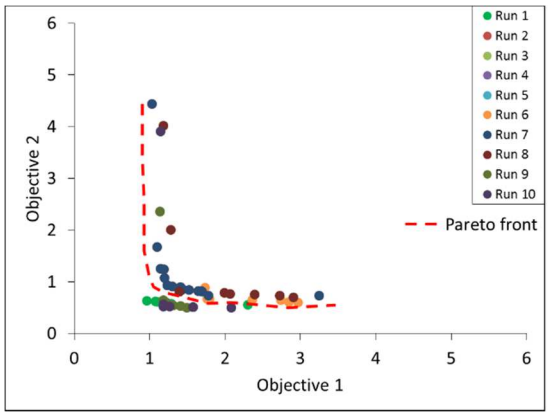

(a-1) Set-1 Single-objective

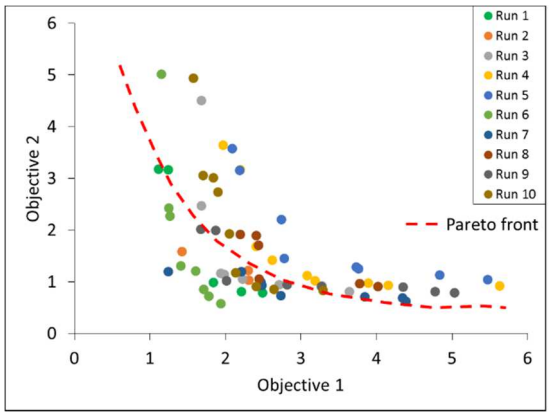

(a-2) Set-1 Multi-objective

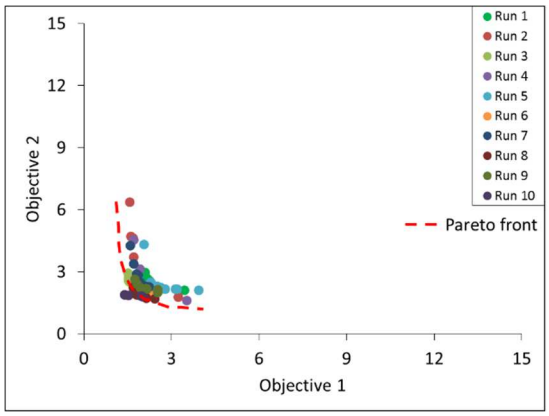

(b-1) Set-2 Single-objective

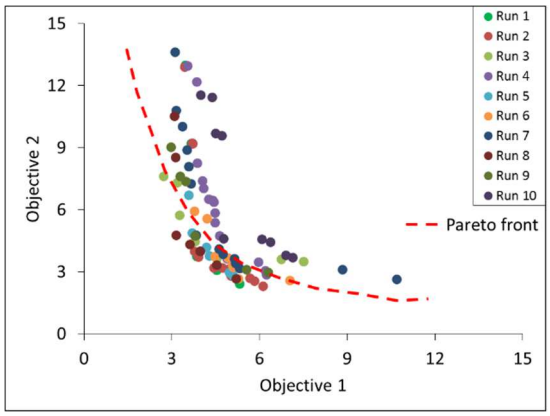

(b-2) Set-2 Multi-objective

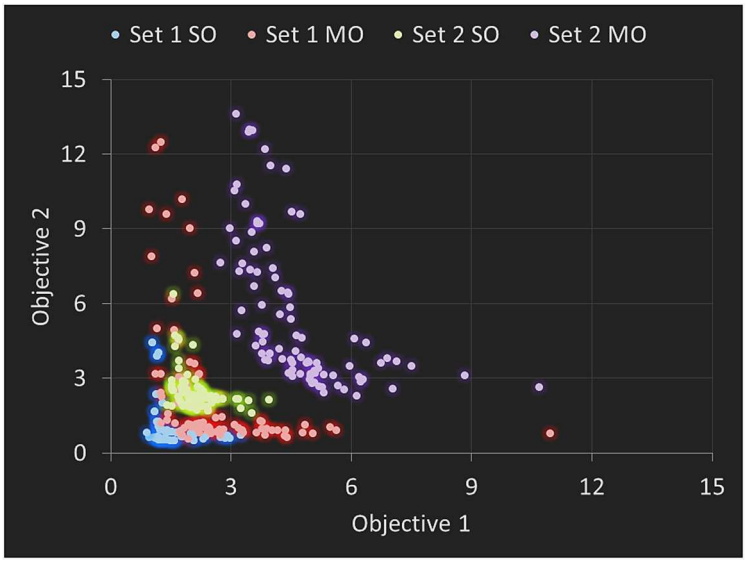

(c) Combined plot

Figure 3.11—Pareto front approximation of history-matched models from all 10 runs of both single and multi-objective approaches for (a) Set-1 and (b) Set-2 parameterisations of PUNQ-S3, and (c) Combined plot of all Pareto solutions in (a) and (b). (SO=single-objective; MO=multi-objective.)

finding a single optimum solution in single-objective, whereas in multi-objective is more explorative as there is a tradeoff between objectives to be optimised. As suggested by Deb [11], smooth and diverse Pareto front is preferable than steep and less diverse one.

3.3.4.3 Forecasting Reliability

After exploring the search space and generating the ensemble of matched models by single- and multi-objective approaches, the next step is to draw inferences from the complete ensemble of each approach. Throughout the thesis, the NAB algorithm [215] is used for posterior inference. NAB infers and evaluates the posterior probability from the complete ensemble. Then, forward reservoir simulations are conducted only for the models that are resampled by NAB. The probabilistic estimates of the forecast were calculated based on the PPD by NAB. More detailed on NAB mechanism on uncertainty prediction is described in Chapter 2.

The configurations for the NAB are as follows:

- Number of chains : 8
- Burn-in period : 50,000
- Chain length : 200,000

We evaluated the uncertainty quantification for the forecast of total oil recovery at the end of production from the field. We used all the 10 runs of single- and multi-objective approaches for both parameterisations. The uncertainty predictions are presented in the form of the *P10*, *P50* and *P90* credible intervals, as shown in Figure 3.12.

Qualitatively, we can see clearly from Figure 3.12 that the forecasting from history-matched models by multi-objective approach is more reliable than from single-objective under different model parameterisation. All 10 runs from multi-objective approach provide forecasting with the *P10–P90* credible interval encapsulating the "truth" case for both model parameterisations, as shown in Figure 3.12 (b). On the contrary, eight out of 10 runs from single-objective history matching in Set-2 model parameterisation resulted in the "truth" case is outside the *P10–P90* credible interval in forecasting, even though all credible intervals encapsulate truth case in Set-1 model parameterisation, as shown in Figure 3.12 (a).

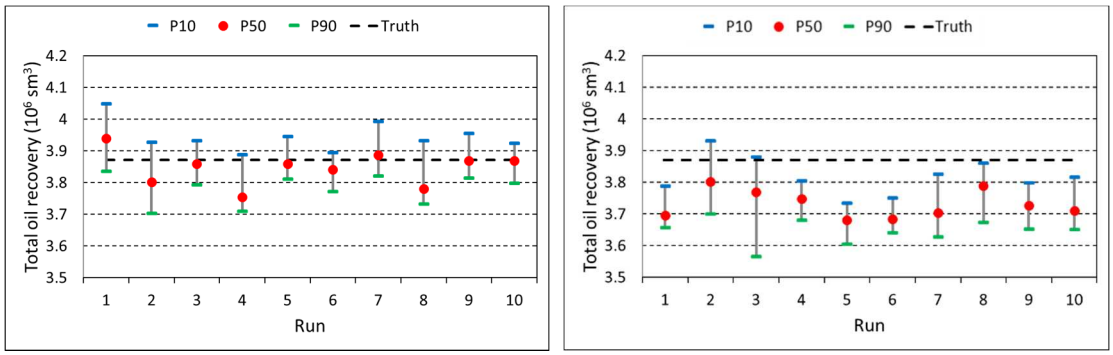

(a-1) Set-1 Single-objective

(a-2) Set-2 Single-objective

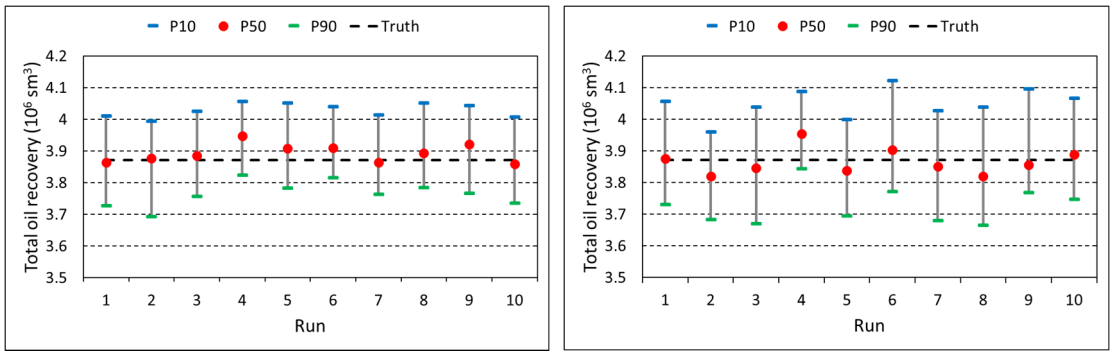

(b-1) Set-1 Multi-objective

(b-2) Set-2 Multi-objective

Figure 3.12—Uncertainty interval in forecasting of total oil recovery from the field at the end of production time from 10 runs of (a) single- and (b) multi-objective history matching for Set-1 and Set-2 parameterisations of PUNQ-S3.

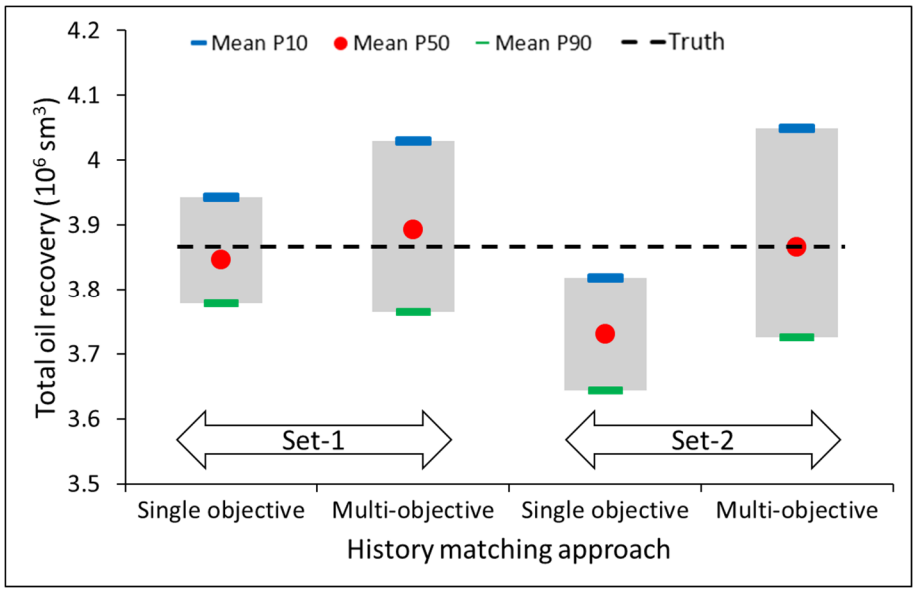

Figure 3.13—Average of each credible interval (*P10*, *P50*, and *P90*) in forecasting of total oil recovery from the field at the end of production time over 10 runs of single- and multi-objective history matching for Set-1 and Set-2 parameterisations of PUNQ-S3.

The uncertainty quantification in forecasting from the history-matched models by multi-objective is more robust than by single-objective approach under different model parameterisations, as shown in Figure 3.13. The robustness is evaluated by computing the mean value of each credible interval (i.e. *P10*, *P50*, and *P90* values) over 10 runs. Then we looked at how these mean values change under different model parameterisations. We can see from Figure 3.13 that over 10 runs, average value of each credible interval from multi-objective is comparable under different parameterisation, whereas from the single-objective is collapsed to different ranges and values of credible interval under different parameterisation.

Quantitatively, we evaluated the forecasting reliability in all the forecast period by using the modified BS defined in Equation (3.2). As suggested by Equation (3.2), the more data points of "truth" case inside the *P10* and *P90* credible intervals, the lower is the BS. Hence, the lower the BS, the better is the forecast as more data points of "truth" case are encapsulated by *P10* and *P90* credible intervals.

Table 3.5 summarises the average of BS for each production data on field and well scales over all 10 runs of single and multi-objective history matching for both model parameterisations. On average, the forecasting reliability from matched models by multi-objective approach is better (lower BS) than single-objective on field and well scales for both model parameterisations. In Set-1, out of 27 production data, 17 have lower BS by multi-objective and only three by a single-objective, and seven have the same BS between both approaches. In Set-2, out of 27 production data, 17 have lower BS by multi-objective and only four by a single-objective, and six have the same BS between both approaches.

Figure 3.14 and Figure 3.15 show the forecasting for the production data both on field and well scales, comparing single and multi-objective history matching in detail for both model parameterisations. The production data were selected to give examples of each of the case from Table 3.5 (i.e. the case of multi-objective is better than single-objective; single-objective is better than multi-objective; and both single-objective and multi-objective are similar).

Production Data	Parameterisation Set-1		Parameterisation Set-2	
	Single-objective	Multi-objective	Single-objective	Multi-objective
FOPT	0.267	0.111	0.402	0.138
FGOR	0.116	0.059	0.160	0.060
FWCT	0.236	0.079	0.235	0.208
WOPT-PRO1	0.210	0.031	0.408	0.308
WOPT-PRO4	0.258	0.258	0.238	0.237
WOPT-PRO5	0.010	0.010	0.010	0.010
WOPT-PRO11	0.044	0.029	0.147	0.015
WOPT-PRO12	0.010	0.010	0.010	0.010
WOPT-PRO15	0.265	0.015	0.346	0.067
WBHP-PRO1	0.374	0.374	0.352	0.359
WBHP-PRO4	0.335	0.321	0.366	0.398
WBHP-PRO5	0.347	0.388	0.410	0.410
WBHP-PRO11	0.163	0.161	0.175	0.173
WBHP-PRO12	0.291	0.262	0.264	0.253
WBHP-PRO15	0.223	0.195	0.238	0.180
WGOR-PRO1	0.085	0.012	0.139	0.088
WGOR-PRO4	0.062	0.042	0.193	0.063
WGOR-PRO5	0.258	0.258	0.258	0.258
WGOR-PRO11	0.258	0.258	0.258	0.258
WGOR-PRO12	0.250	0.238	0.258	0.258
WGOR-PRO15	0.163	0.175	0.212	0.257
WWCT-PRO1	0.101	0.020	0.162	0.085
WWCT-PRO4	0.251	0.172	0.252	0.256
WWCT-PRO5	0.098	0.134	0.077	0.010
WWCT-PRO11	0.137	0.012	0.147	0.012
WWCT-PRO12	0.155	0.147	0.190	0.120
WWCT-PRO15	0.258	0.258	0.135	0.112

Notes:

Multi-objective is better.

Single-objective is better.

Single- and multi-objective are similar.

Table 3.5—Summary of average BS in the forecast period of production data at field and well scale over 10 runs from single- and multi-objective approaches for Set-1 and Set-2 model parameterisations of PUNQ-S3. (FOPT=field oil production total; FGOR=field gas-to-oil ratio; FWCT=field water cut; WOPT=well oil production total; WBHP=well bottom hole pressure; WGOR=well gas-to-oil ratio; WWCT=well water cut.)

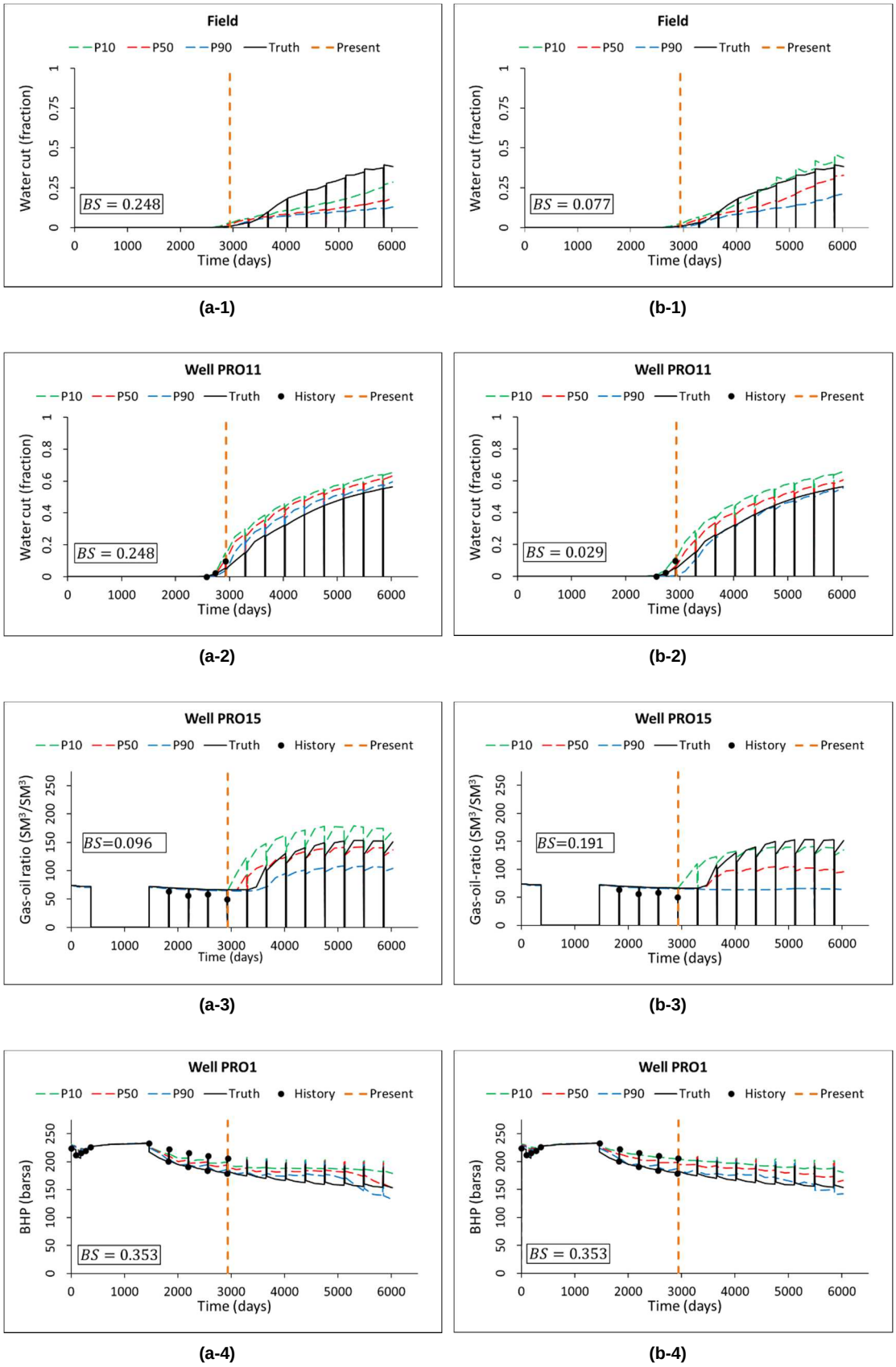

Figure 3.14—Forecasts of some production data at field and well levels comparing (a) single- and (b) multi-objective approaches in history matching for Set-1 model parameterisation of PUNQ-S3. Lower BS value indicates better forecast.

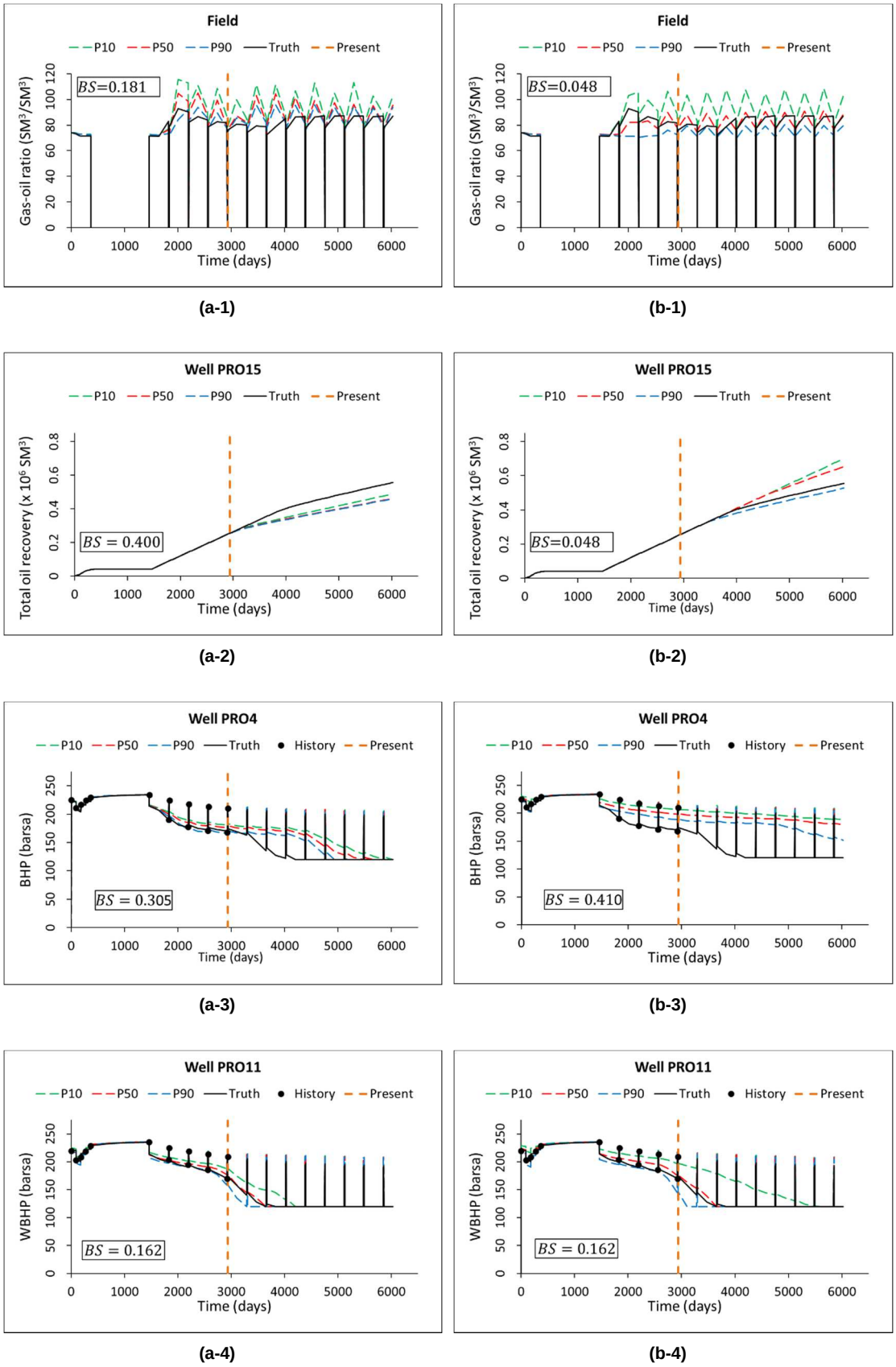

Figure 3.15—Forecasts of some production data at field and well levels comparing (a) single- and (b) multi-objective approaches in history matching for Set-2 model parameterisation of PUNQ-S3. Lower BS value indicates better forecast.

3.4 Discussion

Through the results of the PUNQ-S3 case study, we observed that multi-objective approach in history matching resulted in more diverse sets of history-matched models than the single-objective across different model parameterisations. This is because in multi-objective approach the search for model parameters solutions is guided towards different objectives to trade off between them, whereas the single-objective approach tends to find a global optimum objective value. Hence, multi-objective is more explorative to find the tradeoff of the solutions than single-objective approach.

In both model parameterisations, the exploitative capability by single-objective history matching contributes to faster misfit convergence and lower best-so-far misfit value than multi-objective approach. More complex model parameterisation has less effect on the final best-so-far misfit value by single-objective history matching (2.05 in Set-1 and 4.05 in Set-2) than multi-objective approach (3.20 in Set-1 and 8.20 in Set-2). This is because of the exploitative nature of the single-objective approach to find a single global optimum value is less affected by more model parameters in the search process. In multi-objective approach, the more model parameters to search and the tradeoff mechanism between objectives contribute to slower misfit convergence in the history-matching process of the studied PUNQ-S3 case.

Nonetheless, more complex model parameterisation (i.e. Set-2) contributes to a higher final best-so-far misfit values on both single and multi-objective approaches. Similar findings were highlighted in hydrologic model calibration studies [246–248]. Attempts to use additional model parameters, in the absence of supplementary data to support them, usually fails to notably improve the model fitting and results in poorly identified parameters. In this sense, the formulation of the non-parsimonious (over-parameterised) model increases the uncertainty within the parameter estimation procedure that results in lower match quality in the history matching. Furthermore, even though incorporating more detail may allow a more accurate model description, an over complex model parameterisation will be hard to identify from observations, and this can lead to poor predictions as demonstrated in the single-objective approach case study in this chapter.

Forecasting from multi-objective history-matched models provides more reliable Bayesian credible interval than single-objective in both model parameterisations at field and well levels. Even though single-objective history matching provides better fitness of matched models, it does not necessarily result in a better capability in future prediction, which is aligned with the outcomes from Tavassoli *et al.* [49]. A more diverse set of matched models from multi-objective history matching used in the forecasting has a better forecasting reliability compared to the ones from single-objective. This present study suggests that in the history matching and uncertainty quantification, exploration capability by multi-objective approach is more important for the forecasting reliability than exploitation by a single-objective approach.

The impact of model parameterisation has less effect on the forecasting by multi-objective history-matched models. In the case of more complex models with more model parameters (Set-2), multi-objective history matching provides a favourable framework for preserving parsimony and thus reducing uncertainty. This requires the increase of independent information contained in the calibration, by introducing additional outputs for model fitting in the form of a number of objectives [249]. On the contrary, the use of more complex model parameterisation in the single-objective reveals a critical problem known as *overfitting*, which is demonstrated by the poor forecasting capability of the matched models with good fitting in the history period.

Chapter 4

Optimal Selection of Objective Grouping for Multi-Objective History Matching

4.1 Introduction

In practice, history-matching problem is multi-objective because there are many data sources and match criteria necessary to obtain a good match to field performance. In many cases, these match criteria are conflicting, and no feasible solution optimises them all simultaneously. For instance, an improvement in oil-rate match in one well may cause a deterioration of the gas-rate match in another well. This means that an approach that allows the engineer to explore tradeoffs between matches to various elements of the overall match is useful in seeking the most-reliable and-realistic match. Moreover, as demonstrated in Chapter 3, an ensemble of matched models from multi-objective history matching can provide more robust and reliable reservoir forecasting than single-objective history matching.

Despite its popularity in the last decades, multi-objective algorithms have a critical issue on handling problems with a high number of objectives, i.e. problems with objectives more than three [15,17]. Problems of this type abound in real-world application of science and engineering including petroleum engineering. As the number of objective increases, even the state-of-the-art multi-objective optimisation algorithm incur serious

performance deterioration (slower convergence) in a high-dimensional objective space [15,17].

The petroleum reservoir history-matching problems can potentially have many objectives or criteria to match, i.e. oil rate, water cut, bottom hole pressure, and gas-to-oil ratio data from different wells. This is due to a number of wells and data in a petroleum reservoir can range from the order of tens to thousands. For instance, one of the largest oil fields located in the Eastern Province of Saudi Arabia (Ghawar Field) includes 1500 wells with the total amount of data acquired to date is in the order of hundreds of thousands [250]. In this field, the history-matching task is a highly challenging task for reservoir engineers.

Therefore, in practice, reservoir engineers usually reduce the number of objectives to some form of objectives aggregation, i.e. by grouping. Grouping technique works by lumping several objective components into one group and the other objective components into another group. This technique had been carried out in the petroleum literature particularly in multi-objective history matching [7,9,147,180,181]. However, the existing literature does not present sufficient information on appropriate grouping techniques and ways of combining objective components.

Furthermore, the difficulty in the objective-grouping technique is the number of objective-grouping combinations that increase combinatorically under an increasing number of total objective components. It causes a significant challenge in selecting which objective-grouping combination that gives better history-matching performance (faster convergence and high match quality). The difficulty in this objective-grouping technique is that there are no general principles or guidelines to select the way to group many objective components (such as oil-, water-, and gas-rate matches for each well, or depending on well proximity) into two or three objectives for use by the optimiser.

In this chapter, we present a novel technique for optimal selection of objective grouping by use of nonparametric-conflict information between objective groups. Two case studies are presented with extensive reservoir flow simulations and rigorous statistical test to demonstrate the efficacy of the proposed technique.

4.2 Challenge of a Multi-Objective Approach in Many-Objective Problems

Despite the success of multi-objective algorithms for addressing history-matching problems, their performance reduces dramatically for problems that have more than three objectives, known as many-objective problems. In those problems, Pareto-based multi-objective algorithms are no longer an effective discriminator because the majority of solutions are noncomparable. The concept of dominance and Pareto optimality are less effective in the higher objective dimension because all points tend to become nondominated. In this case, the algorithm effectively becomes a random sampler and consequently compromises the convergence of search procedure.

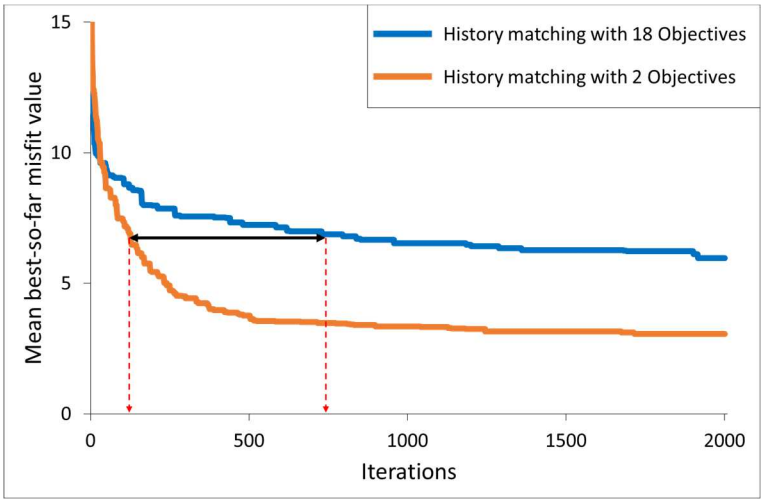

Figure 4.1—Comparison of mean best-so-far misfit-value convergence over 10 runs between multi-objective history matching with grouping (two objectives, in orange) and without grouping (18 objectives, in blue) performed at a synthetic PUNQ-S3 reservoir model.

Figure 4.1 compares the mean best-so-far misfit convergence from two runs: the first a history matching of a synthetic model by use of 18 objectives, and the second the same history match with the objective components grouped to two objectives. The lines represent averages over 10 runs, and the difference in performance is clear. The history-matching runs were performed at a synthetic PUNQ-S3 reservoir model [243].

4.2.1 Initial Study on Multi-Objective History Matching With Different Number of Objectives

We conducted an initial study on the multi-objective history matching of the synthetic PUNQ-S3 reservoir model. The same data sets and misfit definition in Chapter 3 were used (i.e. referring to data sets from [243] and misfit definition described by Equation (4.1)). The Set-1 parameterisation as in Chapter 3 and multi-objective particle swarm optimisation (MOPSO) algorithm [7] were used in the history matching.

$$M = \frac{1}{n_w}\sum_i \frac{1}{n_p}\sum_j \frac{1}{n_t}\sum_k \left(w_{ijk}\frac{\left(obs_{ijk} - sim_{ijk}\right)}{\sigma_{ijk}} \right)^2 \tag{4.1}$$

where n_w is the number of evaluated wells with i runs over it, n_p is the number of observed production data with j runs over it, n_t is the number of timesteps for the j^{th} history data with k runs over it, obs is the observed history, sim is the simulated value, σ^2 is the variance of the measurement errors, and w is the weight factor, with runs over i, j and k.

The multi-objective history matching was set up with a different number of objectives. In PUNQ-S3, there are 18 objective components as the targets to be minimised. These objectives come from six wells (i.e. PRO1, PRO4, PRO5, PRO11, PRO12 and PRO15) and three production data from each well, i.e. well bottom hole pressure (WBHP), well water cut (WWCT) and well gas-to-oil ratio (WGOR). We history matched the model with the 18 components grouped to 2, 4, 6, 8, 10, 12, 14, 16, and 18 objectives. For instance, in two-objective history matching, we grouped 18 objective components into two objectives with unity weighting factor for each objective component. Table 4.1 describes the configuration for each of these different numbers of objectives.

For each different number of objectives scenario, we ran history matching with a different number of flow simulations (i.e. 10, 100, 1000 flow simulations). Then, for each combination of a number of objectives and flow simulations, we repeated the run for 10 times to get more-robust results due to the stochastic algorithm.

Number of Objectives	Objective Configuration, i.e. {obj1}; {obj2}; {obj3}; …
2	{(WBHP,WWCT,WGOR)(PRO1,PRO4,PRO5)}; {(WBHP,WWCT,WGOR)(PRO11,PRO12,PRO15)}
4	{(WBHP,WWCT,WGOR)(PRO1,PRO4)}; {(WBHP,WWCT,WGOR)(PRO5)}; {(WBHP,WWCT,WGOR)(PRO11)}; {(WBHP,WWCT,WGOR)(PRO12,PRO15)}
6	{(WBHP,WWCT,WGOR)(PRO1)}; {(WBHP,WWCT,WGOR)(PRO4)}; {(WBHP,WWCT,WGOR)(PRO5)}; {(WBHP,WWCT,WGOR)(PRO11)}; {(WBHP,WWCT,WGOR)(PRO12)}; {(WBHP,WWCT,WGOR)(PRO15)};
8	{WBHP PRO1,WGOR PRO1}; {WBHP PRO4,WWCT PRO1}; {WBHP PRO5,WGOR PRO4}; {WBHP PRO11,WWCT PRO4}; {WBHP PRO12,WGOR PRO5}; {WBHP PRO15,WWCT PRO5}; {WGOR PRO11,WWCT PRO11}; {WGOR (PRO12,PRO15),WWCT (PRO12,PRO15)}
10	{WBHP PRO1,WGOR PRO1}; {WBHP PRO4,WWCT PRO1}; {WBHP PRO5,WGOR PRO4}; {WBHP PRO11,WWCT PRO4}; {WBHP PRO12,WGOR PRO5}; {WBHP PRO15,WWCT PRO5}; {WGOR PRO11,WWCT PRO11}; {WGOR PRO12,WWCT PRO12}; {WGOR PRO15}; {WWCT PRO15}
12	{WBHP PRO1,WGOR PRO1}; {WBHP PRO4,WWCT PRO1}; {WBHP PRO5,WGOR PRO4}; {WBHP PRO11,WWCT PRO4}; {WBHP PRO12,WGOR PRO5}; {WBHP PRO15,WWCT PRO5}; {WGOR PRO11}; {WWCT PRO11}; {WGOR PRO12}; {WWCT PRO12}; {WGOR PRO15}; {WWCT PRO15}
14	{WBHP PRO1,WGOR PRO1}; {WBHP PRO4,WWCT PRO1}; {WBHP PRO5,WGOR PRO4}; {WBHP PRO11,WWCT PRO4}; {WBHP PRO12}; {WGOR PRO5}; {WBHP PRO15}; {WWCT PRO5}; {WGOR PRO11}; {WWCT PRO11}; {WGOR PRO12}; {WWCT PRO12}; {WGOR PRO15}; {WWCT PRO15}
16	{WBHP PRO1,WGOR PRO1}; {WBHP PRO4,WWCT PRO1}; {WBHP PRO5}; {WGOR PRO4}; {WBHP PRO11}; {WWCT PRO4}; {WBHP PRO12}; {WGOR PRO5}; {WBHP PRO15}; {WWCT PRO5}; {WGOR PRO11}; {WWCT PRO11}; {WGOR PRO12}; {WWCT PRO12}; {WGOR PRO15}; {WWCT PRO15}
18	{WBHP PRO1}; {WGOR PRO1}; {WBHP PRO4}; {WWCT PRO1}; {WBHP PRO5}; {WGOR PRO4}; {WBHP PRO11}; {WWCT PRO4}; {WBHP PRO12}; {WGOR PRO5}; {WBHP PRO15}; {WWCT PRO5}; {WGOR PRO11}; {WWCT PRO11}; {WGOR PRO12}; {WWCT PRO12}; {WGOR PRO15}; {WWCT PRO15}

Table 4.1—Objective configurations for different number of objectives in PUNQ-S3 reservoir history matching.

Figure 4.2 shows the percentage of nondominated solutions with the increasing number of objectives in history-matching runs for synthetic PUNQ-S3 reservoir model. The figure reveals that the more objectives we have, the higher the percentage of nondominated solutions, which causes the algorithm to lose selection pressure (dominance and Pareto optimality concepts) to approximate the Pareto front. This

percentage increases even faster with fewer iterations (i.e. 10 or 100 iterations, shown in red or blue curves, respectively, compared with the green curve for 1,000 iterations). We can also interpret Figure 4.2 that under the increasing number of objectives, it requires a larger number of flow simulations to have the same percentage of nondominated solutions which consequently to reach an acceptable match quality. Similar figures have already been presented in other studies to illustrate the difficulty of multi-objective algorithms for many-objective optimisation problems (MaOPs) [15,16].

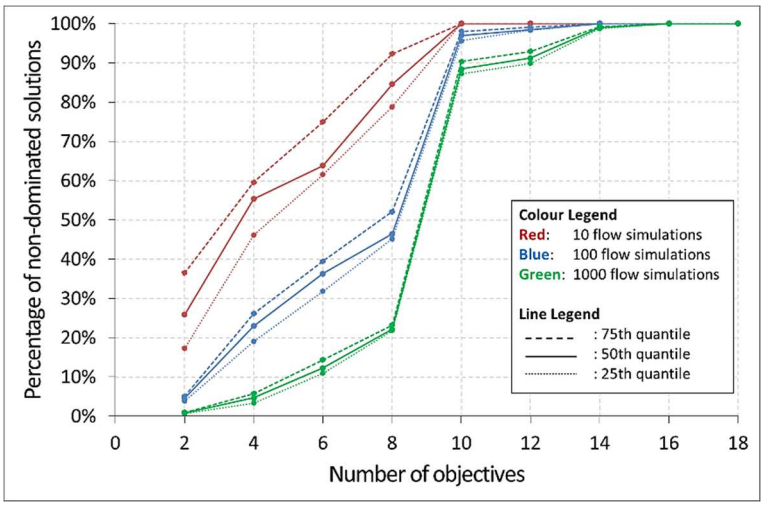

Figure 4.2—Percentage of the nondominated solutions with different number of iterations or flow simulations and configuration of objectives from multi-objective history matching performed at a synthetic reservoir model.

4.2.2 Brief Review on Many-Objective Optimisation Problems Handling

In the general multi-objective optimisation community, attempts at tackling the challenges in MaOPs have been reported in the literature.

In 2005, Hughes [251] showed that it is more effective to use many single-objective optimisations than Pareto-based optimiser on MaOPs. The study was demonstrated on the mathematical test functions with 4 and 6 objectives comparing multiple single-objective Pareto sampling of Hughes [252], repeated single-objective, and elitist nondominated sorting genetic algorithm (NSGA-II) of Deb *et al.* [201].

Brockhoff and Zitzler [253] proposed an objective reduction framework by identifying the redundant objective that can be omitted while preserving the problem structure in MaOPs. They implemented the minimum objective subset (MOSS) algorithms that come in two variants, i.e. a greedy and an exact algorithm for MOSS. The algorithms work by preserving objective functions that are essential for a given problem. The algorithms were tested on the knapsack problem with objectives range of 5–30.

In 2013, Saxena *et al.* [254] introduced a framework that works for both linear and non-linear objective reduction algorithms namely, Linear Principal Component Analysis (L-PCA) and Nonlinear Maximum Variance Unfolding PCA (NL-MVU-PCA), to cope with MaOPs. They tested the framework to both mathematical test functions and real-world problems on a high number of objectives (up to 15 objectives).

Guo *et al.* [255] presented an objective clustering approach on solving MaOPs. They introduced an interdependence coefficient to represent the nonlinear relationship between objectives. They used partition around medoid clustering algorithm to reduce the number of objectives and remove the redundant ones based on the conflict between objectives.

A short review on some challenges and alternative solutions for MaOPs can be found in Ishibuchi *et al.* [15] whereas a more comprehensive survey can be found in von Lücken *et al.* [17].

In the petroleum literature, particularly in history matching, some studies have dealt with problems of more than three objectives. Han *et al.* [186] used multi-objective evolutionary algorithm (MOEA) for history matching with four objective functions. They demonstrated the use of multi-objective history matching to improve the predictability of a model for the estimation of production performance in a waterflooding project. Similarly, Niri and Lumley [189] applied NSGA-II for history matching with four objective functions to measure the mismatch of the geological and seismic data. Adapting technique in [254], Min *et al.* [183] developed an algorithm called DS-MOGA combining dynamic goal programming (DGP) and successive linear objective reduction (SLOR) with NSGA-II. DGP was used as preference ordering whereas SLOR was used

as dimension reduction. The developed algorithm was tested on several scalable mathematical test functions and applied to history matching of a heavy oil reservoir with eight objective functions.

In this chapter, we handle the many-objective history-matching problem by grouping technique. We propose on how to select which groupings that can lead to an improved performance of multi-objective history matching.

4.2.3 Objective Grouping in Multi-Objective History Matching

History matching on the petroleum reservoir can have tens or hundreds of production-data time series to match. It is essential to group these match-quality components into two or three groups to achieve better history-matching performance. The objective grouping chosen by the user can be dependent on geological, engineering, or combination of geological and engineering knowledge. For example, all the pressure terms into one objective and all the water-production rates into another. Grouping the match-quality components by wells in specific parts of the reservoir is another option, although one that makes assumptions regarding their dynamic connectivity. To date, there is no formal study on how to group the match-quality components for multi-objective history matching optimally in the petroleum literature which results in improved history-matching performances.

In the general multi-objective optimisation community, several studies have conducted objective-grouping technique to cope with MaOPs.

Kruisselbrink *et al.* [256] proposed the use of desirability functions to combine groups of objectives to transform the original MaOP into an optimisation problem with a moderate number of objectives. Briefly, a desirability function associates a quality criterion to zero for low quality whereas to one for high quality. Desirability functions are combined according to predefined categories obtaining a single quality value for each category, called as its desirability index. Then, the set of all desirability indexes forms

the new multi-objective optimisation. They applied the technique to the molecular design process.

Murata and Taki [257] proposed a weighted-sum approach based on the correlation between objectives in objective grouping to reduce a MaOP so that can be solved using the multi-objective algorithm. The proposed technique generates a specific number of solutions and is used for calculating the correlation between objectives. These correlations are used to form a predefined number of objective groups, trying to maximise the average correlation of the objectives in each group. They tested the proposed technique on 10 and 40-objective knapsack problems.

Different from [257], Otake *et al.* [258] studied the objective grouping not only based on the correlation between objectives but also based on the meaning of each objective. The study was performed on eight objectives of simplified nurse scheduling problem of which each objective is related to the number on scheduling, such as a number of excessive night shifts, holidays, consecutive shift, prohibited shift sequences, and necessary skills of nurses in one shift.

In the petroleum literature, Hutahaean *et al.* [10] began a comparative study between three different objective-grouping schemes into two-objective history matching on PUNQ-S3 reservoir model. These objective-grouping schemes are based on ad-hoc grouping, Spearman's rank correlation, and geoengineering knowledge. Ad-hoc grouping is based on well grouping adopted from [8]. Spearman's rank correlation grouping is based on the correlation between match-quality components. In this case, a prior history-matching run was used to generate this correlation. Match-quality components with a positive correlation were grouped into one group, and the ones with a negative correlation were grouped into another. In the geoengineering knowledge-based grouping scheme, wells are grouped based on layer completed in each well and the connectivity between each layer (inflow/outflow to/from each layer).

In that study [10], we identified the importance of objective grouping in multi-objective history matching to provide fast misfit convergence speed and the lowest misfit value. Objective grouping based on the geoengineering knowledge, as demonstrated in that

paper, may improve the misfit convergence and match quality in multi-objective history matching. However, as the complexity in the reservoir are different between one reservoir model to another (i.e. the number of wells, layers, completed layers, and faults or compartmentalised region), geoengineering knowledge-based objective grouping can be difficult to use consistently.

In this chapter, we focus on providing the guideline on how to handle multiple objective grouping consistently to improve both convergence rate and final misfit value. We provide a technique for grouping objective components depending on nonparametric-conflict information and selecting the optimal grouping to obtain improved performance in multi-objective history matching. Although we apply this technique to a stochastic optimiser, it can be applied to any multi-objective history-matching procedure.

4.3 Methodology

We introduce the basics of relationships between objectives including *conflicting*, *harmonious*, and *independence*. The different types of conflict and harmony measures are then described. We presented the proposed objective-grouping technique and the methods for performance assessment which are supported by statistical-significance tests.

4.3.1 The General Notions of Relationships Between Objectives

In theoretical multi-objective optimisation, we treat the objectives separately as noncomparable objectives, which are assumed to be conflicting, and a number of solutions can be found to represent the tradeoff between those objectives [11]. However, other relationships can exist between objectives and these may vary within the search space. Purshouse and Flemming [259] offered a basic classification of these possible relationships, as shown in Figure 4.3.

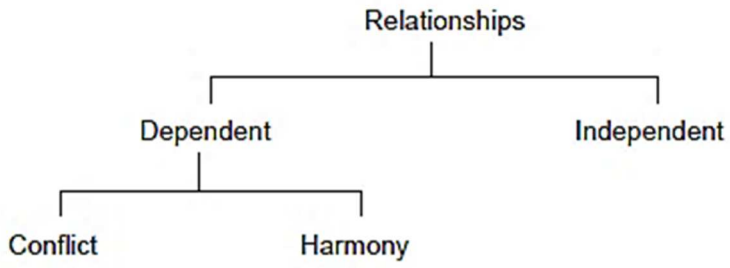

Figure 4.3—Classification of relationships between objectives (after [259]).

4.3.1.1 Notation

The following notations are used in this particular section: M is the number of objectives in the optimisation, $\boldsymbol{X}$ is the set of all feasible objective vectors $\underline{\boldsymbol{x}} \in \mathbb{R}^M$, and $\boldsymbol{X}_R$ is a particular region of interest in objective space, $\boldsymbol{X}_R \subseteq \boldsymbol{X}$. If $\boldsymbol{X}_R = \boldsymbol{X}$ then the relationship is said to be *global*, otherwise it is described as *local*. Let i and j be indices to particular objectives: $i, j \in [1, \dots, M]$. Let a and b be indices to individual objective vector instances: $a, b \in [1 \dots |\boldsymbol{X}_R|] : \underline{\boldsymbol{x}}^a, \underline{\boldsymbol{x}}^b \in X_R$. Also let (a, b) denote a pair of instances for which $a \neq b$. Minimisation is assumed without loss of generality.

Figure 4.4 summarises the identification of the dependency relationships via pairwise analysis. The relationships are dependent on the position of objective vector $\underline{\boldsymbol{x}}^b$ relative to the position of $\underline{\boldsymbol{x}}^a$. These relationships are discussed in more detail in the next section.

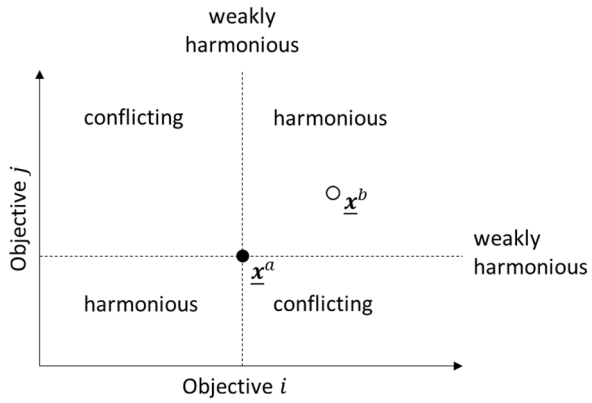

Figure 4.4—Dependency relationship regions between pair of objectives, i and j, identified using the location of sample vector $\underline{x}^b$ relative to that of $\underline{x}^a$ (after [259]).

4.3.1.2 Definition of Conflict

Conflicting is described as a relationship in which the performance in one objective is seen to deteriorate as performance in another is improved. This is summarised by Definition 1 below and can be related to the $\underline{\boldsymbol{x}}^b$-relative-to-$\underline{\boldsymbol{x}}^a$ regions as in Figure 4.4.

Definition 4.1. Objective i and j are conflicting according to the condition $\left(\underline{\boldsymbol{x}}_i^a < \underline{\boldsymbol{x}}_i^b\right) \wedge \left(\underline{\boldsymbol{x}}_j^a > \underline{\boldsymbol{x}}_j^b\right)$. If $\nexists(a, b)$ for which the condition holds then there is *no conflict*, if $\exists(a, b)$ then there is *conflict*, whereas if the condition holds $\forall(a, b)$ then there is *total conflict*.

4.3.1.3 Definition of Harmony

Harmonious is described as a relationship in which performance in one objective is seen to enhance as performance in another is improved. If performance in the objective is unaffected, the relationship is described as *weakly harmonious*. These are summarised by definitions below and can be related to the $\underline{\boldsymbol{x}}^b$-relative-to-$\underline{\boldsymbol{x}}^a$ regions as in Figure 4.4.

Definition 4.2. Objective i and j are harmonious according to the condition $\left(\underline{\boldsymbol{x}}_i^a < \underline{\boldsymbol{x}}_i^b\right) \wedge \left(\underline{\boldsymbol{x}}_j^a < \underline{\boldsymbol{x}}_j^b\right)$. If $\nexists(a, b)$ for which the condition holds then there is *no harmony*, if $\exists(a, b)$ then there is *harmony*, whereas if the condition holds $\forall(a, b)$ then there is *total harmony*.

Definition 4.3. Levels of weak harmony are determined by the condition $\left[\left(\underline{\boldsymbol{x}}_i^a < \underline{\boldsymbol{x}}_i^b\right) \wedge \left(\underline{\boldsymbol{x}}_j^a = \underline{\boldsymbol{x}}_j^b\right)\right] \vee \left[\left(\underline{\boldsymbol{x}}_i^a = \underline{\boldsymbol{x}}_i^b\right) \wedge \left(\underline{\boldsymbol{x}}_j^a < \underline{\boldsymbol{x}}_j^b\right)\right]$. If $\nexists(a, b)$ for which the condition holds then there is *no weak harmony*, if $\exists(a, b)$ then there is *weak harmony*, whereas if the condition holds $\forall(a, b)$ then there is *total weak harmony*.

Definition 4.4. *Neutrality* is determined by the condition $\left(\underline{\boldsymbol{x}}_i^a = \underline{\boldsymbol{x}}_i^b\right) \wedge \left(\underline{\boldsymbol{x}}_j^a = \underline{\boldsymbol{x}}_j^b\right)$. If $\nexists(a, b)$ for which the condition holds then there is *no neutrality*, if $\exists(a, b)$ then there is *neutrality*, whereas if the condition holds $\forall(a, b)$ then there is *total neutrality*.

4.3.1.4 Definition of Independence

Independence means that the objectives can, in theory, be optimised completely separated from each other. In this case, different objectives and parameters will be allocated to different subproblems. If two objectives are independent, then they do not form part of the same tradeoff front. Therefore, multiple and distinct tradeoff fronts exist, each of which should be represented separately.

4.3.2 Conflict and Harmony Measures

We considered the relationships between pairs of objectives by comparing pairs of objective vectors. In this sense, methods that are closely linked to the general definitions of conflict and harmony described earlier are discussed further in the next section.

4.3.2.1 Qualitative Methods

One popular qualitative method to compare pairs of objectives is through a scatterplot matrix visualisation [260]. In this plot, each element of the matrix shows a particular bi-objective section of the tradeoff surface. However, it can sometimes be difficult to extract information from these plots, especially as the number of objectives increases.

The parallel coordinates plot, first described in [262] and subsequently applied to multi-objective optimisation in [193], reduces high-dimensional objective space to two-dimensions. Objective labels are located at discrete intervals on the horizontal axis, and the value of each objective is indicated on the vertical axis. A particular objective vector is displayed by joining the objective values in all adjacent objectives by straight lines. Then, considering two objective vector instances for a pair of objectives, the lines representing the two instances will cross if there is a conflict according to Definition 4.1 or will not cross if there is a harmony according to Definition 4.2 or Definition 4.3. The lines will be superimposed in the case of Definition 4.4. Therefore, the magnitude of conflict is heuristically visualised as ‘many’ crossing lines.

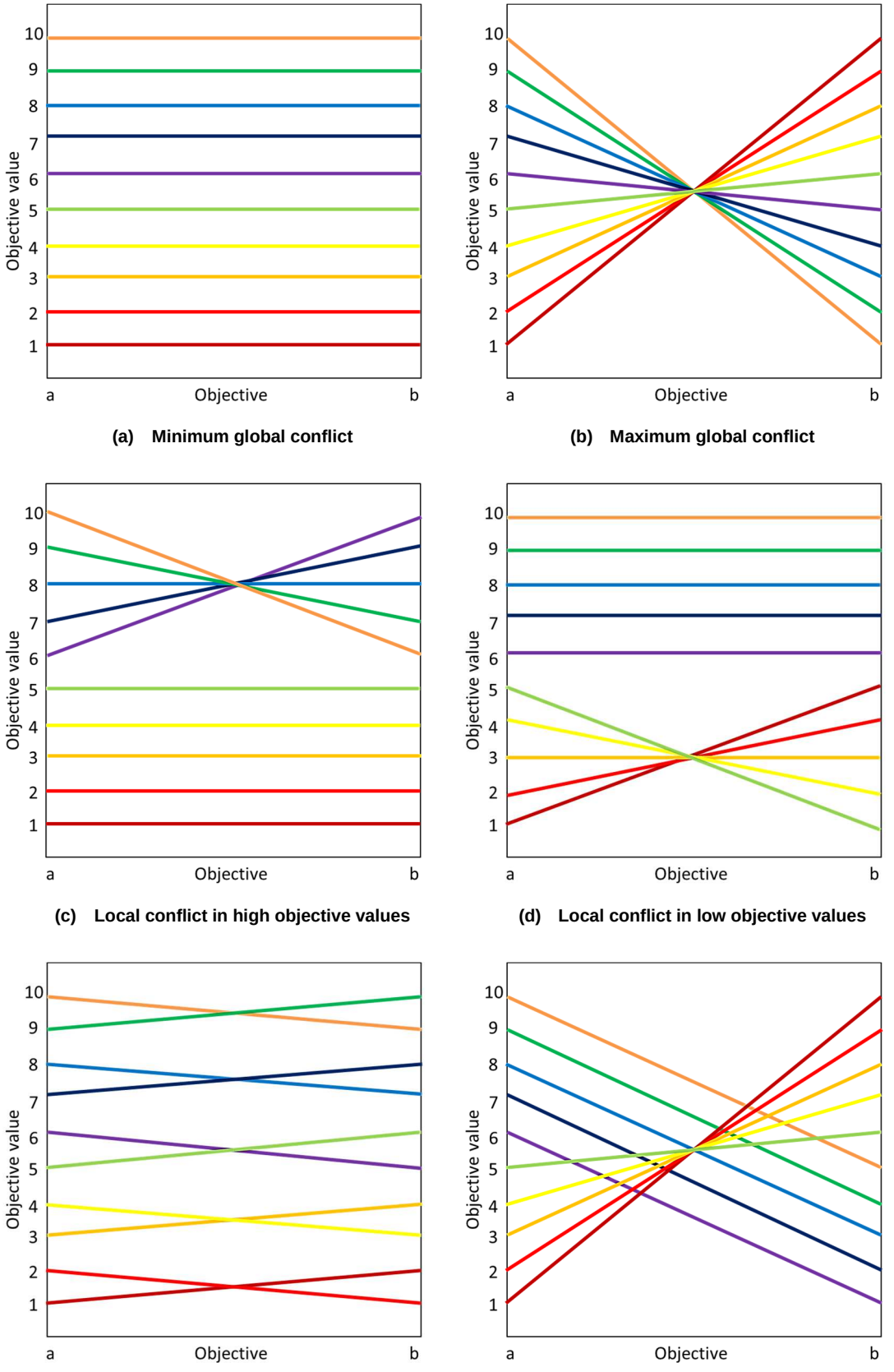

(a) Minimum global conflict

(b) Maximum global conflict

(c) Local conflict in high objective values

(d) Local conflict in low objective values

(e) Global medium conflict

(f) Local conflict in different locations in each objective

Figure 4.5—Illustrative example on six of different possible kinds of conflict in parallel plot (after [261]).

Figure 4.5 illustrates six different possible kinds of conflict and harmony in a parallel coordinate plot of hypothetical problems with two objectives, a and b. In this figure, conflicting objectives are shown by crossing lines, whereas harmonious objectives are represented by noncrossing lines. For instance, Figure 4.5 (a) shows minimum global conflict, whereas Figure 4.5 (b) shows maximum global conflict between objectives. We can see that not only can the amount of conflict vary, but the conflict can also be concentrated in a certain region of the objective space. Thus, the concept of conflict may depend on what we expect as "good" and "bad" values for each objective.

4.3.2.2 Quantitative Methods

As the conflict can be concentrated in a certain region of the objective space, the concept of conflict may depend on what we expect as "good" and "bad" values for each objective. For instance, in the minimisation problems the lower objective values, the better, whereas in the maximisation problems, the higher objective values, the better. Comparing Figure 4.5 (c) and (d), if we assume a minimisation problem, Figure 4.5 (c) shows the conflict exists at the "bad" objective values, whereas Figure 4.5 (d) shows the conflict exists at the "good" objective values.

On the contrary, the concept of harmony implies that improvement in one objective leads to improvement in another. In this sense, harmony may not always be the exact opposite of conflict. The fact that harmony is represented by noncrossing lines in parallel coordinate plot infers the possibility of joining the objectives through summation without loss of quality in the Pareto front. Therefore, if we want to group two objectives into a new compound objective, it is best to group those objectives with greater harmony even if there is some degree of conflict between them.

According to these loose definitions, de Freitas *et al.* [16] proposed specific mathematical formulations of conflict and harmony by specifying three types of conflict: *direct, maximum/minimum,* and *nonparametric conflict*. Harmony, on the other hand, is inversely proportional to nonparametric conflict. Table 4.2 shows the mathematical formulation of those three kinds of conflict which are described in more detail in the next section.

Conflict	Formula	c_{min}	c_{max}
Direct conflict	$C_{ab} = \sum_i \lvert X'_{ia} - X'_{ib} \rvert$ $X'_{ij} = X_{ij} - \min(X_{.j})$	0	–
Maximum/minimum conflict	$C_{ab} = \sum_i \lvert X'_{ia} - X'_{ib} \rvert$ $X'_{ij} = \frac{X_{ij} - \min(X_{.j})}{\max(X_{.j}) - \min(X_{.j})}$	0	n
Nonparametric conflict	$C_{ab} = \sum_i \lvert X'_{ia} - X'_{ib} \rvert$ $X'_{ij} = R_{ij}$	0	$\sum_{i=1}^{n} \lvert 2i - n - 1 \rvert$

Table 4.2—Mathematical formulation of three different types of conflict (after [16]).

C_{ab} represents the conflict measure between objectives a and b, whereas c_{min} and c_{max} represent the possible minimum and maximum values of conflict for each type of conflict. These values are useful for normalising the results if required. $\boldsymbol{X}_{ij}$ is the objective value of the solution or Iteration i (of a total of n solutions or iterations) on objective j from history matching. $\boldsymbol{R}_{ij}$ is the rank of $\boldsymbol{X}_{ij}$ within $\boldsymbol{X}_{.j}$ dependent on the objective value in that particular objective (i.e. the solution with smallest objective value has the top rank, and hence is Rank 1 in that particular objective). $\boldsymbol{X}_{.j}$ is the objective value of all solutions on objective j.

Direct Conflict

Direct conflict measures the absolute difference between the values for the objectives (Table 4.2). If the range of values is different for each objective, the objective value of $\boldsymbol{X}$ is normalised to zero in a new $\boldsymbol{X}'$ formed by the subtraction of the minimum values in $\boldsymbol{X}$ for each objective. With this normalisation, the direct conflict measure is:

- Insensitive to summation or subtraction in the original objective values;
- Useful when the objectives have the same units;
- Assuming all objectives are equally important.

However, because the multi-objective optimisation is designed to treat incomparable objectives in the general case, it is not sensible to directly compare the objective values unless they have the same units.

Maximum/Minimum Conflict

Different from the direct conflict, maximum/minimum conflict normalises objective values on a range from zero to unity before measuring the conflict between objectives, which implies that the importance of the objectives is inversely proportional to their achievable range of values, as suggested by the formula in Table 4.2. With this normalisation, the maximum/minimum conflict measure is:

- Insensitive to any previous linear normalisation;
- Useful when all the objectives are equally important;
- The importance of each objective is linearly proportional to its range of values.

The maximum/minimum conflict measure has more loss of information because of the lack of direct comparability in the same units. However, it is better than direct conflict because there are fewer assumptions, such as the possibility of objectives with different units.

Nonparametric Conflict

A nonparametric-conflict measure works without the assumption of comparability between objectives. It ranks the absolute value in each objective before they are compared, as suggested by the formula in Table 4.2. Rank differences in the objectives are used to compare the objectives without considering the distance between their values.

Figure 4.6 illustrates an example of a nonparametric-conflict calculation from six solutions in a two-objective minimisation problem (objectives a and b). For instance, for solution 1, S_1, the rank in objective a is 4 as it is the 4th smallest objective value amongst all solutions in objective a whereas in objective b its rank is 6 as it is the 6th smallest objective value amongst all solutions in objective b. Then, the absolute value of the rank difference is calculated and summed up for all solutions along with the possible maximum value of conflict, as shown in the last column. We then normalise the conflict score with the possible maximum value of conflict, as shown in the last row.

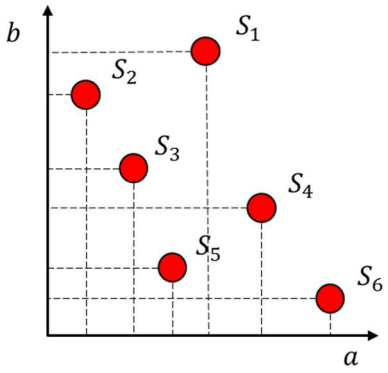

S_i $i = (1,2,\dots,n)$	Rank		$\lvert S'_{ia} - S'_{ib} \rvert$	$\lvert 2i - n - 1 \rvert$
	$S'_{ia} = R_{ia}$	$S'_{ib} = R_{ib}$		
S_1	4	6	2	5
S_2	1	5	4	3
S_3	2	4	2	1
S_4	5	3	2	1
S_5	3	2	1	3
S_6	6	1	5	5
			$C_{ab} = 16$	$C_{max} = 18$
			$Conflict = 88.9\%$	

Figure 4.6—An example of nonparametric-conflict calculation from six solutions in a two-objective minimisation problem.

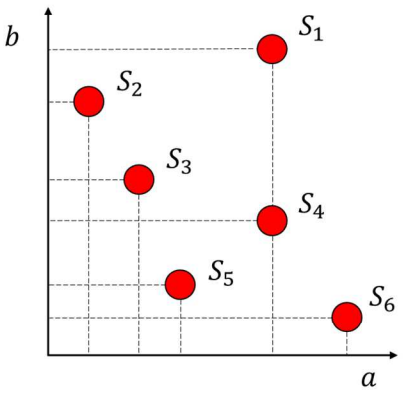

Scenario 1

S_i $i = (1,2,\dots,n)$	Rank		$\lvert S'_{ia} - S'_{ib} \rvert$	$\lvert 2i - n - 1 \rvert$
	$S'_{ia} = R_{ia}$	$S'_{ib} = R_{ib}$		
S_1	4	6	2	5
S_2	1	5	4	3
S_3	2	4	2	1
S_4	5	3	2	1
S_5	3	2	1	3
S_6	6	1	5	5
			$C_{ab} = 16$	$C_{max} = 18$
			$Conflict = 88.9\%$	

Scenario 2

S_i $i = (1,2,\dots,n)$	Rank		$\lvert S'_{ia} - S'_{ib} \rvert$	$\lvert 2i - n - 1 \rvert$
	$S'_{ia} = R_{ia}$	$S'_{ib} = R_{ib}$		
S_1	5	6	1	5
S_2	1	5	4	3
S_3	2	4	2	1
S_4	4	3	1	1
S_5	3	2	1	3
S_6	6	1	5	5
			$C_{ab} = 14$	$C_{max} = 18$
			$Conflict = 77.8\%$	

Figure 4.7—An example of how to break the ties on the rank from Solution 1 (S_1) and Solution 4 (S_4) from six solutions in the two-objective minimisation problem. Scenario 2 results in the least conflict between objectives a and b.

The ties in the rank calculation in a particular objective occur if there are solutions with the same objective value in that particular objective (i.e. solution S_1 and S_4 in objective a, as shown in Figure 4.7). We break these ties by use of the rank that causes the least conflict with the other objective being compared, as illustrated in Figure 4.7.

From these illustrations, we can infer that the nonparametric-conflict measure is:

- Insensitive to any previous non-disruptive normalisation;
- Useful when the objectives use either the same or different units and are either comparable or not;
- Useful when a value of importance of each objective cannot be inferred, but we want to understand the relationship between them.

The nonparametric-conflict measure reflects the degree by which lines would be crossing between objectives a and b in a parallel coordinate plot. Therefore, this metric can be used to formulate the measure of harmony, as defined in Equation (4.2). This harmony measure (H_{ab}) returns values that range between 0 and 1.

$$H_{ab} = 1 - \frac{C_{ab}}{c_{max}} \tag{4.2}$$

The nonparametric-conflict measure is more robust because it is less sensitive to any previous normalisation and it relies on fewer assumptions, such as of having different units of objectives without any conversion between them. It is robust to measure the conflict and to work with any data in general. Therefore, in this thesis we use nonparametric-conflict measures between all solutions generated from the initial run as the basis for objective grouping.

4.3.3 Proposed Objective-Grouping-Selection Technique

We proposed objective-grouping-selection technique for an improved multi-objective history matching. The technique consists of three steps, as shown in Figure 4.8.

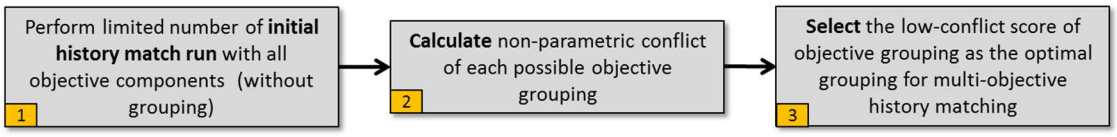

Figure 4.8—Proposed objective-grouping-selection technique for an improved multi-objective history matching dependent on nonparametric-conflict information between objectives.

In ***Step 1***, we perform a limited number of initial history-matching iterations with the multi-objective algorithm at hand without any grouping on the objective component. For instance, if we have a total 18 objectives or misfit components, we perform a limited number of history-matching iterations in a multi-objective with 18 objective functions. The reason behind this is the analogue to the studied optimisation problem in [253], [259]. By performing history-matching run without grouping, the problem structure or objective components relation in history-matching problem is more preserved than the one with any grouping scheme. We then use the solutions from the initial run to find the relationships between objectives, represented by the nonparametric-conflict scores between objectives.

The output from *Step 1* is the vector of objective values from all objective components. The number of element in each objective vector is determined by the number of iterations from the initial run.

In the literature, there is no formal study on how many initial iterations should be performed to identify the relationship between objectives in the multi-objective optimisation. Therefore, we conducted an initial experiment to determine how many initial iterations should be performed, presented in Section 4.4.1.5. This experiment suggested that 5–10% of intended iterations in the history matching can be used as starting point. For instance, if we want to run history matching with 500 iterations, we can use all solutions from 25 initial iterations (5% of 500) as an input to the next step. Note that although we performed this as a separate step, in a practical implementation, this information would be generated during the initial setup of a stochastic optimiser.

In ***Step 2***, we calculate the nonparametric-conflict score, by use of the formula in Table 4.2, of each possible objective grouping. In this study, we show how to group the objective components down to two objectives for use in the optimiser. The total number of objective-grouping combinations for two objectives can be calculated by

$$n_G = 2^{M-1} - 1 \tag{4.3}$$

where n_G is the number of total possibilities of objective grouping and M is the number of objective components. For instance, there will be $n_G = 3$ total possibilities of grouping from an $M = 3$ objectives problem to be reduced to the two objectives, as illustrated in Table 4.3.

Grouping	Objective 1	Objective 2
1	a	$b + c$
2	$a + b$	c
3	$a + c$	b

Table 4.3—An illustration of all $n_G = 3$ possibilities objective-grouping combinations from $M = 3$ objective components ($a, b,$ and c) to be grouped for a two-objective problem.

We provide the proof of (4.3) as below.

Proof (4.3). According to the *Binomial theorem*, it is possible to expand any power of $x + y$ into a sum of the form:

$$(x + y)^M = \sum_{k=0}^{M} \binom{M}{k} x^{M-k} y^k = \sum_{k=0}^{M} \binom{M}{k} x^k y^{M-k} \tag{4.4}$$

where

$$\binom{M}{k} = \frac{M!}{(M-k)!\,k!} \tag{4.5}$$

is a specific positive integer that gives the number of different combination of k elements that can be chosen from an M-element set and known as *binomial coefficient*. The final expression in Equation (4.4) follows from the previous one by the symmetry of x and y in the first expression, and by comparison it follows that the sequence of binomial coefficients in the formula is symmetrical. A simple variant of the binomial formula in Equation (4.4) is obtained by substituting 1 for both x and y. In this form, the formula reads:

$$2^M = \sum_{k=0}^{M} \binom{M}{k} \tag{4.6}$$

which states that there are 2^M subsets of an M-element set. Then, for every subset of M-element set except for { } and $\{M\}$, one gets partition with two non-empty sets and, there are $2^M - 2$ subsets. Because every (non-ordered) partition is counted twice, we can divide by 2 to obtain $= 2^{M-1} - 1$, as in Equation (4.3).

The number of possible objective groupings to be reduced to the two-objective problem increases exponentially with the total number of objectives, as suggested in Equation (4.3). For instance, there will be $n_G = 511$ total possibilities of grouping from an $M = 10$ objectives problem to be reduced to a two-objective problem; $n_G = 16{,}383$ possibilities from an $M = 15$ objectives problem; and $n_G = 524{,}287$ possibilities from an $M = 20$ objectives problem. In a petroleum reservoir with tens or hundreds of wells, the number of possibilities of objective grouping in the multi-objective history matching is enormous. This results in a challenge on how to select which objective-grouping combination for a good performance of history matching.

The output *Step 2* is a pool of objective-grouping combinations (total of n_G combinations) with a nonparametric-conflict score attached to each grouping combination.

In **S*tep 3***, we select the low nonparametric-conflict score of objective-grouping combination as the optimal grouping. For instance, for grouping schemes in Table 4.3, if Grouping 1 has relatively lower nonparametric-conflict score amongst other grouping combinations, we select Grouping 1 as the optimal grouping.

The output of *Step 3* is the selected optimal grouping combinations for an improved multi-objective history-matching performance (faster convergence and higher match quality).

4.3.4 Performance Measures and Statistical-Significance Test

We evaluate the performance of the history matching with different groupings by use of their misfit convergences, final misfit values, and speedup ratio (SUR). We then perform statistical-significance tests to evaluate the significance of the improvement. For each of these measures and tests, we use a related plot for the comparison study.

4.3.4.1 Misfit Convergence, Final Misfit Value, and SUR

Because one of the primary goals in history matching assisted by the optimisation algorithm is to obtain reservoir models with the lowest misfit value, we look at the minimum or best-so-far misfit-value convergence plot over iterations. In this thesis, the misfit is the sum (with equal unity weights) of the predefined objective functions for each case study. Because the algorithm is stochastic, we repeat the experiments 10 times and then compute the mean and standard deviation (SD) of the results to ensure that stochastic variability does not alter the conclusions.

In this chapter, we also perform the bootstrap [263] on the mean final misfit value from each grouping to obtain a more-robust comparison between groupings on the final outcome of history matching. Ideally, the statistical measure (mean or SD) to compare between groupings should come from a large number of samples for a robust comparison. However, in history matching, the computational cost can be expensive to obtain a large number of samples or trial runs. In the present study, for reasons of computational cost, we only perform 10 replicates of each history match for each objective-grouping scheme. Therefore, we use a bootstrap-resampling technique to cope with a small sample of history-matching trial runs, as described below.

In a bootstrap, we repeatedly sample (with replacement) from the pool of N samples to create another "N samples" for several times (usually a high number, such as 10,000 times to reduce the resampling error). We then use these bootstrapped resamples to compute the sampling distribution of the statistics in which we are interested (mean or SD). Let $\mathbf{X} = (X_1, X_2, \ldots, X_N)$ be the original N samples, and $\theta = S(\mathbf{X})$ is the statistic (i.e.

mean or SD) of the original samples. The bootstrap technique resamples from the original sample $\mathbf{X}$ to create b bootstrap resamples with length of N for each resample; i.e. $\mathbf{X}^* = \{\mathbf{X}^{1*}, \mathbf{X}^{2*}, \dots, \mathbf{X}^{b*}\}$, with $\mathbf{X}^{i*} = (X_1^*, X_2^*, \dots, X_N^*)$ and $i = (1,2, \dots, b)$. Then, the statistic for each bootstrap resample is computed and the distribution of these statistics is constructed, i.e. $\theta^* = S(\mathbf{X}^*) = \{S(\mathbf{X}^{1*}), S(\mathbf{X}^{2*}), \dots, S(\mathbf{X}^{b*})\}$. Finally, the mean and SD of this bootstrapped-resampling distribution can be computed.

Finally, we use a metric to evaluate the convergence-speed ratio of misfit-value evolutions between different objective groupings, called the SUR, as illustrated in Figure 4.9 and given by Equation (4.7) comparing Groupings *A* and *B*.

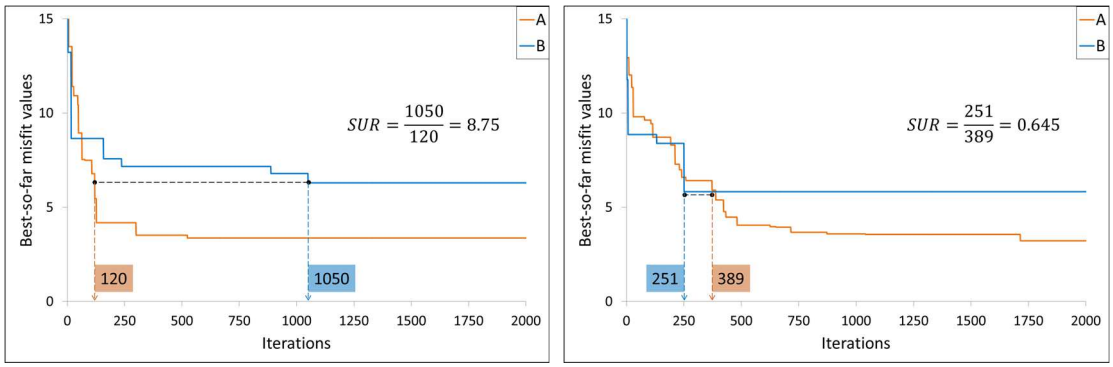

Figure 4.9— An example of the SUR calculation from history-matching runs with Groupings *A* to *B*. The SUR is calculated at the maximum of the lowest misfit values of history-matching results with Groupings A and B.

$$SUR_m = \frac{(n_{iter})_B}{(n_{iter})_A} \tag{4.7}$$

where SUR_m is the SUR of history matching with Groupings *A* to *B* at misfit value *m*, and $(n_{iter})_B$ and $(n_{iter})_A$ are the number of iterations to reach misfit *m* from Groupings *B* and *A*, respectively. It is worth to point out that the misfit value *m* is the maximum of the lowest misfit values between grouping *A* and *B*, and the number of iterations are taken at the first time of each grouping reach this misfit value, as illustrated in Figure 4.9. By this, we can get a fair pairwise comparison to the grouping that never reach the misfit value by the other grouping.

4.3.4.2 Statistical-Significance Test

The use of a statistical test has become a widespread technique in computational intelligence to confirm whether a new proposed method or algorithm offers a significant improvement, or not, over the existing methods for a given problem. In our case, these are the performances of different grouping schemes in the multi-objective history matching.

In this study, hypothesis testing is used for the statistical-significance test. The aim is to draw inferences regarding one or more populations from given samples or results that comprise the definition of two hypotheses: the null hypothesis H_0 and the alternative hypothesis H_1. The null hypothesis is a statement of no difference or no effect, whereas the alternative hypothesis represents the presence of a difference or an effect (in our case, significant differences or improvements between different objective groupings). A level of significance α is then used to determine at which level the hypothesis is rejected when applying this statistical procedure to reject a hypothesis.

The smallest level of significance that results in the rejection of H_0 can be computed instead of specifying an a priori level of significance α. This is the definition of the *p*-value, which is the probability of obtaining a result at least as extreme as the one that was actually observed, assuming that H_0 is true. A *p*-value provides information whether a hypothesis test is significant and indicates how significant the result is (i.e. the smaller *p*-value, the stronger the evidence against H_0). In this thesis, the level of significance $\alpha = 0.05$ is used such that the improvement of one grouping to the other one is significant if the *p*-value is less than 0.05, whereas if the *p*-value value is equal or more than 0.05, the improvement is not significant [264].

In this thesis, the Wilcoxon signed rank test procedures are conducted on pairwise comparison between 10 trial history-matching runs from two different groupings, respectively, for all iterations. The Wilcoxon signed rank significance test and its computation of *p*-value is usually included in well-known statistical-software packages, such as R.

The Wilcoxon signed rank test [265] is used to evaluate the significance improvement of history matching by one grouping to the other. It is a nonparametric statistical procedure in hypothesis testing used for answering the following questions: Do two samples of groupings generate two different history-matching performances, and if so, how significant is the difference or improvement? It is analogous to the paired *t*-test in nonparametric statistical tests. However, as suggested by Derrac *et al.* [266], the Wilcoxon signed rank test is more robust and safer than the paired *t*-test because it does not assume a normal distribution. Derrac *et al.* [266] also noted that the outliers have less effect on the Wilcoxon signed rank test than on the paired *t*-test.

In this chapter, the Wilcoxon signed rank test procedures are conducted on pairwise comparison between 10 trials of the history-matching run from two different groupings, respectively, for all iterations. The test procedure is described as follows. Let d_i be the difference between the misfit values of the two groupings on ith out of n pairs (each pair is selected randomly and independently from each grouping). Then, the differences are ranked dependent on their absolute values; in case of ties, use the average of rank (for instance, if two differences are tied in the assignation of Ranks 2 and 3, assign Rank 2.5 to both differences) and continue the rank assignment from Rank 4 as Rank 2 and 3 are both occupied by Rank 2.5. Let R^+ be the sum of ranks for the problems in which the first grouping outperformed the second (i.e. $d_i < 0$), let R^- be the sum of ranks for the opposite (i.e. $d_i > 0$), and let ranks of $d_i = 0$ be split evenly amongst the sums, as in Equation (4.8).

$$R^+ = \sum_{d_i<0} \text{rank}(d_i) + \frac{1}{2}\sum_{d_i=0} \text{rank}(d_i)$$
$$R^- = \sum_{d_i>0} \text{rank}(d_i) + \frac{1}{2}\sum_{d_i=0} \text{rank}(d_i) \tag{4.8}$$

Whichever of the sums in Equation (4.8) is the smaller is the test statistic value T; i.e. $T = \min(R^+, R^-)$. If T is less than or equal to the critical value of the distribution of Wilcoxon's test (see for example Statistical Table 8.1 in [267]), the H_0 is rejected. This means that a given grouping outperforms the other one with the associated *p*-value to determine its significance.

4.4 Field Applications

We have applied the proposed objective-grouping-selection technique to two case studies of multi-objective history matching on an industry-standard reservoir model for benchmarking and a real-field case study. We have tested the proposed technique to group the objective components into two-objective history matching. For both case studies, we used MOPSO [7] with the following algorithm parameters [123]:

- Number of particles : 20
- Inertia weight, w : 0.729
- Cognitive component, c_1 : 1.494
- Social component, c_2 : 1.494

4.4.1 Case Study 1: PUNQ-S3

We applied the proposed objective-grouping technique to the history-matching problem of the PUNQ-S3 reservoir [235]. We used the same data sets from [243], the Set-1 model parameterisation described in Chapter 3, and the same misfit definition described in Equation (4.1).

4.4.1.1 Objective Grouping in Multi-Objective History Matching

As the first step in the proposed objective-grouping-selection technique, we perform an initial history-matching run without any grouping for 100 iterations because we intend to run the history matching for 2,000 iterations (100 is 5% of 2,000, as described in Section 4.4.1.5). In *Step 2*, we use the solutions from the first step to calculate the nonparametric conflict for each possible objective grouping. As suggested by Equation (4.3), 131,071 possible-objective-grouping combinations can be generated from 18 objective components to make the problem become a two-objective one. In *Step 3*, we select the low-conflict objective grouping as the optimal grouping for multi-objective history matching. We then select another grouping that has the high-conflict score to contrast the results. Table 4.4 describes both low- and high-conflict groupings on the PUNQ-S3 case study.

Group ID	Objective 1	Objective 2	Conflict (%)
Low	WBHP[12] + WGOR[4,5,11,15]	WBHP[1,4,5,11,15] + WGOR[1,12] + WWCT[1,4,5,11,12,15]	39.1
High	WWCT[15]	WBHP[ALL] + WGOR[ALL] + WWCT[1,4,5,11,12]	83.6

Table 4.4—The description of low- and high-conflict-score groupings on PUNQ-S3. The number in brackets indicates the well number in the model; as an example, WBHP[12] refers to the misfit of WBHP at well PRO12.

4.4.1.2 Results

Misfit Convergence, Final Misfit Value, and SUR

Figure 4.10 shows the mean and SD of the best-so-far misfit values from 10 runs of low- and high-conflict groupings. On average, history matching with low- and high-conflict groupings has the same misfit convergence on the first few iterations (during the random-search stage in the algorithm), and the low-conflict grouping outweighs the high-conflict grouping afterwards. Moreover, the lower bound of best-so-far misfit values from high-conflict grouping is mostly above the mean of low-conflict grouping and the upper bound of best-so-far misfit values from low-conflict grouping is mostly below the mean of high-conflict grouping.

We performed 10,000 bootstrap resamplings on the mean final misfit value from 10 trials of each grouping, as shown in Figure 4.11. We can see that on average, the low-conflict grouping provides a lower bootstrapped mean final misfit value than high-conflict grouping. The SD of the bootstrapped mean final misfit value from low-conflict grouping is also smaller than the high-conflict grouping. In this sense, history matching with low-conflict grouping provides higher-match-quality models (lower mean final misfit value) and more-robust misfit evaluations than the high-conflict grouping towards stochastic nature of the algorithm (i.e. smaller SD of mean final misfit value).

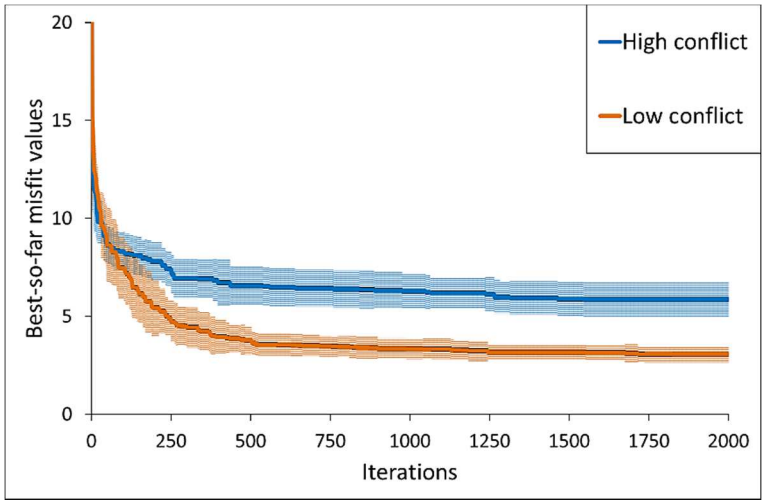

Figure 4.10—Mean and SD of the best-so-far misfit value over 10 trials of multi-objective history matching with low- and high-conflict-score groupings on PUNQ-S3.

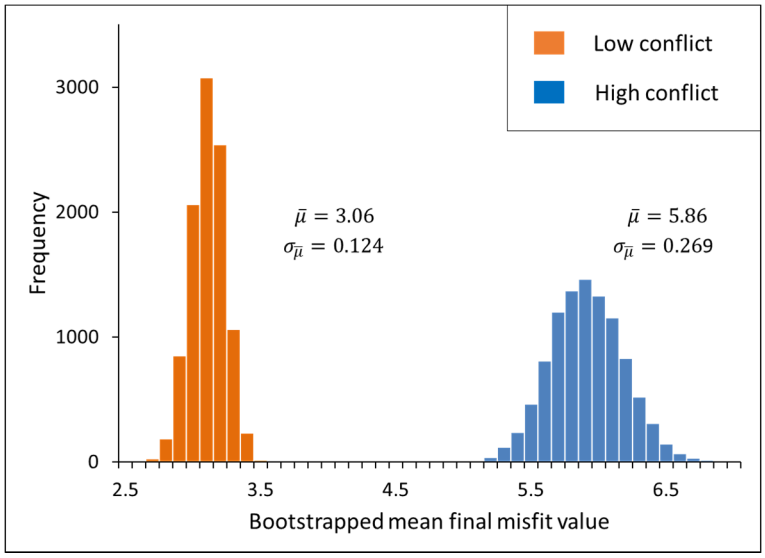

Figure 4.11—Histogram of the bootstrapped mean final misfit values (*b*=10,000 resamples) from 10 trials of multi-objective history matching with low- and high-conflict-score groupings on PUNQ-S3.

We then calculated the SUR of low/high-conflict grouping, as described in Equation (4.7). Out of 10 trials from each low- and high-conflict grouping, respectively, we can derive 100 pairwise comparisons between low- and high-conflict groupings. We then computed the SUR from these 100 pairwise comparisons. Figure 4.12 shows the histogram of these 100 SURs comparing history matching with low/high-conflict grouping. On average, the SUR between low/high-conflict grouping is 7.92 over these 100 pairwise runs.

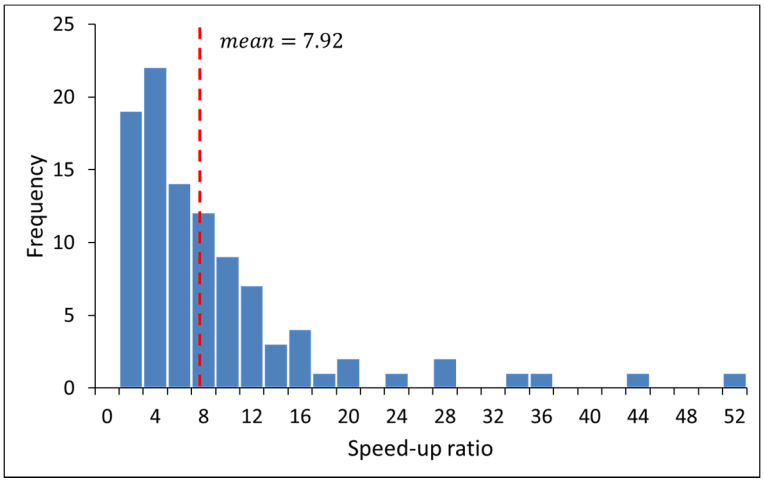

Figure 4.12—Histogram of SUR from history matching with low- to high-conflict groupings on PUNQ-S3. 100 SURs are derived from pairwise comparison of 10 trials of history matching from each grouping.

Statistical Significance of Observed Differences

The significant improvement of the low-conflict grouping from high-conflict grouping is shown in Figure 4.10. We evaluated the statistical significance of this difference by use of the Wilcoxon signed rank test on 10 trials of each grouping with the significance threshold of 0.05 (p-value < 0.05). We took the negative logarithmic value of p-value and plotted over all iterations, as shown in Figure 4.13. In this case, the significant threshold is converted to $-\log(0.05)$ which is 1.30, above which the improvement is significant.

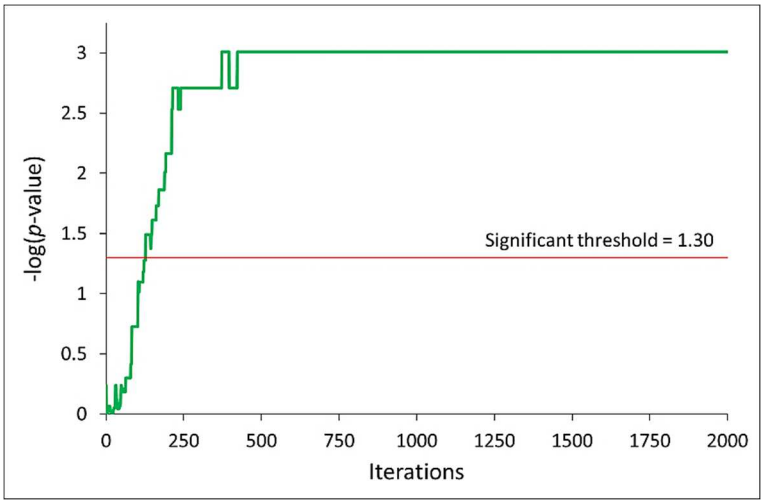

Figure 4.13—Significant level of history matching with low-conflict to high-conflict groupings over 10 trials of history matching on PUNQ-S3.

We can see from Figure 4.13 that the history matching from low-conflict grouping is not significantly different from the high-conflict grouping for the first 125 iterations, and it improves significantly for the rest of the iterations. This plot is aligned with the result in Figure 4.10, where the upper bound of best-so-far misfit value from low-conflict grouping starts to be below the mean of high-conflict grouping at approximately Iteration 125.

Reservoir Engineering Perspective

The superiority of multi-objective history matching from the low-conflict grouping with the high conflict is also assessed by comparing simulated production data from the matched models to the observed production data at the well level. The simulated production data at several wells from the five-best matched models by each grouping are plotted as in Figure 4.14. Each of five curves in a graph represents the iteration number for that particular model as in the legend of the plot.

We can see from Figure 4.14 that all five-best matched models from the low-conflict grouping match well all the observed production data. On the other hand, most of the five-best matched models from high-conflict grouping fail to match some of the observed production data. Moreover, the low-conflict history matching provides the best matched models faster than high conflict (at Iterations 810–1,134 for low conflict, whereas for high conflict, are higher than Iteration 1,545 to provide equally good matched models).

These results demonstrate that history matching with low-conflict grouping is able to provide an ensemble of best matched models that can match observed production data locally better and faster than the high-conflict grouping.

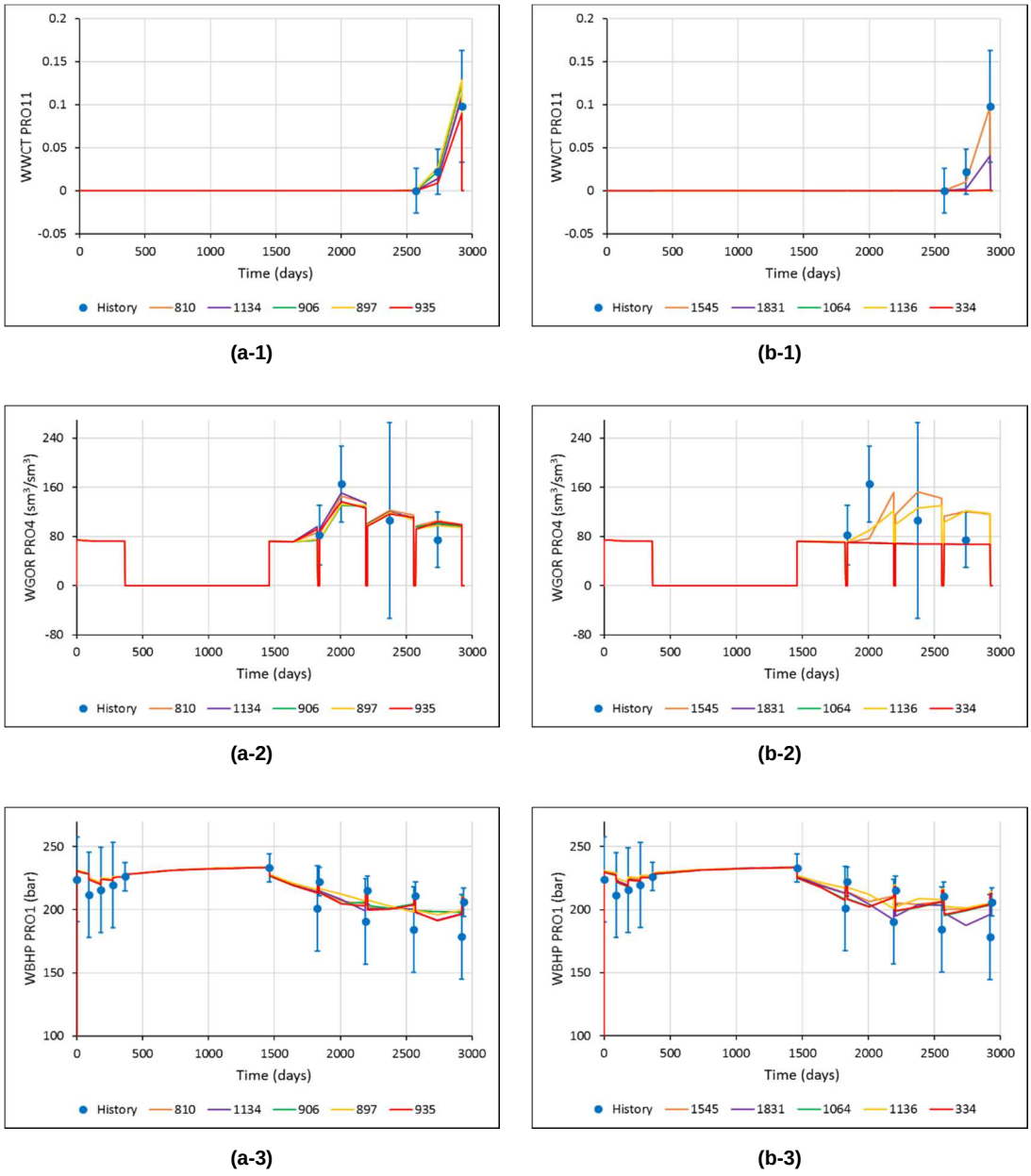

Figure 4.14—History-matching results on production data at several producer wells from (a) low- and (b) high-conflict groupings on PUNQ-S3. Each plot shows the five-best matched models as different coloured lines, the observed production data as blue dots, and data SD as a blue vertical line. Numbers in the legend are the iterations number of the five-best models.

4.4.1.3 Low-Conflict Grouping with Other Groupings

We randomly selected 10 groupings on PUNQ-S3 covering a wide range of conflict score, as described in Table 4.5. The optimal grouping is identified as the one with the relatively low conflict. We then ran the history matching for 10 times for each respective grouping.

Group ID	Objective 1	Objective 2	Conflict (%)
1	WBHP[12] + WGOR[4,5,11,15]	WBHP[1,4,5,11,15] + WGOR[1,12] + WWCT[1,4,5,11,12,15]	39.1
2	WBHP[1,4,12] + WGOR[1,4,12] + WWCT[1,4,12]	WBHP[5,11,15] + WGOR[5,11,15] + WWCT[5,11,15]	46.2
3	WBHP[4,11,12]	WBHP[1,5,15] + WGOR[ALL] + WWCT[ALL]	54
4	WBHP[5] + WGOR[4,15]	WBHP[1,4,11,12,15] + WGOR[1,5,11,12] + WWCT[ALL]	59
5	WBHP[1,4,11] + WGOR[1,11,12] + WWCT[4,12,15]	WBHP[5,12,15] + WGOR[4,5,15] + WWCT[1,5,11]	63.6
6	WBHP[1] + WGOR[1] + WWCT[15]	WBHP[4,5,11,12,15] + WGOR[4,5,11,12,15] + WWCT[1,4,5,11,12]	69
7	WBHP[1,4,5,12,15] WGOR[1,11,12,15] + WWCT[1,5,12]	WBHP[11] WGOR[4,5] + WWCT[4,11,15]	72.6
8	WWCT[4,15]	WBHP[ALL] + WGOR[ALL] + WWCT[1,5,11,12]	76.9
9	WBHP[ALL] + WGOR[1,4,5,11,15] + WWCT[5,11]	WGOR[12] + WWCT[1,4,12,15]	79
10	WWCT[15]	WBHP[ALL] + WGOR[ALL] + WWCT[1,4,5,11,12]	83.6

Table 4.5—The description of 10 randomly selected groupings on PUNQ-S3, covering a wide range of conflict score for sensitivity study. The number in brackets indicates the well number in the model.

Final Misfit Value

We performed bootstrap resampling with 10,000 samples on the mean final misfit value on each grouping with the sample size of 10 for each resampling and calculated the mean and SD from the bootstrapped resamples, as shown in Table 4.6. We can see from this table that the history matching with low-conflict score provides lower mean final misfit values than high-conflict score. Even though there are similar SD amongst groupings, there is a slightly lower SD value of the lowest conflict than the highest conflict which demonstrates the robustness of the lowest-conflicted grouping.

Correlation Between Final Misfit Value and Conflict Score

We evaluated the correlation between final misfit value and conflict score by use of the 10 groupings described in Table 4.5. Figure 4.15 (a) shows the plot of bootstrapped mean final misfit value against the conflict score. We can see from this figure that the final

misfit value is less sensitive to the choice of grouping for low-conflict scores (less than 57% in this case), whereas for higher conflict scores the choice of grouping affects the performance of history matching. Nonetheless, there is a high positive monotonic relationship between final misfit value and the conflict score with Spearman's rank correlation of 0.988, as shown in Figure 4.15 (a).

Group ID	$\bar{\mu}$	$\sigma_{\bar{\mu}}$
1	3.060	0.124
2	3.198	0.178
3	3.110	0.168
4	3.304	0.131
5	3.518	0.184
6	3.619	0.109
7	4.423	0.164
8	4.957	0.272
9	5.393	0.171
10	5.866	0.269

Table 4.6—Mean and SD of the bootstrapped mean final misfit values (*b*=10,000 resamples) for each grouping described in Table 4.5.

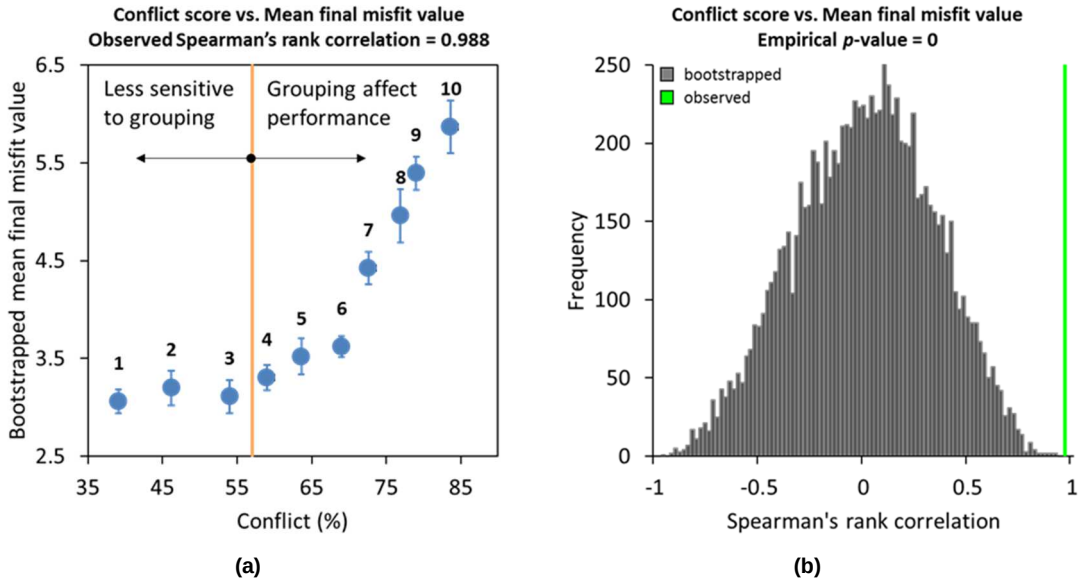

(a) **(b)**

Figure 4.15—Mean and SD of bootstrapped mean final misfit values (*b*=10,000 resamples) over 10 trials of the history-matching run vs. conflict score from 10 randomly selected groupings (a), and Histogram of 10,000 Spearman's rank correlations derived from bootstrap resampling on shuffled 10 groupings (b), on PUNQ-S3, as described in Table 4.5. The real observed correlation is shown as a green line.

We tested whether the observed value of Spearman's rank correlation is significantly different from zero (the case when there is no relationship between conflict score and final misfit value). We performed 10,000 bootstrap resamplings on the shuffled 10 groupings and computed the correlation on each resample. We then calculated the number of resamples that have correlations greater than or equal to the observed value in the form of probability or *p*-value. Figure 4.15 (b) shows the histogram of the Spearman's rank correlation from these bootstrapped resamples compared with the observed value. We can see from this figure that there are no bootstrap resamples with correlation higher than or equal to the observed value (*p*-value = 0). We can infer from these results that the correlation between final misfit value and conflict score is highly significant and has not happened by chance.

4.4.1.4 Sensitivity Test for the Optimal Grouping Selection

We performed sensitivity analysis of the effect of the random selection of the groupings by randomly selecting another 10 different groupings covering a wide range of conflict scores, as described in Table 4.7. We conducted the same computation as before, i.e. mean final misfit value bootstrapping and final misfit value vs. conflict score correlation evaluation, and plotted the results, as shown in Table 4.8 and Figure 4.16, respectively.

We found similar results from the sensitivity study that the low-conflict history matching provides lower mean final misfit value than the high-conflict grouping, as shown in Table 4.8.

Figure 4.16 (a) shows that the conflict-score boundary is approximately 57%, less than when the choice of grouping is less sensitive to the final misfit value and higher than when the choice of grouping affects the performance in history matching. There is also a high positive monotonic relationship between final misfit value and conflict score from this sensitivity study with the Spearman's rank correlation of 1.0, as shown in Figure 4.16 (b).

Group ID	Objective 1	Objective 2	Conflict (%)
S1	WBHP[1,4,5,11,15] + WGOR[1] + WWCT[4,5,11,15]	WBHP[12] + WGOR[4,5,11,12,15] + WWCT[1,12]	39.2
S2	WBHP[1,4,5,11,15] + WGOR[1,5,15] WWCT[5,11,12]	WBHP[12] + WGOR[4,11,12] + WWCT[1,4,15]	43
S3	WBHP[1,5,15] + WWCT[4,11,15]	WBHP[4,11,12] + WGOR[ALL] + WWCT[1,5,12]	49
S4	WBHP[1,4,5,15] + WGOR[1,4,5,11] + WWCT[4,5,12]	WBHP[11,12] + WGOR[12,15] + WWCT[1,11,15]	56
S5	WBHP[1,5] + WGOR[5,11,15] + WWCT[1,11,12]	WBHP[4,11,12,15] WGOR[1,4,12] + WWCT[4,5,15]	61
S6	WBHP[1] + WGOR[5,12,15] + WWCT[1,15]	WBHP[4,5,11,12,15] WGOR[1,4,11] + WWCT[4,5,11,12]	66
S7	WBHP[1] + WGOR[5,12,15] + WWCT[4,5,11,12,15]	WBHP[4,5,11,12,15] + WGOR[1,4,11] + WWCT[1]	70
S8	WBHP[ALL] WGOR[ALL] + WWCT[5,11,12]	WWCT[1,4,15]	77
S9	WBHP[ALL] + WGOR[1,4,5,11,15] + WWCT[11]	WGOR[12] + WWCT[1,4,5,12,15]	80
S10	WBHP[ALL] WGOR[ALL] + WWCT[4,5,11,12]	WWCT[1,15]	83.4

Table 4.7—The description of another 10 randomly selected groupings on PUNQ-S3, covering a wide range of conflict score for sensitivity study. The number in brackets indicates the well number in the model.

Group ID	$\bar{\mu}$	$\sigma_{\bar{\mu}}$
1	3.093	0.124
2	3.103	0.117
3	3.110	0.181
4	3.208	0.238
5	3.401	0.137
6	3.525	0.114
7	4.253	0.208
8	4.955	0.272
9	5.416	0.117
10	5.815	0.267

Table 4.8—Mean and SD of the bootstrapped mean final misfit values (*b*=10,000 resamples) for each grouping described in Table 4.7.

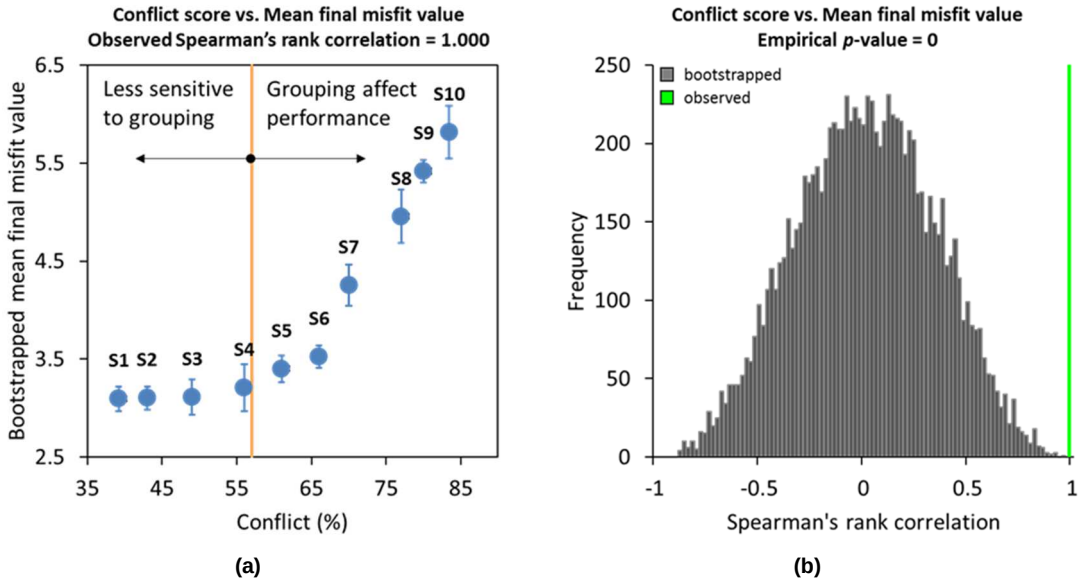

Figure 4.16—Mean and SD of bootstrapped mean final misfit values (*b*=10,000 resamples) over 10 trials of the history-matching run vs. conflict score from 10 randomly selected groupings (a), and Histogram of 10,000 Spearman's rank correlations derived from bootstrap resampling on shuffled 10 groupings (b), on PUNQ-S3, as described in Table 4.7. The real observed correlation is shown as a green line.

4.4.1.5 Sensitivity Analysis on the Initial Run

In this section, we report the sensitivity study on the number of iterations required in the initial history-matching run in *Step 1* of the proposed grouping selection technique shown in Figure 4.8.

In *Step 1* of the proposed technique, we perform a limited number of initial history-matching iterations, which are used in the next step. We may ask how many iterations should be performed in this initial run so we still can select the optimal grouping from the pool of all grouping combinations. Because we are interested in the low-conflict grouping combinations, we limit the search of selecting the optimal grouping in the top 1 or 5% of the total number of groupings. In other words, we consider what the probability is that the optimal grouping will be in the top 1 or 5% of the total groupings if we use a different number of iterations for the initial run.

To answer this question, we performed a sensitivity test on the number of iterations in the initial history-matching run against the probability of the optimal grouping in the top 1 or 5% of the total groupings. The number of iterations is represented with the percentage of the total of intended history-matching iterations. For instance, if we intend

to perform history matching with n iterations as the stopping criterion, the number of iterations in the initial run is represented by the percentage from n iterations.

We used the PUNQ-S3 case study with stopping criterion of 2,000 iterations in this sensitivity test. We performed a different number of iterations on the initial run—20, 40, 60, 80, 100, 120, 140, 160, 180, 200, 400, and 600 iterations—that represent the percentage of initial run of 1, 2, 3, 4, 5, 6, 7, 8, 9, 10, 20 and 30%, respectively, from 2,000 iterations. The runs were repeated for 10 times for each percentage scheme because of the stochastic nature of the algorithm. We then chose the five-best groupings depending on the lowest conflict score from the top 1% pool of a total number of groupings. We calculated the probabilities of these best groupings would appear in the top 1% pool of total possible-grouping combinations out of 10 trials of history-matching run for each percentage scheme.

Figure 4.17 (a) shows the probability to find the five-best groupings in the top 1% pool of total possible-grouping combinations under different percentages of the initial run. Figure 4.17 (a) shows that it requires 5–10% of the intended history-matching iterations for the initial run to have a high probability of selecting the best objective-grouping combinations. It also shows that adding more iterations (more than 10%) in the initial run does not significantly increase the probability to select the best groupings.

We then increase the pool size of selecting the best groupings from 1 to 5% of the total number of groupings to see the sensitivity on the probability of finding the best groupings. For instance, if we have 1,000 possible-objective-grouping combinations, the top 1% pool represents 10 groupings with the low conflict, whereas the top 5% pool has 50 groupings with low conflict. Figure 4.17 (b) shows the sensitivity on the probability of selecting these five-best groupings by increasing the pool of objective-grouping combinations from the top 1% to top 5% from total groupings. Figure 4.17 (b) shows that our chance to select the five-best groupings is increased if we increase the pool size from the top 1% to the top 5% of the total possible-grouping combinations. Figure 4.17 (b) also suggests that it requires 5–10% of the intended history-matching iterations for the initial run to have a high probability of selecting the best objective-grouping combinations. Moreover, adding more iterations (more than 5%) in the initial run of the

intended history-matching run does not significantly increase the probability to select the best groupings.

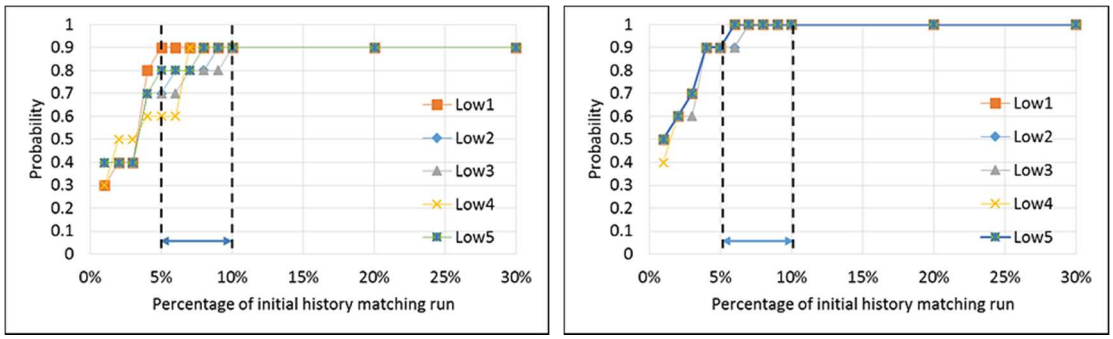

Figure 4.17—(a) Probability to select five low-conflict groupings in the top 1% pool of total possible-grouping combinations in PUNQ-S3 history matching. (b) Probability to select five low-conflict groupings in the top 5% pool of total possible-grouping combinations in PUNQ-S3 history matching.

4.4.2 Case Study 2: Zagadka Field, Western Siberia

We applied the proposed technique to the real-field case study to see its applicability in a real and more complex reservoir.

4.4.2.1 Field and History-Matching Overview

The Zagadka Field is located in western Siberia and is a medium-size oil field. It has 95 wells, some of which have 10–15 years of history, in nine groups. The field is produced by a combination of waterflooding and aquifer drive. The reservoir model has approximately 100,000 active grid cells. The field is compartmentalised with possible sealing faults creating seven compartments. Figure 4.18 shows the multiplier region map of the Zagadka Field reservoir model.

We used the same model parameterisation described in [9] for the history-matching study. The parameterisation depicts geological structure zonation of the field. It has 19 parameters: seven global k_h multiplier, one global k_v multiplier, three capillary pressure (P_c) values, four oil relative permeability (k_{ro}) values, one water relative permeability (k_{rw}) value, one fault transmissibility, and two aquifer-support multipliers. Table 4.9 gives the description and prior range of these parameters.

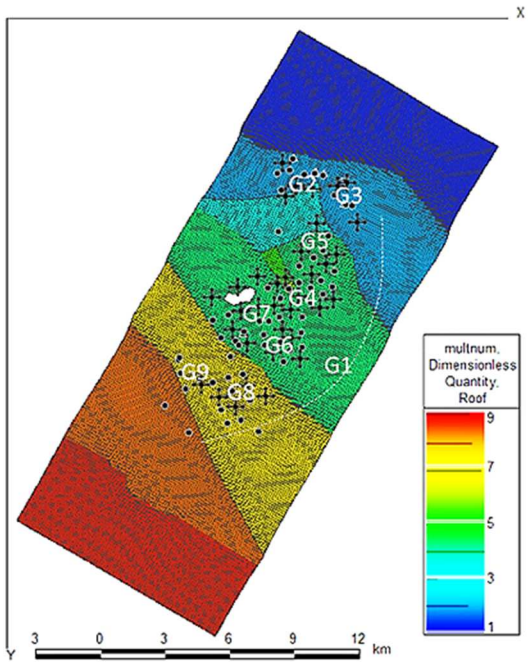

Figure 4.18—Zagadka Field region map showing the location of well groups.

Parameter	Number	Range
k_h multiplier	7	1–30
k_v multiplier	1	0.1–0.9
Capillary pressure 1	1	18–23
Capillary pressure 2	1	9–13
Capillary pressure 3	1	1.01–3.0
Oil relative permeability 1	1	0.5–1
Oil relative permeability 2	1	0.6–0.9
Oil relative permeability 3	1	0.1–0.3
Oil relative permeability 4	1	0.02–0.095
Water relative permeability	1	0.2–1.25
Fault transmissibility	1	0.0–1.0
Aquifer-support multiplier	2	2.5–4.5

Table 4.9—Parameters and prior range in the model parameterisation of the Zagadka Field case study.

In the Zagadka Field, all wells are grouped into nine groups, G1–G9, dependent on the geological structure, fault block in the model, and the time when the wells are drilled. Wells in Group G1 are the exploration wells in different regions across the field, whereas wells in the other groups are clustered in particular regions of the field following the drilling schedule. The wells are drilled progressively from northeast/southwest direction in the field.

We use the group level of historical data of oil rate (GOPR) and water rate (GWPR) for history matching. The objective function to be minimised is defined as

$$M = \sum_{i}^{n_g} \sum_{j}^{n_p} w_{ij} \sum_{k}^{n_t} \frac{\left(obs_{ijk} - sim_{ijk}\right)^2}{2\sigma_{ijk}^2} \tag{4.9}$$

where n_g is the number of groups, n_p is the number of observed production data, n_t is the number of timesteps for the jth history data, obs is the observed history, sim is the simulated value, σ^2 is the variance of the measurement errors, and w is the weight factor. We can see from Equation (4.9) that there are 18 misfit components in the Zagadka Field (misfits from nine groups with two production data from each group to match).

4.4.2.2 Objective Grouping in Multi-Objective History Matching

We applied the proposed objective-grouping-selection technique shown in Figure 4.8 for multi-objective history matching of Zagadka Field. An initial history-matching run of 25 iterations was used to calculate the conflict between objective-grouping combinations because we intend to run the history matching for 500 iterations (5% criterion). We then selected the low-conflict grouping for history matching and contrasted the results with the high-conflict one, as described in Table 4.10.

Group ID	Objective 1	Objective 2	Conflict (%)
Low	GOPR[G1+G2+G3+G9] + GWPR[G6]	Rest	19.5
High	GOPR[G3+G8] + GWPR [G3+G8]	Rest	85.8

Table 4.10—The description of low- and high-conflict-score groupings in the Zagadka Field. G1, G2, …, G9 refer to the groups of wells in the model.

4.4.2.3 Results

We report the results of the objective-grouping study on Zagadka Field case study with the same computation procedure as on PUNQ-S3 reservoir model. We evaluate misfit convergence, final misfit value and SUR between low- and high-conflict groupings.

Misfit Convergence, Final Misfit Value, and SUR

Figure 4.19 through Figure 4.21 show the results from 10 runs of history matching from low- and high-conflict groupings.

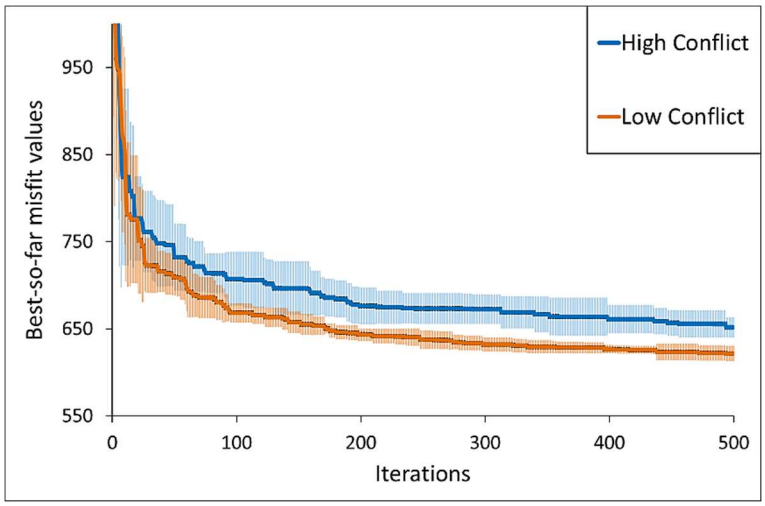

Figure 4.19—Mean and SD of the best-so-far misfit value over 10 trials of multi-objective history matching with low- and high-conflict-score groupings on Zagadka.

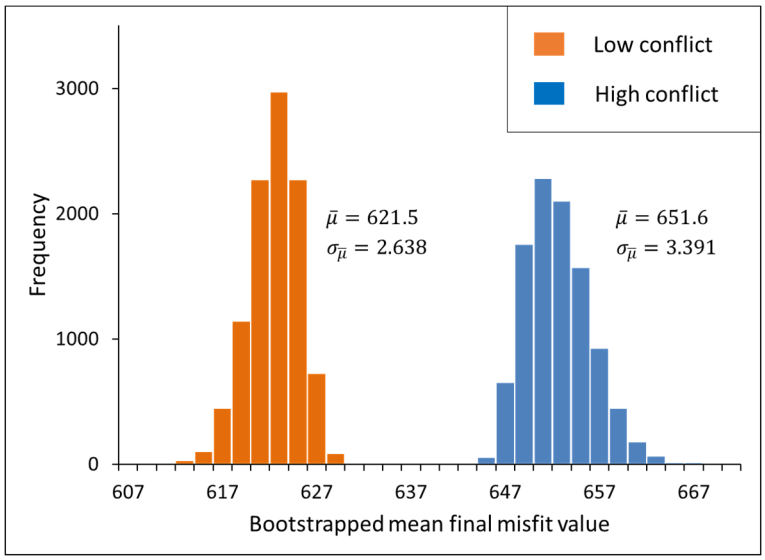

Figure 4.20—Histogram of the bootstrapped mean final misfit values (n=10,000 resamples) with a sample size of ten from ten trials of multi-objective history matching with low- and high-conflict-score groupings on Zagadka.

We can see from Figure 4.19 that the mean of best-so-far misfit value from low-conflict grouping is similar to the high-conflict grouping during the early iterations, and it separates from the high-conflict grouping afterwards. The lower bound of the best-so-

far misfit values from the high-conflict grouping is mostly above the mean of low-conflict grouping and the upper bound of the best-so-far misfit values from low-conflict grouping is mostly below the mean of high-conflict grouping.

The low-conflict grouping provides a lower mean and SD of bootstrapped mean final misfit value than high-conflict grouping, as shown in Figure 4.20. This implies that the history-matched models from low-conflict grouping are better in match quality and more robust towards the randomness of stochastic optimiser than the ones from high-conflict grouping.

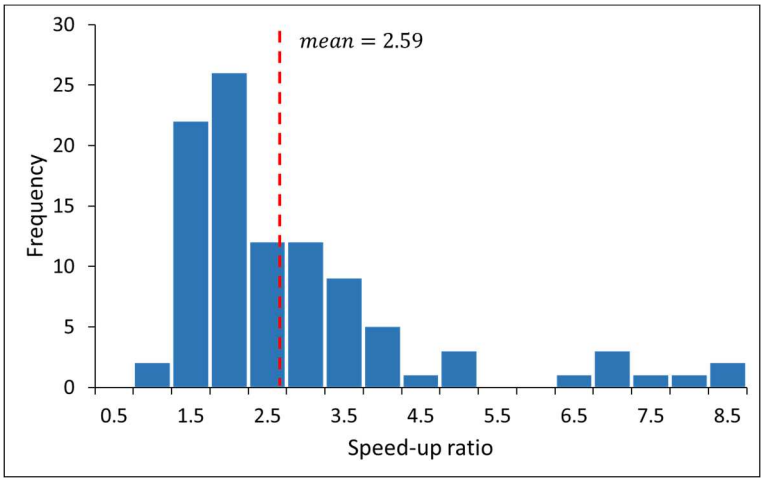

Figure 4.21—Histogram of SUR from history matching with low- to high-conflict groupings on Zagadka. 100 SURs are derived from a pairwise comparison of 10 trials history matching from each grouping.

The history matching with low-conflict grouping also provides faster misfit convergence than high-conflict grouping with an average SUR of 2.59, as shown in Figure 4.21. This implies that history matching with low-conflict grouping obtains good matched models faster than the history matching with high-conflict grouping.

In summary, the results presented in Figure 4.19 through Figure 4.21 demonstrate that history matching with low-conflict grouping provides higher-match-quality models (lower mean final misfit value), more-robust misfit evaluations towards the stochastic nature of the algorithm (smaller SD of mean final misfit value), and faster misfit convergence than high-conflict grouping in the real-field case study.

Statistical-significance Test

The significant improvement of the low-conflict grouping from high-conflict grouping is observed on the Zagadka Field case study, as shown in Figure 4.22. Aligned with the result in Figure 4.19, Figure 4.22 shows that there is no significant improvement from low-conflict history matching on the earlier iterations. The history matching from low-conflict grouping started to improve significantly from high conflict after Iteration 25, and becomes superior from Iteration 60, as shown in Figure 4.22.

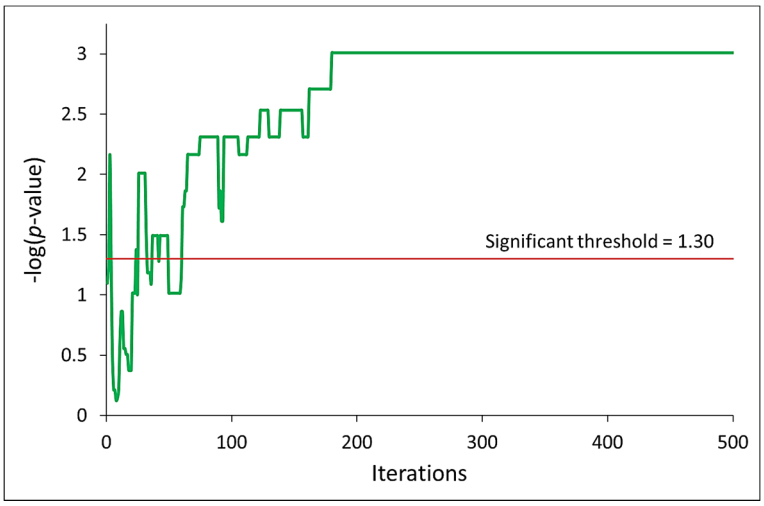

Figure 4.22—Significant level of history matching with low- to high-conflict groupings over 10 trials of history matching on Zagadka.

Reservoir Engineering Perspective

We evaluated the production-data match in several groups to demonstrate the superiority of low-conflict multi-objective history matching to the high-conflict, as shown in Figure 4.23. Overall, we can see from Figure 4.23 that the five-best matched models from the low-conflict grouping match better to the observed data. On the other hand, most or all of the five-best matched models from the high-conflict grouping fail to match the observed data.

These results demonstrate that history matching with low-conflict grouping is able to provide an ensemble of best matched models that can match observed production data in the group level better than the high-conflict grouping.

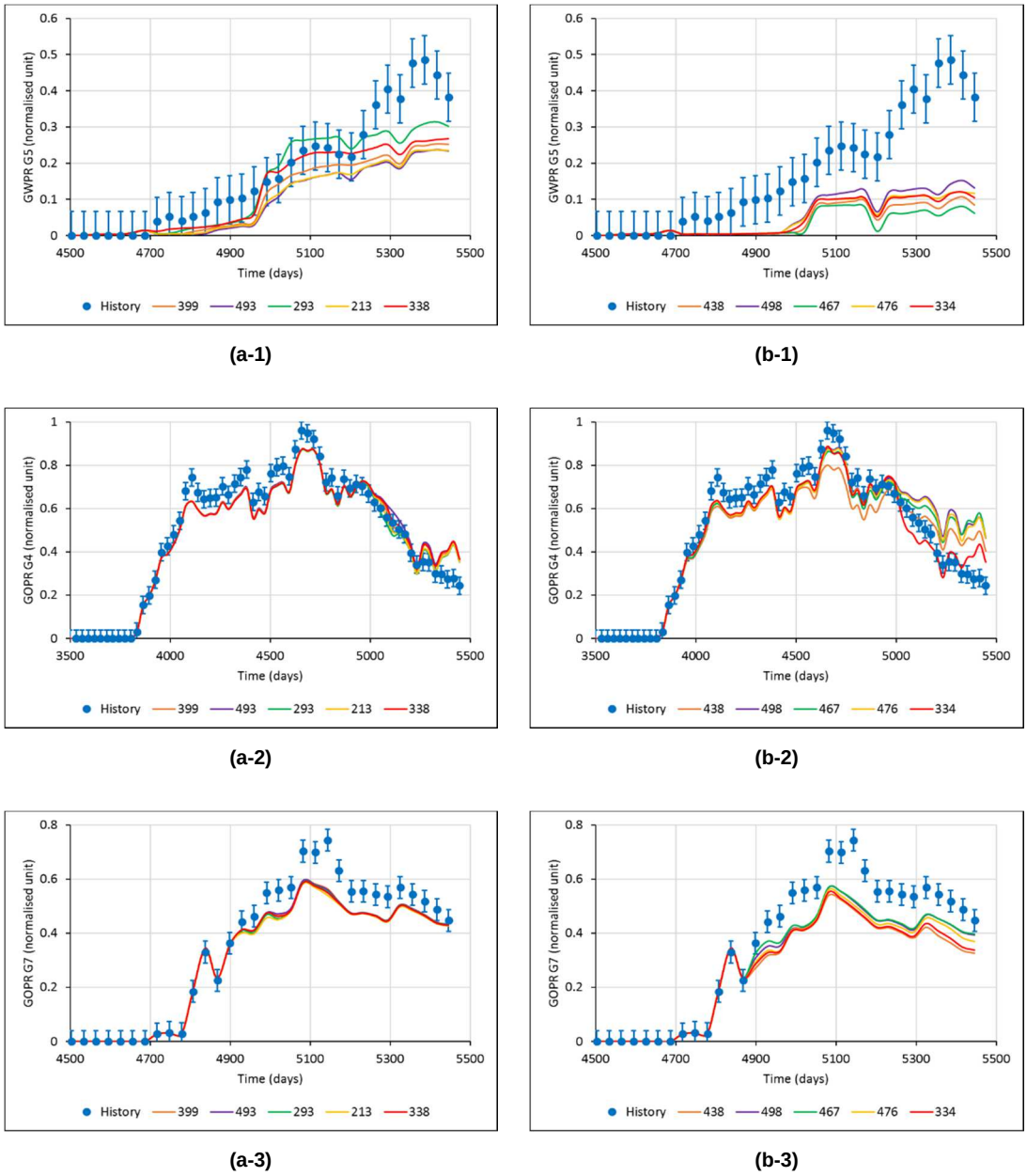

Figure 4.23—History-matching results on production data at several groups of producer wells from (a) low- and (b) high-conflict groupings on Zagadka Field. Each plot shows the five-best matched models as different coloured lines, the observed production data as blue dots, and data SD as a blue vertical line. Numbers in the legend are the iterations number of the five-best models.

4.5 Discussion

This chapter demonstrates that a key challenge of the multi-objective approach in history matching is that an increasing number of objectives cause any Pareto-based multi-objective algorithm to lose its selection pressure because most or all solutions become

nondominated. This loss of selection pressure can cause the sampling algorithm to become a random-search sampler with consequent poor performance (lower match quality and slower misfit convergence).

We showed that a novel technique to select an optimal objective-grouping combination was able to produce faster and more-robust history matches with better quality. The algorithm reduces the high number of objective components to two objectives by combining the misfit components with the lowest conflict to yield two objectives that provide optimal performance.

We applied the proposed technique to two field examples: the synthetic PUNQ-S3 reservoir model and a real-field case study in the Zagadka Field. The PUNQ-S3 case has 18 misfit components; when grouped optimally to two components, we observed a factor of 7.9 speedup average in the performance of multi-objective history matching compared with the performance of the high-conflict grouping. In the case of the Zagadka Field, we show a speedup of between 1.5 and 8, with an average of 2.59, over the high-conflict grouping.

The conclusions on the effectiveness of the proposed grouping technique are supported by rigorous statistical and sensitivity tests. For PUNQ-S3, these tests also show a significantly high correlation between misfit values and conflict measures. These tests are dependent on average behaviour over 10 identical runs, where the variation between runs was caused by the initial choice of the random seed and the subsequently generated random numbers in the stochastic optimiser.

On the basis of the extensive numerical simulations on both synthetic and real-field case studies in this chapter, we can conclude that grouping the less-conflicted objective components to select two objective components yields a significant improvement in the performance of multi-objective optimisation for history matching.

Chapter 5

Many-Objective Optimisation Algorithm for History Matching

5.1 Introduction

Multi-objective algorithms have gained good reputation since its first application for history matching in 2007 [180]. The algorithm allows the engineer to explore tradeoffs between matches to various elements of the overall match, hence is useful in seeking the most reliable and realistic match. Due to this mechanism, the multi-objective algorithm is able to obtain a diverse set of history-matched models, as demonstrated in Chapter 3. Moreover, in some cases, multi-objective algorithm provides faster misfit convergence and more robust towards stochastic nature of optimisation algorithm [7,8].

Some multi-objective algorithms and their successful applications in history matching are reported in the literature. Amongst these algorithms are strength Pareto evolutionary algorithm 2 (SPEA2) in [180], [188], multi-objective genetic algorithm (MOGA) in [181,186,187,190], differential evolution multi-objective Pareto ranking (DEMOPR) in [8], multi-objective neighbourhood algorithm (MONA) in [41], multi-objective particle swarm optimisation (MOPSO) in [7,9,10,96], differential evolution Markov chain Monte Carlo in [184] and the elitist nondominated sorting genetic algorithm (NSGA-II) in [147,182,189].

Figure 5.1 summarises the different multi-objective algorithms applied during 25 years of research on multi-objective history matching. Even though it was identified as a multi-objective problem by the theoretical study of Chung and Kravaris [179] in 1991, the first application of a multi-objective algorithm for history matching was performed in 2007 by the study of Schulze-Riegert *et al.* [180]. Since then, many multi-objective history matching studies appear, and typically only production data are involved. In 2013, the first inclusion of seismic data into multi-objective history matching was demonstrated by the study of Stephen [41].

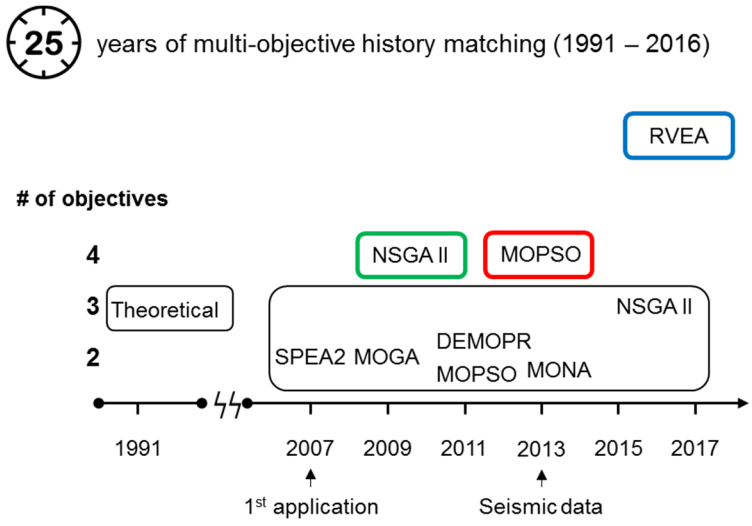

Figure 5.1—25 years of multi-objective history matching.

All of these noted multi-objective algorithms have a similar elitism strategy in their search procedure which is by using Pareto and dominance optimality concepts [11]. Amongst them, there are two multi-objective algorithms that are successfully implemented for real-field reservoir, namely MOPSO [9], [96] and NSGA-II [182], [189]. Therefore, these two algorithms can be considered as the current state-of-the-art in multi-objective history matching of the reservoir model. Nonetheless, it is worth to point out that the number of objectives involved by these multi-objective algorithms for history-matching studies is in the range from two to four objectives.

However, reservoir history matching may feature far too many objectives or criteria to match. For example, a medium-size oil field can have more than 100 wells and multiple production data to match in history matching. In this case, history matching problems

cannot be efficiently handled anymore by conventional Pareto dominance-based multi-objective algorithms.

The Pareto dominance-based algorithms have experienced substantial difficulties when they are adopted to tackle multi-objective optimisation problems with more than three objectives [15], often referred to as the many-objective optimisation problems (MaOPs). In these problems, the performance of the algorithms is severely deteriorated (lower match quality and slower misfit convergence), as demonstrated in Chapter 4. The performance deterioration can be attributed to the loss of selection pressure, i.e. the pressure for the population to converge towards the Pareto front when dominance is adopted as a criterion for selecting individuals with a limited population size [268].

Another critical reason for the degraded performance of the Pareto dominance-based multi-objective algorithms on MaOPs is the difficulty in maintaining a good population diversity in a high-dimensional objective space. Conventional Pareto dominance-based multi-objective algorithms aim to find a set of evenly distributed representative solutions to approximate the Pareto front. In two or three objectives, where the Pareto front is typically a one-dimensional curve or two-dimensional surface, maintaining a good diversity of the solutions is relatively straightforward. However, as the number of objective increases, it becomes increasingly challenging to maintain a good population diversity. The candidate solutions distribute sparsely in the high-dimensional objective space, causing immense difficulties to the diversity management strategies widely used in conventional multi-objective algorithms, e.g. the crowding distance method in both MOPSO and NSGA-II [201,206].

A number of approaches have been proposed to enhance the performance of conventional multi-objective algorithms in solving MaOPs [15,17,269,270]. The most common way is to modify the dominance relationships to increase the selection pressure towards the Pareto front, which includes ϵ-dominance [271], preference order ranking [272], and fuzzy dominance [273]. The other way is known as the performance indicator-based approaches, e.g. the indicator-based algorithm [274,275], the S-metric selection-based evolutionary algorithm (SMS-EMOA) [276], and the fast hypervolume-based evolutionary algorithm (HypE) [277]. Unfortunately, the computational cost for the

calculation of the performance becomes expensive when the number of objective is large [278].

The decomposition-based approach introduced in [279] is one way of multi-objective algorithms deal with MaOPs. It works by dividing a complex multi-objective problem into a number of single-objective problems using a set of *weight vectors* and solve them in a collaborative manner (see [279–281] for more detail). More recently, Liu *et al.* in [282] proposed a decomposition strategy by using a set of *direction vectors* to divide the whole Pareto front into a number of segment, each segment being a multi-objective subproblem, known as the multi-objective evolutionary algorithm based on decomposition (MOEA/D). Similar to the MOEA/D, the elitist decomposition-based nondominated sorting genetic algorithm (NSGA-III) used a set of *reference points* to manage diversity in each subspace for MaOPs that effectively enhances convergence by giving priority to solutions closer to the reference points. The most recent decomposition-based multi-objective algorithm is proposed in [283], known as reference vector guided evolutionary algorithm (RVEA), to solve MaOPs.

In this chapter, we introduce for the first time the application of one of the many-objective algorithms, called RVEA [283], for history matching. We describe the RVEA underlining its mechanisms as one of the decomposition-based multi-objective algorithms. We perform comparative studies between RVEA with the state-of-the-art of conventional multi-objective algorithms (namely MOPSO and NSGA-II) on several benchmark test problems with more than three objectives to show the effectiveness of the algorithm. Then, we apply the algorithm for history matching a synthetic reservoir model and a real-field case study with more than three objectives, emphasising the potential of many-objective optimisation algorithm paradigm for further research in history matching.

5.2 Reference Vector Guided Evolutionary Algorithm

In this section, we describe RVEA [283], a recently proposed algorithm to solve MaOPs.

5.2.1 General Framework

The general framework of the RVEA algorithm is shown in Algorithm 2.1. RVEA adopts an elitism strategy similar to that of NSGA-II [201], where traditional genetic operations such as crossover and mutation are used to generate the offspring population and then is combined with the parent population to go through an elitism selection.

However, RVEA has three main differences with NSGA-II: (1) a set of predefined reference vectors is required for the input in RVEA; (2) reference vectors are used to guide the selection of elitist solutions; and (3) there is a reference vector adaptation strategy to cope with different scales between objectives.

In the following subsections, we describe the four main components in Algorithm 2.1, i.e. reference vector, offspring creation, reference vector guided selection, and reference vector adaptation.

Algorithm 5.1—The general framework of RVEA [283].

1: **Input**: maximum number of generations t_{max}, a set of unit reference vectors $V_0 = \{\mathbf{v}_{0,1}, \mathbf{v}_{0,2,\ldots,}, \mathbf{v}_{0,N}\}$;
2: **Output**: final population $P_{t_{max}}$;
3: /*Initialisation*/
4: **Initialisation**: create the initial Population P_0 with N randomised individuals;
5: /*Main Loop*/
6: **while** $t < t_{max}$ **do**
7: Q_t = offspring creation (P_t);
8: $P_t = P_t \cup Q_t$;
9: P_{t+1} = reference vector guided selection (t, P_t, V_t);
10: V_{t+1} = reference vector adaptation (t, P_{t+1}, V_t, V_0);
11: $t = t + 1$;
12: **end while**

5.2.2 Reference Vector

Reference vectors are used to divide the objective space into smaller subspaces. Its use has been demonstrated successfully to improve the convergence and diversity of MaOP [283,284].

In this work, without loss of generality, we use unit reference vectors generated uniformly in the first quadrant with the origin as the initial point. The *canonical simplex-lattice design method* [285] is used to generate a set of uniformly distributed points on the hyperplane, as in Equation (5.1):

$$\begin{cases} \mathbf{u_i} = (u_i^1, u_i^2, \dots, u_i^M) \\ u_i^j \in \left\{\frac{0}{H}, \frac{1}{H}, \dots, \frac{H}{H}\right\}, \sum_{j=1}^{M} u_i^j = 1 \end{cases} \tag{5.1}$$

where $i = 1, \dots, N$ with N being the number of uniformly distributed points, M is the number of objectives, and H is a positive integer for the simplex-lattice design. Then, the reference points $\mathbf{u_i}$ are mapped from a hyperplane to a hypersphere to obtain the corresponding unit reference vectors $\mathbf{v_i}$ by the transformation in Equation (5.2).

$$\mathbf{v_i} = \frac{\mathbf{u_i}}{\|\mathbf{u_i}\|} \tag{5.2}$$

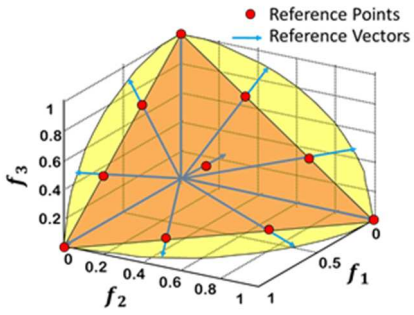

Figure 5.2—An example of generating 10 uniformly distributed unit reference vectors in a three-objective optimisation problem (after [283]).

According to the property of simplex-lattice design, a total number of $N = \binom{H+M-1}{M-1}$ uniformly distributed reference vectors can be generated, given M and H. For instance,

there are $N = 10$ reference vectors if we define $H = 3$ in a $M = 3$-objective problem, an example of which is shown in Figure 5.2.

5.2.3 Offspring Creation

In RVEA, the traditional genetic operators, i.e. simulated binary crossover (SBX) [144] and polynomial mutation [145], are used to generate the offspring population and then this population is combined with the parent population for elitism selection. Then, instead of an explicit mating selection strategy to create the parents, RVEA randomly generates a number of $\lfloor N/2 \rfloor$ pair of parents from N individuals in the current population P_t, such that each of individual in N has an equal probability to participate in the reproduction procedure. This mechanism can be done by employing the reference vector guided selection strategy that makes the individual inside each subspace to have an equal contribution to the population.

5.2.4 Reference Vector Guided Selection

In RVEA, selection of the next generation is made separately on each subspace partitioned by the reference vectors. This selection strategy consists of three steps: (1) objective value translation; (2) population partition; and (3) angle-penalised distance (APD) calculation, followed by the elitism selection [283], which are described in the following subsections.

Objective Value Translation

The objective value translation makes sure the initial point of the reference vectors is always the origin, and all the translated objective values are in the first quadrant, as illustrated in Figure 5.3 for the two-objective optimisation problem.

The role of this translation also to set the ideal point to be the origin of the coordinate system. Objective values in population P_t, denoted as $F_t = \{\mathbf{f}_{t,1}, \mathbf{f}_{t,2}, \ldots, \mathbf{f}_{t,|P_t|}\}$, where t is the generation index, are translated into F_t' by the transformation in Equation (5.3).

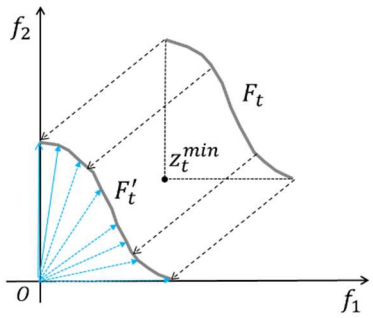

Figure 5.3—An illustration of the objective value translation in two-objective optimisation problem (after [283]).

$$\mathbf{f}'_{t,i} = \mathbf{f}_{t,i} - \mathbf{z}_t^{min} \tag{5.3}$$

where $i = 1, \ldots, |P_t|$, $\mathbf{f}_{t,i}$, $\mathbf{f}'_{t,i}$ are the objective vectors of individual i before and after the translation, and $\mathbf{z}_t^{min} = (z_{t,1}^{min}, z_{t,2}^{min}, \ldots, z_{t,m}^{min})$ represents the minimal objective values calculated from F_t.

Population Partition

The translated objective values in population P_t are partitioned to N subpopulations $P_{t,1}, P_{t,2}, \ldots, P_{t,N}$ by associating each individual to the closest reference vector, as illustrated in Figure 5.4, where N is the number of reference vectors.

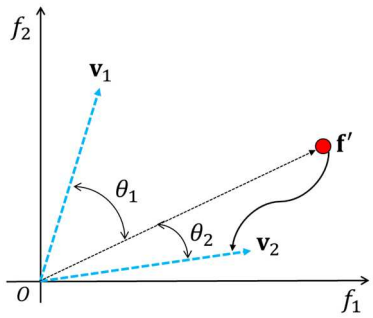

Figure 5.4—An illustration of an individual association with a reference vector. Because $\theta_2 < \theta_1$, the individual denoted by $\mathbf{f}'$ is associated with reference vector $\mathbf{v}_2$.

The spatial relationship between each translated individual subpopulation to the reference vector is determined by the *acute angle*, as in Equation (5.4). In this way, the closest reference vector to which the individual subpopulation will be allocated is based on the largest cosine value of Equation (5.4) (i.e. the acute angle is minimal), as in Equation (5.5).

$$cos\,\theta_{t,i,j} = \frac{\mathbf{f}'_{t,i} \cdot \mathbf{v}_{t,j}}{\left\|\mathbf{f}'_{t,i}\right\|} \tag{5.4}$$

$$\bar{P}_{t,k} = \{I_{t,i} | k = \underset{j\in\{1,\dots,N\}}{\operatorname{argmax}} cos\,\theta_{t,i,j}\} \tag{5.5}$$

where $\theta_{t,i,j}$ is the angle between objective vector $\mathbf{f}'_{t,i}$, and the reference vector $\mathbf{v}_{t,j}$, $I_{t,i}$ denotes the *I*-th individual allocated to a subpopulation in P_t, with $i = 1, \dots, |P_t|$.

APD Calculation

In RVEA, the elitist solutions are selected from each subpopulation $\bar{P}_{t,1}, \bar{P}_{t,2}, \dots, \bar{P}_{t,N}$ to create P_{t+1} for the next generation. The selection criteria consist of the convergence and diversity criteria with respect to the reference vector that the candidate solutions are associated with.

Because the ideal point is always the axis origin due to the objective values translation by transformation in Equation (5.3), the convergence criterion can be represented by the distance of $\mathbf{f}'_{t,i}$ to the origin, i.e. $\left\|\mathbf{f}'_{t,i}\right\|$, whereas the diversity criterion is naturally represented by the angle $\theta_{t,i,j}$ defined in Equation (5.4). APD, $d_{t,i,j}$, is introduced to balance these criteria (convergence and diversity) with a scalarisation approach, as in Equation (5.6).

$$d_{t,i,j} = \left(1 + P\left(\theta_{t,i,j}\right)\right) \cdot \left\|\mathbf{f}'_{t,i}\right\| \tag{5.6}$$

with $P(\theta_{t,i,j})$ being a penalty function related to $\theta_{t,i,j}$, i.e.:

$$P(\theta_{t,i,j}) = M \cdot \left(\frac{t}{t_{max}}\right)^{\alpha} \cdot \frac{\theta_{t,i,j}}{\gamma_{\mathbf{v}_{t,j}}} \tag{5.7}$$

and

$$\gamma_{\mathbf{v}_{t,j}} = \min_{i \in \{1,\ldots,N\}, i \neq j} \langle \mathbf{v}_{t,i}, \mathbf{v}_{t,j} \rangle \tag{5.8}$$

where M is the number of objectives, N is the number of reference vectors, t_{max} is the maximum number of generations, α is the parameter governing the rate of change of $P(\theta_{t,i,j})$, and $\gamma_{\mathbf{v}_{t,j}}$ is the smallest angle value between reference vector $\mathbf{v}_{t,j}$ and the other reference vectors in the current generation.

The basic idea in the APD calculation is not to apply constant pressure on both convergence and diversity in the entire search process due to the sparseness of the candidate solutions in high-dimensional objective space of many-objective optimisation. Instead, the high selection pressure on convergence is exerted at the early stage of the search process to push the population towards the Pareto front. On the later stage, the population diversity is emphasised in selection to generate well-distributed candidate solutions once the population is close to the Pareto front.

The penalty function $P(\theta_{t,i,j})$ in Equation (5.7) works in this sense in the APD calculation defined in Equation (5.6). At the early stage (i.e. $t \ll t_{max}$), $P(\theta_{t,i,j}) \approx 0$, and hence $d_{t,i,j} \approx \|\mathbf{f}'_{t,i}\|$, prioritising the convergence criterion. At the later stage (i.e. $t \approx t_{max}$), the $P(\theta_{t,i,j})$ is gradually accumulated emphasising the diversity criterion $\theta_{t,i,j}$. Moreover, the penalty function $P(\theta_{t,i,j})$ is proportionally related to the value of M because the sparsity of the candidate solutions is directly related to the dimension of objective space.

RVEA uses an angle normalisation in the APD calculation, i.e. it uses the angle $\gamma_{\mathbf{v}_{t,j}}$ to normalise the angle specified by $\mathbf{v}_{t,j}$. This normalisation is useful when the distribution of some reference vectors is either too dense (or too sparse), resulting in extremely small

(or large) angle between the candidate solutions and the reference vectors. By normalising the angles in each subspace independently, the actual positions of candidate solutions will not change and does not affect the distribution of the candidate solutions in other subspaces.

Algorithm 5.2—The reference vector guided selection strategy in RVEA [283].

Input: generation index t, population P_t, unit reference vector set $V_t = \{\mathbf{v}_{t,1}, \mathbf{v}_{t,2}, \dots, \mathbf{v}_{t,N}\}$;
Output: population P_{t+1} for the next generation;
/*Objective Value Translation*/
Calculate the minimal objective values $\mathbf{z}_t^{min}$;
for $i = 1$ to $|P_t|$ **do**
  $\mathbf{f}'_{t,i} = \mathbf{f}_{t,i} - \mathbf{z}_t^{min}$; //refer to (5.3)
end for
/*Population Partition*/
for $i = 1$ to $|P_t|$ **do**
  for $j = 1$ to N **do**
    $cos\,\theta_{t,i,j} = \frac{\mathbf{f}'_{t,i} \cdot \mathbf{v}_{t,j}}{\|\mathbf{f}'_{t,i}\|}$; //refer to (5.4)
  end for
end for
for $i = 1$ to $|P_t|$ **do**
  $k = \underset{j \in \{1,\dots,N\}}{\operatorname{argmax}} cos\,\theta_{t,i,j}$;
  $\bar{P}_{t,k} = \bar{P}_{t,k} \cup \{I_{t,i}\}$; //refer to (5.5)
end for
/*APD Calculation*/
for $i = 1$ to N **do**
  for $i = 1$ to $|\bar{P}_{t,j}|$ **do**
    $d_{t,i,j} = \left(1 + P\left(\theta_{t,i,j}\right)\right) \cdot \|\mathbf{f}'_{t,i}\|$; //refer to (5.6), (5.7), (5.8)
  end for
end for
/*Elitism Selection*/
for $i = 1$ to N **do**
  $k = \underset{i \in \{1,\dots,|\bar{P}_{t,j}|\}}{\operatorname{argmin}} d_{t,i,j}$;
  $\bar{P}_{t+1} = \bar{P}_{t+1} \cup \{I_{t,k}\}$;
end for

The individual in each subpopulation with the minimal APD is then selected as the elitist to the population for the next generation. The pseudo code for the reference vector guided selection strategy is summarised in Algorithm 5.2.

5.2.5 Reference Vector Adaptation

In real-world problems such as in history matching, we often encounter an issue with different scales of objective values ranges from different objectives. For instance, in oil-rate match criteria the misfit values can range from 0–10, whereas in water-rate match criteria it can range from 0–50. However, RVEA is expected to obtain a set of uniformly distributed Pareto optimal solutions that are the intersection points between each reference vector and the Pareto front, as shown in Figure 5.5 (a). In problems with different range of objective values, uniformly distributed reference vectors used in RVEA will not produce uniformly distributed solutions, as illustrated in Figure 5.5 (b).

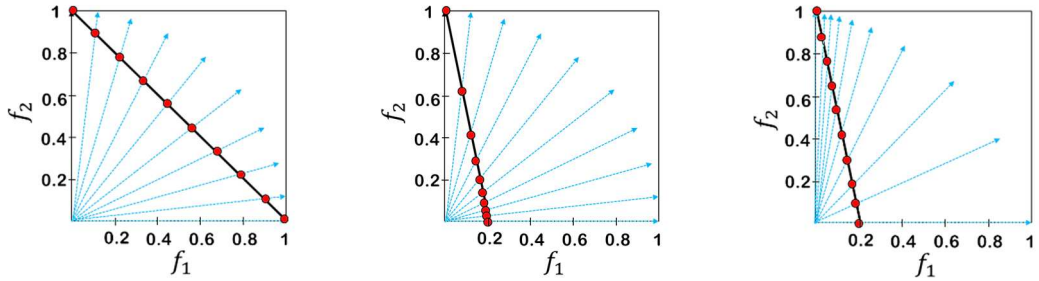

(a) 10 uniformly distributed reference vectors on a Pareto front with the same range of objective values

(b) 10 uniformly distributed reference vectors on a Pareto front with objectives scaled different range

(c) 10 adapted reference vectors on a Pareto front with objectives scaled different range

Figure 5.5—The Pareto optimal solutions (red dots) specified by different reference vectors (blue arrows) on different Pareto front (solid black line).

Therefore, a reference vector adaptation strategy is employed in RVEA to cope with this problem, as illustrated in Figure 5.5 (c). It works by adapting the reference vectors based on the ranges of the objective values, as in Equation (5.9):

$$\mathbf{v}_{t+1,i} = \frac{\mathbf{v}_{0,i} \text{ o } (\mathbf{z}_{t+1}^{max} - \mathbf{z}_{t+1}^{min})}{\left\| \mathbf{v}_{0,i} \text{ o } (\mathbf{z}_{t+1}^{max} - \mathbf{z}_{t+1}^{min}) \right\|} \tag{5.9}$$

where $i = 1, \dots, N$, $\mathbf{v}_{t+1,i}$ represents the i-th adapted reference vector for the next generation $t+1$, $\mathbf{v}_{0,i}$ represents the i-th initial uniformly distributed reference vectors, $\mathbf{z}_{t+1}^{max}$ and $\mathbf{z}_{t+1}^{min}$ represent the maximum and minimum values of the objective in the $t+1$ generation respectively, and the o operator denotes the Hadamard product that element wisely multiplies two vectors (or matrices) of the same size.

By applying this adaptation strategy, the RVEA can obtain uniformly distributed solutions on the problem with different scale of objective value ranges, as illustrated in Figure 5.5 (c). As suggested in [286], the reference vector adaptation strategy should not be used too frequently during the search process to ensure a stable convergence. Thus, a parameter f_r is introduced in RVEA to control the frequency of using the adaptation strategy. The reference vector adaptation strategy is summarised in Algorithm 5.3.

Algorithm 5.3—The reference vector adaptation strategy in RVEA [283].

Input: generation index t, population P_{t+1}, current unit reference vector set $V_t = \{\mathbf{v}_{t,1}, \mathbf{v}_{t,2}, \dots, \mathbf{v}_{t,N}\}$, initial unit reference vector set $V_0 = \{\mathbf{v}_{0,1}, \mathbf{v}_{0,2}, \dots, \mathbf{v}_{0,N}\}$;
Output: reference vector set V_{t+1} for the next generation;
if $\left(\frac{t}{t_{max}} mod\ f_r\right) == 0$ **then**
  Calculate the minimal and maximal objective values $\mathbf{z}_{t+1}^{min}$ and $\mathbf{z}_{t+1}^{max}$;
  for $i = 1$ to N **do**
    $\mathbf{v}_{t+1,i} = \frac{\mathbf{v}_{0,i}\ o\ (\mathbf{z}_{t+1}^{max} - \mathbf{z}_{t+1}^{min})}{\|\mathbf{v}_{0,i}\ o\ (\mathbf{z}_{t+1}^{max} - \mathbf{z}_{t+1}^{min})\|}$; //refer to Equation (5.9);
  end for
else
  $\mathbf{v}_{t+1} = \mathbf{v}_{t,i}$;
end if

5.2.6 Computational Complexity of the RVEA

The main computational complexity in RVEA is contributed from the reference vector guided selection strategy (objective value translation, population partition, APD calculation and elitism selection) and reference vector adaptation mechanism, apart from genetic operations such as crossover and mutation. Suppose the M is the number of

objectives and N is the population size, then the computational complexity for objective value translation and population partition is $O(MN)$ and $O(MN^2)$, respectively. The computational complexity for APD calculation and elitism selection is $O(MN^2)$ and $O(N^2)$, respectively. The computational complexity for the reference adaptation strategy is $O\left(MN/(f_r \cdot t_{max})\right)$, where f_r and t_{max} denotes the frequency to use the reference vector adaptation strategy and maximal number of generations, respectively. The overall computation complexity is therefore $O(MN^2)$.

5.3 Numerical Experiment

As in the original paper [283], the performance of the RVEA is evaluated using widely used scalable test functions designed for testing population-based multi-objective optimisation algorithms, i.e. Deb, Thiele, Laumanns, Zitzler (DTLZ) test suites [287]. The RVEA results are then compared with the state-of-the-art multi-objective optimisation algorithms for history matching, namely MOPSO and NSGA-II. Both MOPSO and NSGA-II algorithms are the most successful multi-objective algorithms for history matching and are already applied to real-field case studies [9,96,183,190].

In the following subsections, we first present a brief introduction to the test functions and the performance measure used. Then, the parameter settings used for each algorithm are given, followed by the results of each algorithm from 20 independent runs on each test function. Finally, the parameter sensitivity analysis on RVEA is presented as a guideline for its application for reservoir history matching case studies.

The aim of this numerical experiment is to demonstrate the significant improvement of RVEA performance compared with the two state-of-the-arts multi-objective algorithms known in petroleum industry (i.e. MOPSO and NSGA-II), particularly in the problems with more than three objectives. Moreover, the closely replication of RVEA on the test functions in this chapter to the original paper [283] serves for the self-content chapter in the thesis for RVEA numerical experiments in addition to its application for history matching. Nonetheless, more numerical experiments of RVEA to other test functions, i.e. walking fish group (WFG) test suites compared with other many-objective algorithms, i.e. MOEA/DD, NSGA-III, MOEA/D-PBI, grid based evolutionary

algorithm and knee point driven evolutionary algorithm can be found in the original paper [283].

5.3.1 Test Function Description

The first four test functions for the numerical experiments are DTLZ1–DTLZ4 [287], as described in Table 5.1. Similar to the original paper by Cheng *et al.* [283], the number of parameters is $n = M + k - 1$, where M is the number of objectives and, $k = 5$ is used for DTLZ1, whereas $k = 10$ is used for DTLZ2, DTLZ3 and DTLZ4 as recommended in [287]. However, we used $M = 3, 4, 6, 8, 10$ objectives in this study, whereas in the original paper of Cheng *et al.* [283] only $M = 3, 6, 8, 10$ objectives are studied.

Name	Description	Parameter Domains	Pareto Front Requirements
DTLZ1	$f_1 = (1+g)0.5\prod_{i=1}^{M-1} x_i$ $f_{m=2:M-1} = (1+g)0.5\left(\prod_{i=1}^{M-m} x_i\right)(1-x_{M-m+1})$ $f_M = (1+g)0.5(1-x_i)$ $g = 100\left[k + \sum_{i=1}^{k}\left((x_i-0.5)^2 - \cos\left(20\pi(x_i-0.5)\right)\right)\right]$	[0, 1]	$\sum_{i=1}^{M} f_i = 0.5$
DTLZ2	$f_1 = (1+g)\prod_{i=1}^{M-1}\cos(x_i\pi/2)$ $f_{m=2:M-1} = (1+g)\left(\prod_{i=1}^{M-m}\cos(x_i\pi/2)\right)\sin(x_{M-m+1}\pi/2)$ $f_M = (1+g)\sin(x_i\pi/2)$ $g = \sum_{i=1}^{k}(x_i-0.5)^2$	[0, 1]	$\sum_{i=1}^{M} f_i^2 = 1$
DTLZ3	As DTLZ2, except the equation for g is replaced by the one from DTLZ1.	[0, 1]	$\sum_{i=1}^{M} f_i^2 = 1$
DTLZ4	As DTLZ2, except all $x_i \in x$ are replaced by y_i^{α}, where $\alpha = 100$.	[0, 1]	$\sum_{i=1}^{M} f_i^2 = 1$

Table 5.1—The description of DTLZ1–DTLZ4 test functions. M is the number of objectives and x is the parameter. All objectives are to be minimised.

The DTLZ test suite of benchmark problem is scalable to any number objectives, which is an important characteristic to facilitate the investigation of many-objective problems. These test functions have different fitness landscape and Pareto optimal geometry. For instance, DTLZ1 and DTLZ3 have multi-modal fitness landscape in common with the linear and concave geometry of Pareto optimal, respectively. On the other hand, both DTLZ2 and DTLZ4 have a unimodal landscape with a concave geometry, with bias

characteristic on DTLZ4 towards particular objectives. These characteristics ensure that the performed benchmark tests cover various type of problems.

Similar to Cheng *et al.* [283], we have also used the scaled version of the DTLZ1 and DTLZ3 (denoted as SDTLZ1 and SDTLZ3) to investigate the algorithm's performance on problems that have differently scaled objective values. We followed the scaling approach as in [284], where each objective is multiplied by a coefficient p^{i-1}, where p is a parameter that defines the scaling size and $i = 1, \dots, M$ is the objective index. For instance, given $p = 10$, the objectives of a 3-objective problem is scaled to be $10^0 \times f_1$, $10^1 \times f_2$ and $10^2 \times f_3$. In our study, the values of p are set to 10, 10, 5, 3, 2 for problems with an objective number $M = 3$, 4, 6, 8, 10, respectively. This scaling approach is also followed in Cheng *et al.* [283] for the scaled version of DTLZ test functions.

5.3.2 Performance Measures

We used *hypervolume* (HV) metric [288] to measure the performance of an algorithm in each test function. The HV is a well-known and single metric that can provide a combined information about the convergence and diversity of the obtained solutions, as given by Equation (5.10).

$$HV(S, R) = volume\left(\bigcup_{i=1}^{n_S} v_i\right) \tag{5.10}$$

where S is the obtained solutions, R is the reference points and v_i is a hypercube constructed with the reference points.

Figure 5.6 illustrates an example of the HV calculation in a hypothetical bi-objective and minimisation problem. The HV(S, R) is thus the area $ABCWA$ enclosed by the discontinuous boundary where reference points $R = \{W\}^2$. This figure suggests that the closer the obtained solutions set $S = \{A, B, C\}$ to the true Pareto front and the more diverse of those solutions in objective space, the higher value of HV. Thus, a higher value of HV implies a good convergence-diversity and is preferable.

In this study, given M as the number of objectives, we used reference points $R = \{1.5\}^M$ for DTLZ1–DTLZ4, $R = \{1600\}^M$ for SDTLZ1, and $R = \{3200\}^M$ for SDTLZ3. All HV values presented in this study are all normalised to [0,1] by dividing to $\prod_{i=1}^{M} R_i$.

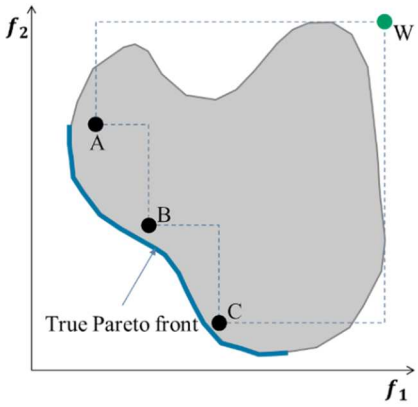

Figure 5.6—An illustration of a HV calculation in a hypothetical two-objective minimisation problem.

5.3.3 Parameter Settings for Algorithms

We used the specific recommended parameter settings from the literature in each algorithm, as described in Table 5.2, i.e. following [207] for MOPSO and following [144,145,201] for NSGA-II. In RVEA, similar to Cheng *et al.* [283], the distribution index is set to $\eta_c = 30$ for the simulated binary crossover [144], the crossover probability $p_c = 1.0$; for the polynomial mutation [145], the distribution index and the mutation probability are set to $\eta_m = 20$ and $p_m = 1/n$, respectively, as recommended in [144,145,283].

We used the same population size of 105, 120, 126, 128, 230 on all three algorithms for 3, 4, 6, 8, 10 objectives, respectively. The population size is determined by the simplex-lattice design factor H together with the objective number M, as referred to Equation (5.1). In comparison with Cheng *et al.* [283], the same population size of 105 is used in RVEA for 3-objective problems. However, there are different population size used in this thesis for 6, 8 and 10-objective problems compared to the original paper of RVEA [283] (i.e. population size of 126, 128 and 230 are used here, whereas the population size of 132, 156 and 275 are used in [283] for 6, 8 and 10-objective problems, respectively). We used a two-layer vector generation strategy to generate reference vectors on

the outer and inner layers of the Pareto fronts from problems with $M \geq 8$, as recommended in [284]. Hence, we started to use both layers (i.e. H_1, H_2 settings) from $M \geq 8$, as shown in Table 5.2, whereas in Cheng *et al.* [283] the authors started to use both layers from $M \geq 6$ (i.e. H_1, H_2 are set to 4 and 1).

M	RVEA				MOPSO		NSGA-II
	(H_1, H_2)	Ref. Vectors	(α, f_r)	$(\eta_c, p_c, \eta_m, p_m)$[a]	$(\omega, c_1, c_2, p_{mut})$[b]	Archive size	$(\eta_c, p_c, \eta_m, p_m)$[a]
3	(13, 0)	105	(2, 0.1)	(30, 1, 20, $1/n$)	(0.729, 1.494, 1.494, 0.5)	262	(30, 1, 20, $1/n$)
4	(7, 0)	120	(2, 0.1)	(30, 1, 20, $1/n$)	(0.729, 1.494, 1.494, 0.5)	300	(30, 1, 20, $1/n$)
6	(4, 0)	126	(2, 0.1)	(30, 1, 20, $1/n$)	(0.729, 1.494, 1.494, 0.5)	315	(30, 1, 20, $1/n$)
8	(3, 1)	128	(2, 0.1)	(30, 1, 20, $1/n$)	(0.729, 1.494, 1.494, 0.5)	320	(30, 1, 20, $1/n$)
10	(3, 1)	230	(2, 0.1)	(30, 1, 20, $1/n$)	(0.729, 1.494, 1.494, 0.5)	575	(30, 1, 20, $1/n$)

a SBX distribution index (η_c), SBX probability (p_c), polynomial mutation distribution index (η_m), polynomial distribution probability (p_m), and the number of parameters (n).
b Inertia weight (ω), cognitive (c_1) and social (c_2) component, and mutation probability (p_{mut}) parameters.

Table 5.2—Specific parameter settings in each algorithm.

The stopping condition for each run is set to the maximal number of generations. Differ from numerical experiments in [283], in this chapter the maximal number of generations is set to 500 for all cases. In [283], the maximal number of generations is set to 1,000 for DTLZ1, SDTLZ1, DTLZ3 and SDTLZ3. For DTLZ2 and DTLZ4, the maximal number of generations is set to 500.

5.3.4 Results

Table 5.3 summarises the statistical results of the HV values obtained by the three algorithms over 20 independent runs where the best results are highlighted in bold. We used the Wilcoxon signed rank test to compare the results obtained by the RVEA and those of by two compared algorithms at a significance level of 0.05. Symbol '+' indicates that the compared algorithm is significantly outperformed by RVEA, whereas '−' indicates that RVEA is significantly outperformed by the compared algorithm, and '≈' means that there is no statistically significant difference between the results obtained by RVEA and the compared algorithm according to the Wilcoxon signed rank test.

It can be seen from Table 5.3 that RVEA shows the best overall performance amongst the two compared algorithms on the six test functions. NSGA-II is able to compete with RVEA on the low number of objectives, i.e. 3 or 4 objectives. However, its performance is outweighed by RVEA on the high number of objectives, i.e. 6, 8 and 10 objectives. MOPSO shows the worst overall performance amongst others both in a low and high number of objectives.

The MOPSO results corresponding to problems DTLZ1, DTLZ3 and their scaled versions deserve additional comments. The HV value equal to zero means that the obtained solutions by MOPSO are outside the limits of the Pareto front. Hence, when applying the HV calculation, these solutions are not taken into account because otherwise, the calculated results would be unreliable.

Figure 5.7 shows the obtained Pareto front from all three algorithms for the three-objective DTLZ1–DTLZ4, SDTLZ1 and SDTLZ3 problems. These plots are taken from a particular run that is associated with the median value of HV performance metric from each algorithm. It is clear from Figure 5.7 that RVEA is able to find solutions with good convergence and diversity consistently in test problems with various characteristics.

Aligned with the results in Table 5.3, Figure 5.7 shows that NSGA-II is also able to find a good distribution of solutions similar to that of RVEA in a low number of objectives, i.e. three objectives. MOPSO performance suffered in the problem with multi-modal fitness landscape, i.e. DTLZ1, DTLZ3, SDTLZ1 and SDTLZ3 even in the three-objective problem, as shown in Figure 5.7. In DTLZ4, a test problem with bias characteristic, both RVEA and NSGA-II are able to obtain well-distributed solutions, whereas MOPSO suffered from the bias characteristic of DTLZ4.

In general, the results presented in both Table 5.3 and Figure 5.7 in this chapter show similar performances of RVEA compared with the results in Cheng *et al.* [283] on each respective test functions tested (i.e. DTLZ test suites). A slightly lower HV value in this thesis than in [283] on some test functions (i.e. DTLZ2 and DTLZ3) can be caused by different population size and the maximal number of generations used, though the difference is not significant.

Problem	M	RVEA	MOPSO	NSGA-II
DTLZ1	3	**0.992234 (0.000048)**	0 (0) +	0.991314 (0.000188) ≈
	4	**0.998903 (0.000008)**	0 (0) +	0.729822 (0.388067) +
	6	**0.999966 (0.000005)**	0 (0) +	0 (0) +
	8	**0.999997 (0.000004)**	0 (0) +	0 (0) +
	10	**0.999987 (0.000038)**	0 (0) +	0 (0) +
DTLZ2	3	**0.826879 (0.000092)**	0.821970 (0.003530) +	0.813499 (0.003607) ≈
	4	**0.914134 (0.000066)**	0.859111 (0.029900) +	0.879261 (0.005228) +
	6	**0.970678 (0.027682)**	0.181819 (0.097958) +	0.318051 (0.186968) +
	8	**0.981996 (0.024021)**	0.135446 (0.079010) +	0.033898 (0.063516) +
	10	**0.977899 (0.028060)**	0.118097 (0.089831) +	0.021733 (0.069107) +
DTLZ3	3	**0.806762 (0.011304)**	0 (0) +	0.775184 (0.150606) ≈
	4	**0.902896 (0.005571)**	0 (0) +	0 (0) +
	6	**0.832588 (0.304695)**	0 (0) +	0 (0) +
	8	**0.844201 (0.335317)**	0 (0) +	0 (0) +
	10	**0.980410 (0.019070)**	0 (0) +	0 (0) +
DTLZ4	3	**0.814312 (0.002594)**	0.796320 (0.050396) +	0.807979 (0.084152) ≈
	4	**0.913908 (0.000119)**	0.883374 (0.017658) +	0.885692 (0.004634) +
	6	**0.976192 (0.002166)**	0.861008 (0.035004) +	0.020423 (0.060544) +
	8	**0.979864 (0.023233)**	0.833295 (0.058728) +	0.015345 (0.045235) +
	10	**0.978673 (0.025803)**	0.873593 (0.034799) +	0.051505 (0.071803) +
SDTLZ1	3	**0.999999 (0)**	0 (0) +	**0.999999 (0)** ≈
	4	**0.999999 (0)**	0 (0) +	**0.999999 (0)** ≈
	6	**0.999915 (0.000071)**	0 (0) +	0.749579 (0.110492) +
	8	**0.999959 (0.00005)**	0 (0) +	0.638631 (0.134979) +
	10	**0.999997 (0.000011)**	0 (0) +	0.872210 (0.047958) +
SDTLZ3	3	**0.999999 (0)**	0 (0) +	**0.999999 (0)** ≈
	4	**0.999963 (0.000093)**	0 (0) +	0.999367 (0.001035) ≈
	6	**0.999906 (0.000294)**	0 (0) +	0.359346 (0.265173) +
	8	**0.999882 (0.000213)**	0 (0) +	0.091898 (0.225488) +
	10	**0.999999 (0.000001)**	0 (0) +	0.047630 (0.120678) +

Table 5.3—The statistical results (mean and SD) of the HV values obtained by RVEA, MOPSO and NSGA-II on DTLZ1–DTLZ4, SDTLZ1 and SDTLZ3. The best results are highlighted in bold.

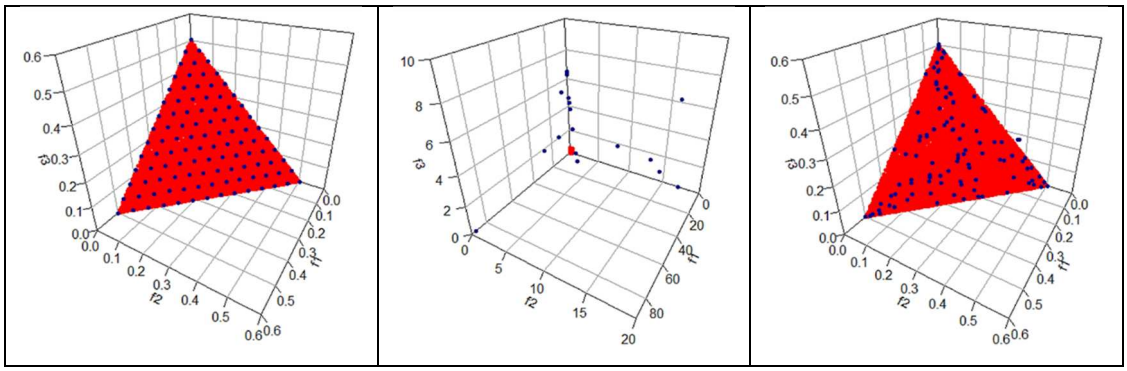

DTLZ1

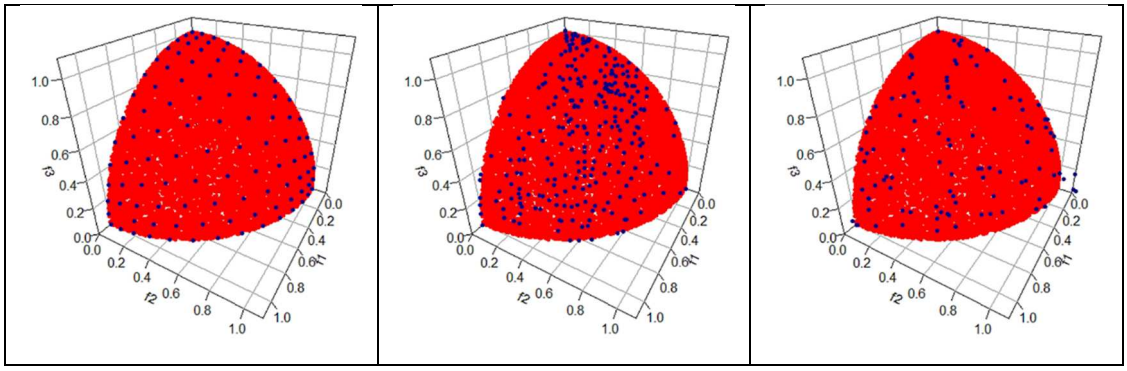

DTLZ2

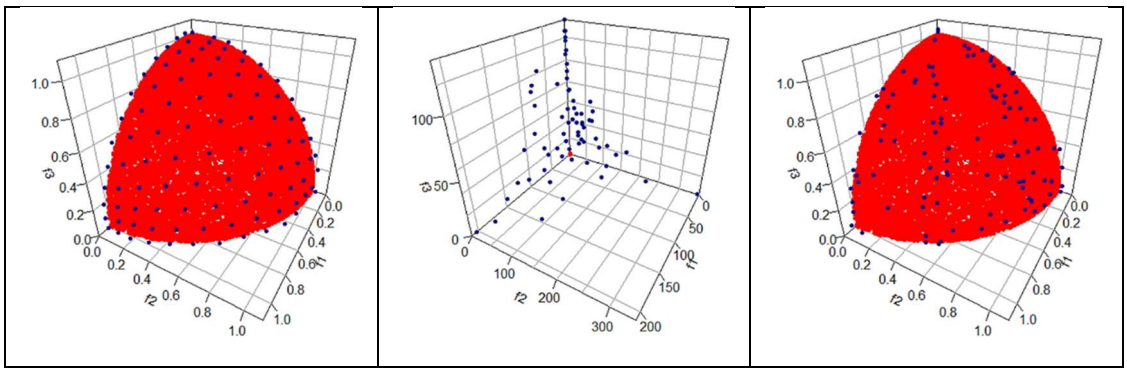

DTLZ3

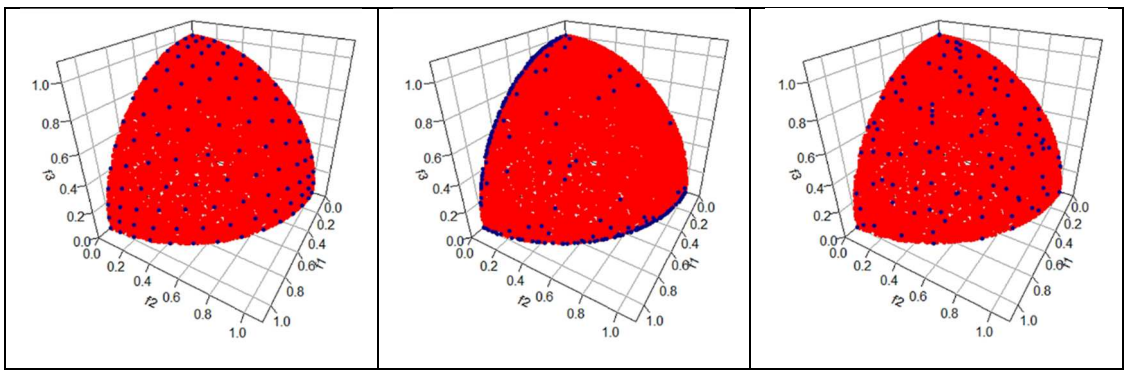

DTLZ4

(a) RVEA (b) MOPSO (c) NSGA-II

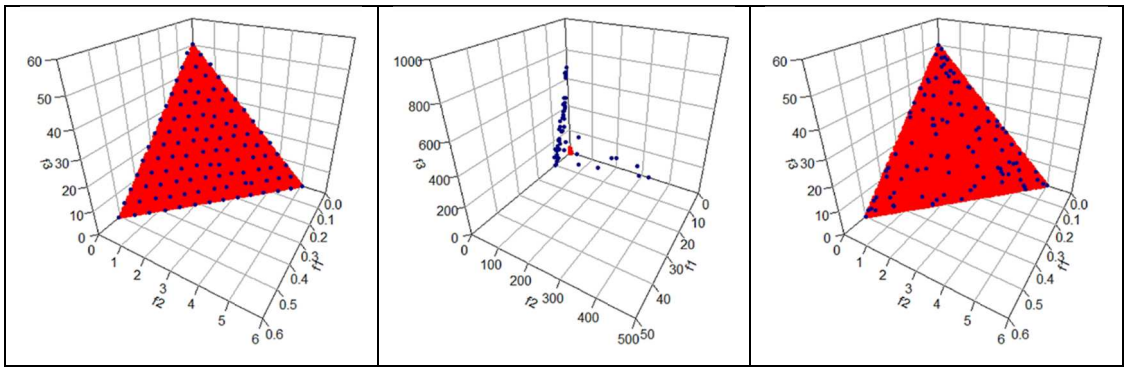

SDTLZ1

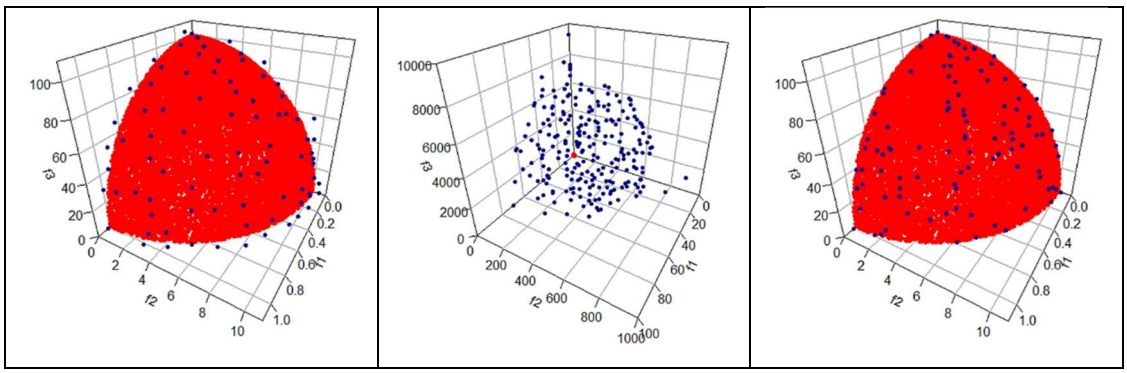

SDTLZ3

(a) RVEA (b) MOPSO (c) NSGA-II

Figure 5.7—Obtained solutions (in blue) by (a) RVEA, (b) MOPSO, (c) NSGA-II for the three-objective problem of DTLZ1–DTLZ4, SDTLZ1 and SDTLZ3. True Pareto front is shown in red.

5.3.5 Parameter Sensitivity Analysis

We conducted sensitivity studies on two predefined parameters in RVEA, i.e. α (used to control the rate of change of the penalty function in Equation (5.7)) and f_r (used to define the frequency of reference vector adaptation in Algorithm 5.3). We performed additional runs with various setting of α and f_r on DTLZ3 and SDTLZ1 test functions, which covers both normal and scaled test problems.

We carried out sensitivity analysis of parameter α by fixing the f_r to 0.1 and varying the α from 1 to 9, as shown in Figure 5.8. We can see that the performance of RVEA is in general insensitive to the settings of α for both problems (note the HV values scales in Figure 5.8 (b) is the zoom-in scale). In DTLZ3, there are slightly increase of HV values with the increase of α, except for 10-objective problem. In SDTLZ3, the HV started to

slightly deteriorate with the increase of α, especially on high-dimensional scaled objective space. In this problem, the candidate of solutions is sparsely distributed and a relatively small α will help to maintain population diversity. Thus, based on these observations, a small value of α is preferred, i.e. 2 or 3.

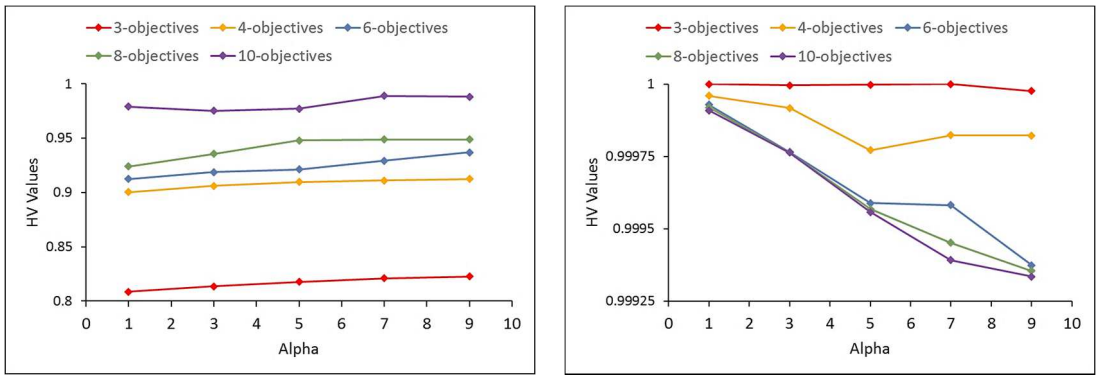

(a) DTLZ3 **(b) SDTLZ1**

Figure 5.8—The HV values obtained by RVEA averaged over 20 independent runs with f_r fixed to 0.1 and α varying from 1 to 9.

We then carried out sensitivity analysis of f_r by fixing α to 2 and varying f_r from 0.01 to 0.5, as shown in Figure 5.9. We can see that in SDTLZ1, the performance of RVEA is generally insensitive to the settings of f_r, as shown in Figure 5.9 (b) (note that the HV values scale is the zoom-in scale in this figure). On the contrary, on DTLZ3, a problem with complex multi-modal fitness landscape, a too small f_r (frequent reference vector adaptation) leads to a significant deterioration of the RVEA performance. Nonetheless, the f_r values larger than 0.1 will not affect the performance of RVEA significantly. Therefore, based on these observations, the f_r value of 0.1 is preferred.

The results in this section confirms the previous experiment results in [283] on the RVEA parameter sensitivity analysis which are tested on both DTLZ3 and WFG4 test functions. In this section, the parameter sensitivity tests on RVEA also conducted on SDTLZ1 that represents a scaled test problem. The results presented in this section suggest parameters values of $\alpha = 2$ and $f_r = 0.1$ for RVEA on the field application in the next section.

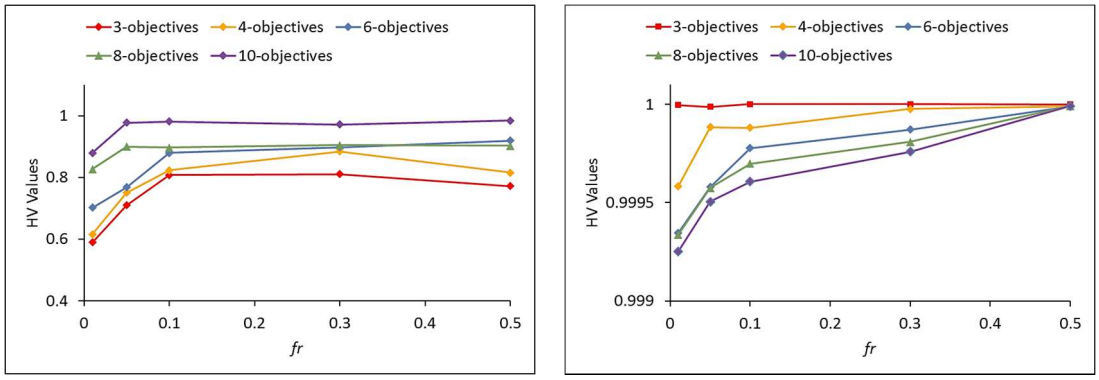

(a) DTLZ3 (b) SDTLZ1

Figure 5.9—The HV values obtained by RVEA averaged over 20 independent runs with α fixed to 2 and f_r varying from 0.01 to 0.5.

5.4 Field Application

The three algorithms (RVEA, MOPSO, and NSGA-II) were applied to the synthetic PUNQ-S3 [235] and real-field Zagadka Field case studies. The objective is to compare the many-objective history matching results obtained by these algorithms. The Set-1 model parameterisation described in Chapter 3 was used for PUNQ-S3 history matching. For Zagadka Field, the same model parameterisation described in Chapter 4 was used.

5.4.1 PUNQ-S3 Many-Objective History Matching Formulation

Eight years of production history data including bottom hole pressure (BHP), water cut (WCT) and gas-to-oil ratio (GOR) from all wells are used for the history matching of PUNQ-S3. The data are uncorrelated and following the original dataset [243]. The objective function, misfit M, to be minimised is defined as:

$$M = \frac{1}{n_w}\sum_i \frac{1}{n_p}\sum_j \frac{1}{n_t}\sum_k \left(w_{ijk}\frac{(obs_{ijk} - sim_{ijk})}{\sigma_{ijk}} \right)^2 \tag{5.11}$$

where n_w is the number of evaluated wells, n_p is the number of observed production data, n_t is the number of timesteps for the j^{th} history data, obs is the observed history, sim is the simulated value, σ^2 is the variance of the measurement errors, and w is the

weight factor. In PUNQ-S3, $n_w = 6$, $n_p = 3$, and the misfit for each production data will be lumped over all timesteps. Hence, we can see from Equation (5.11) that there are 18 misfit components in PUNQ-S3 which are the misfits from six wells with three production data (BHP, WCT, and GOR) from each well to minimise.

We formulated the history matching with many-objective optimisation of six objective functions by decomposing the misfit function in Equation (5.11) based on production wells, as described in Equation (5.12):

$$\begin{cases} minimize\ \left(M_1(p), M_2(p), \dots, M_6(p)\right) \\ \quad \boldsymbol{p} = \{BHP, WCT, GOR\} \end{cases} \tag{5.12}$$

where M_1 to M_6 correspond to the misfits from production wells PRO-1, PRO-4, PRO-5, PRO-11, PRO-12 and PRO-15 respectively, which are summed up on all production variable $\boldsymbol{p}$ over all timesteps with unity weights. For instance, $M_1 = (M_{BHP} + M_{WCT} + M_{GOR})_{PRO-1}$, $M_2 = (M_{BHP} + M_{WCT} + M_{GOR})_{PRO-4}$, and so on.

5.4.2 Zagadka Field Many-Objective History Matching Formulation

We used the historical data of field level of oil-rate (GOPR) and water-rate (GWPR) from all well groups in the history matching of Zagadka Field. In Zagadka Field, there are nine groups of wells in total, G1–G9, based on the geological structure, fault block in the model, and the time when the wells were drilled, as shown in Figure 5.10.

The objective function to be minimised is defined as:

$$M = \sum_i^{n_g} \sum_j^{n_p} w_{ij} \sum_k^{n_t} \frac{\left(obs_{ijk} - sim_{ijk}\right)^2}{2\sigma_{ijk}^2} \tag{5.13}$$

where n_g is the number of groups, n_p is the number of observed production data, n_t is the number of timesteps for the j^{th} history data, obs is the observed history, sim is the simulated value, σ^2 is the variance of the measurement errors, and w is the weight factor.

In Zagadka Field, $n_g = 9$, $n_p = 2$, and the misfit for each production data will be lumped over all timesteps. Hence, we can see from Equation (5.13) that there are 18 misfit components in Zagadka Field which are the misfits from nine well groups with two production data (GOPR and GWPR) from each group to minimise.

We grouped the 18 misfit components in Zagadka Field into four objectives, as in Equation (5.14), based on the predominant clusters where the wells are located shown in Figure 5.10 and the production start time from each group shown in Figure 5.11.

$$\begin{cases} minimize\ \left(M_1(p), M_2(p), \dots, M_4(p)\right) \\ \boldsymbol{p} = \{GOPR, GWPR\} \end{cases} \tag{5.14}$$

where M_1, M_2, M_3 and M_4 correspond to the misfit from groups (G1), (G2 and G3), (G4 to G7), and (G8 and G9), respectively, which are summed up on all production variable $\boldsymbol{p}$ over all timesteps with unity weights. For instance, $M_1 = (M_{GOPR} + M_{GWPR})_{G1}$, $M_2 = (M_{GOPR} + M_{GWPR})_{G2} + (M_{GOPR} + M_{GWPR})_{G3}$, and so on.

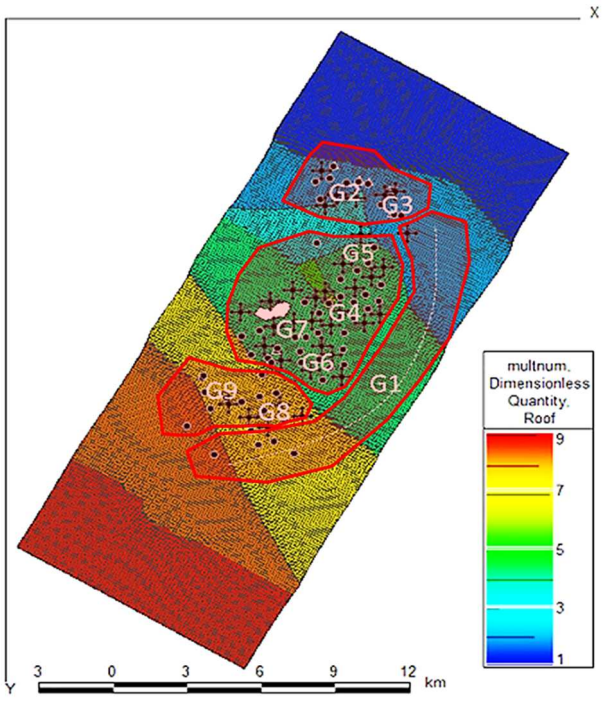

Figure 5.10—Zagadka Field region map highlighting the location of four clusters (G1, G2 & G3, G4–G7, and G8 & G9) for many-objective history matching.

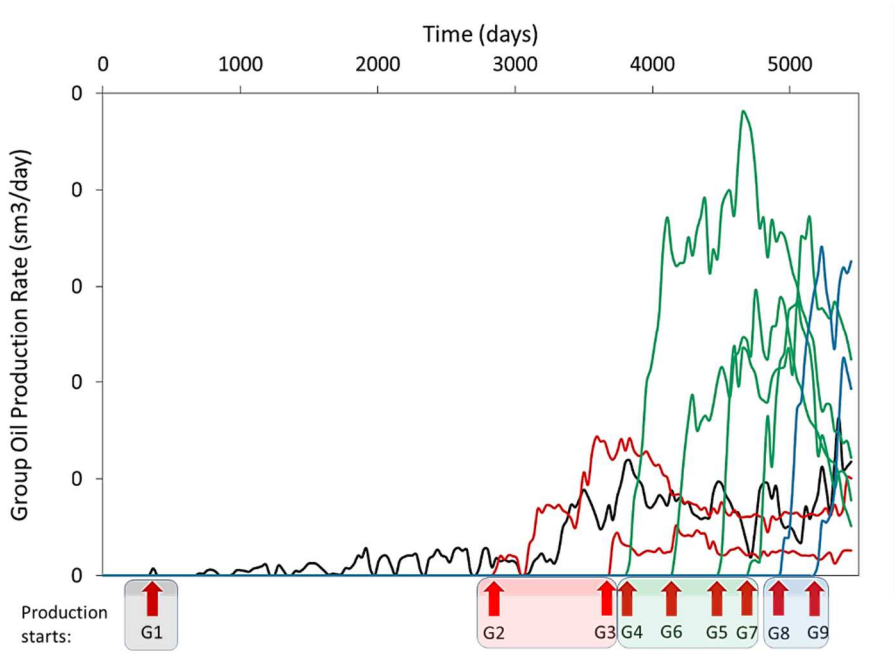

Figure 5.11—Production profile in Zagadka Field from all of the nine groups of wells highlighting the way of grouping for many-objective history matching.

5.4.3 Results

In this section, we compare the many-objective history matching results on both case studies from RVEA [283] with MOPSO [7] and NSGA-II [201]. For each case study, 10 independent history-matching runs were performed, where the variation between run is caused by the initial choice of random seed and the subsequently generated random numbers in the stochastic optimiser.

5.4.3.1 Parameter Settings for Algorithms

Table 5.4 describes the parameter settings for each algorithm in both case studies. A termination criterion of 1,500 and 250 function evaluations is set for PUNQ-S3 and Zagadka Field case studies, respectively, as there is no significant improvement of misfit value beyond these iterations.

Algorithm	Parameters	PUNQ-S3 (6 Objectives)	Zagadka Field (4 Objectives)
RVEA	(H_1, H_2)	(2, 0)	(2, 0)
	(α, f_r)	(2, 0.1)	(2, 0.1)
	$(\eta_c, p_c, \eta_m, p_m)$[a]	(30, 1, 20, 1/24)	(30, 1, 20, 1/19)
	Population size	21	20
	Reference vectors	21	10
MOPSO	$(\omega, c_1, c_2, p_{mut})$[b]	(0.729, 1.494, 1.494, 0.5)	(0.729, 1.494, 1.494, 0.5)
	Population size	20	20
	Archive size	250	250
NSGA-II	$(\eta_c, p_c, \eta_m, p_m)$[a]	(30, 1, 20, 1/24)	(30, 1, 20, 1/19)
	Population size	20	20

[a] SBX distribution index (η_c), SBX probability (p_c), polynomial mutation distribution index (η_m), polynomial distribution probability (p_m).

[b] Inertia weight (ω), cognitive (c_1) and social (c_2) component, and mutation probability p_{mut} parameters.

Table 5.4—Parameter settings in each algorithm for PUNQ-S3 and Zagadka case studies.

5.4.3.2 Misfit Convergence

We calculated the global sum of misfit after many-objective history-matching runs from all three algorithms and looked at the best-so-far misfit values. Figure 5.12 (a) and (b) show the mean and standard deviation (SD) of best-so-far misfit values from 10 trials history-matching run from each algorithm on PUNQ-S3 and Zagadka Field case studies, respectively. In both case studies, the mean of best-so-far misfit values of history matching with RVEA is predominantly below the lower bound of best-so-far misfit values from history matching with MOPSO and NSGA-II. These figures also show that the upper bound of best-so-far misfit values from RVEA are predominantly below the mean of best-so-far misfit values from MOPSO and NSGA-II.

History matching with RVEA also provides faster misfit convergence than MOPSO and NSGA-II in both PUNQ-S3 and Zagadka Field case studies, as shown in Figure 5.12. In PUNQ-S3, RVEA is 6.8 and 3.6 times faster than MOPSO and NSGA-II, respectively, as shown in Figure 5.12 (a). In Zagadka Field, history matching with RVEA is 6.25 and 3.1 times faster than MOPSO and NSGA-II, respectively, as shown in Figure 5.12 (b).

Similar to Chapter 4, we performed 10,000 bootstrap resamplings on the mean final misfit value from 10 trials of each algorithm, as shown in Figure 5.13. We can see that the RVEA provides a lower bootstrapped mean final misfit value than MOPSO and

NSGA-II on both case studies. In PUNQ-S3, the SD of the bootstrapped mean final misfit value from RVEA is also lower than MOPSO and NSGA-II, as shown in Figure 5.13 (a). In Zagadka Field, even though the SD of the bootstrapped mean final misfit value from RVEA is higher than MOPSO, the mean value from RVEA is significantly lower than MOPSO. This result implies that RVEA provides consistently history-matched models with low misfit values, whereas MOPSO generates consistently history-matched models with high misfit values. Compared to NSGA-II, both mean and SD of the bootstrapped mean final misfit value from RVEA is lower than NSGA-II, as shown in Figure 5.13 (b). These results demonstrate that history matching with RVEA provides consistently higher-match-quality models (lower mean final misfit value) than MOPSO and NSGA-II, and relatively robust misfit evaluations (i.e. relatively low SD of mean final misfit value).

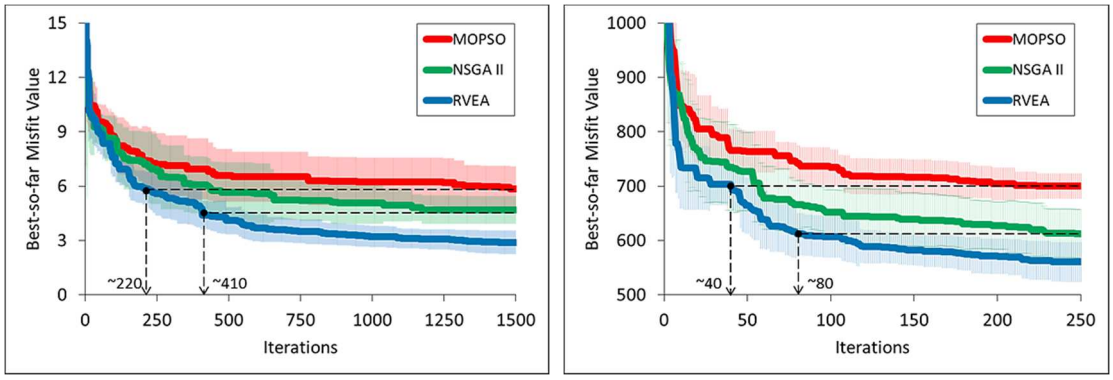

(a) PUNQ-S3 (b) Zagadka

Figure 5.12—Mean and SD of the best-so-far misfit value over 10 trials history-matching run from RVEA, MOPSO, and NSGA-II algorithms on (a) PUNQ-S3 and (b) Zagadka Field.

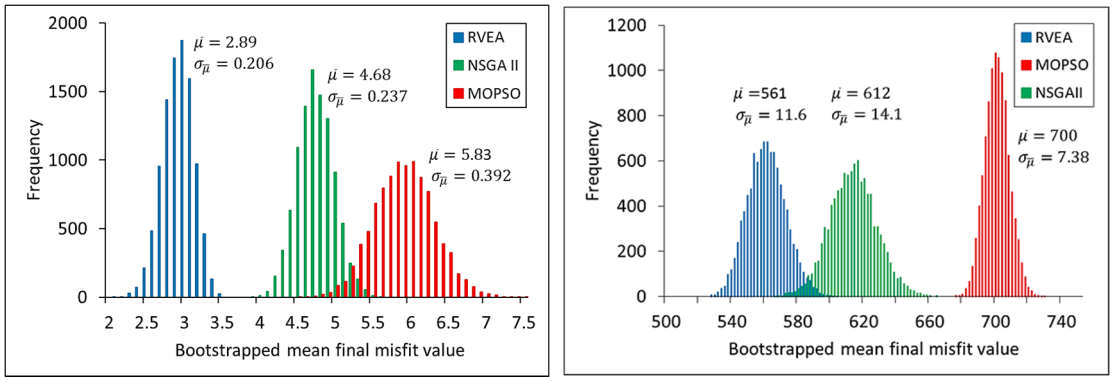

(a) PUNQ-S3 (b) Zagadka

Figure 5.13—Histogram of the bootstrapped mean final misfit values (*b*=10,000 resamples) from 10 trials history-matching run from RVEA, MOPSO, and NSGA-II algorithms on (a) PUNQ-S3 and (b) Zagadka Field.

The significant improvements of RVEA from MOPSO and NSGA-II on both case studies are shown in Figure 5.14. Similar to Chapter 4, we evaluated the statistical significance of this difference by using the Wilcoxon signed rank test on 10 trials of each grouping with the significance threshold of 0.05 (p-value < 0.05). We took the negative logarithmic value of p-value and plotted over all iterations, as shown in Figure 5.14 (a) and (b) for PUNQ-S3 and Zagadka Field, respectively. In this case, the significant threshold is converted to $-\log(0.05)$ which is 1.30.

In PUNQ-S3, there is no significant different between RVEA and MOPSO for the first 60 iterations, and then RVEA improves significantly afterwards, as shown in Figure 5.14 (a). RVEA outweighs NSGA-II significantly from approximately Iteration 400 in PUNQ-S3, as shown in Figure 5.14 (a). In Zagadka Field, RVEA outperforms MOPSO significantly since the early iteration, i.e. Iteration 6, whereas it outperforms NSGA-II significantly since Iteration 45, as shown in Figure 5.14 (b).

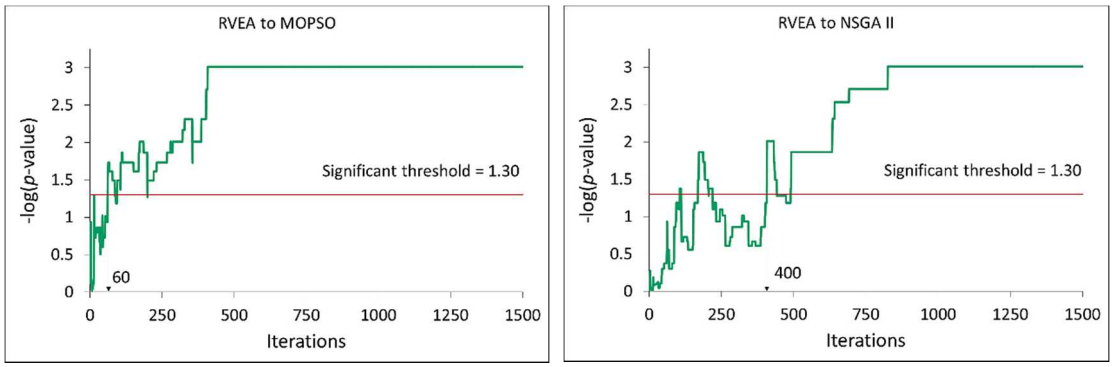

(a) PUNQ-S3

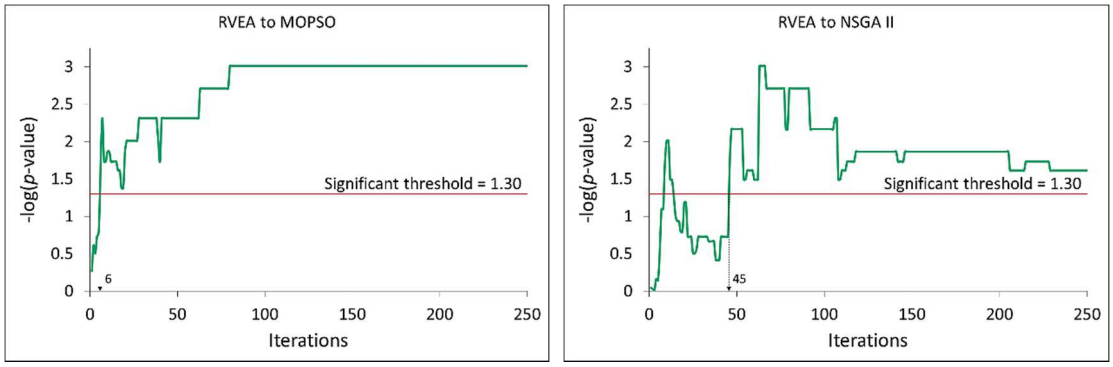

(b) Zagadka Field

Figure 5.14—Significant level of history-matching runs with RVEA compared to both NSGA-II and MOPSO algorithms on (a) PUNQ-S3 and (b) Zagadka Field.

5.4.3.3 Diversity of Matched Models

We looked at the diversity of matched models in the objective space from the history matching with each algorithm by using radial coordinate visualisation (RadViz) [289]. RadViz is a multi-dimensional visualisation technique that can display data of three or more objectives in a two-dimensional projection. The objectives (called dimensional anchors) are distributed evenly along the perimeter of the unit circle after normalisation. Each objective vector is then held with springs that are attached to the anchors, and the spring force is proportional to the value of the corresponding objective or anchor. The objective vector is depicted as a point in the circle and located in which the spring forces are in equilibrium. For example, a point that is located close to an anchor of one objective have a higher value in that objective than in any other objective. Objective vector with all equal objective values is located exactly in the centre of the circle.

As an illustration, Figure 5.15 (a) and (b) show RadViz plots of obtained nondominated solutions from RVEA and MOPSO on the three-objective DTLZ2 problem, and its true Pareto front is showed in Figure 5.15 (c) as a reference. A diverse set of solutions can be identified by the distribution of the points to different areas in the circle, as shown in Figure 5.15 (a), whereas the points where are concentrated or clustered in one particular area in the circle indicate less diverse solutions, as shown in Figure 5.15 (b).

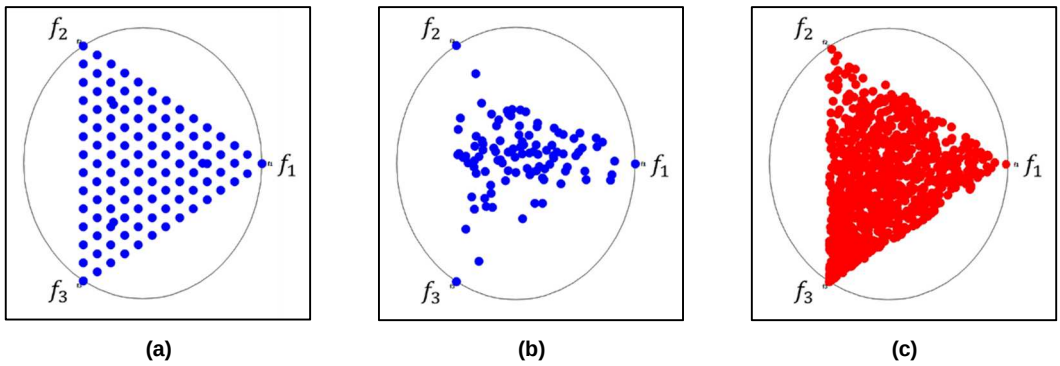

Figure 5.15—The RadViz plot of nondominated solutions obtained by (a) RVEA and (b) MOPSO on the three-objective DTLZ2 problem. The true Pareto front of three-objective DTLZ2 is shown in (c) as a reference. RVEA obtains more diverse solutions than MOPSO.

Figure 5.16 shows the RadViz plot of all the nondominated matched models obtained by each algorithm on PUNQ-S3 and Zagadka Field case studies in the run associated

with the median final misfit value. The plot is colour-coded according to the total misfit values.

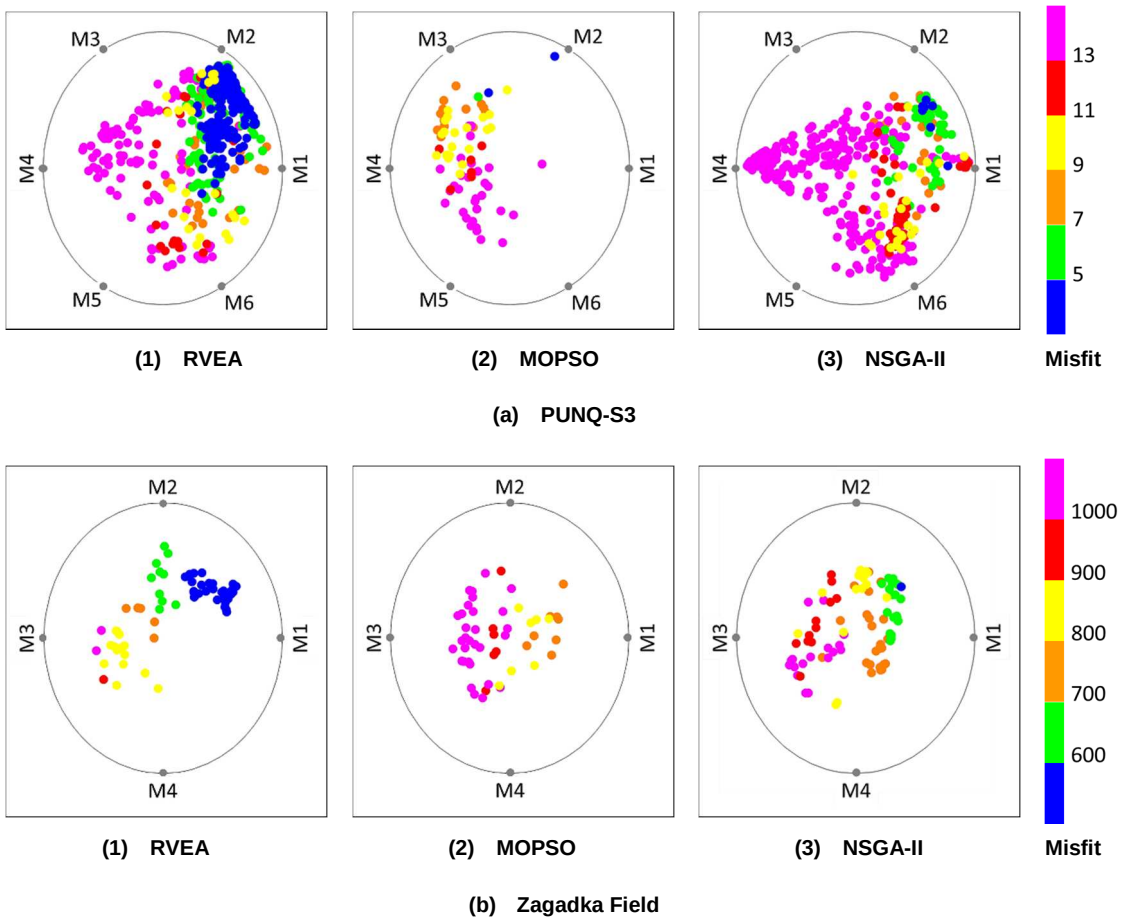

Figure 5.16—The RadViz plots of the nondominated matched models obtained by each algorithm on (a) PUNQ-S3 and (b) Zagadka Field, in the run associated with the median final misfit value. The plots are colour-coded according to the total misfit values. M_i is the objective defined in Equation (5.12) and (5.14) for PUNQ-S3 (6 objectives) and Zagadka Field (4 objectives), respectively, with their values are normalised.

In PUNQ-S3, history matching with RVEA provides more diverse set and higher quality of matched models than MOPSO, as shown Figure 5.16 (a1) and (a2), respectively. The diversity of the matched models from RVEA is comparable with NSGA-II, as shown in Figure 5.16 (a1) and (a3), respectively.

However, the number of high quality nondominated matched models (i.e. total misfit value < 5) from RVEA is larger (245 models) than MOPSO (two models) and NSGA-II (seven models), as shown in Table 5.5. History matching with MOPSO results in the worst performance amongst others (low match quality and the least diverse set of

matched models), as shown in Figure 5.16 (a2) and Table 5.5. In Zagadka Field, history matching from all algorithms provides a similarly diverse set of the matched models, as shown in Figure 5.16 (b). However, history matching from RVEA results in more matched models (33 models) with higher quality (i.e. misfit value < 600) than NSGA-II (one model) and MOPSO (none), as shown in Table 5.5.

These results demonstrate that RVEA successfully obtained high quality and yet diverse set of history-matched models.

Algorithm	PUNQ-S3 (6 objectives)			Zagadka (4 objectives)		
	Total number of simulations	Number of nondominated models	Number of nondominated models below total misfit (M < 5)	Total number of simulations	Number of nondominated models	Number of nondominated models below total misfit (M < 600)
RVEA	1,500	530	245	250	65	33
MOPSO	1,500	74	2	250	51	0
NSGA-II	1,500	418	7	250	94	1

Table 5.5—Results of the performance of RVEA, MOPSO and NSGA-II on PUNQ-S3 and Zagadka Field case studies on the number of obtained nondominated solutions and their quality in the run associated with the median final misfit value.

5.5 Discussion

Having reviewed population-based multi-objective optimisation algorithms and observed their niche on various practical problems involving mostly two or three objectives [202,208], there is now a growing need for an algorithm for handling many-objective (having four or more objectives) problems. In this chapter, we introduce a recently proposed many-objective optimisation algorithm, termed RVEA, for history matching problems.

The effectiveness of the reference vector in the evolutionary algorithm search on a high number of objectives is demonstrated on some numerical experiments by use of test functions. When tested to the well-known scalable test suites DTLZ and its scaled version, RVEA can obtain solutions with good diversity and convergence to the true Pareto front on 3, 4, 6, 8 and 10 objectives. Compared to two of the state-of-the-art multi-

objective algorithms, namely MOPSO and NSGA-II, RVEA outperforms both algorithms by having significantly higher HV values.

We demonstrated that the reference vector mechanism had shown high efficiency in dealing with history matching problems where the number of objective functions is high and the objective values are not always well scaled (i.e. different ranges of objective values in all objectives). When applied to the history matching problems with high number of objectives, i.e. six objectives on PUNQ-S3 and four objectives on Zagadka Field history matching case studies, RVEA can achieve fast misfit convergence, obtain high quality and a diverse set of matched models. Compared to MOPSO and NSGA-II, RVEA improves the history-matching performance significantly based on statistical tests over 10 independent runs. History matching with RVEA results in more-robust misfit evaluation (smaller variation between 10 runs) and better match quality (lower misfit values) than MOPSO and NSGA-II. In PUNQ-S3, history matching with RVEA can achieve up to 6.8 and 3.6 times faster misfit convergence than history matching with MOPSO and NSGA-II, respectively. In the real-field case study, Zagadka Field, the misfit convergence speed from history matching by RVEA can be up to 6.25 and 3.1 times faster than MOPSO and NSGA-II, respectively.

RVEA also successfully maintains the diversity of the matched models in both case studies, which are essential for better forecasting. In general, history matching with RVEA provides a more diverse set of models than MOPSO and NSGA-II. The diversity on the ensemble of these models ensures an improved uncertainty quantification in the forecasting period from these models [7–10].

These results demonstrate that, from the three compared algorithms and presented case studies, RVEA is the best algorithm to provide high quality and diverse matched models on the many-objective history matching, followed by NSGA-II and MOPSO algorithms, consecutively.

Chapter 6

Reservoir Development Optimisation Under Uncertainty for Infill Well Placement

6.1 Introduction

In an uncertain and volatile oil price environment, mature field rejuvenation or brownfield redevelopment is becoming an increasingly attractive option to manage the production decline. At this stage, the assets are already owned, understood to a certain extent, and offer diverse enhanced oil recovery opportunities.

One of the essential strategies in brownfield redevelopment is optimally placing infill wells to maximise oil recovery from the field and to minimise operational expenditure. This strategy ensures the company will gain a positive cash flow to sustain their business. Moreover, due to an extensive period of low oil price environment, this strategy can accommodate the company portfolio on cutting the operational budget including the field development budget while still keep on improving the oil recovery from the field.

Infill well drilling is a substantial capital investment decision. For instance, it needs around 15–30 million dollars to drill and complete an offshore oil well with a standard

jack-up oil rig (http://www.rigzone.com/data/dayrates/). Hence, well-informed and robust decision-making on infill well placement based on available knowledge of the reservoir has always been a critical component in a reservoir development.

A company uses reservoir model flow simulation as the standard tool to justify the decision to achieve their objectives. At brownfield life stage, the reservoir model is calibrated to match flow simulation response closely to the production data. Uncertainty in the model parameters arises due to limitations in the understanding of the reservoir. A proper uncertainty quantification strategy is needed to account for these factors in decision-making processes. This uncertainty prediction is used to manage the expectation of returns within the company portfolio. The forecast optimisation of the recovered oil to justify the decision to determine optimal infill well location should be robust and reliable to avoid any disappointment from the outcome.

Well placement optimisation problems are affected not only by design variables (i.e. well location) but also by often unmanageable stochastic parameters, such as noise and sparse nature of reservoir and well data (i.e. core data, well logs, seismic data) that are used to construct a reservoir model. Hence, uncertainty is an inherent characteristic of any reservoir model and the unique true distribution of reservoir properties will remain unknown.

Jin and Branke [290] made a distinction between optimisation problems considering uncertainty in:

(a) Objective function evaluation subjected to noise originated by different sources. In reservoir modelling, this type of uncertainty can be mimicked by different realisations that result in a different value of the objective function in the same set of decision variable.
(b) Perturbations or changes occur after the optimal solution was found.
(c) The estimated fitness function is obtained by an approximation of the real one.
(d) Fitness may vary with time, i.e. optimisation algorithm must be updated continuously.

In the present chapter, we deal with the problems of category (a) where the geological uncertainty is propagated to the optimisation decision-making through the variation of objective function evaluation across different model realisations. The main reason behind this as pointed out by Demirmen in 2009 [291], one of the most difficult factors to account for in decision-making is geological uncertainty. Hence, any attempt that can contribute to handle this difficulty would be useful.

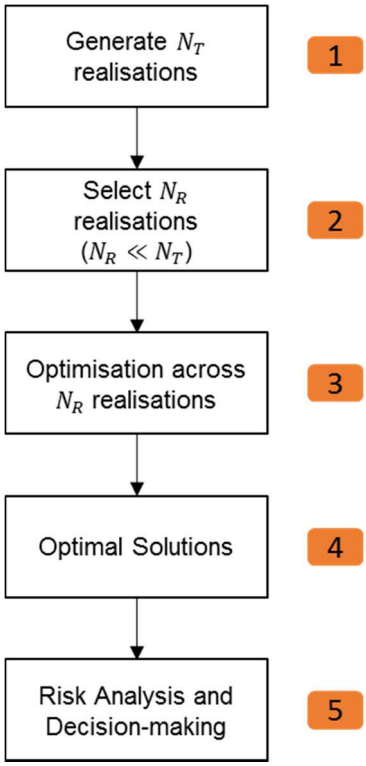

Figure 6.1—General diagram of decision-making on well placement optimisation across multiple model realisations.

Figure 6.1 shows a general diagram for decision-making to identify the optimal well location with a reservoir model simulation subject to geological uncertainty. The uncertainty quantification of the forecast optimisation is constructed through generation of finite number of model realisations θ_d that represents the unknown uncertainty space Θ. Then, a small set of representative realisations θ_R are selected for optimisation across multiple model realisations to reduce computational cost, i.e. the number of flow simulations.

$$\theta_R = \{\theta_1, \theta_2, \dots, \theta_{N_R}\} \in \theta_d = \{\theta_1, \theta_2, \dots, \theta_{N_T}\} \in \Theta \quad (6.1)$$

where N_T is the total of generated model realisations and N_R is the number of representative realisations ($N_R \ll N_T$).

From the general diagram in Figure 6.1, we can identify several challenges that arise in justifying the decision on where to place the infill well in the brownfield development stage:

1. *How to generate the model realisations?*

Production data is available abundantly from the brownfield. These data can be used to calibrate a reservoir model through history-matching process. Multiple realisations are then generated to represent many plausible property distributions of a reservoir model that reasonably match to the production data.

2. *How to select the models for the development optimisation task?*

As the ensemble of matched-models can include hundreds or thousands of realisations, the optimisation of infill well locations on all of these models will involve high computational costs. Therefore, a small set of model realisations should be selected. The models to be selected should be diverse and representative regarding possible geological uncertainty to make the computation visible and yet result in robust optimal solutions between different history-matching runs.

Following up to this second question is, *how to quantify the range of uncertainty from all of the selected models?*

Assigning a weight or probability to each selected model is also an important task (history matching realisations are not necessarily equally probable) to get a reliable and accurate range of uncertainty estimation. The standard way is to estimate a posterior probability distribution (PPD) which leads to high computational costs.

3. *How to perform the optimisation across multiple model realisations?*

In this chapter, we perform two different ways of performing optimisation across multiple model realisations: the extended nominal optimisation and the robust optimisation, which is described in Sections 6.3.3.1 and 6.3.3.2 respectively. We evaluate the feature and limitation of both ways through the demonstration from two case studies.

4. How to select the optimal well locations?

Different selected model realisations provide either the same or different optimal solutions. It is necessary to ensure the solutions are optimal across all possible history-matched geological realisations to support a robust decision and to avoid suboptimal solutions. Different optimisation approach has a different way of selecting the optimal solutions that will be demonstrated through the case study.

5. How to perform risk analysis and decision-making?

Even though there is no definitive way of doing this step (i.e. depends on the project portfolio, the behaviour of decision-maker, and decision criteria), we attempt to demonstrate the process of risk analysis and decision-making through two case studies on field applications.

In this chapter, we propose a workflow for optimisation of well placement under uncertainty at a brownfield development stage in an attempt to address the challenges above. We tested our workflow on the infill well placement optimisation problem and the decision-making process for PUNQ-S3 [243], a standard reservoir model for benchmarking, and evaluate the consistency of the output from the workflow across different history-matching runs. We validated our proposed technique for selecting the representative optimal well locations with exhaustive flow simulation runs and “truth” case scenario.

6.2 A Brief History on Well Placement Optimisation

In the last few decades, many works have been done in well placement optimisation exercises to help decision-makers. Methods have shifted gradually, from the traditional use of quality maps [292–294] to automated processes using either gradient-based [295–

297], local optimisation method [298], or global optimisation search strategies such as genetic algorithm (GA) [19,134,299–304] and particle swarm optimisation (PSO) [114,305], and ensemble-based data assimilation [22,306–308].

The gradient-based technique has the advantage of converging to the optimal solutions quickly but suffers from problems of high-nonlinearity as it can easily get trapped in the local optimum solutions, as reviewed in Chapter 2. Recent studies in the area of optimisation using the gradient-based techniques can be found in [309,310] . In [309], gradient-based multi-objective optimisation was applied to waterflooding optimisation. In [310], the same authors demonstrated a multi-objective steepest descent method applied to well control optimisation. Both studies suggested the use of multi-objective optimisation for handling multiple conflicting objectives in the optimisation and demonstrated the superior efficiency of the algorithm compared to other competing multi-objective optimisation algorithms.

The global search capability has the significant advantage in stochastic approaches over gradient-based approaches, given the often significantly nonsmooth objective functions associated with the well placement optimisation problem, as reviewed in Chapter 2. Several studies have dealt with the combination of this technique with others in the area of well placement optimisation [311–313]. In [311], Bouzarkouna *et al.* applied the derivative-free optimiser covariance matrix adaptation evolution strategy (CMA-ES) and meta models. In [312], Nwankwor *et al.* hybridised the differential evolution (DE) algorithm and PSO for well placement optimisation, whereas in [313] Ding *et al.* combined the modified PSO with the quality map technique. These combinations and modifications were successfully implemented and demonstrated improvements in the performances either in the optimisation process itself or the outcome from the optimisation.

Extensions of global search optimiser to multi-objective optimisation in the well placement optimisation have also been implemented successfully in the literature [173, 314–319]. The multi-objective optimisation approach overcomes the difficulty of the single-objective optimisation to address objectives with differing data types, to accommodate multiple objectives, and to handle conflicts between objectives.

Ensemble-based optimisation has gained popularity recently due to its ability to capture uncertainty represented by multiple realisations of the reservoir model. Instead of deterministic optimal objective function values, optimisation based on multiple realisations provides a probability of the expected optimal objective function value. History matching, as a model calibration process, can be used to generate an ensemble of model realisations consistent with the prior geological information and able to provide flow simulation response that matches with observed production data. The combination of history matching with reservoir management has been studied previously in [22,306–308] to update the model for optimisation in the closed-loop reservoir development framework. In [306,307], history matching is done by ensemble Kalman filter (EnKF), whereas in [22], Shirangi and Durlofsky accomplished the history matching with an adjoint-gradient-based randomised maximum likelihood (RML). In [308], Bukshtynov *et al.* developed and applied a unified adjoint-based data assimilation in the history-matching component of the workflow.

There have been several published attempts to account for uncertainty in well placement. Aanonsen *et al.* [18] presented a method for optimising well location while taking into account uncertainty in geological modelling. Guyaguler and Horne [19] assessed the uncertainties associated with different well placement using the utility theory framework. They used 23 realisations of history-matched models and truth case of the synthetic reservoir model to demonstrate the applicability of the utility framework. Ozdogan and Horne [320] included time-dependent information in the well placement optimisation to achieve better decisions in terms of reduced uncertainty and increased probable net present value (NPV). Van Essen *et al.* [20] studied a robust optimisation from two different sets of 100 realisations of reservoir models in the waterflooding. They compared the results with the reactive and nominal optimisation. Bouzarkouna *et al.* [21] presented an approach to handle geological uncertainty, represented by 20 geological realisations, for the well placement with a reduced number of reservoir simulations by using simulated well configurations in the neighbourhood of each well configuration. They combined this approach with the stochastic optimiser CMA-ES.

However, all of these noted optimisation studies account for uncertainty by using the assumption of equally probable multiple realisations, which is most likely not the case.

In real life, we know that we are not certain about the likelihood of each model, but we can constraint each model to the observed data to obtain the likelihood based on the discrepancy between model responses to observed data. Hence, assigning an equal probability for each model in the optimisation is rather a "*naïve*" approach that may lead to unreliable uncertainty prediction.

Another challenge in the optimisation under uncertainty is the high computational cost, as the optimisation involves simulating many model realisations. Various approaches for the model selections out of large set of models have been carried out in previous studies within a different context. Scheidt and Caers [321] used kernel k-means clustering from the equally probable model realisations. The representative models are weighted based on the number of members in each cluster. They used this technique for uncertainty estimation with streamline simulation. Wang *et al.* [322] also applied k-means clustering on selecting model realisations for well placement optimisation and assigned an equal probability to each model realisation. In their study, the weight for each selected model depends on the number of models in each cluster. Yang *et al.* [323] selected the models by ranking all realisations (which are assigned as equally probable) in terms of the NPV for a base case and then selecting nine realisations corresponding to *P10*, *P20*, *P30*, …, *P90* of the NPV distribution. They applied this technique in the optimisation of steam-assisted gravity drainage (SAGD) operations.

6.2.1 Some Remaining Problems

There are some remaining problems that have been identified from all of these noted studies on: (1) how to select a diverse set of models for optimisation; (2) how to approximate posterior probability for the reliability of optimisation uncertainty prediction; and (3) how to reduce high computational (or CPU=central processing unit) costs without compromising uncertainty quantification.

In the present work, we use the multi-objective approach in the history matching that allows us to obtain a diverse set of the model realisations which should lead to better forecasting, as shown in [7–10] and Chapter 3 in this thesis. We use the multi-objective variants of PSO [102], so-called multi-objective particle swarm optimisation (MOPSO)

[207], both in the history matching and in the well placement optimisation. We then use the history-matched models to infer their PPD under the Bayesian framework and then propagate uncertainty to the optimisation of well placement. The multi-objective approach in the optimisation allows us to maximise recovery and to minimise cost, or to maximise the expected oil recovery over multiple model realisation and to minimise its variance. These objectives are the key factors in the successful brownfield development.

Our approach accounts for uncertainty represented by a weighted probability of the selected models from a pool of not only calibrated but also weighted geological realisations. Calibrated models are the models whose responses mimic the observed production data, whereas the weighted geological realisations are those calibrated models that are associated with the PPD attached to each model. Accurate PPD is essential in uncertainty quantification studies but often limited to the CPU demands. We propose an accurate and yet manageable way to approximate the PPD for optimisation under uncertainty studies.

In this chapter, we perform optimisation under geological uncertainty to place infill well to increase the oil recovery by using multi-objective formalism. We use multi-objective history matching to generate multiple model realisations combined with Bayesian analysis for uncertainty quantification. We select the Pareto models (PMs) as the diverse set of good matched models and perform multi-objective optimisation across these selected models (i.e. by extended nominal optimisation or robust optimisation). The Pareto front solutions are selected as the optimal solutions and analysed for the decision-making by imposing the assigned calculated model probability. This workflow enables us to reduce the computational cost to a manageable amount while still obtaining representative and reliable optimal solutions.

6.3 Methodology: The Proposed Workflow

Figure 6.2 shows the general diagram of the proposed workflow for the optimisation under uncertainty used in the present chapter. The numbers in orange correspond to the general workflow steps in Figure 6.1. We describe each step in the following sections.

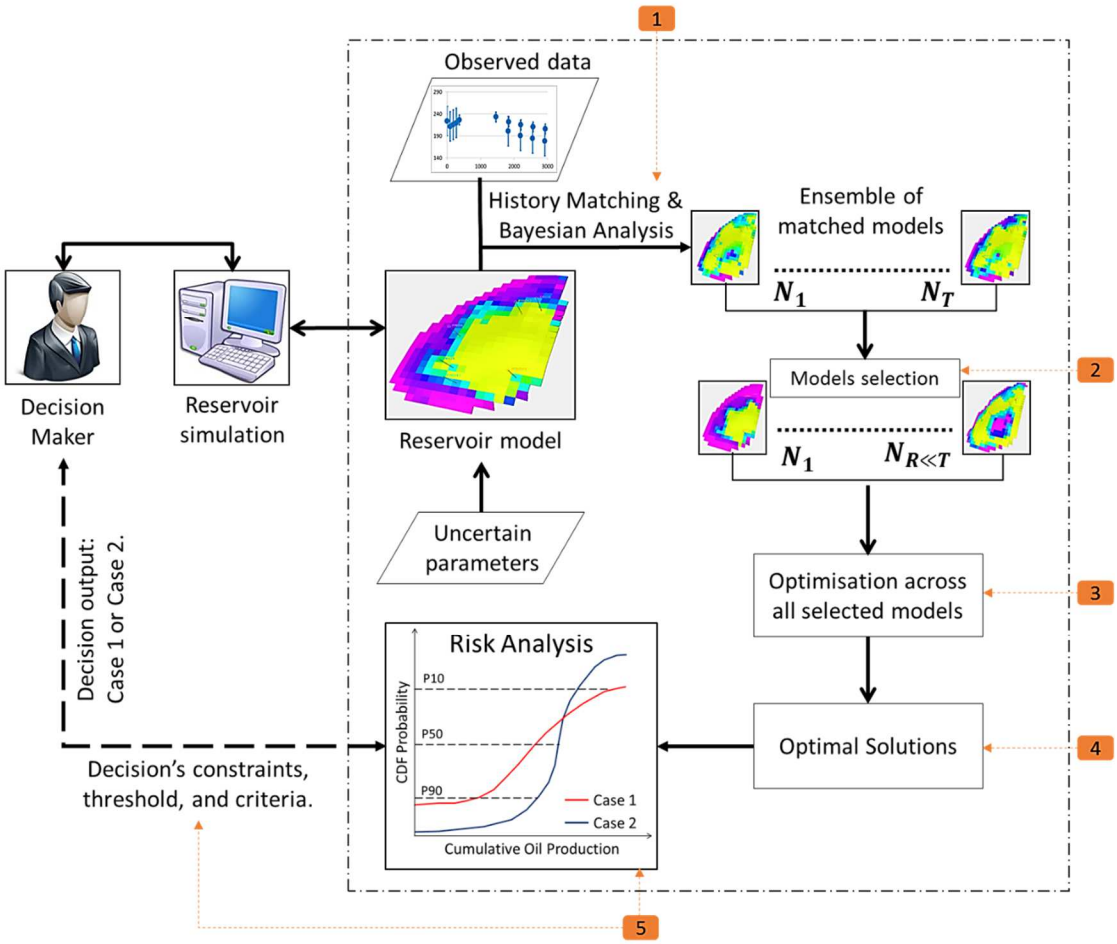

Figure 6.2—General diagram of the proposed workflow for the optimisation under uncertainty.

6.3.1 Step 1: History Matching and Bayesian Analysis

The objective in the first step is to generate N_T model realisations along with their PPD. Given production data at the mature stage of a field, we perform history matching to get an ensemble of good matched models. We use a multi-objective approach in the history matching as it will result in a diverse set of matched-models. These models are more likely to produce different flow responses, leading to a better (more robust) optimisation forecast [7–10]. Then, we perform Bayesian analysis to approximate the PPD for each matched-model. As in the previous chapter, we use neighbourhood algorithm coupled with Bayesian, i.e. neighbourhood algorithm Bayes (NAB) [215] to construct the PPD for each matched-model and filter out the low-quality models with low likelihood (i.e. high misfit value and zero PPD).

6.3.2 Step 2: Model Selection

The objective of the second step is to select a small subset of N_R representative model realisations. As in the multi-objective optimisation the nondominated solutions are located on the Pareto front in the objective space, we select the PMs from the previous multi-objective history matching. Pareto optimality and non-dominance mechanisms ensure the high match quality and diversity of the selected history-matched models.

6.3.2.1 Posterior Inference

The range of uncertainty estimate in the optimisation forecasting is evaluated by assigning a posterior probability for each selected model. A proper posterior probability estimation for each model used in the optimisation is essential to have a good uncertainty estimation of optimal solutions. In the present chapter, we use Bayesian framework for this task which involves three steps:

1. Computing *posterior probability* for each matched-model by using NAB [48]. This step is done in *Step 1* of the proposed workflow.
2. *Clustering* NAB models in a standardised parameter space between the Pareto nondominated solutions.
3. *Estimating the probability* for each PM by calculating a sum of posterior probabilities in each cluster.

The reapproximation of PPD for each PM is done by clustering resampled posterior of NAB models in the standardised parameter space, as defined in Equation (6.2). This standardisation is required as the ranges of values in each model parameters are not necessarily the same (i.e. one parameter can have a range of value from zero to one, whereas the other from zero to 10). The standardisation ensures that the distance calculation to cluster centre from each model will have the same scale.

$$Z_{ij} = \frac{X_{ij} - \mu_i}{\sigma_i}; i = (1,2, \dots, n_p), j = (1,2, \dots, N_T) \tag{6.2}$$

where Z_{ij} is the standardised value of a particular parameter i in a model j, X_{ij} is the original value of a particular parameter i in a model j that is being standardised, μ_i and σ_i is the mean and the standard deviation, respectively, of the distribution of a particular parameter i in all N_T models, and n_p is the number of model parameters.

The centre of each cluster is fixed to PMs. The members of each cluster are classified by computing the Euclidean distance between the PMs to the other models in the standardised parameter space, as defined in Equation (6.3). Then, the nearest neighbour model will be allocated to each cluster based on the closest Euclidean distance of Equation (6.3), as described in Equation (6.4).

$$d(P_c, Q_j)_{P_c \neq Q_j} = \sqrt{\sum_{i=1}^{n_p} (P_{c,i} - Q_{j,i})^2} \tag{6.3}$$

$$\overline{P_c} = \left\{ I_j \middle| \underset{j \in (1,2,\ldots,N_T)}{\operatorname{argmin}} d(P_c, Q_j) \right\} \tag{6.4}$$

where P_c is the PM as the fixed centre of a cluster, c is the number of cluster, i.e. $c = (1,2,..,N_R)$, Q_j is the models other than the PM, $j = (1,2,\ldots,N_T - N_R)$, n_p is the number of model parameters, and I_j denotes the I-th model allocated to a cluster with the centre of P_c. Then, the sum of probabilities in each cluster will be assigned as the new probability to each cluster centre (i.e. the PM), as defined in Equation (6.5).

$$\mathbb{P}_{P_c} = \sum_{k=1}^{n_c} \mathbb{P}_{k,c}(m|O) \tag{6.5}$$

where $\mathbb{P}_{P_c}$ is the recalculated posterior probability for the PM P_c, n_c is the number of models in cluster c, and $\mathbb{P}_{k,c}(m|O)$ is the posterior probability of each model in the cluster c.

Figure 6.3 shows how the model clustering and the PPD recalculation is done in a one-dimensional case. In reality, this clustering and probability recalculation will be done in multi-dimensional parameter space where history matching is performed. The output

from *Step 2* are the selected models (i.e. PMs) with the recalculated posterior probability assigned to each of them.

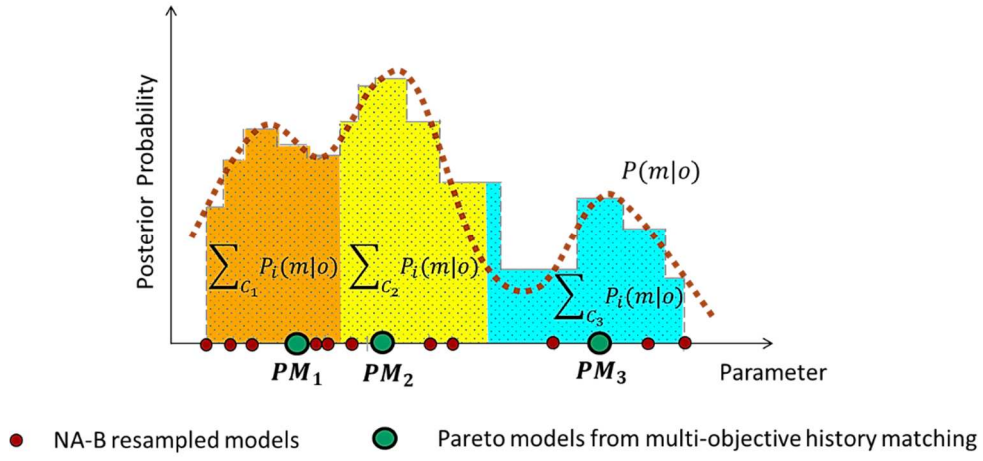

Figure 6.3—An illustration of NAB model clustering and posterior probability recalculation in a hypothetical one-dimensional problem.

6.3.3 Step 3 and 4: Optimisation Across Multiple Models and Optimal Solution Selection

We describe two different ways of conducting optimisation across multiple model realisations, i.e. the extended nominal optimisation and robust optimisation.

6.3.3.1 Extended Nominal Optimisation

The nominal optimisation is based on a single model realisation. After N_T model realisations are generated and ranked, usually a "*P50* realisation" is selected as the best guess. Then, the objective function is calculated based on the simulation results of the "*P50* realisation" only. Afterwards, the resulting optimal solutions are subsequently applied to the N_T realisations resulting in N_T predictions. These N_T predictions can be further used for risk analysis of the decision-making (see for example [20,323] where the nominal optimisation is used and compared with the robust optimisation).

However, the "*P50* realisation" is non-unique. As this realisation is obtained by a ranking process based on a particular production data, i.e. oil rate, different production data may result in the different rank of models, and consequently different "*P50* realisation".

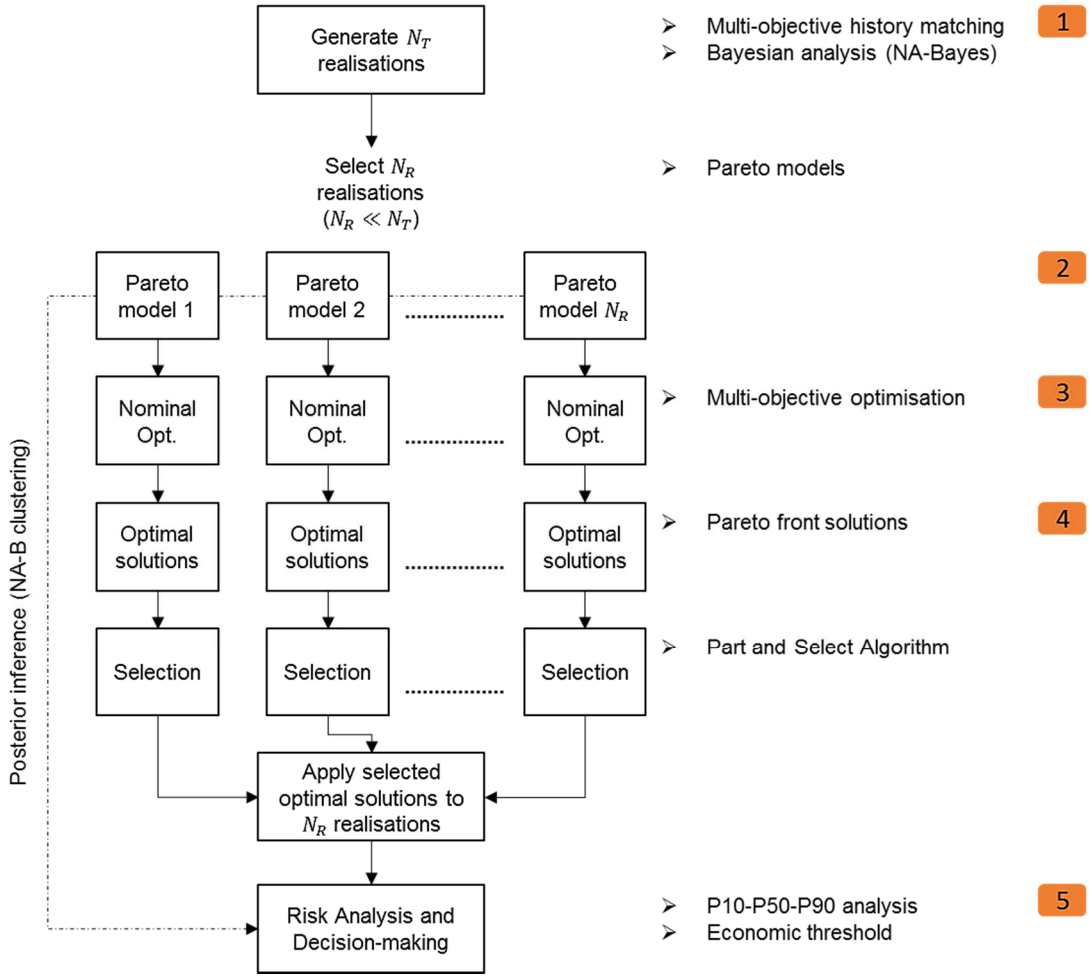

Figure 6.4—The workflow diagram of the extended nominal optimisation.

In the present chapter, we extend the nominal optimisation which is based on several selected model realisations from history matching, hence the extended nominal optimisation. After N_T model realisations are generated by multi-objective history matching and the Bayesian analysis is performed, we select N_R PMs. Then, we perform a multi-objective optimisation individually for each selected PMs. Afterwards, the resulting Pareto front solutions as the optimal solutions are selected and subsequently applied to the other N_R model realisations. These N_R predictions can be further used for risk

analysis of the decision-making. Figure 6.4 shows the workflow diagram of the extended nominal optimisation for the optimisation across multiple model realisations.

Challenges

One of the challenges in the optimisation across multiple model realisations by the extended nominal optimisation is the optimal solutions found by the optimiser are not always the same across different model realisations, as illustrated in Figure 6.5. From Figure 6.5, we can see that both model realisations (i.e. Model 1 at the left and Model 2 at the right) have some common optimal solutions at Grids (11,25), (16,23), and (17,23). However, optimal solutions at Grids (11,20) and (12,10) from Model 1 are not found in the set of optimal solutions from Model 2. Similarly, the optimal solution at Grid (7,22) from Model 2 is not found in the optimal solutions on Model 1, as shown in Figure 6.5.

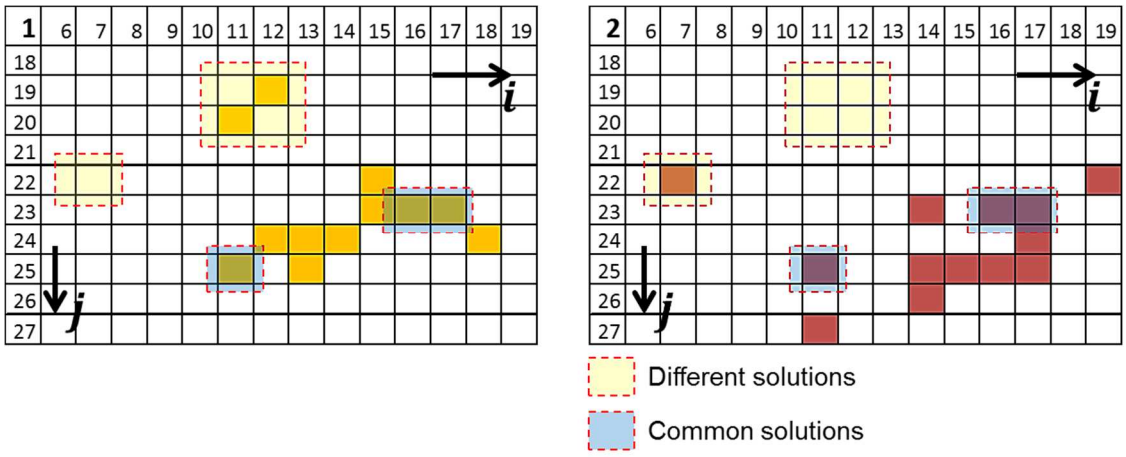

Figure 6.5—An illustration of different and common optimal solutions found by two independent optimisations from two different model realisations' optimisation (i.e. left for Model 1 and right for Model 2).

A straightforward way of solving this problem is by rerunning all optimal solutions found from each model to the other models that have different solutions. However, this approach can potentially lead to an exhaustive flow simulations effort across all optimum solutions across all the models that can be computationally expensive. As an illustration, if there are five geological model realisations in the optimisation and each of them has 10 different optimal solutions between each model, in total there are 50 different optimal solutions. All of these must then be run for each model realisation to avoid suboptimal solutions. For instance, in one model we need to run the simulation for

another 40 optimal solutions, and the same optimal solutions with the next models. In total, we need to run an additional 200 flow simulations, a total of which may increase if we have more model realisations and more optimal solutions. To tackle this issue, we use *part and select algorithm* (PSA) [324] to select a small set of optimal solutions to be rerun across all models, which will be representative of the optimal solutions if they are run exhaustively.

PSA

Salomon *et al.* [324] originally introduced PSA as a selection mechanism in MOEA. It works by partitioning a given set of points in the objective space into smaller subsets. PSA performs $(m-1)$ divisions of one single set into two subsets to partition a set into m subsets. At each step, the set with the biggest dissimilarity amongst its members is the one that is divided. This is repeated until the stopping criteria is met, i.e. a predefined number of subsets or a maximal dissimilarity amongst each of the subsets.

Let $A \coloneqq \{\mathbf{f}_1 = [f_{11}, \dots, f_{1k}], \dots, \mathbf{f}_n = [f_{n1}, \dots, f_{nk}]\} \subset \mathbb{R}^k$ (i.e. n objective vectors $\mathbf{f}_i = F(x_i)$ for points $x_i \in Q$), and denote

$$a_j \coloneqq \min_{i=1,\dots n} f_{ij}, b_j \coloneqq \max_{i=1,\dots n} f_{ij}, \Delta_j \coloneqq b_j - a_j, j = 1, \dots, k \tag{6.6}$$

$$\emptyset A \coloneqq \max_{j=1,\dots k} \Delta_j \tag{6.7}$$

The pseudocode of PSA for a fixed value of m (i.e. the size of the representative subset) is shown in the Algorithm 6.1 below. The dissimilarity of a set A is defined by the measure in Equation (6.7). Once the set A has been divided into m subsets, the representative from each subset is chosen by the closest Euclidean distance to the centre of hyper rectangle circumscribing A_i. If there is more than one member closest to the centre, one of them is chosen randomly.

Figure 6.6 illustrates the steps of the PSA on choosing $m = 3$ representatives of Pareto solutions from 13 points in a hypothetical optimisation problem with two objectives. By

Algorithm 6.1—Partitioning a set A into m subsets by PSA [324].

1: $A_1 \leftarrow A$

2: Evaluate $\emptyset A_1$ according to Equation (6.7) and store $\emptyset A_1$ in an archive

3: $i \leftarrow 2$

4: **while** $i < m$ **do**

i) Find A_j and coordinate p_j such that $\emptyset A_j = \Delta_{p_j} = \max_{l=1,\dots i-1} \emptyset A_l$

ii) Part A_j to subsets A_{j1}, A_{j2}:

$A_{j1} \leftarrow \{\mathbf{f} = [f_1, \dots, f_{p_j}, \dots, f_k] \in A_j, f_{p_j} \leq a_{p_j} + \emptyset A_j/2\}$

$A_{j2} \leftarrow \{\mathbf{f} = [f_1, \dots, f_{p_j}, \dots, f_k] \in A_j, f_{p_j} > a_{p_j} + \emptyset A_j/2\}$

iii) Evaluate $\emptyset A_{j1}$ and $\emptyset A_{j2}$ according to (6.7), and replace in the archive $\emptyset A_j$ and p_j with the pairs $\emptyset A_{j1}$, $\emptyset A_{j2}$ and p_{j1}, p_{j2} accordingly.

iv) $S \leftarrow \{A_1, \dots, A_{j1}, A_{j2}, \dots, A_i\}$

v) $i \leftarrow i + 1$

5: **end while**

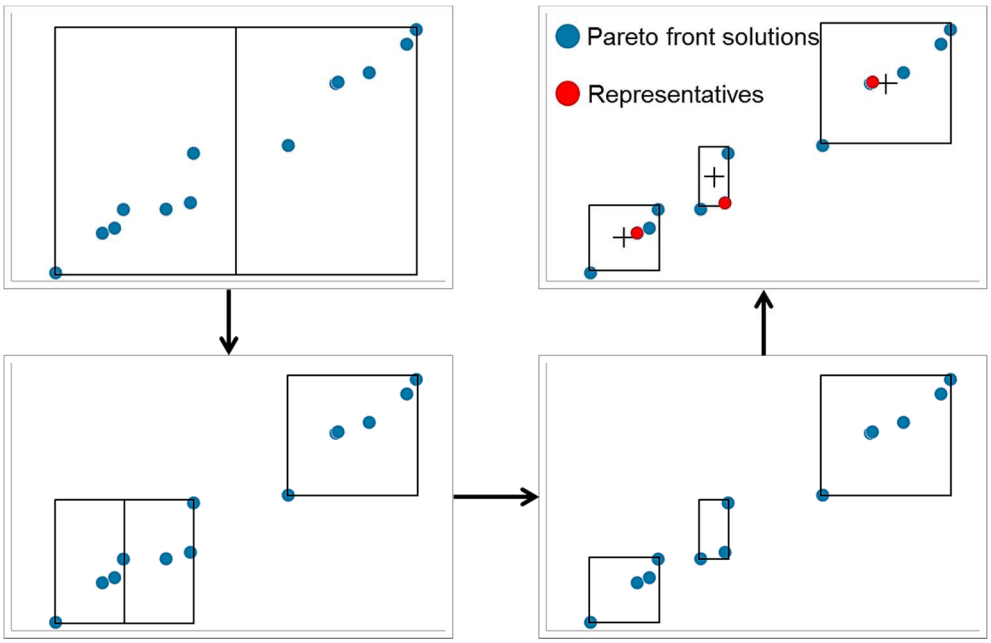

Figure 6.6—An illustrative example of the steps in PSA for choosing three representative solutions from 13 solutions in a hypothetical optimisation problem with two objectives (after [324]).

looking at Figure 6.6 in counter-clockwise from top-left, we can see that the first partition is made by vertical incision (the vertical line in the middle of the rectangle)

because the horizontal length of the given set has the biggest dissimilarity. The result of this partition is depicted in the bottom-left of Figure 6.6 as two rectangles. From these two rectangles, the lower-left has the biggest dissimilarity amongst its member and will be divided. Because the horizontal section on this rectangle has the biggest dissimilarity, the partition is made by the vertical incision. The result of this is shown in the lower-right as three rectangles and these are the three subsets from the PSA. The representatives of each subset are found by the closest Euclidean distance to the centre of each rectangle amongst the point in each subset, as shown by the red circle in the upper-right.

6.3.3.2 Robust Optimisation

The robust optimisation is based on multiple model realisations with expected measures as the objective functions. After N_T model realisations are generated, N_R model realisations are selected for robust optimisation. In the robust optimisation, the objective function is replaced by the expected outcome over the set of selected model realisations to account for the uncertainty, as defined in Equation (6.8). Afterwards, the resulting optimal solutions are selected and the risk analysis is performed for decision-making.

$$J_{RO}(\vec{x}) = \frac{1}{N_R}\sum_{i=1}^{N_R} J(\vec{x}, \theta_i) \tag{6.8}$$

where $J(\vec{x}, \theta_i)$ is the objective function of solution parameters $\vec{x}$ and model realisations θ_i, N_R is the number of selected model realisations, and J_{RO} is the objective function from robust optimisation.

Without loss of generality, extending the robust optimisation to the multi-objective optimisation of:

$$\left.\begin{array}{c}\text{maximise } \left(J_1(\vec{x}), J_2(\vec{x}), \dots, J_M(\vec{x})\right) \\ \text{subject to } \vec{x} \in S\end{array}\right\} \tag{6.9}$$

where $J_i(\vec{x})$ is the objective function, $i = (1,2,\dots,M)$, M is the number of objective functions, S is the parameter search space, all the M objective functions are replaced by

the expectation measure, as defined in Equation (6.8). Hence, in the robust multi-objective optimisation, the objective functions formulation becomes:

$$\left.\begin{array}{l}\text{maximise } \left(J_{RO,1}(\vec{x}), J_{RO,2}(\vec{x}), \ldots, J_{RO,M}(\vec{x})\right) \\ \text{subject to } \vec{x} \in S\end{array}\right\} \tag{6.10}$$

where $J_{RO,i}(\vec{x})$ is the robust optimisation objective function, as defined in Equation (6.8).

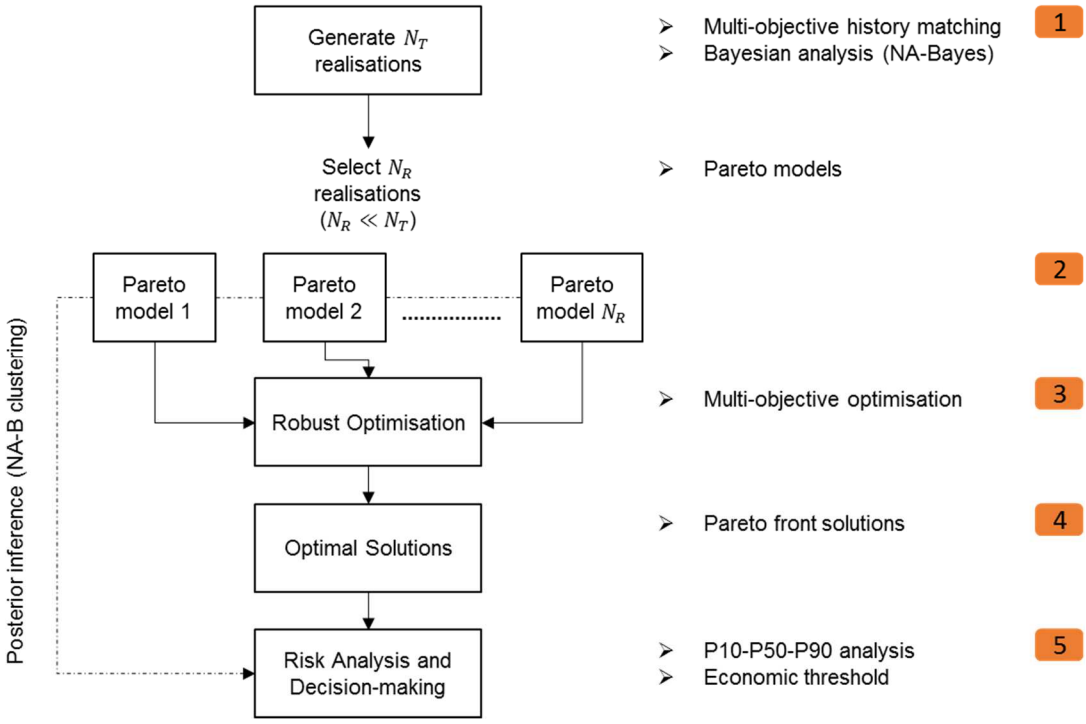

Figure 6.7—The workflow diagram of robust optimisation.

Figure 6.7 shows the workflow diagram of the robust optimisation used in this chapter. Multi-objective history matching is used to generate N_T model realisations. Then, the Bayesian analysis (i.e. NAB) is used to compute the PPD for each of N_T history-matched models. N_R PMs are then selected for optimisation under uncertainty. The robust multi-objective optimisation across these selected models are conducted based on the expected measure, as defined in Equation (6.8). Then, Pareto front solutions are selected as the optimal solutions which can be further analysed for decision-making.

The extended nominal optimisation and the robust optimisation have similarities and differences. Both of optimisation approaches are based on multiple realisations to account for the uncertainty, and in this chapter, both of them are used with the multi-objective approach. The main difference between them is in the objective functions definition. In the extended nominal optimisation, objective functions are evaluated separately from each optimisation model and then reevaluated across all optimisation models based on found optimal solutions. In the robust optimisation, objective functions are evaluated across all optimisation models simultaneously based on found optimal solutions, and the expectation measure is computed. Another difference is in the extended nominal solutions there is an extra step to account for different optimal solutions found by each optimisation model (i.e. with PSA), whereas in the robust optimisation this step is not required as all the found optimal solutions are common to all optimisation models.

6.3.4 Step 5: Risk Analysis and Decision-Making

The last step in the workflow is to perform the risk analysis for each selected optimal solution. In the present chapter, the risk analysis relies on the *P10*, *P50*, and *P90* Bayesian credible intervals on the optimisation forecast. PPD inference is used to construct these credible intervals. Then, based on decision's criteria, such as an economic threshold or tradeoff between objectives, the optimal infill well locations can be confidently decided.

6.4 PUNQ-S3 Field

We demonstrate the application of the proposed workflow to the PUNQ-S3 reservoir model on two case studies. In the first case study, we optimise an infill well location to maximise the oil recovery from the field and to minimise the water production rate from the field. We apply the extended nominal optimisation workflow, assess its decision consistency between different history-matching runs, validate the PSA method for selecting the representative of optimal solutions, and compare the results with the robust optimisation workflow.

In the second case study, we optimise three infill well locations to maximise the mean of oil recovery and to minimise the variance of oil recovery over multiple model realisations. We apply only the robust optimisation to achieve these objectives because it is the method that can accommodate the expectation and variance measures during optimisation run.

For both case studies, we use the same production history and profile that is described in the following section.

6.4.1 Present State

Initial oil-in-place at the beginning of production in 1967 was 17.37 million SM^3. Initial free gas was 0.36 billion $SM^{3,}$ and there were 1.28 billion SM^3 of dissolved gas in the reservoir. The field had been produced for 16.5 years until mid-1983 from the six producer wells. Producers 1 (PRO1), 4 (PRO4) and 12 (PRO12) are perforated in Layers 4 and 5. Producers 5 (PRO5) and 11 (PRO11) are perforated in Layers 3 and 4, whereas producer 15 (PRO15) is completed only in Layer 4.

"Truth" Case Reference

The truth case scenario [243] is used as a reference and for validation in both case studies. Several data can be acquired by simulating the truth case which mimics the real-life scenario when the data are available until the present day. For instance, at the present state (i.e. mid-1983), the PUNQ-S3 field had produced a total of 3.87 million SM^3 of oil from truth case simulation. In real life, this data can be acquired from the production report. The remaining oil left is 13.5 million SM^3 which become the target amount of oil need to be recovered.

We evaluated more details the initial- and current-oil-in-place in each layer of the PUNQ-S3 reservoir to determine the optimisation strategy on the well completion. Table 6.1 shows the initial- and current-oil-in-place in each layer of the PUNQ-S3 reservoir from the simulation of the truth case. We can see from Table 6.1 that there is a potential amount of oil that can be recovered from each layer of the PUNQ-S3 reservoir. Hence,

in the optimisation of the well placement, we complete and open all the layers to contribute in the oil production.

Layer	Initial-oil-in-place (million SM^3)	Current-oil-in-place (million SM^3)	Current recovery factor (%)
1	3.51	3.09	11.96
2	1.91	1.63	14.43
3	5.14	4.16	19.03
4	3.60	2.68	25.59
5	3.21	1.94	39.78
Total	**17.37**	**13.5**	**22.29**

Table 6.1—The initial- and current-oil-in-place in each layer of PUNQ-S3 reservoir.

Figure 6.8 shows the reservoir properties (porosity and permeability) and the current oil saturation map of the PUNQ-S3 reservoir in each layer based on the truth case scenario. We can see from the porosity and permeability maps that the PUNQ-S3 is a heterogeneous reservoir. Hence, it is necessary to perform optimisation of infill well placement based on different model realisations to capture this heterogeneity. From the current oil saturation map, we can see that each layer of the reservoir can contribute to increase the oil recovery from the field.

Note that in real life, we never know the exact truth of the reservoir such as the exact values of porosity and permeability and their spatial distribution. Hence, it is not a plausible choice to assume that the reservoir is homogeneous with no uncertainty on its properties. Therefore, it is important to conduct reservoir simulation for field development optimisation (e.g. infill well placement optimisation) based on multiple plausible model realisations to quantify the uncertainty. However, we have to make sure that the model realisations we use can robustly produce reliable optimisation forecasts. Hence, the necessity of a reference case such as a “truth” case scenario.

The truth case presented in this subsection serves as a reference and validation for the proposed methodology. The optimisation routine with the same objective functions will be applied deterministically to the “truth” case for the validation purpose on each case study presented in the next sections.

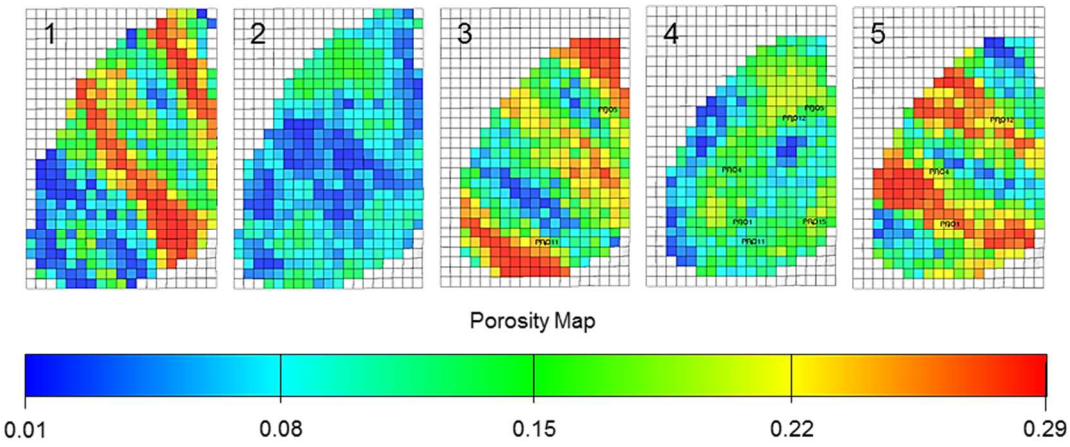

(a)

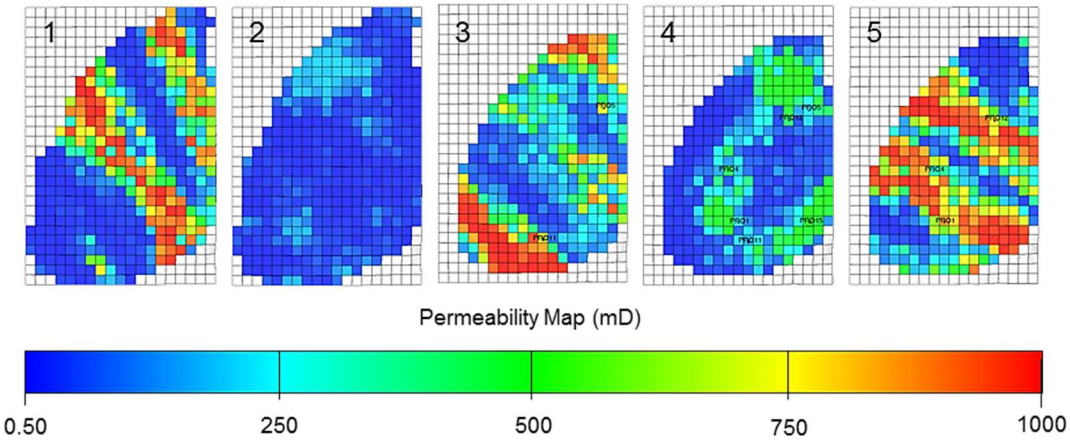

(b)

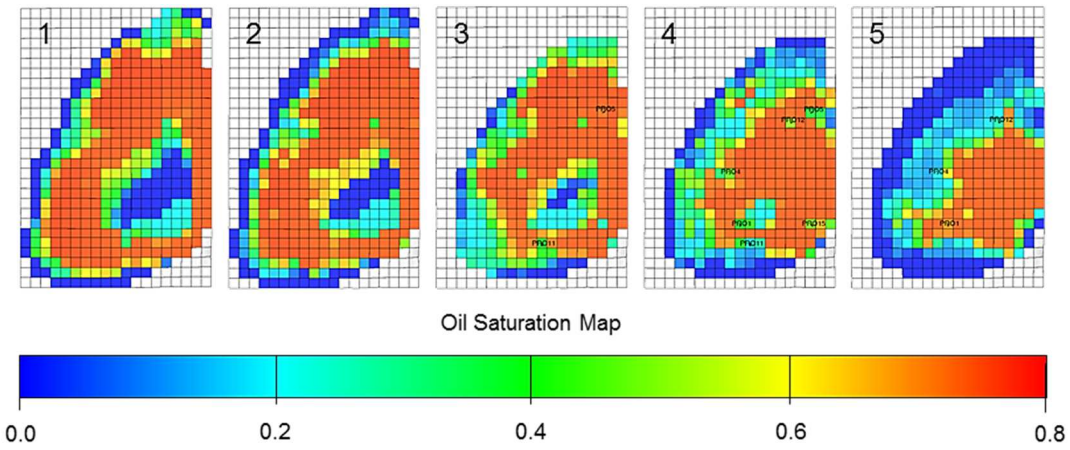

(c)

Figure 6.8—(a) Porosity, (b) Permeability, and (c) Current-oil-saturations maps in PUNQ-S3 reservoir based on the truth case scenario. The truth case is used as a reference and for validation.

6.5 Case Study 1: An Infill Well Placement

6.5.1 Production and Optimisation Setup

In the first case study, the PUNQ-S3 mature field is further developed by drilling a new vertical infill well after been produced for 16.5 years to increase oil recovery. The setup of production schedule in the reservoir for optimisation is listed as follows:

- Additional one vertical infill well to put on production for the next 10 years;
- Oil is produced with continuous condition (i.e. without any periodic shut-in as in history period) with a maximum oil production rate of 150 SM^3/day. There is only one-time shut-in period for 14 days for all wells before the new well is on production;
- Each producer well will produce with the maximum gas-to-oil ratio (GOR) 200 SM^3/day as the limiting factor, and when this limit is reached, the oil rate will be reduced with a factor of 0.75 with minimum 120 bars of grid block pressure.

The optimisation will be a two-objective problem, whose objectives are set to maximise the cumulative oil production from the field (a production variable that is related to value) and to minimise the maximum value of the water production rate from the field (a production variable that is related to cost). The objective functions are scalar-valued functions on a given model realisation, as formulated in Equation (6.11). These objective functions will be evaluated across all the selected models for optimisation.

$$J_1 = \sum_{w=1}^{N_w} \sum_{k=1}^{N_t-1} q_{o(w,k)} \cdot \Delta_{k,k+1}$$
$$J_2 = \underset{k}{\text{argmax}} \sum_{w=1}^{N_w} q_{w(w,k)} \tag{6.11}$$

where J_1 and J_2 are the first and second objective function values to be maximised and minimised, respectively; $q_{o(w,k)}$ and $q_{w(w,k)}$ represents the oil and water rate from a producer well at the simulation timestep k, respectively; $\Delta_{k,k+1}$ represents the period of

time from timesteps k to $k+1$; N_w is the number of producer wells, and N_t is the number of timestep at the end of simulation time.

The constraint in the optimisation is the new infill well could not be drilled in the inactive cells of reservoir model nor overlap with the current existing wells. These constraints ensure that the proposed new well will not be drilled outside the reservoir of interest and through the same well head with the existing well in the field.

6.5.2 Tests Overview

Several tests are conducted to evaluate the applicability of the proposed workflow with regard to decision-making and its robustness towards variation in history-matching outcomes. There are four tests altogether. Tests 1, 2, and 3 are related to the workflow using the extended nominal optimisation, as in Figure 6.4, whereas Test 4 is related to the workflow using the robust optimisation, as in Figure 6.7. The list of tests performed is as follows:

1. *Test 1*: in Section 6.5.3, we applied the proposed workflow by use of the extended nominal optimisation, as in Figure 6.4, for the decision-making on an infill well placement.
2. *Test 2*: in Section 6.5.4, we applied the same workflow as in Test 1 to different history-matching runs to test the consistency of the decision-making outcome with the different history-matching runs given the same optimisation setup and decision's criteria.
3. *Test 3*: in Section 6.5.5, we presented the validation of PSA as the method to select the optimal solutions for reducing the computational cost.
4. *Test 4*: in Section 6.5.6, we applied the proposed workflow by use of the robust optimisation, as in Figure 6.7, for decision-making on an infill well placement.

6.5.3 Test 1: Simulation Results by the Extended Nominal Optimisation

We report simulation results of the proposed workflow by use of the extended nominal optimisation on PUNQ-S3 case study.

6.5.3.1 Multi-Objective History Matching and Bayesian Analysis

We performed multi-objective history matching to generate model realisations. The Set-1 model parameterisation described in Chapter 3 and 16.5 years of production history data including bottom hole pressure (BHP), water cut (WCT), and GOR from all wells are used for history matching. The data are uncorrelated and following the original dataset [243]. The misfit to be minimised is defined as:

$$M = \frac{1}{n_w}\sum_i \frac{1}{n_p}\sum_j \frac{1}{n_t}\sum_k \left(w_{ijk}\frac{(obs_{ijk} - sim_{ijk})}{\sigma_{ijk}} \right)^2 \tag{6.12}$$

where n_w is the number of evaluated wells with i runs over it, n_p is the number of observed production data with j runs over it, n_t is the number of timesteps for the j^{th} history data with k runs over it, obs is the observed history, sim is the simulated value, σ^2 is the variance of the measurement errors, and w is the weight factor, with runs over i, j and k. We can see from Equation (6.12) that there are 18 misfit components in PUNQ-S3 (i.e. misfits from six production wells with three production data from each well to match).

We formulated the multi-objective history matching to two objective functions by de-composing the misfit function in Equation (6.12) based on production wells, as in Equation (6.13).

$$\begin{aligned} M_1 &= M_{PRO1} + M_{PRO4} + M_{PRO12} \\ M_2 &= M_{PRO5} + M_{PRO11} + M_{PRO15} \end{aligned} \tag{6.13}$$

where M_{PROi} corresponds to the misfit from production wells PRO-i, i = (1, 4, 5, 11, 12, 15), that are summed up on all production data (BHP, WCT, GOR) over all timesteps with unity weights.

We performed 2,000 flow simulations in the multi-objective history matching with objective functions described in (6.13) by use MOPSO algorithm [7] with the parameter setting as follows [123]:

- Number of particles : 20
- Inertia weight, w : 0.729
- Cognitive component, c_1 : 1.494
- Social component, c_2 : 1.494

Afterwards, we ran the NAB to approximate the posterior probability for each resampled matched-model. NAB resamples all the matched-models and infers the posterior probability for each model without further solving the forward simulation. Figure 6.9 shows all the generated 2,000 models from multi-objective history matching and the 745 NAB models in the objective space. We can see from Figure 6.9 that NAB filtered out the models with high misfit value (i.e. models with total misfit values > 16) which have a posterior probability of zero. This procedure ensures that the models selected for optimisation are the models that are plausible and not the ones with low likelihood given the observed production data.

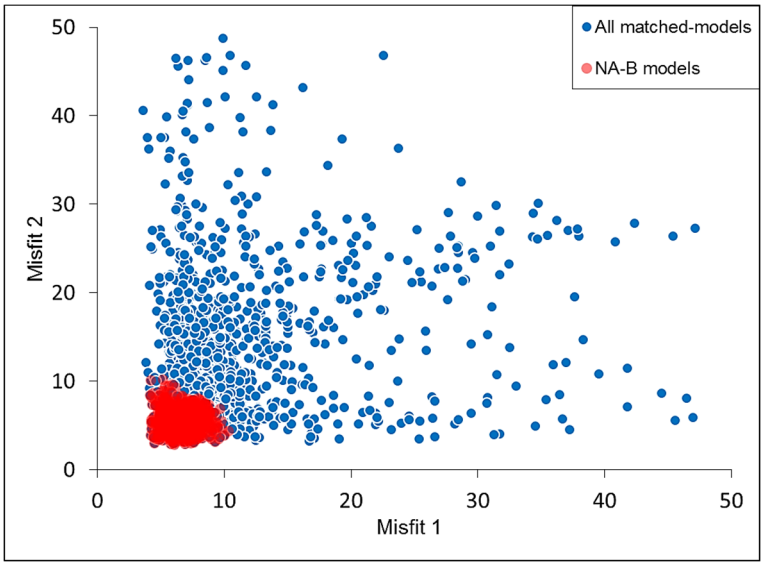

Figure 6.9—All the generated history-matched models and the NAB models in the objective space.

6.5.3.2 Model Selection

The models with low misfit values will tend to have high likelihood and consequently may have high posterior probability given a uniform prior. However, in the case of sparse clustering, a lower likelihood model may get higher posterior probability value,

and when high likelihood models are over refined or clustered in parameter space, their posterior probability may get decreased. This problem is rectified by reapproximating the PPD for PMs which are sparse and consequently ensuring the diversity.

We select the models for optimisation based on the PMs from multi-objective history matching. Initially, there are 11 PMs out of 2,000 history-matched models and after running the NAB, there are only seven good match PMs out of 745 NAB models. These seven PMs are then selected for optimisation, as shown in Figure 6.10. We can see from Figure 6.10 that PMs have a wide spread to approximate the front in the objective space of multi-objective history matching to ensure the diversity of models for optimisation.

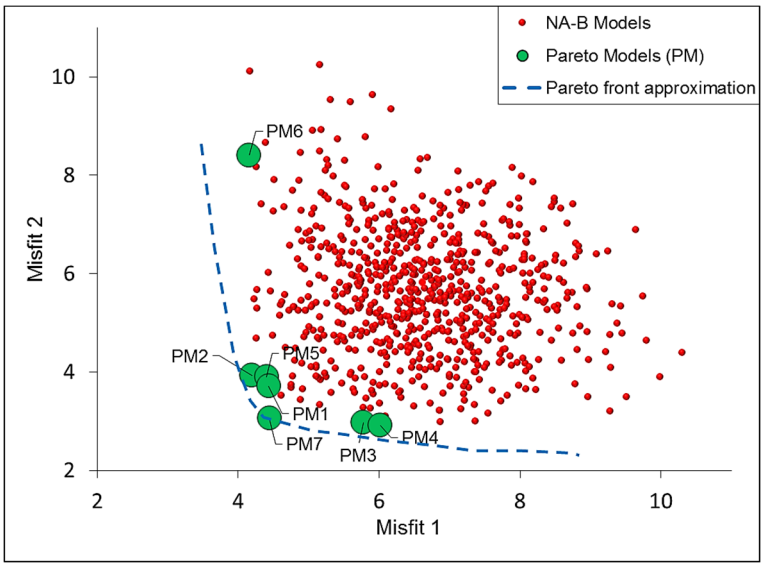

Figure 6.10—Seven models (coloured green) selected for optimisation based on the PMs from multi-objective history matching and Bayesian analysis.

Posterior Inference for Selected Models

We recalculated the PPD for the selected seven PMs based on 745 NAB models. First, these 745 models are clustered in the standardised parameter space, as in Equation (6.2), around seven cluster centres (PMs). Then the NAB posterior probability for each cluster is summed up to be assigned to the seven PMs, as described in Equations (6.3) and (6.4). Table 6.2 shows the recalculated probability for each PM. We can see from Table 6.2 that the probability estimations for PM1, PM7, PM2, and PM5 have a relatively higher probability than the others. This result is expected as those solutions are closer to the origin in the objective space than the others and are preferred hence higher probability.

Cluster	# of models	Centre	Probability
C1	145	PM1	0.3602
C2	89	PM2	0.1176
C3	146	PM3	0.1010
C4	68	PM4	0.055
C5	71	PM5	0.0718
C6	48	PM6	0.0372
C7	178	PM7	0.2567
Total	**745**	**7**	**1.0**

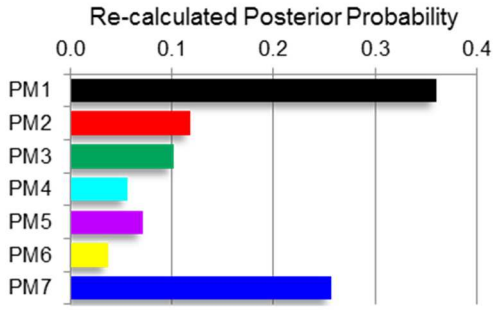

Table 6.2—Recalculated posterior probability for each of the seven PMs from NAB-clustering process.

6.5.3.3 Extended Nominal Optimisation

We ran the multi-objective optimisation for each of selected seven PMs to place an infill well with the objective functions defined in Equation (6.11). We performed 500 flow simulations for each optimisation run on each PM by MOPSO [7] with the same algorithm's parameter setting with history matching.

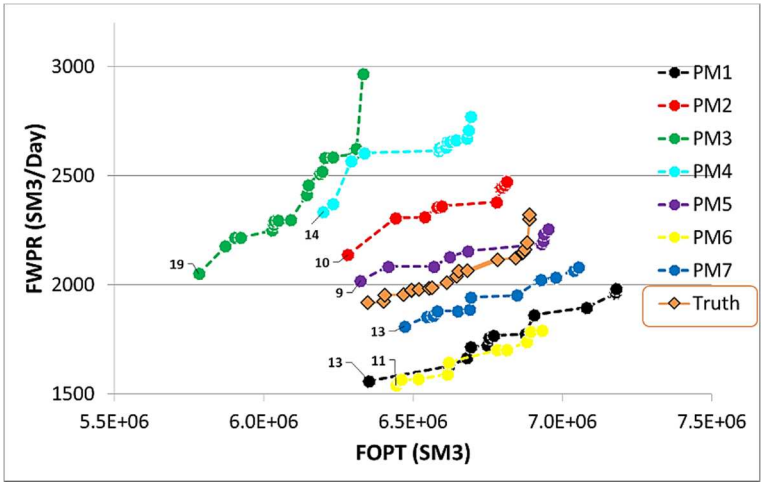

Figure 6.11—Pareto front solutions from the optimisation of the seven selected PMs in the objective space (FOPT=field oil production total; FWPR=field water production rate). Optimised case from the truth is plotted as a reference.

Figure 6.11 shows the Pareto front solutions from each optimisation on each PM in the objective space along with the optimisation results from the truth case as a reference. Each point in one Pareto front in Figure 6.11 represents one set of optimal solutions (i.e.

the infill well location) found by the optimiser, and the number on each Pareto front indicates the number of optimal solutions found by each selected PM. In total, there are 56 different optimal solutions from the optimisation across all seven selected PMs.

The results shown in Figure 6.11 indicate that the model selection based on PMs from multi-objective history matching is a good method to select the model realisations for optimisation. The range of objective values from the optimal solutions found from PMs' optimisation encapsulates the optimised case from the truth case scenario. We can also see from Figure 6.11 that the optimisation from three PMs (i.e. PM1, PM6, and PM7) are economically better than the truth case (i.e. models are optimistic) and from four PMs (i.e. PM2, PM3, PM4, and PM5) are economically worse than the truth case (i.e. models are pessimistic).

In the extended nominal optimisation, we reevaluated objective functions based on all optimal solutions found by each Pareto history-matched model. However, to run all of these optimal solutions will require high CPU costs. Hence, we only select representative optimal solutions from the results of each PM's optimisation and apply to all seven PMs.

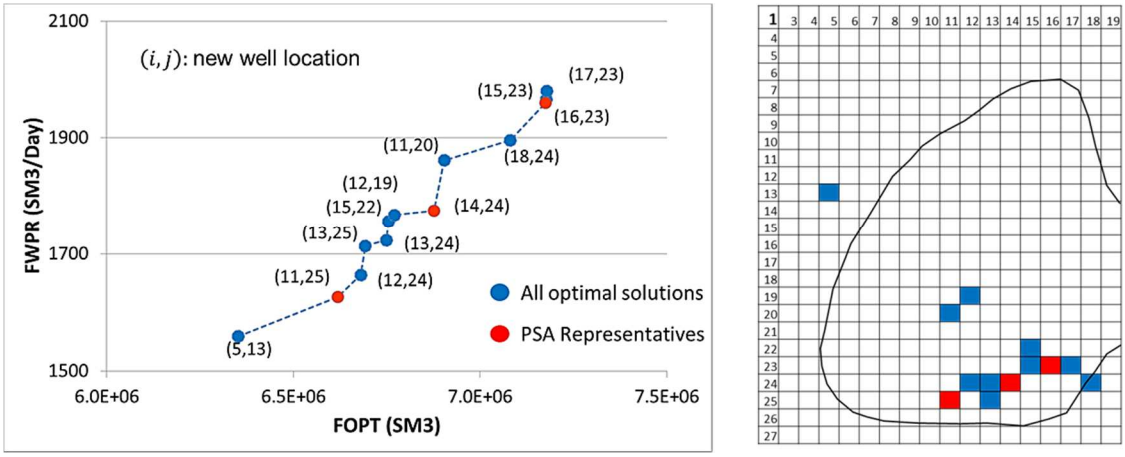

Figure 6.12—Pareto front solutions obtained from the optimisation of PM1 and the red-highlighted PSA representatives in the objective space (left), and their corresponding locations on a grid (right).

We use PSA [324] to select three representatives from each Pareto front solutions to represent high-, mid-, and low-case scenarios from each Pareto front. Figure 6.12 shows

an example of selecting three representatives from 13 optimal solutions obtained by the optimisation of PM1 by PSA along with their corresponding locations map. These three optimal locations are then applied to the other PMs.

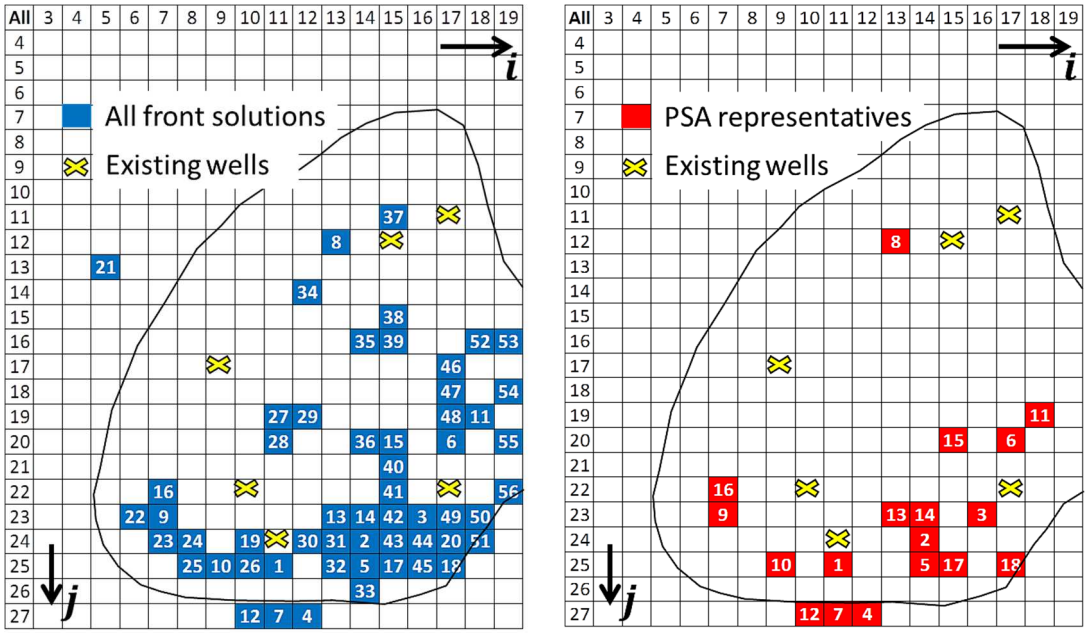

(a) All optimal solutions on a grid **(b) PSA's representatives of optimal solutions**

Figure 6.13—(a) Joint optimal solutions from the optimisation of seven PMs on a grid. (b) The representative optimal solutions selected by PSA. The number in each grid represents the location index.

Figure 6.13 (a) shows all the optimal solutions from the optimisation of all seven PMs on a grid. The number on each grid cell is the location index to represent an optimal well location. We can see from Figure 6.13 (a) that the optimal well locations are predominantly located in the southern and eastern part of the field. There are two possible reasons for this. First, this is possibly due to the fact of there is strong aquifer from the western and northern parts of the field to sweep the remaining oil towards the east bounding sealing fault. Second, as one of the objective in the optimisation is to minimise the water production rate from the field, the optimiser tries to find the tradeoff from maximising the oil recovery and minimising the water production rate from the field. Hence, the optimal locations should be further away from the aquifer drive.

Figure 6.13 (b) shows the representative of the optimal solutions from the optimisation of all seven PMs. We can see that from Figure 6.13 (b) that PSA reasonably preserves

the optimal solutions to cover different parts of optimal well locations in the field. These representative optimal solutions are applied to all seven PMs and will be further analysed in the decision-making.

6.5.3.4 Risk Analysis and Decision-Making

The final step in the workflow is to conduct probabilistic risk analysis and to choose the optimal solution accordingly. Risk analysis can be performed by evaluating the expected upside (*P10*) and downside (*P90*) of oil recovery from each optimal solution. There are few different criteria to choose the optimal decision, such as the infill well location should provide the oil recovery that exceeds an economic threshold, the highest possible oil recovery both in the upside and downside, or the smallest possible spread between the expected upside and downside of the uncertainty estimation.

In the present case study, we define the optimal decision as the one that satisfies both of the following conditions:

1. The expected *P50* of oil recovery from the optimal infill well location is above a given economic threshold.
2. There is a small variation in the oil recovery due to geological uncertainty (i.e. a smaller spread of *P10* and *P90* value is preferred).

Economic Threshold

The economic threshold is determined by the minimum incremental of oil recovery required to ensure a positive (or at least zero) cash flow during the next period of 10 years. We used a typical spreadsheet for cash flow calculation in the production sharing contract scheme (i.e. 80:20 ratio between the government and operator) and excluded the produced gas in the calculation, as described in Equation (6.14).

$$CF = (1 - G) \sum_{t=1}^{T} \frac{p_o Q_t^o - C^{opex}}{(1 + r)^t} - C^{capex} \tag{6.14}$$

where CF is the cash flow, T is the total production time in years; r is the annual discount rate; G is the government share; p_o represents the oil price in \$/STB (STB=stock tank

barrel); Q_t^o represents the total volumes of oil in STB, produced at time t; C^{opex} represents the operational expenditure ($), and C^{capex} is the capital expenditure ($) that represents the total cost to drill a new well, build a new facility and add additional flowline.

Table 6.3 shows the input parameter used for the cash flow calculation defined in Equation (6.14). Assuming these input parameters are fixed and considering the oil depreciation on each year in the form of a discount factor, the field should be producing oil at the rate of 5.1 MBBLS/day (MBBLS=thousand barrels) for the next 10 years to achieve a positive cash flow, as depicted in Figure 6.14. At this production rate, the minimum incremental of oil recovered from the field is 2.98 × 10^6 SM^3 from the reference case (i.e. truth case) that gives an economic threshold of **6.85 × 10^6 SM^3** that should be produced at the end of production time, as illustrated in Figure 6.15.

Parameter	Value	Unit
Oil price, p_0	50	$/STB
Drilling cost, C^{capex}	25	$mm
Additional facility, C^{capex}	5	$mm
Additional flowline cost, C^{capex}	5	$mm
Operational cost, C^{opex}	1	$mm/year
Discount rate, r	0.1	-
Government share, G	0.8	-

Table 6.3—Economic parameters for the cash flow calculation.

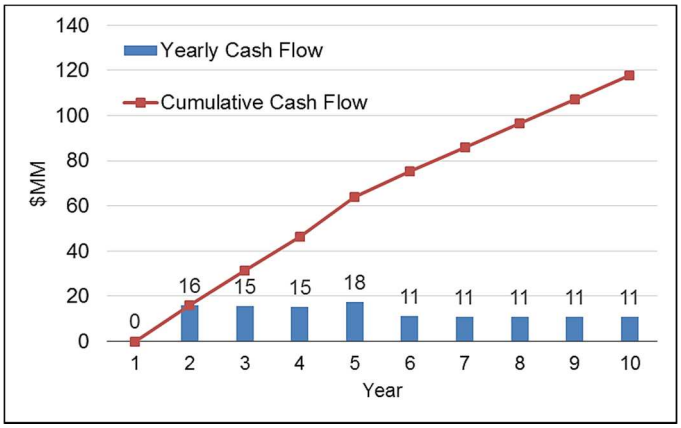

Figure 6.14—Yearly and cumulative cash flow at the average field oil production rate of 5.1 MBBLS/day (MBBLS=thousand barrels).

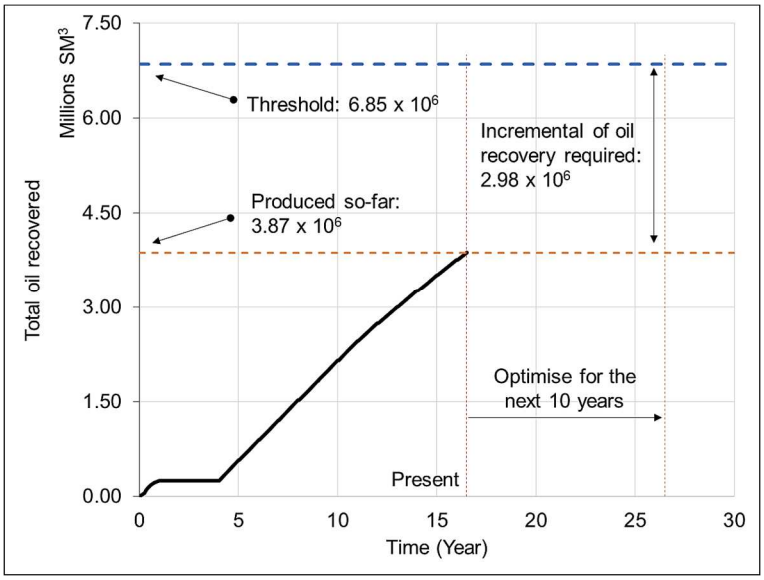

Figure 6.15—Production profile of the truth case to determine the minimum incremental oil recovery from the field for the next 10 years to achieve positive (or at least zero) cash flow (i.e. the economic threshold of total oil recovered at the end of production time is 6.85 x 10^6 SM^3).

Decision on Optimal Location

The decision on optimal well location is based on the risk analysis of each solution. The risk analysis is based on the probability of each obtained solutions of either achieving or not achieving the economic threshold. We used the *P50* value from each solution and compared with the economic threshold.

We used the recalculated probability for each PM, as given in Table 6.2, to generate the *P10*, *P50*, and *P90* credible intervals on each representative of the optimal solution shown in Figure 6.13 (b) for the risk analysis and decision-making. Figure 6.16 shows the box plot of all 18 representative optimal solutions shown in Figure 6.13 (b) along with the economic threshold (i.e. Figure 6.16 becomes our decision panel). We can see from Figure 6.16 that there are only four location indices i.e. Location indices 3, 6, 11, and 18 that have *P50* of the recovered oil above the economic threshold. These location indices will be taken further for analysis.

The *P50* value and the spread of expected oil recovery (*P10–P90*) of Location indices 6, 11 and 18 are slightly smaller than Location index 3. A risk-taker decision-maker will tend to choose Location index 3 where there is an opportunity to have a slightly higher

expected recovery with a risk of larger downside (i.e. larger range between *P50* and *P90* values). A risk-averse decision-maker will tend to choose either Location index 6 or 11 where there is a smaller downside of expected recovery even though the expected *P50* is slightly lower than Location index 3. Location index 18 is not a better choice than the others as it has a slightly lower expected *P50* oil recovery and a larger downside than Location indices 3, 6, and 11.

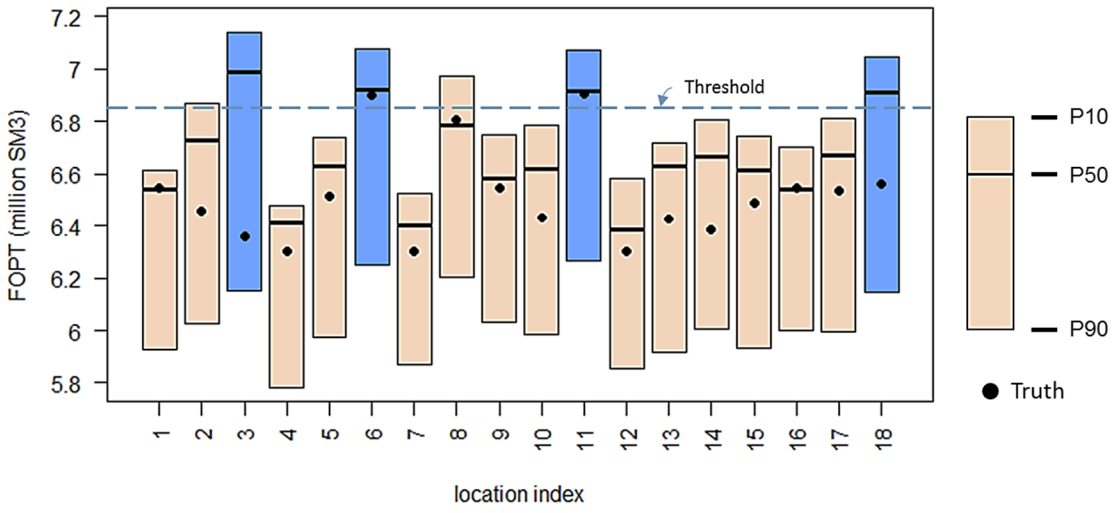

Figure 6.16—Box plot of total oil recovery on 18 representative optimal solutions from the optimisation across all seven Pareto history-matched models with the truth case as a reference for each location index. Location indices that result *P50* of FOPT more than the economic threshold are highlighted in blue.

Validation with the "Truth" Case

The validation of uncertainty estimation is performed with the truth case to see the reliability of the optimisation forecast. We evaluated each location index as if the new infill well is drilled based on the truth case data sets of the model [235,243]. We aim to check how reliable the calculated expected oil recovery at the end of field production time is in each location (i.e. the encapsulation of the truth case within *P10–P90* range).

We can see from Figure 6.16 that the truth values of the total recovered oil at the end of field production time are encapsulated within *P10–P90* range for all representative op-

timal location indices. This result demonstrates that the proposed workflow in uncertainty estimation of optimisation forecast is reliable to support the decision-making process.

This validation also shows that Location 3 selected by risk-taker decision-maker is proved to be risky, i.e. the truth case value is below the economic threshold. The Location indices 6 and 11 selected by risk-averse decision-maker is proved to be economically sustainable, i.e. the truth case optimised production to match the *P50* value.

6.5.3.5 CPU Computational Cost

Due to the potential high computational cost of a model simulation, one of the considerations for choosing a proper optimisation workflow is the number of simulations required by the optimisation process. Table 6.4 compares the number of flow simulation runs between the proposed workflow and the conventional method (where simulations are run exhaustively for each history-matched model). Even though we run history matching with 2,000 flow simulations, realistically we only select the models with low misfit for optimisation (see Figure 6.10).

Step	Conventional Workflow		Proposed Workflow	
	Simulation runs	Optimisation flow simulation runs	Selected from multi-objective (Pareto)	Optimisation flow simulation runs
1.PPD approximation (NAB)	745	372,500[a]	7	3,500[a]
2.Optimised Decision	100	425[b]	21	18[b]
	Total	372,925	Total	3,518

[a]: 500 flow simulations per optimisation run; [b]: flow simulations of all optimal solution across seven Pareto history-matched models.

Table 6.4—Comparison of the number of flow simulation runs between proposed and conventional workflow.

The first row of Table 6.4 shows the number of good matched models (models with low misfit, i.e. 745 models) and the seven selected PMs. The numbers on the second row are calculated manually based on the number of optimal solutions from the selected PMs comparing conventional (i.e. exhaustive simulations run) and the proposed workflow (i.e. optimal solutions selection by PSA). We can see from Table 6.4 that conventional

optimisation workflow using the full set of 745 realisations is unrealistic at the current level of computing resources.

Therefore, the proposed optimisation workflow with a small set of representative realisations can be recommended for an infill well placement optimisation because it provides more confident decision-making process at affordable computational cost.

6.5.4 Test 2: Decision Consistency Between History-Matching Runs

The nature of history matching powered by the stochastic optimiser is known for its randomness in generating the solutions which give us a different set of matched-models. The question arises whether the decision in the optimal well location from one history-match run holds for different history-match runs. This section describes the same workflow as before (see Figure 6.4) with different history-matching runs for decision-making on optimal solutions to drilling a new infill well. We defined the previous run in Test 1 and its results as Run 1 whereas the run and results presented in this section as Run 2.

We used the same setup on both history matching and optimisation, as described in Equations (6.13) and (6.11), respectively. We also used the same algorithm setting and number of simulations, i.e. 2,000 flow simulations in history matching and 500 flow simulations per each selected model in the optimisation. In the risk analysis and decision-making, we used the same criteria as before, i.e. an economic threshold of *P50* > 6.85 x 10^6 SM^3 and low variance of the expected oil recovery (i.e. lower range of *P10*–*P90* values).

6.5.4.1 Model Selection and Posterior Inference

We selected the models for the optimisation based on the PMs of multi-objective history matching. Figure 6.17 shows the selected PMs from the history matching and NAB analysis out of all generated history-matched models. We can see from the Figure 6.17 (a) that the NAB is able to filter out the low-quality models and assign a posterior probability for the rest of models (there are 830 NAB models out of 2,000 history-

matched models in total). Then, eight PMs from the NAB models are selected for optimisation, as shown in Figure 6.17 (b), from which we can see that higher misfit value in Misfit 1 (i.e. misfits from production data at Wells PRO1, PRO4, and PRO12) does not help to decrease significantly Misfit 2 (i.e. misfits from production data at Wells PRO5, PRO11, and PRO15).

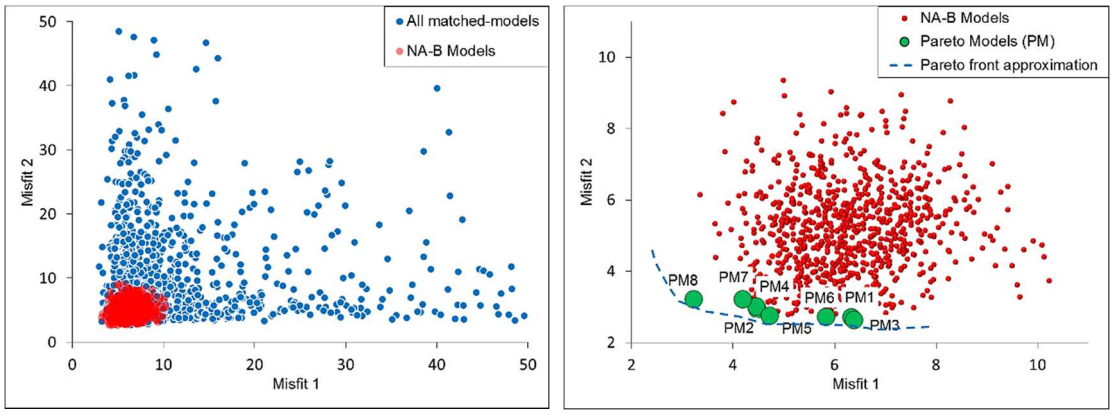

(a) (b)

Figure 6.17—(a) All the generated history-matched models and the NAB models in the objective space. (b) Eight selected models (coloured green) for optimisation based on the PMs from multi-objective history matching and NAB analysis.

Cluster	# of models	Centre	Probability
C1	19	PM1	0.0545
C2	48	PM2	0.0473
C3	69	PM3	0.0995
C4	141	PM4	0.1783
C5	133	PM5	0.1264
C6	63	PM6	0.0808
C7	196	PM7	0.1952
C8	161	PM8	0.2178
Total	**830**	**8**	**1.0**

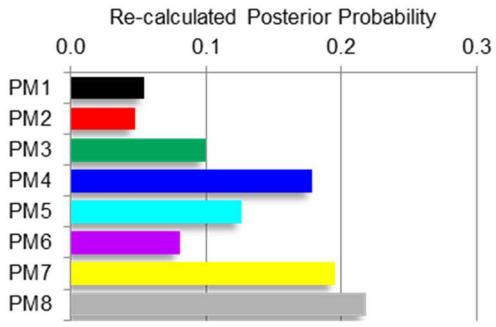

Table 6.5—Recalculated posterior probability for each of the 8 PMs from NAB-clustering process on Run 2.

We recalculated the probability for the selected 8 PMs based on 830 NAB models clustering, as described in Equations (6.3) and (6.4). Table 6.5 shows the recalculated probability for each PM. We can see from Figure 6.17 (b) and Table 6.5 that the recalculated posterior probabilities for most of the models closer to the origin are larger

than the others, as expected. For instance, PM8, PM7, and PM4, which are the closest three to the origin, have a larger assigned probability than the others.

6.5.4.2 Optimisation and Optimal Solutions Selection

In Run 2, the multi-objective optimisation for each of selected 8 PMs was conducted with the same setup as in Run 1. Figure 6.18 shows the Pareto front solutions from each PM optimisation in the objective space along with the truth case optimisation as a reference. We can see from Figure 6.18 that model selection based on the PMs provides a good estimation of the objective values (oil recovery and water production rate from the field) because it encapsulates the optimised case from the truth case. The number attached to each Pareto front is the number of optimal solutions from the optimisation from each PM.

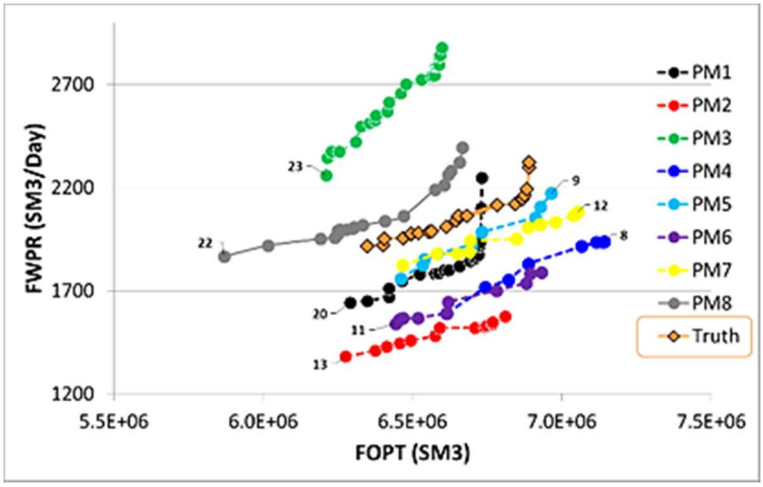

Figure 6.18—Pareto front solutions from the optimisation of the eight selected PMs in the objective space (FOPT=total cumulative produced oil from the field, FWPR=field water production rate) from Run 2. Optimised case from the truth is plotted as a reference.

We selected representative optimal solutions from the results of each PM's optimisation by PSA and applied to all of the eight PMs. Out of 57 optimal solutions in total, there are 20 optimal solutions selected across all the PMs' optimisation, as shown in Figure 6.19 (a) and (b), respectively. Comparing Figure 6.19 (a) and Figure 6.13 (a), we can see from both figures that the optimal well locations are consistent between different history-match run, i.e. the solutions are predominantly located in the southern and eastern part of the field. From Figure 6.19 (b) we can see that PSA reasonably preserves

the optimal solutions to cover different parts of optimal well locations in the field. All of these representative optimal solutions are applied to all eight PMs and will be further analysed in the decision-making.

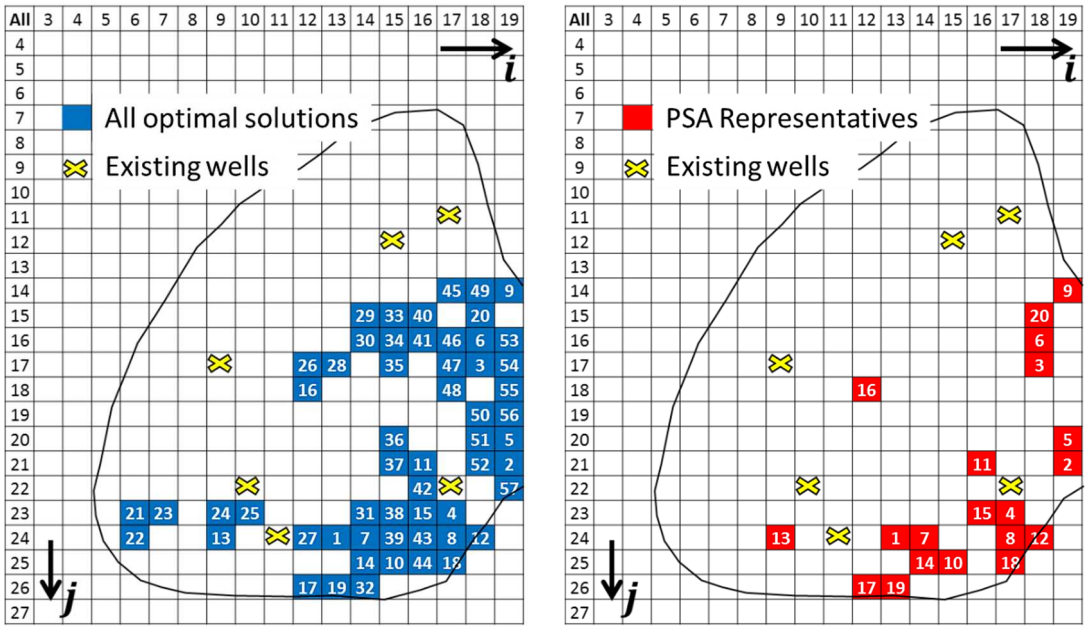

(a) All optimal solutions on a grid (b) PSA's representatives of optimal solutions

Figure 6.19—(a) Joint optimal solutions from the optimisation of eight PMs on a grid on Run 2 and (b) The representative optimal solutions selected by PSA. The number in each grid represents the well location index.

6.5.4.3 Risk Analysis and Decision-Making

As in Run 1, the final step in the workflow is to conduct risk analysis and to choose the optimal solutions based on the economic threshold (i.e. *P50* of FOPT > 6.85 x 10^6 SM^3) and the range of *P10–P90* value to evaluate the upside and downside of each optimal solution. Figure 6.20 shows the box plot of all 20 representative optimal solutions shown in Figure 6.19 (b) along with the economic threshold (i.e. Figure 6.20 becomes our decision panel). We can see from Figure 6.20 that there are five location indices, i.e. Location indices 3, 4, 6, 15, and 20 that have *P50* values of the recovered oil above the economic threshold. These location indices will be further analysed.

The *P50* and the spread (P10–P90) of expected oil recovery of Location indices 3, 6 and 20 are slightly smaller than Location indices 4 and 15. A risk-taker decision-maker will tend to choose Location index 4 or 5 where there is an opportunity to have a slightly

higher expected recovery with a risk of larger downside (i.e. larger range of *P50* and *P90* values). A risk-averse decision-maker will tend to choose either Location index 3, 6 or 20 where there is a smaller downside of expected recovery even though the expected *P50* is slightly lower than Location index 4 or 15.

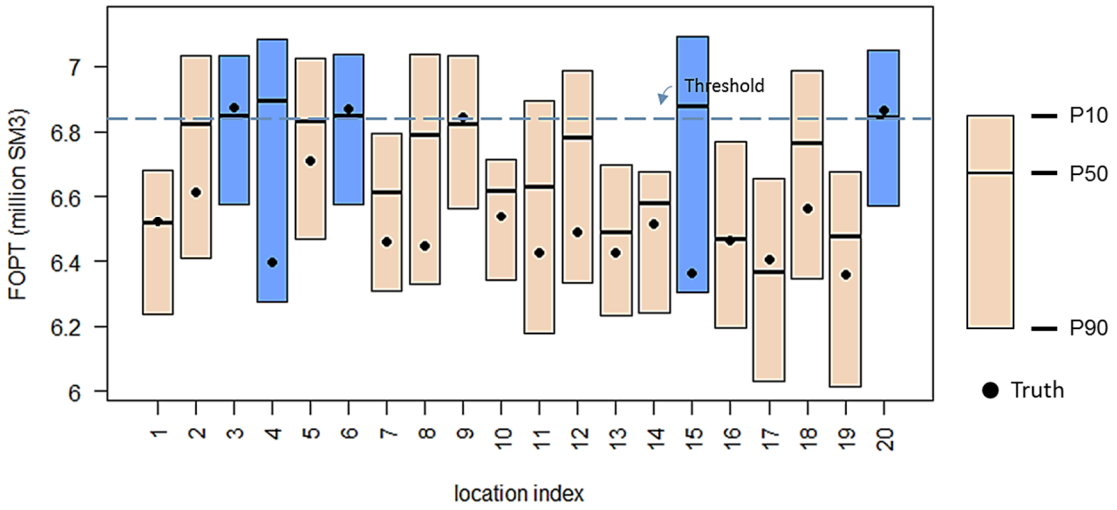

Figure 6.20—Box plot of total oil recovery on 20 representative optimal solutions from the optimisation across all eight Pareto history-matched models on Run 2 with the truth case as a reference for each location index. Location indices that result *P50* of FOPT more than the economic threshold are highlighted in blue.

The results presented in this section demonstrate the consistency of the decision outcome between stochastic history-matching runs from the proposed optimisation workflow. Location indices 6 and 11 from Run 1 are comparable with Location indices 3, 6, and 20 from Run 2 in terms of the expected oil recovery. The region for these wells is consistently found in the mid-eastern part of the field, as shown in Figure 6.13 and Figure 6.19. On the other hand, Location indices 3 and 18 from Run 1 are comparable with Location indices 4 and 15 from Run 2 in terms of the expected oil recovery. The region for these wells is also consistently found in the south-eastern part of the field. These results also give flexibility to the decision-maker given constraints that they might have, such as pipeline route, well platform, and the environment. The consistency of the decision output ensures that decision-maker associated with their risk behaviour (i.e. risk-averse or risk-taker) can be more confident of the expected result.

The validation of uncertainty estimation is performed with the truth case to see the reliability of the optimisation forecast of the oil recovery at the end of field production time, as shown in Figure 6.20. We can see from Figure 6.20 that the truth values of the total recovered oil from the field are encapsulated within *P10–P90* range for all location indices. This result demonstrates that the proposed workflow in uncertainty estimation of optimisation forecast is reliable to support the decision-making process.

6.5.5 Test 3: Validation on PSA As a Method for Optimal Solution Selection

We validated the representativeness of selected optimal solutions by PSA with the ones based on optimising over the exhaustive sets of Pareto front solutions. To do this, all the joint optimal solutions shown in Figure 6.13 (a) and Figure 6.19 (a) are run exhaustively to each Pareto history-matched model, for Run 1 and Run 2, respectively. There are 56 and 57 joint optimal solutions from Run 1 and Run 2, respectively, which are applied to seven and eight PMs' optimisation for Run 1 and Run 2, respectively. Afterwards, the PDFs are constructed based on the respective posterior probability of each PM.

Figure 6.21 and Figure 6.22 show the PDFs of the expected recovery from exhaustive runs on all optimal locations of Run 1 and Run 2, respectively. We can see from Figure 6.21 (a) and Figure 6.22 (a) that the PDFs of the expected recovery from the PSA's subset selection are well represented, as shown in Figure 6.21 (c) and Figure 6.22 (c), respectively. The validation on exhaustive runs is then extended to all optimal locations that satisfy the economic threshold. We can see from Figure 6.21 (b) and Figure 6.22 (b) that the PDFs of the expected recovery from the PSA's subset selection are well represented, as shown in Figure 6.21 (d) and Figure 6.22 (d), respectively.

6.5.6 Test 4: Simulation Results by Robust Optimisation

We applied robust optimisation workflow shown in Figure 6.7 to the same optimisation job in Section 6.5.3 (i.e. an infill well placement optimisation). The objective is to compare the results of robust optimisation with the extended nominal optimisation shown in Figure 6.4. The objective functions in the robust optimisation are the same i.e.

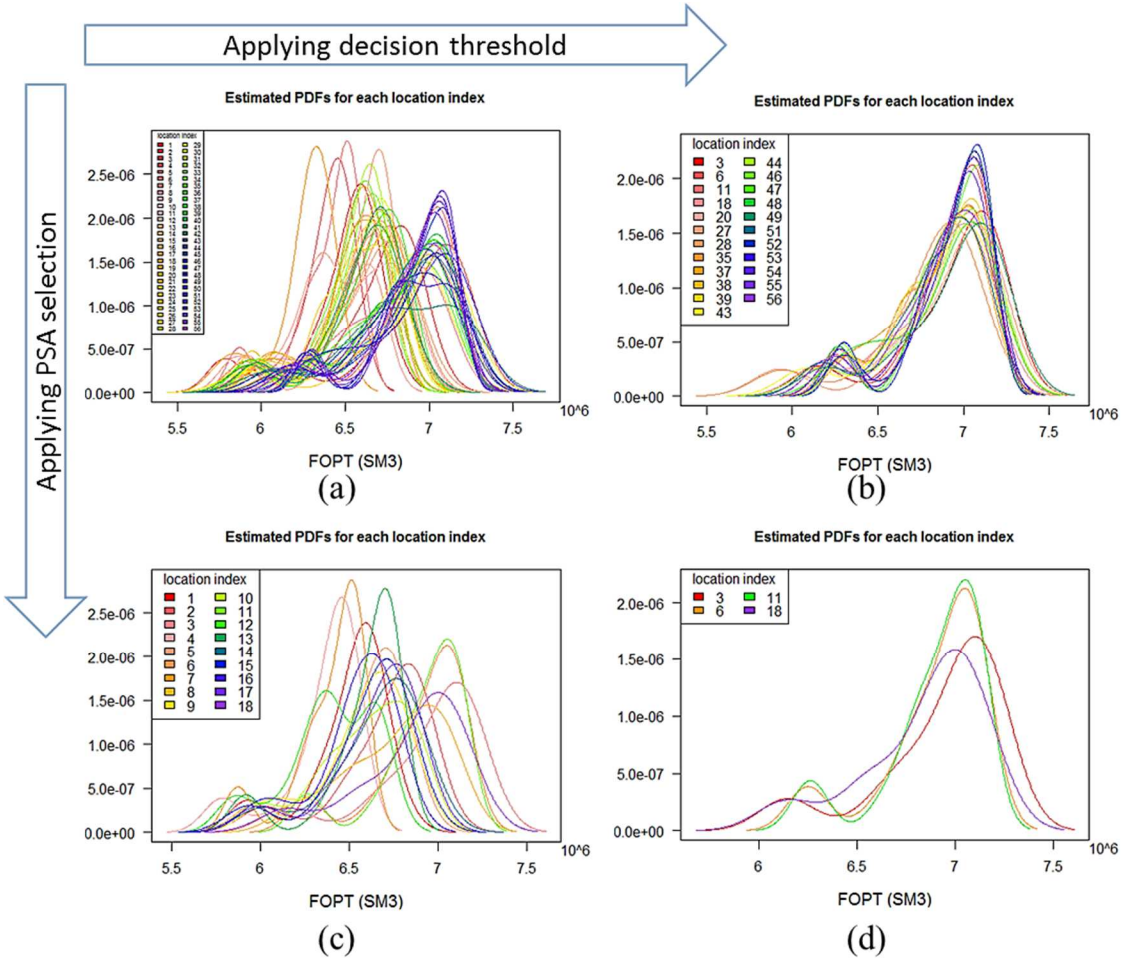

Figure 6.21—Run 1 results: (a) Estimated PDF of expected recovery for each location index for all 56 optimal locations; (b) All optimal locations satisfying the economic threshold; (c) PSA's subset optimal locations; (d) PSA's subset optimal locations satisfying the economic threshold.

to maximise the oil recovery and minimise the water production rate from the field, as defined in Equation (6.11). However, in the robust optimisation, the objective functions are the expectation values of each objective function in (6.11) across all the selected models formulated in (6.8). We used the same seven PMs as in the previous Run 1 which are described in Table 6.2. We also used the same algorithm setting and number of flow simulations for each PM's optimisation, i.e. 500 simulations each.

Figure 6.23 shows the results of the robust optimisation for placing an infill well in PUNQ-S3 reservoir. The Pareto front solutions are selected as the optimal solutions and further analysed, as shown in Figure 6.23 (a). Figure 6.23 (b) shows the corresponding location of each optimal solutions in a grid. The number on each grid is the location in-

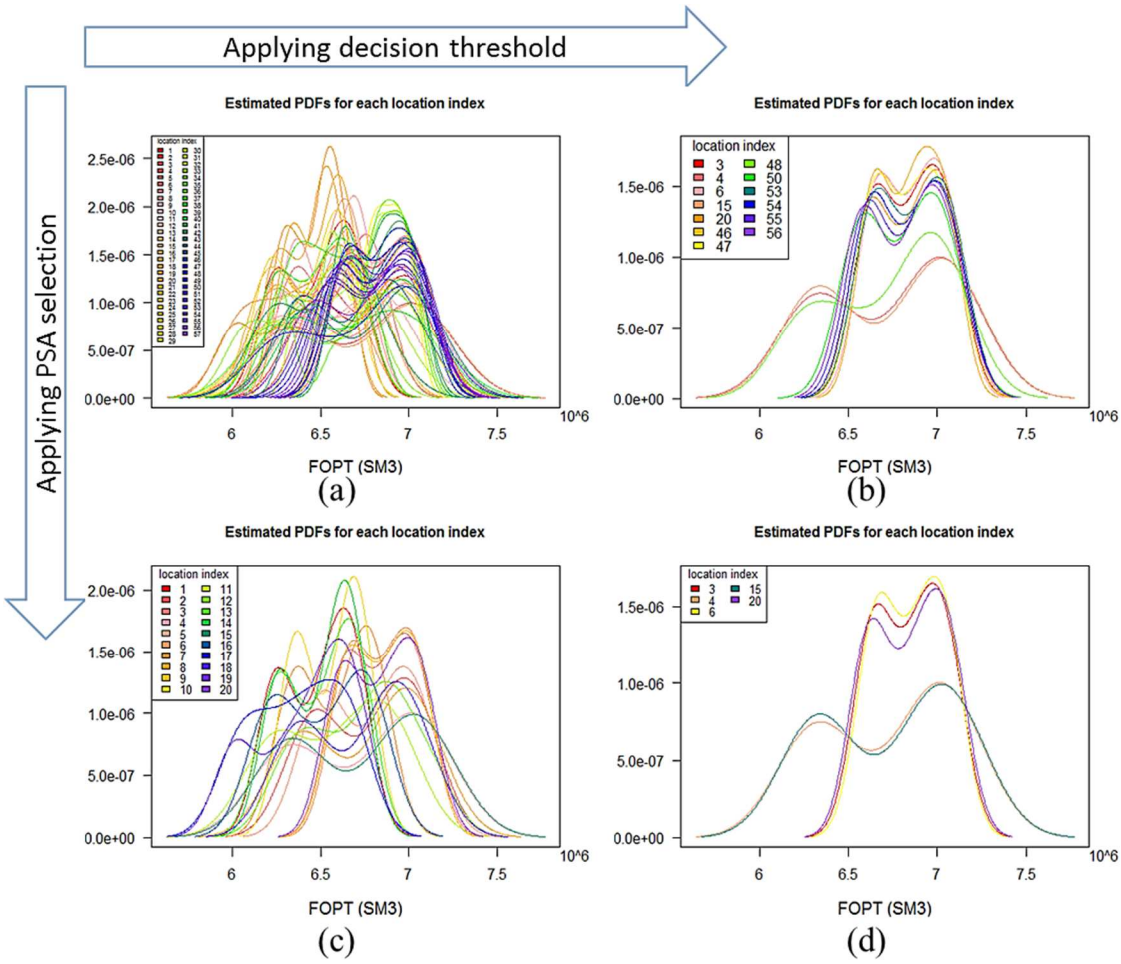

Figure 6.22—Run 2 results: (a) Estimated PDF of expected recovery for each location index for all 57 optimal locations; (b) All optimal locations satisfying the economic threshold; (c) PSA's subset optimal locations; (d) PSA's subset optimal locations satisfying the economic threshold.

dex to represent an optimal well location. We can see from Figure 6.23 (b) that the optimal well locations are predominantly located in the southern part of the field and only one location in the mid-eastern part of the field. The optimal well locations are reasonably similar to the ones from the extended nominal optimisation workflow shown in Figure 6.13.

Because the objective functions in the robust optimisation are the expected objectives values across all the models, all the optimal solutions will be the same for all the models. Hence, further application of optimal solutions found by a model's optimisation to the other models is not required as in the extended nominal optimisation. Consequently, the selection of optimal solutions by PSA is not required in the robust optimisation. Hence,

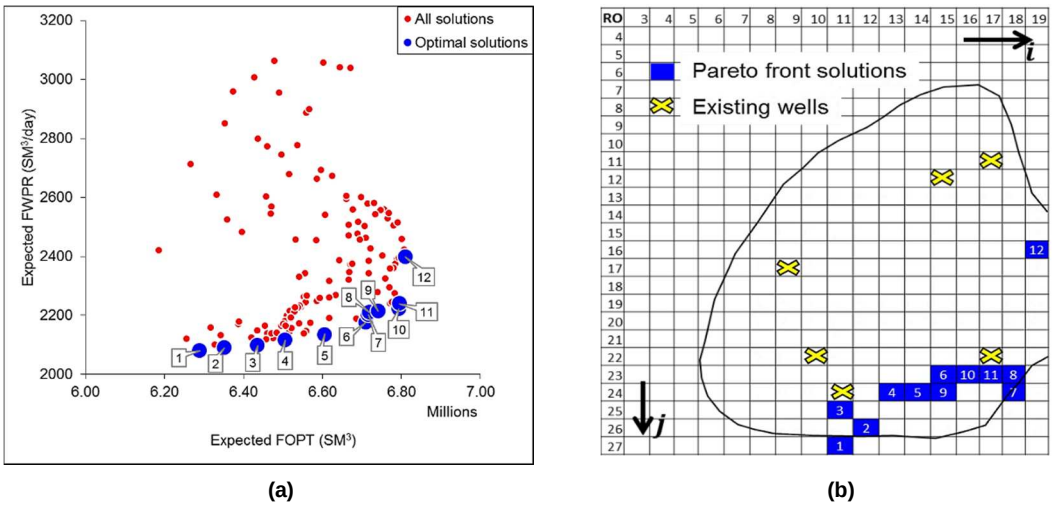

Figure 6.23—(a) Robust optimisation results depicting all and the optimal solutions in the objective space, and (b) The corresponding location of the optimal solutions in a grid for an infill well placement optimisation on PUNQ-S3 reservoir. The number in each grid represents the location index.

robust optimisation requires a lesser number of flow simulations than the extended nominal optimisation (i.e. only 7 × 500 = 3,500 flow simulations for the optimisation job). All of the 12 optimal solutions shown in Figure 6.23 (a) are further analysed.

We use the recalculated probability for each PM given in Table 6.2 to generate the *P10*, *P50*, and *P90* credible intervals on each optimal solution showed in Figure 6.23 for the risk analysis and decision-making. Figure 6.24 shows the box plot of all 12 optimal solutions along with the same economic threshold (i.e. *P50* > 6.85 x 10^6 SM^3). We can see from Figure 6.24 that there is no location that has *P50* of the recovered oil above the economic threshold. However, the closest *P50* of FOPT to the economic threshold is the results from drilling a new well at the Location index 12 or 10. A risk-taker decision-maker will tend to choose Location index 10 where there is an opportunity to have a slightly higher *P10* value of recovery with a risk of larger downside (i.e. larger range of *P50* and *P90* values). A risk-averse decision-maker will tend to choose Location index 12 where there is a smaller downside of expected recovery even though the *P10* value is slightly lower than Location index 10.

We compared the results of the robust optimisation workflow (Figure 6.24) and the extended nominal optimisation (Figure 6.16). We used the truth case value as the validation for the comparison. We can see from Figure 6.16 that there are four location indices

from the extended nominal optimisation that have a *P50* values of FOPT larger than the economic threshold (i.e. Location indices 3, 6, 11, and 18). Out of these 4 locations, there are two location indices that the truth case values are larger than the economic threshold which aligns with the result from the optimisation (i.e. Location indices 6 and 11). The other two locations (i.e. Location indices 3 and 18) are the unfortunate events when the risk-taker decision-maker choose either of these locations as the final solution. On the other hand, there is one location (i.e. Location index 12) from the truth case that the oil recovery is more than the economic threshold, but was not found by the robust optimisation, as shown in Figure 6.24.

Nonetheless, if the decision-maker decided to use *P10* instead of *P50* value (i.e. P10 value of FOPT > 6.85×10^6 SM^3) as the economic threshold reference, both of the results from the extended nominal and robust optimisation become comparable. For instance, there are six location indices i.e. Location indices 2, 3, 6, 8, 11 and 18 and eight location indices i.e. Location indices 5, 6, 7, 8, 9, 10, 11 and 12 that satisfy this criterion from the extended nominal optimisation and robust optimisation, respectively, as shown in Figure 6.16 and Figure 6.24. The locations of these solutions are also similar from both optimisations workflow, i.e. all of them are located predominantly in the eastern part of the field across from the middle to south of the field.

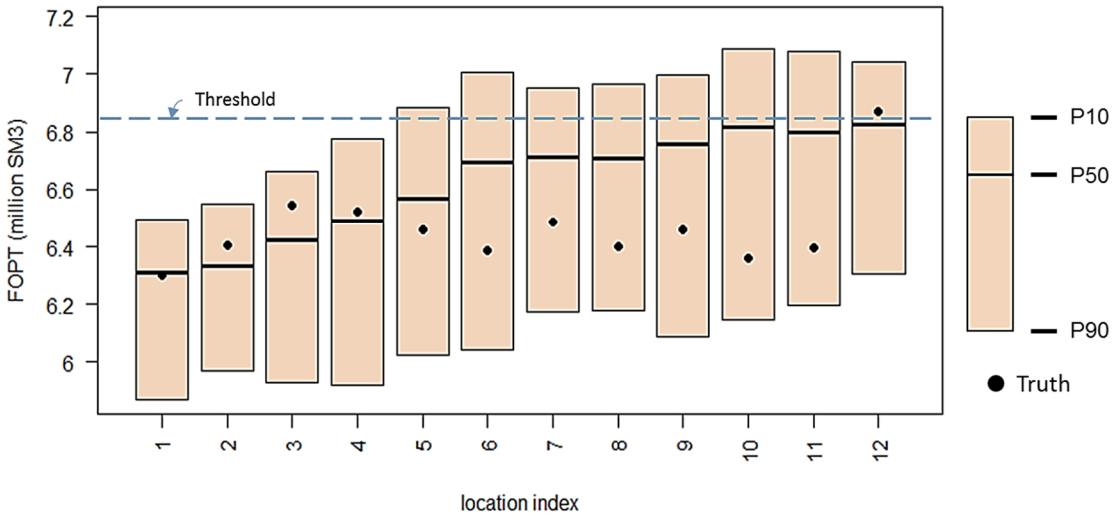

Figure 6.24—Box plot of total oil recovery on 12 optimal solutions from the robust optimisation across all seven Pareto history-matched models with the truth case as a reference for each location index. No location index results in *P50* of FOPT more than the economic threshold.

The validation of uncertainty estimation from the robust optimisation is also performed with the truth case to see the reliability of the optimisation forecast. We can see from Figure 6.24 that the truth values of the total recovered oil at the end of field production time are encapsulated within *P10–P90* range for all location indices. This result demonstrates that the proposed methods (i.e. model selection based on the Pareto models and posterior inference based on the NAB clustering) in uncertainty estimation of optimisation forecast in the robust optimisation workflow is reliable to support the decision-making process.

6.6 Case Study 2: Three Infill Wells Placement

A key feature in the robust optimisation workflow is its viability to handle complex cases, i.e. more than one well to be placed. As the number of wells or decision variables increases, the robust optimisation can evaluate an objective function(s) simultaneously across all the model realisations, i.e. in the form of expectation measure, for all the found common solutions.

Another robustness criterion can be added in the robust optimisation workflow by use of the multi-objective optimisation. For instance, variance measure can be added as the additional objective function that measures the variation of the original objective function across the selected model realisations at the solution parameter. This approach will be demonstrated in the case study presented in this section.

6.6.1 Optimisation Setup

In the second case study, the PUNQ-S3 mature field is further developed by drilling three new vertical infill wells to be produced for the next 10 years after been produced for 16.5 years to increase the oil recovery. The setup of production schedule is similar with the first case study in Section 6.5.

The optimisation will be a two-objective problem whose objectives are set to maximise the expected cumulative oil production and to minimise the variance cumulative oil production from the field across all model realisations, as given in Equation (6.15). The

constraint in the optimisation is the new infill well could not be drilled in the inactive cells of reservoir model nor overlap with the current existing wells. These constraints ensure that the proposed new wells will not be drilled outside the reservoir of interest and through the same well head with the existing well in the field.

$$J_1 = J_{(\theta_{1:N_R})} = \frac{1}{N_R}\sum_{i=1}^{N_R} J(\theta_i)$$

$$J_2 = \frac{1}{N_R}\sum_{i=1}^{N_R} (J(\theta_i))^2 - \frac{1}{N_R}\sum_{i=1}^{N_R} J(\theta_i)\,, \text{where} \tag{6.15}$$

$$J_{(\theta_i)} = \left(\sum_{w=1}^{N_w}\sum_{k=1}^{N_t-1} q_{o(w,k)} \cdot \Delta_{k,k+1}\right)_i$$

where J_1 and J_2 are the first and second objective function values to be maximised and minimised, respectively; $q_{o(w,k)}$ represents the oil rate from a producer well at the simulation timestep k; $\Delta_{k,k+1}$ represents the period of time from timesteps k to $k+1$; N_w is the number of producer wells; θ_i is the model realisation i ($i = 1, 2, \ldots, N_R$); and N_t is the number of timestep at the end of simulation time.

6.6.2 Optimisation Results

We applied the robust optimisation workflow to place three new vertical infill wells with the objective functions defined in Equation (6.15). We used all eight selected PMs described in Table 6.5 for the optimisation. The algorithm setting is the same with the previous optimisation runs with 500 flows simulations for each PMs which results in 4,000 reservoir flow simulations in total.

Figure 6.25 shows the results of the robust optimisation of placing three new vertical wells on PUNQ-S3 reservoir in the objective space. We selected the Pareto front solutions as the optimal locations and these locations are analysed further. There are three selected scenarios, i.e. Scenarios 1, 2, and 3 to represent three types of decision-maker behaviour, i.e. risk-averse, risk-neutral, and risk-taker, respectively, as shown in Figure 6.25. The risk-averse decision-maker tends to be more conservative in terms of a

lower expected oil recovery and its variance, whereas the risk-taker one is more aggressive on expecting a higher oil recovery with the higher risk of larger variance of oil recovery. The risk-neutral decision-maker tends to be in between risk-averse and risk-taker.

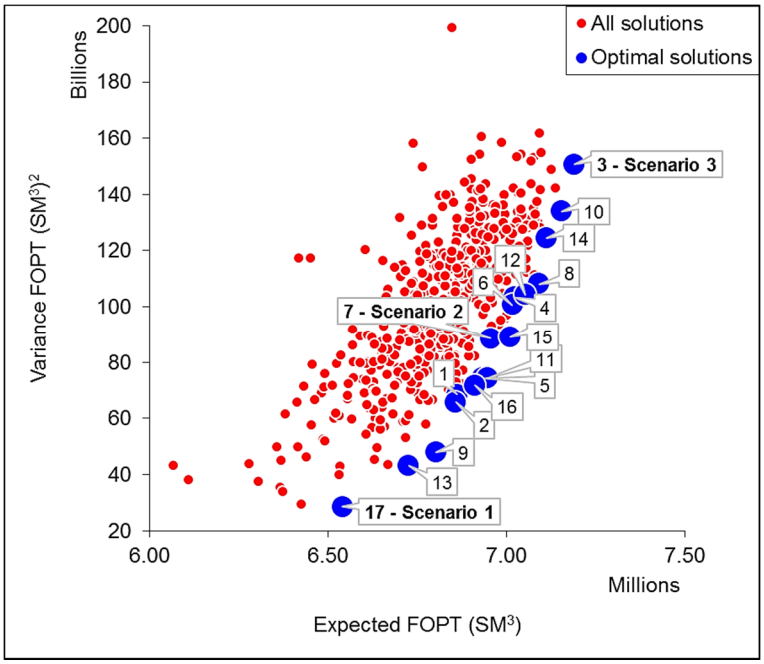

Figure 6.25—Robust optimisation results of placing three new vertical wells in PUNQ-S3 showing all and the optimal solutions in the objective space. The number on each blue dot represents solution index. Three scenarios are selected based on different types of decision-maker behaviour, i.e. Scenario 1 for risk-averse, Scenario 2 for risk-neutral, and Scenario 3 for risk-taker decision-makers.

Figure 6.26 shows the corresponding locations of the selected three scenarios in a grid. We can see from Figure 6.26 that drilling wells in both northern and southern part result in low expected oil recovery with low variance, as shown in green boxes (i.e. Scenario 1). Well locations at the middle across from the western to the eastern part of the field result in high expected oil recovery with high variance, as shown in red boxes (i.e. Scenario 3). In Scenario 2, well locations are located across from the western to the eastern part of the field with a slightly towards southern part of the field, as shown in blue boxes.

The validation of uncertainty estimation from the robust optimisation is also performed with the truth case to see the reliability of the optimisation forecast, as shown in Figure

6.27. We can see from Figure 6.27 that the truth values of the total recovered oil at the end of field production time are encapsulated within *P10–P90* range for all location indices. This result demonstrates that the proposed methods (i.e. models selection based on the Pareto models and posterior inference based on the NAB clustering) in uncertainty estimation of optimisation forecast in the robust optimisation workflow is reliable to support the decision-making process.

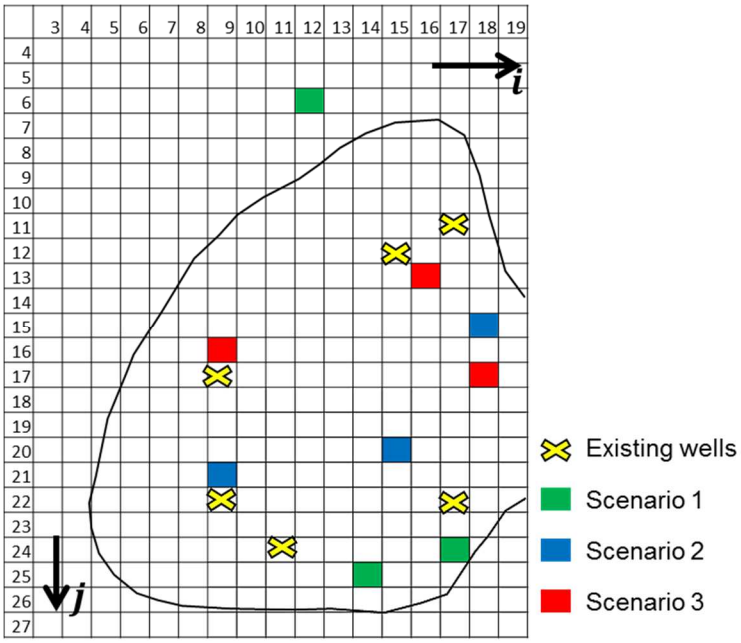

Figure 6.26—The corresponding well locations for the selected three scenarios in Figure 6.25.

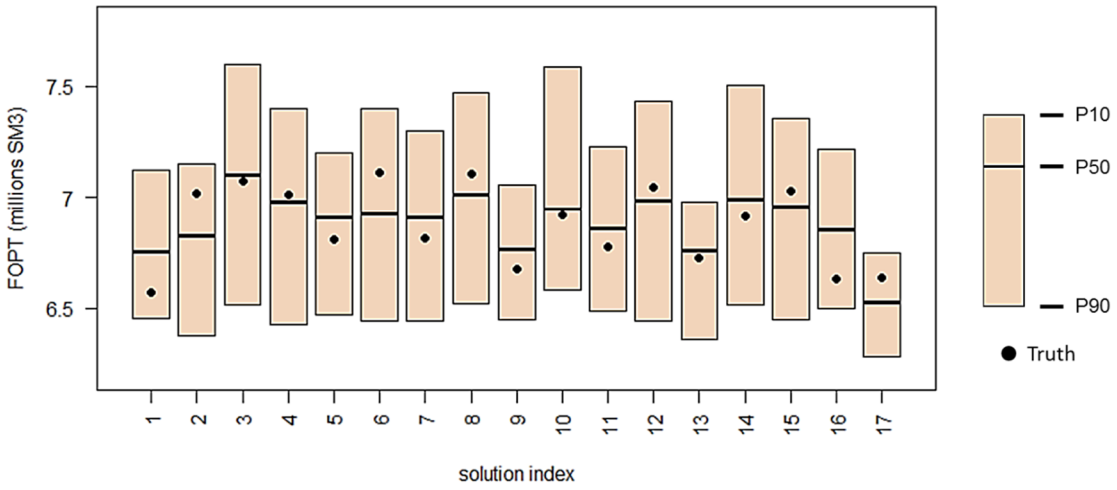

Figure 6.27—Box plot of total oil recovery on 17 optimal solutions from the robust optimisation across all eight Pareto history-matched models with the truth case as a reference for each solution index.

6.7 Discussion

In this chapter, we have presented a new workflow to place an infill well or group of wells while considering geological uncertainty. The workflow combines the history-matching run, posterior inference calculation and optimisation run. We applied this workflow to find the optimal infill well location(s) in a brownfield. The proposed workflow addresses five challenges mentioned at the beginning of this chapter as follows:

1. How to generate the model realisations?
   Proposed method: multi-objective history matching and NAB to assign the PPD for each history-matched models.

2. How to select the models for the development optimisation task?
   Proposed method: Pareto models from multi-objective history matching.

   How to quantify the range of uncertainty from all of the selected models?
   Proposed method: Pareto-centred NAB clustering.

3. How to perform the optimisation across multiple model realisations?
   Proposed method: the extended multi-objective nominal optimisation or the robust multi-objective optimisation.

4. How to select the optimal well locations?
   Proposed method: PSA can be used in the extended nominal optimisation for the optimal well locations, whereas in the robust optimisation all the optimal solutions can be selected which requires no PSA.

5. How to perform risk analysis and decision-making?
   Proposed method: economic threshold, Pareto front solutions, and *P10*, *P50*, and *P90* Bayesian credible intervals.

The multi-objective approach in the history matching provides diverse sets of matched-models that should lead to a better forecast on the optimisation outcomes. This is

demonstrated in both case studies presented in this chapter. The results show that the forecasting optimisation based on the Pareto history-matched models results in *P10–P90* range encapsulating the truth case values.

The chapter emphasises that the uncertainty estimation with inference approximation based on multi-objective history matching produces robust optimal development solutions between different history-match runs. We applied the proposed workflow to an industry-standard reservoir model for benchmarking. Different optimal regions found with different uncertainty range can accommodate different types of decision-maker behaviour, i.e. risk-averse and risk-taker, which offers a flexibility to the decision-maker given possible constraints.

This chapter shows that the proposed extended nominal optimisation under uncertainty workflow can be used to obtain robust and reliable decisions regarding location of a new infill well with a high oil recovery and a low range of uncertainty at a manageable computational cost. This was achieved by the introduction of the PSA application in the extended nominal optimisation, which enables us to obtain representative optimal solutions while reducing the computational cost. The representativeness of the selected optimal solutions from PSA is then validated by running all optimal solutions across all models exhaustively.

This chapter also shows that the proposed robust optimisation workflow can be used to obtain comparable results with the ones from the extended nominal optimisation in an infill well placement optimisation. The robust optimisation addresses the limitation of the extended nominal optimisation to cope with the objective functions such as expectation and variance measures. Both of these objective functions can be optimised by the multi-objective approach that is able to obtain a group of optimisation solutions, and the decision-maker could make decisions based on their risk attitude. Again, coupled with the proposed model selection and posterior inference, the forecasting optimisations are validated with the truth case and demonstrated to be reliable.

Chapter 7

Summary and Future Work

This thesis is succeeded in demonstrating that multi-objective approach to history matching and reservoir development optimisation can provide reliable forecasting uncertainty and robust decision-making. The multi-objective approach on history matching can find an ensemble of a diverse set of good history-matched models. This diverse set of good history-matched models is essential for reliable and yet realistic uncertainty prediction of future field behaviours. The models from multi-objective history matching also are then used in the reservoir development optimisation to obtain robust decisions under uncertainty.

This thesis contributes to the research of methods for multi-objective history matching and uncertainty quantification in reliable forecasting and field development optimisation. Several challenges in the framework of multi-objective history matching, uncertainty quantification and optimisation have been outlined in Chapter 1 and investigated in this thesis. These challenges include: (1) impact of the uncertainty in the model parameterisation on the forecast reliability; (2) history matching efficiency in case of many matched criteria and the way they can be grouped into multiple objectives; (3) the problem with a high number of objectives; and (4) reservoir development optimisation under uncertainty.

This thesis proposes solutions for each of the challenges mentioned above through extensive studies on both synthetic and real field cases supported by rigour statistical

evaluations. This chapter summarises the main contributions and key findings from the thesis and suggests recommendations for future work.

7.1 Summary

7.1.1 Challenge in the Uncertainty of Model Parameterisation

Chapter 3 demonstrated that the multi-objective approach in history matching improves the reliability of predictions under uncertainty in the model parameterisation. The key finding in Chapter 3 is that the uncertainty envelope from the ensemble of history-matched models from a multi-objective approach is more accurate, more robust and more reliable than the one from single-objective history matching across different model parameterisations on the PUNQ-S3 reservoir study.

Additionally, the results of the investigation in Chapter 3 confirm previous findings in [7–9] and contribute to our understanding that inherently, history matching is a multi-objective problem which should be approached by a methodology that preserves this nature. It was demonstrated that the multi-objective approach in history matching obtains a more diverse set of good matched models than the single-objective approach across different model parameterisations. This is due to the nature of the multi-objective approach to trade off between objectives that results in a more explorative search of the algorithm to find the solutions than the single-objective approach.

7.1.2 Challenge in the Uncertainty of Objective Grouping

Chapter 4 demonstrated that the low conflicted objective grouping results in significantly better history-matching performance (i.e. high match quality and faster convergence) than the high conflicted objectives. Chapter 4 introduced a novel technique on how to group and optimally select the objective grouping for multi-objective history matching. The proposed technique reduces the number of objectives to two objectives by grouping and then selecting the lowest conflicted grouping based on nonparametric-conflict score as the optimal grouping. The technique was demonstrated through history

matching studies on the synthetic PUNQ-S3 model and the real case study Zagadka Field.

Additionally, through studies on the synthetic PUNQ-S3 history matching, more key findings in Chapter 4 are:

- There is a significantly high correlation between misfit values and conflict measure. This finding is supported by rigorous statistical tests.
- Multi-objective history matching encounters the same problem with general multi-objective optimisation problems on a high number of objectives, i.e. performance deterioration in terms of slow misfit convergence. The study in Chapter 4 has shown that the more objectives we have, the higher the percentage of nondominated solutions, that causes the algorithm to lose selection pressure to approximate the Pareto front, consequently slowing the misfit convergence and lowering the match quality.

The practical implication from Chapter 4 is to increase the reservoir engineers' awareness of the limitations of certain algorithms for history matching, particularly the multi-objective algorithm. Given the limitation of the present Pareto-based multi-objective optimisation algorithm, the proposed technique presented in Chapter 4 can be used as a practical guideline on how to properly handle multiple match criteria in multi-objective history matching. The proposed technique can be used to help reservoir engineers on how to deal with the explosion of the choices on objective grouping in multi-objective history matching due to its combinatory nature.

7.1.3 Challenge in a High Number of Objectives

Chapter 5 succeeded in showing, for the first time, the application of one of the many-objective algorithms, called the reference vector guided evolutionary algorithm (RVEA) to cope with the high number of objectives in multi-objective history matching.

Key findings in Chapter 5 through studies on the synthetic PUNQ-S3 and the Zagadka Field history matchings which are supported by rigorous statistical tests are:

- RVEA was able to obtain fast misfit convergence, high quality and yet a diverse set of matched models for the history matching problems with six objectives on PUNQ-S3 and four objectives on Zagadka Field.
- RVEA outperformed both multi-objective particle swarm optimisation (MOPSO) and the elitist nondominated sorting genetic algorithm (NSGA-II) significantly in terms of fast misfit convergence and providing high quality matched-models.
- In PUNQ-S3, the matched models by RVEA are significantly more diverse than MOPSO and are comparable with NSGA-II. Moreover, RVEA obtained a significantly larger number of high quality matched models than NSGA-II and MOPSO that should lead to better uncertainty prediction.
- In Zagadka Field, the diversity of matched models obtained by all three algorithms is similar. However, RVEA successfully obtained more matched-models with lower misfit values than MOPSO and NSGA-II.

The practical implication of these findings is that the many-objective history matching paradigm should be highly considered in the practice of reservoir simulation study. Given the nature of a petroleum reservoir that may feature far too many objectives to match (i.e. multiple production data from multiple wells), the capability offered by many-objective optimisation algorithms such as RVEA may help to obtain a diverse set of good matched models fast.

7.1.4 Challenge in the Reservoir Development Optimisation Under Uncertainty

Chapter 6 proposed and demonstrated successfully a workflow for reservoir development optimisation under uncertainty to obtain robust decision-making and reliable uncertainty prediction, and yet with a manageable computational cost. The workflow comprises model selection from multi-objective history matching; posterior probability distribution (PPD) reapproximation for each selected Pareto model (with Bayesian analysis and clustering); multi-objective optimisation across the selected models; optimal solution selection and decision-making based on risk analysis. Specifically, in the optimisation step, we tested the workflow with the extended nominal optimisation and the robust optimisation approaches.

Through experimental studies on infill well placement optimisation in a brownfield PUNQ-S3 reservoir model with various tests, key findings in Chapter 6 are as follows:

- The proposed workflow can be applied to obtain a consistent and reliable decision-making outcome on infill well placement optimisation under geological uncertainty with a reduced computational cost, i.e. a number of flow simulations.
- Nondominated Pareto models from multi-objective history matching can be used for the optimisation of infill well placement under geological uncertainty.
- PPD for each nondominated Pareto model is approximated with a combination of NAB technique and clustering. This recalculated PPD is then used for uncertainty quantification in the optimisation forecast across all optimisation models.
- The combination of nondominated model selection with the proposed PPD approximation successfully provides reliable uncertainty estimation for infill well optimisation. The *P10–P90* credible interval of each optimal solution found by either the extended nominal optimisation or the robust optimisation scheme encapsulates the "truth" case value for each respective optimal solution.
- Part and select algorithm (PSA) can be used to select representatives of optimal solutions in the multi-objective optimisation to reduce computational cost in the extended nominal optimisation. The validation test conducted in Chapter 6 has demonstrated that the subset of optimum solutions selected by PSA preserves the estimated probability distribution function (PDF) from exhaustive simulations on all optimum solutions in the extended nominal optimisation scheme.
- Multi-objective optimisation can effectively handle different types of objectives (i.e. the expected and variance measures of oil recovery) to accommodate different behaviours of decision-maker (i.e. risk-taker, risk-neutral, or risk-averse). It was demonstrated in Chapter 6 that different types of decision-maker would choose different optimal solutions based on the tradeoff between expected oil recovery and its variance.

7.2 Recommendations for Future Work

The author's recommendations for future work are discussed below.

7.2.1 Guideline for the Parsimonious Representation

Chapter 3 identified that the multi-objective approach in history matching can cope with model parameterisation uncertainty by providing better and more robust uncertainty quantification in the forecasting than single-objective optimisation approach. It is demonstrated in Chapter 3 that in the case of more complex models (i.e. more model parameters), the multi-objective history matching provides a favourable approach for preserving parsimony. This is due to the increase of independent information contained in the history matching by introducing additional outputs during model calibration in the form of objective functions. However, the findings are subject to the presented case studies which involve 24 and 38 model parameters, and two objectives in the multi-objective case.

Further research should be done to investigate the capability of the multi-objective approach in history matching to preserve the parsimony representation of a reservoir model calibration. A guideline based on the empirical studies of the ratio between the number of objectives and the number of model parameters can be a starting point to provide a parsimonious representation of the multi-objective history matching problem. This will guide the choice of algorithm and approach used for history matching and at the same time raise the reservoir engineers' awareness of the limitation of the outcome.

7.2.2 Recognition of Model Parameterisation Errors

Some studies of hydrological model calibration have used a multi-objective calibration framework to identify a wrongly parameterised model (see for example [325,326]). This was done by investigating the tradeoffs between different objectives of the Pareto optimal solutions. An irregular shape of the Pareto front such as significant tradeoffs between two or more objectives may indicate that the model is not parameterised correctly. Further research can concentrate on this to help reservoir engineers to reparameterise the model during history matching.

7.2.3 Extension of the Proposed Objective Grouping Technique

In Chapter 4, the proposed objective grouping selection technique was applied and demonstrated on two-objective history matching case studies. Further extension of the objective grouping selection technique should be done on three or more objectives. Given the present availability of many-objective optimisation algorithms in the literature, this extended technique should be a fruitful line of investigation.

Another possible extension of the proposed objective grouping is production data mining or learning from the grouping with low conflict to reveal the answer to some engineering questions, such as flow connectivity. A combination of data mining or learning techniques such as variable importance with an engineering perspective may lead to meaningful results.

7.2.4 Time-Based Objective Grouping Technique

Similar to work in Chapter 4, further research may concentrate on objective grouping based on the time of production data from the field. As an example, this framework can be seen in the work of Khu *et al.* [327] on the hydrologic model calibration which classifies multi-site data measurements into groups based on their temporal dynamics. In history matching, this can be grouping the production data from the wells in the field according to their production time (i.e. early and later period).

7.2.5 Comparative Study Between Many-Objective Algorithms

In Chapter 5, we demonstrated the superiority of one of the many-objective optimisation algorithms, i.e. RVEA to MOPSO and NSGA-II for history matching problems with more than three objectives. We can argue that the comparison is not fair as MOPSO and NSGA-II algorithms are designed for the problems with two or three objectives. However, an important finding to emerge in this study is that reservoir engineers need to be

aware of the limitation of the current state-of-the-art multi-objective optimisation algorithms (i.e. MOPSO and NSGA-II) on multi-objective history matching with a high number of objective (i.e. more than three objectives). A practical implication of this finding is that when dealing with multi-objective history matching with more than three objectives, reservoir engineers should use many-objective optimisation algorithms instead of a multi-objective one.

As the development of many-objective optimisation algorithms is increasing in the computer science field, further research should be done to compare the performance of many-objective optimisation algorithms (such as RVEA, MOEA/D, and NSGA III) in history matching problems.

7.2.6 Application of the Preference Articulation

Inherently, the reference vectors-based method RVEA is capable of articulating user preference in the objective space during optimisation. In real-world optimisation problems such as oil production facility optimisation, this feature is advantageous as it should accommodate the term of *"what you get is (nearly with) what you want"* from the optimisation. Figure 7.1 illustrates the user preference articulation on the corners and centre of the Pareto front of a three-objective hypothetical problem during an optimisation run. This user preference articulation is an interesting line of further research on optimisation problems in the petroleum domain, such as production facility optimisation, combined with a many-objective algorithm.

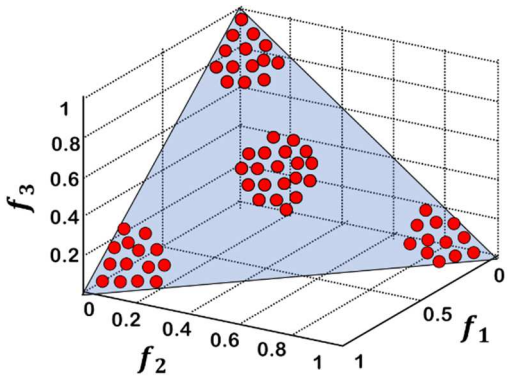

Figure 7.1—The approximate Pareto optimal solutions distributed on the corners and centre of the Pareto front of a three-objective hypothetical problem (red dots) obtained by applying preference articulation. The blue-shaded area is the true Pareto front.

7.2.7 PPD Reapproximation for Uncertainty Prediction

In Chapter 6, we proposed a weighting procedure on the selected model for optimisation under uncertainty by recalculating the approximated PPD from Bayesian analysis within a multi-objective formalism and using a clustering technique. The proposed technique is demonstrated for the problem of optimisation across multiple realisations to keep the computational cost manageable. It will be interesting to see the applicability of this technique in reducing the computational cost in the forecasting uncertainty quantification from an ensemble of history-matched models. In this technique, as the nondominated models are selected, the framework can be tested with either multi- or many-objective optimisation algorithms.

7.2.8 Bayesian Statistical Significant Test

Recently in 2016, the American Statistical Association (ASA) issued a statement on the context, process, and purpose of *p*-values [328]. This statement was issued due to concerns about the *reproducibility* and *replicability* of scientific conclusions based on the *p*-values measure. The use of *p*-values is commonly misused and misinterpreted even though they can be a useful statistical measure. The other concern is about the use of a *p*-values threshold of 0.05 for statistical-significance testing which is *ill-defined* (the reasons for it still being used are merely that is still what the scientific community and journal editors use and is what many people were taught in college or grad school). The ASA statement provides several principles regarding *p*-values and significance testing which should be accompanied during its use.

In light of this ASA's statement, a careful study is required to investigate other approaches in significance testing comparing two different groups, approaches, or algorithms for history matching problems. Bayesian estimation supersedes the *t*-test (BEST) [329] is one of those other significance testing approaches. In BEST, the *p*-values concept is not used eliminating the concerns about its use. Moreover in [329], the article claimed that BEST always provides much richer information than *t*-test significance testing. For a starting point to give some flavour of BEST, interested readers can access its online version at http://sumsar.net/best_online/.

7.2.9 Large-Scale Problems

With the (1) advanced development of forward simulation and algorithms; (2) the arrival of the petascale computing era; and (3) the explosion of available observed data, solving large-scale problems in history matching and uncertainty quantification becomes viable (i.e. involving large amounts of data and high-dimensional parameter space). Future research should focus on the development and application of stochastic optimisation algorithms that can cope with large numbers of model parameters and/or objectives, such as those often encountered in history matching. Furthermore, these algorithms can also be applied to the optimisation problems in the petroleum domain, such as production optimisation, production facility optimisation, and the optimisation of mature field redevelopment which may consist of hundreds or thousands of wells.

There are some recently developed algorithms that can cope with these large-scale problems. The competitive swarm optimisation (CSO) [330] and social learning particle swarm optimisation (SL-PSO) [331] algorithms are two PSO variants for solving large-scale single-objective optimisation problems. The inverse model based MOEA (IM-MOEA) which uses Gaussian process-based inverse modelling can be tested for solving large-scale multi-objective optimisation problems (problems with two or three objectives). Applying these optimisation algorithms to history matching problems with hundreds or thousands of model parameters may be a worthwhile line of investigation.

7.2.10 Data-Physics Paradigm

Finally, a recent defeat of one of the world's best Go players by AlphaGo, a Go-playing artificial intelligence developed by Google's DeepMind, reaffirms a major milestone for artificial intelligence. Go is a board game orders of magnitude more computationally complex than chess game which cannot be solved by brute force. It was thought that a solution to Go was at least 10 years away. Nonetheless, DeepMind's approach to solving this became visible through huge amounts of data training, the use of Google's extra-large graphics processing unit clusters, and significant advanced development in data science over the past decade.

Routinely, the oil and gas industry has been collecting a variety of data, such as well logs, production data, artificial lift, completion data, permanent downhole sensors, and maintenance data. More often than not, most of these data are not used to the fullest extent possible and almost certainly are not used to help in proactive decision-making. Oil operators often rely on a reactive approach, i.e. trying to remediate the producer well after it water breakthrough. These reactive controls are usually "too late", and can be costly.

Even though generally lagging in the uptake of new technology, the oil and gas industry has also seen a surge in the application of data science (terms such as "digital oil field", "closed-loop reservoir management", and "smart field" are amongst the technologies that adopt data science). By general definition, data science is an interdisciplinary field about processes and systems to extract knowledge or insights from data in various forms. Data science can help in shifting from reactive remedial approaches to proactive decision-making. Data science enables this through the integration of collected data, modelling, and optimisation. Predictive models (predictive analytics) are built from different kinds of data and used to predict future well, reservoir, and production facility performance, and then optimise such decisions. This additional optimisation and decision-making step leads to "prescriptive" analytics providing particular recommendations to the operator to solve a particular problem.

In one of his books, L.P. Dake said that *"it is only through having a complete understanding of the physics that the engineer can hope to appreciate and solve complex reservoir engineering problems in a practical manner"* [32]. Such a heavily data-driven process in data science should be considered and aligned with physics. In light of this, a new paradigm called "*data-physics*" should be aimed for to be included in history matching, reservoir forecasting, and optimisation assisted by artificial intelligence.

The knowledge of reservoir physics is important in the context of multi-objective approach. Multi-objective has the advantage of producing good tradeoff solutions, however has drawback of usually producing too many solutions. Hence, the inclusion of domain knowledge for the problems at hand is useful to help the decision-maker to pick the optimal solutions from the results of multi-objective approaches.

Another good opportunity offered by multi-objective approaches in the context of data-physics paradigm is to help the integration of more reservoir knowledge and data mining task for a problem at hand. The knowledge of reservoir can either to speed up the search process, to improve the quality of the obtained solutions or to tune the algorithm itself. This integration can be realised by enabling the combination of objective functions specific to the data mining task with separate objective that exploit reservoir knowledge. Corne *et al.* [332] provide an excellent review on the emerging use of multi-objective approaches in operations research and data mining that can be a starting point on this promising route of research.

Ultimately, the inclusion of physics with data-driven process such as history matching and optimisation should help improve understanding of reservoir engineering phenomena in a timely manner, solving specific encountered problem in reservoirs confidently, and ultimately lead towards better-informed decision-making.

§§§ • §§§

It is my hope that the research presented in this thesis will lay the foundations of a new and exciting field of study, combining multi or many-objective optimisation within reservoir simulation studies (i.e. history matching, forecasting uncertainty quantification and optimisation) in a principled and practical way.

References

[1] BP, 'BP Energy Outlook 2017 Edition', 2017.

[2] J. C. Rivenæs, P. Sørhaug, and R. Knarud, 'Introduction to reservoir modelling', in *Petroleum Geoscience: From Sedimentary Environments to Rock Physics*, K. Bjørlykke, Ed. Berlin, Heidelberg: Springer Berlin Heidelberg, 2015, pp. 559–580.

[3] L. Mohamed, 'Novel sampling techniques for reservoir history matching optimisation and uncertainty quantification in flow prediction', PhD Thesis, Heriot-Watt University, Edinburgh, 2011.

[4] Y. Hajizadeh, 'Population-based algorithms for improved history matching and uncertainty quantification of petroleum reservoirs', PhD Thesis, Heriot-Watt University, Edinburgh, 2011.

[5] D. S. Oliver, A. C. Reynolds, and N. Liu, *Inverse theory for petroleum reservoir characterization and history matching*. Cambridge: Cambridge University Press, 2008.

[6] A. Tarantola, *Inverse problem theory and methods for model parameter estimation*. Philadelphia: SIAM, 2005.

[7] L. Mohamed, M. A. Christie, and V. Demyanov, 'History matching and uncertainty quantification: multiobjective particle swarm optimisation approach', in *SPE EUROPEC/EAGE Annual Conference and Exhibition, SPE-143067-MS*, Vienna, Austria, 2011.

[8] Y. Hajizadeh, M. A. Christie, and V. Demyanov, 'Towards multiobjective history matching: Faster convergence and uncertainty quantification', in *SPE Reservoir Simulation Symposium, SPE-141111-MS*, The Woodlands, Texas, USA, 2011.

[9] M. Christie, D. Eydinov, V. Demyanov, J. Talbot, D. Arnold, and V. Shelkov, 'Use of multi-objective algorithms in history matching of a real field', in *SPE Reservoir Simulation Symposium, SPE-163580-MS*, The Woodlands, Texas, USA, 2013.

[10] J. J. Hutahaean, V. Demyanow, and M. A. Christie, 'Impact of model parameterisation and objective choices on assisted history matching and reservoir forecasting', in *SPE/IATMI Asia Pacific Oil & Gas Conference and Exhibition, SPE-176389-MS*, Nusa Dua, Bali, Indonesia, 2015.

[11] K. Deb, *Multi-objective optimization using evolutionary algorithms*. West Sussex: John Wiley & Sons Ltd., 2001.

[12] N. Liu, S. Betancourt, and D. S. Oliver, 'Assessment of uncertainty assessment methods', in *SPE Annual Technical Conference and Exhibition, SPE-71624-MS*, New Orleans, Louisiana, 2001.

[13] D. Erbas, 'Sampling strategies for uncertainty quantification in oil reservoir prediction', PhD Thesis, Heriot-Watt University, Edinburgh, 2006.

[14] D. Arnold, 'Geological parameterisation of petroleum reservoir models for improved uncertainty quantification', PhD Thesis, Heriot-Watt University, Edinburgh, 2008.

[15] H. Ishibuchi, N. Tsukamoto, and Y. Nojima, 'Evolutionary many-objective optimization: A short review', in *Proceedings of the IEEE Congress on Evolutionary Computation (CEC)*, Hong Kong, p. 2419–2426, 2008.

[16] A. R. R. de Freitas, P. J. Fleming, and F. G. Guimarães, 'Aggregation Trees for visualization and dimension reduction in many-objective optimization', *Information Sciences*, vol. 298, no. 20 March, pp. 288–314, 2015.

[17] C. von Lücken, B. Barán, and C. Brizuela, 'A survey on multi-objective evolutionary algorithms for many-objective problems', *Computational Optimization and Applications*, vol. 58, no. 3, pp. 707–756, 2014.

[18] S. I. Aanonsen, A. L. Eide, L. Holden, and J. O. Aasen, 'Optimizing reservoir performance under uncertainty with application to well location', in *SPE Annual Technical Conference and Exhibition, SPE-30710-MS*, Dallas, Texas, 1995.

[19] B. Güyagüler and R. N. Horne, 'Uncertainty assessment of well-placement optimization', *SPE Reservoir Evaluation & Engineering, SPE-87663-PA*, vol. 7, no. 01, pp. 24–32, Feb. 2004.

[20] G. van Essen, M. Zandvliet, P. Van den Hof, O. Bosgra, and J.-D. Jansen, 'Robust waterflooding optimization of multiple geological scenarios', *SPE Journal, SPE-102913-PA*, vol. 14, no. 01, pp. 202–210, Mar. 2009.

[21] Z. Bouzarkouna, D. Y. Ding, and A. Auger, 'Well placement optimization under uncertainty with CMA-ES using the neighborhood', in *ECMOR XIII-13th European Conference on the Mathematics of Oil Recovery*, Biarritz, France, 2012.

[22] M. G. Shirangi and L. J. Durlofsky, 'Closed-loop field development under uncertainty by use of optimization with sample validation', *SPE Journal, SPE-173219-PA*, vol. 20, no. 05, pp. 908–922, Oct. 2015.

[23] L. Cosentino, *Integrated reservoir studies*. Paris: Editions Technip, 2001.

[24] L. C. Uren, *Petroleum production engineering*, 4th ed., vol. 1. McGraw-Hill, 1956.

[25] K. H. Coats, 'Use and misuse of reservoir simulation models', *Journal of Petroleum Technology, SPE-2367-PA*, vol. 21, no. 11, pp. 1391–1398, Nov. 1969.

[26] D. Katz, 'A method of estimating oil and gas reserves', *Transactions of the AIME, SPE-936018-G*, vol. 118, no. 01, pp. 18–32, Dec. 1936.

[27] S. E. Buckley and Mc. Leverett, 'Mechanism of fluid displacement in sands', *Transactions of the AIME, SPE-942107-G*, vol. 146, no. 01, pp. 107–116, Dec. 1942.

[28] D. Dietz, 'A theoretical approach to the problem of encroaching and by-passing edge water', in *Proceedings of the Akad. van Wetenschappen*, Amsterdam, 1953, vol. 56, pp. 83–92.

[29] J. S. Archer and C. G. Wall, *Petroleum engineering: Principles and practice*, 1st ed. Springer Netherlands, 1986.

[30] L. P. Dake, *The practice of reservoir engineering*, Revised. Amsterdam: Elsevier, 2001.

[31] J. J. Arps, 'Analysis of decline curves', *Transactions of the AIME, SPE-945228-G*, vol. 160, no. 01, pp. 228–247, Dec. 1945.

[32] L. P. Dake, *Fundamentals of reservoir engineering*, vol. 8. Elsevier, 1983.

[33] K. Zhang, Y. Wu, C. Ding, K. Pruess, and E. Elmroth, 'Parallel computing techniques for large-scale reservoir simulation of multi-component and multiphase fluid flow', in *SPE Reservoir Simulation Symposium, SPE-66343-MS*, Houston, Texas, 2001.

[34] J. A. Pita, J. C. Tan, L. S. Fung, and A. H. Dogru, 'Highly-parallel, implicit compositional reservoir simulator for multi-million-cell models', US7526418 B2, 28-Apr-2009.

[35] P. Bhambri and K. Mohanty, 'Compositional streamline simulation: A parallel implementation', *Transport in Porous Media*, vol. 90, no. 3, pp. 741–761, Dec. 2011.

[36] Y.-S. Wu, K. Zhang, and K. Pruess, 'Massively parallel simulation of flow and transport in variably saturated porous and fractured media', *Developments in Water Science*, vol. 47, pp. 289–296, 2002.

[37] J. R. Fanchi, *Principles of applied reservoir simulation*, 3rd ed. Colorado: Gulf Professional Publishing, 2005.

[38] M. G. Gerritsen and L. J. Durlofsky, 'Modeling fluid flow in oil reservoirs', *Annual Review of Fluid Mechanics*, vol. 37, pp. 211–238, Jan. 2005.

[39] A. Odeh, 'Reservoir simulation... What is it', *Journal of Petroleum Technology, SPE-2790-PA*, vol. 21, no. 11, pp. 1383–1389, Nov. 1969.

[40] Schlumberger, 'Oilfield Review', *April 1990*, vol. 2, no. 2, pp. 18–30, Apr-1990.

[41] K. D. Stephen, 'Seismic history matching with saturation indicators combined with multiple objective function optimization.', in *EAGE Annual Conference & Exhibition incorporating SPE Europec, SPE-164857-MS*, London, 2013.

[42] K. D. Stephen, J. Soldo, C. Macbeth, and M. A. Christie, 'Multiple model seismic and production history matching: A case study', *SPE Journal, SPE-94173-PA*, vol. 11, no. 04, pp. 418–430, Dec. 2006.

[43] A. Kazemi, K. Stephen, and A. Shams, 'Seismic history matching of Nelson using time-lapse seismic data: An investigation of 4D signature normalization', *SPE Reservoir Evaluation & Engineering, SPE-131538-PA*, vol. 14, no. 05, pp. 621–633, Oct. 2011.

[44] M. Litvak, M. Christie, D. Johnson, J. Colbert, and M. Sambridge, 'Uncertainty estimation in production predictions constrained by production history and time-lapse seismic in a GOM oil field', in *SPE Reservoir Simulation Symposium, SPE-93146-MS*, The Woodlands, Texas, 2005.

[45] K. D. Stephen and C. Macbeth, 'Reducing reservoir prediction uncertainty by updating a stochastic model using seismic history matching', *SPE Reservoir Evaluation & Engineering, SPE-100295-PA*, vol. 11, no. 06, pp. 991–999, Dec. 2008.

[46] F. Sedighi-Dehkordi and K. Stephen, 'Faster convergence in seismic history matching by dividing and conquering the unknowns', *SPE Journal, SPE-121210-PA*, vol. 15, no. 04, pp. 1077–1088, Dec. 2010.

[47] D. D. Jackson, 'Interpretation of inaccurate, insufficient and inconsistent data', *Geophysical Journal International*, vol. 28, no. 2, pp. 97–109, Jun. 1972.

[48] A. Tarantola, 'Popper, Bayes and the inverse problem', *Nature Physics*, vol. 2, no. 8, pp. 492–494, 2006.

[49] Z. Tavassoli, J. N. Carter, and P. R. King, 'Errors in history matching', *SPE Journal, SPE-86883-PA*, vol. 9, no. 03, pp. 352–361, Sep. 2004.

[50] J. Hadamard, 'Sur les problèmes aux dérivées partielles et leur signification physique', *Princeton University Bulletin*, vol. 13, no. 49–52, p. 28, 1902.

[51] M. A. Williams, J. F. Keating, and M. F. Barghouty, 'The stratigraphic method: A structured approach to history matching complex simulation models', *SPE Reservoir Evaluation & Engineering, SPE-38014-PA*, vol. 1, no. 02, pp. 169–176, Apr. 1998.

[52] A. Abdollahzadeh, 'Adaptive algorithms for history matching and uncertainty quantification', PhD Thesis, Heriot-Watt University, Edinburgh, 2013.

[53] C. C. Mattax and R. L. Dalton, 'Reservoir simulation (includes associated papers 21606 and 21620)', *Journal of Petroleum Technology*, vol. 42, no. 06, pp. 692–695, Jun. 1990.

[54] N. Saleri, R. Toronyi, and D. Snyder, 'Data and data hierarchy', *Journal of Petroleum Technology, SPE-21369-PA*, vol. 44, no. 12, pp. 1286–1293, Dec. 1992.

[55] H. Cheng, K. Dehghani, and T. C. Billiter, 'A structured approach for probabilistic-assisted history matching using evolutionary algorithms: Tengiz field applications', in *SPE Annual Technical Conference and Exhibition, SPE-116212-MS*, Denver, Colorado, USA, 2008.

[56] M. Kelkar and G. Perez, *Applied geostatistics for reservoir characterization*. Texas: Society of Petroleum Engineers, 2002.

[57] J. Watts, 'Reservoir simulation: Past, present, and future', *SPE Computer Applications, SPE-38441-PA*, vol. 9, no. 06, pp. 171–176, Nov. 1997.

[58] C. S. Kabir, M. C. H. Chien, and J. L. Landa, 'Experiences with automated history matching', in *SPE Reservoir Simulation Symposium, SPE-79670-MS*, Houston, Texas, 2003.

[59] M. Gruenwalder, S. Poellitzer, and T. Clemens, 'Assisted and manual history matching of a reservoir with 120 wells, 58 years production history and multiple well re-Completions', in *EUROPEC/EAGE Conference and Exhibition, SPE-106039-MS*, London, 2007.

[60] M. A. Christie, J. Glimm, J. W. Grove, D. M. Higdon, D. H. Sharp, and M. M. Wood-Schultz, 'Error analysis and simulations of complex phenomena', *Los Alamos Science*, vol. 29, pp. 6–25, 2005.

[61] T. Rojas, 'Controlling realism and uncertainty in reservoir models using intelligent sedimentological prior information', PhD Thesis, Heriot-Watt University, Edinburgh, 2013.

[62] G. R. Gavalas, P. C. Shah, and J. H. Seinfeld, 'Reservoir history matching by Bayesian estimation', *SPE Journal, SPE-5740-PA*, vol. 16, no. 06, pp. 337–350, Dec. 1976.

[63] S. Shah, G. R. Gavalas, and J. H. Seinfeld, 'Error analysis in history matching: The optimum level of parameterization', *SPE Journal, SPE-6508-PA*, vol. 18, no. 03, pp. 219–228, Jun. 1978.

[64] H. O. Jahns, 'A rapid method for obtaining a two-dimensional reservoir description from well pressure response data', *SPE Journal, SPE-1473-PA*, vol. 6, no. 04, pp. 315–327, Dec. 1966.

[65] G. J. J. Williams, M. Mansfield, D. G. MacDonald, and M. D. Bush, 'Top-down reservoir modelling', in *SPE Annual Technical Conference and Exhibition, SPE-89974-MS*, Houston, Texas, 2004.

[66] L. K. Thomas, L. J. Hellums, and G. M. Reheis, 'A nonlinear automatic history matching technique for reservoir simulation models', *SPE Journal, SPE-3475-PA*, vol. 12, no. 06, pp. 508–514, Dec. 1972.

[67] K. H. Coats, J. R. Dempsey, and J. H. Henderson, 'A new technique for determining reservoir description from field performance data', *SPE Journal, SPE-2344-PA*, vol. 10, no. 01, pp. 66–74, Mar. 1970.

[68] A. C. Bertolini and D. J. Schiozer, 'Influence of the objective function in the history matching process', *Journal of Petroleum Science and Engineering*, vol. 78, no. 1, pp. 32–41, Jul. 2011.

[69] Z. Bi, D. S. Oliver, and A. C. Reynolds, 'Conditioning 3D stochastic channels to pressure data', in *SPE Annual Technical Conference and Exhibition, SPE-56682-MS*, Houston, Texas, 1999.

[70] F. Anterion, R. Eymard, and B. Karcher, 'Use of parameter gradients for reservoir history matching', in *SPE Symposium on Reservoir Simulation, SPE-18433-MS*, Houston, Texas, 1989.

[71] W. H. Chen, G. R. Gavalas, J. H. Seinfeld, and M. L. Wasserman, 'A new algorithm for automatic history matching', *SPE Journal, SPE-4545-PA*, vol. 14, no. 6, pp. 593–608, Dec. 1974.

[72] R. Li, A. C. Reynolds, and D. S. Oliver, 'History matching of three-phase flow production data', *SPE Journal, SPE-87336-PA*, vol. 8, no. 04, pp. 328–340, Dec. 2003.

[73] D. S. Oliver and Y. Chen, 'Recent progress on reservoir history matching: A review', *Computational Geosciences*, vol. 15, no. 1, pp. 185–221, Jan. 2011.

[74] S. I. Aanonsen, G. Nævdal, D. S. Oliver, A. C. Reynolds, and B. Vallès, 'The ensemble Kalman filter in reservoir engineering: A review', *SPE Journal, SPE-117274-PA*, vol. 14, no. 03, pp. 393–412, Sep. 2009.

[75] J. Skjervheim and G. Evensen, 'An ensemble smoother for assisted history matching', in *SPE Reservoir Simulation Symposium, SPE-141929-MS*, The Woodlands, Texas, USA, 2011.

[76] G. Evensen, J. Hove, H. Meisingset, E. Reiso, K. S. Seim, and Ø. Espelid, 'Using the EnKF for assisted history matching of a North Sea reservoir model', in *SPE Reservoir Simulation Symposium, SPE-106184-MS*, Houston, Texas, 2007.

[77] G. Evensen, 'The ensemble Kalman filter: Theoretical formulation and practical implementation', *Ocean Dynamics*, vol. 53, no. 4, pp. 343–367, 2003.

[78] J.-A. Skjervheim, G. Evensen, S. I. Aanonsen, B. O. Ruud, and T.-A. Johansen, 'Incorporating 4D seismic data in reservoir simulation models using ensemble Kalman filter', in *SPE Annual Technical Conference and Exhibition, SPE-95789-MS*, Dallas, Texas, 2005.

[79] M. Valjak, 'History matching and forecasting with uncertainty: Challenges and proposed solutions for real field applications', PhD Thesis, Heriot-Watt University, Edinburgh, 2008.

[80] L. Mohamed, B. Calderhead, M. Filippone, M. Christie, and M. Girolami, 'Population MCMC methods for history matching and uncertainty quantification', *Computational Geosciences*, vol. 16, no. 2, pp. 423–436, 2012.

[81] A. J. Sultan, A. Ouenes, and W. W. Weiss, 'Automatic history matching for an integrated reservoir description and improving oil recovery', in *Permian Basin Oil and Gas Recovery Conference, SPE-27712-MS*, Midland, Texas, 1994.

[82] C. E. Romero, J. N. Carter, R. W. Zimmerman, and A. C. Gringarten, 'Improved reservoir characterization through evolutionary computation', in *SPE Annual Technical Conference and Exhibition, SPE-62942-MS*, Dallas, Texas, 2000.

[83] C. Romero, J. Carter, A. Gringarten, and R. Zimmerman, 'A modified genetic algorithm for reservoir characterisation', in *International Oil and Gas Conference and Exhibition, SPE-64765-MS*, Beijing, China, 2000.

[84] D. Erbas and M. A. Christie, 'Effect of sampling strategies on prediction uncertainty estimation', in *SPE Reservoir Simulation Symposium, SPE-106229-MS*, Houston, Texas, 2007.

[85] R. W. Schulze-Riegert, J. K. Axmann, O. Haase, D. T. Rian, and Y.-L. You, 'Optimization methods for history matching of complex reservoirs', in *SPE Reservoir Simulation Symposium, SPE-66393-MS*, Houston, Texas, 2001.

[86] R. Schulze-Riegert, J. Axmann, O. Haase, D. Rian, and Y.-L. You, 'Evolutionary algorithms applied to history matching of complex reservoirs', *SPE Reservoir Evaluation & Engineering, SPE-77301-PA*, vol. 5, no. 02, pp. 163–173, Apr. 2002.

[87] V. Demyanov, S. Subbey, and M. Christie, 'Uncertainty assessment in PUNQS3–Neighbourhood algorithm framework for geostatistical modelling', in *9th European Conference on the Mathematics of Oil Recovery*, Cannes, France, 2004.

[88] Y. Hajizadeh, M. A. Christie, and V. Demyanov, 'History matching with differential evolution approach: A look at new search strategies', in *SPE EUROPEC/EAGE Annual Conference and Exhibition, SPE-130253-MS*, Barcelona, Spain, 2010.

[89] Y. Hajizadeh, M. Christie, and V. Demyanov, 'Ant colony optimization for history matching and uncertainty quantification of reservoir models', *Journal of Petroleum Science and Engineering*, vol. 77, no. 1, pp. 78–92, 2011.

[90] L. Mohamed, M. A. Christie, and V. Demyanov, 'Reservoir model history matching with particle swarms: Variants study', in *SPE Oil and Gas India Conference and Exhibition, SPE-129152-MS*, Mumbai, India, 2010.

[91] A. Abdollahzadeh, A. Reynolds, M. Christie, D. W. Corne, G. J. J. Williams, and B. J. Davies, 'Estimation of distribution algorithms applied to history matching', *SPE Journal, SPE-141161-PA*, vol. 18, no. 03, pp. 508–517, Apr. 2013.

[92] A. Abdollahzadeh, A. Reynolds, M. Christie, D. W. Corne, B. J. Davies, and G. J. J. Williams, 'Bayesian optimization algorithm applied to uncertainty quantification', *SPE Journal, SPE-143290-PA*, vol. 17, no. 03, pp. 865–873, Sep. 2012.

[93] A. Abdollahzadeh, A. Reynolds, M. A. Christie, and D. Corne, 'A parallel GA-EDA hybrid algorithm for history-matching', in *SPE Oil and Gas India Conference and Exhibition, SPE-153750-MS*, Mumbai, India, 2012.

[94] A. P. Reynolds, A. Abdollahzadeh, D. W. Corne, M. Christie, B. Davies, and G. Williams, 'A parallel BOA-PSO hybrid algorithm for history matching', in *Proceedings of the IEEE Congress on Evolutionary Computation (CEC)*, Luxembourg, 2011, pp. 894–901.

[95] E. C. Santhosh and J. S. Sangwai, 'A hybrid differential evolution algorithm approach towards assisted history matching and uncertainty quantification for reservoir models', *Journal of Petroleum Science and Engineering*, vol. 142, pp. 21–35, Jun. 2016.

[96] Y. Kato, H. Okano, and S. Takahashi, 'Application of PSO and MOPSO to gas injection analysis', in *International Petroleum Technology Conference, IPTC-18074-MS*, Kuala Lumpur, Malaysia, 2014.

[97] M. Sambridge, 'Geophysical inversion with a neighbourhood algorithm—I. Searching a parameter space', *Geophysical Journal International*, vol. 138, no. 2, pp. 479–494, Aug. 1999.

[98] S. Subbey, M. Christie, and M. Sambridge, 'Prediction under uncertainty in reservoir modeling', *Journal of Petroleum Science and Engineering*, vol. 44, no. 1, pp. 143–153, 2004.

[99] G. Voronoï, 'Nouvelles applications des paramètres continus à la théorie des formes quadratiques. Deuxième mémoire. Recherches sur les parallélloèdres primitifs.', *Journal für die reine und angewandte Mathematik*, vol. 134, pp. 198–287, 1908.

[100] A. Okabe, B. Boots, K. Sugihara, and S. N. Chiu, *Spatial tessellations: Concepts and applications of Voronoi diagrams*, 2nd ed., vol. 501. West Sussex: John Wiley & Sons, 2000.

[101] M. Christie, A. Cliffe, P. Dawid, and S. S. Senn, *Simplicity, complexity and modelling*. West Sussex: John Wiley & Sons, 2011.

[102] J. Kennedy and R. Eberhart, 'Particle swarm optimization', in *Proceedings of the IEEE International Conference on Neural Networks*, Perth, Australia, 1995, vol. 4, pp. 1942–1948.

[103] R. Eberhart, P. Simpson, and R. Dobbins, *Computational intelligence PC tools*. San Diego, California: Academic Press Professional, Inc., 1996.

[104] A. P. Engelbrecht, *Computational intelligence: An introduction*, 2nd ed. West Sussex: John Wiley & Sons, 2007.

[105] A. P. Engelbrecht, *Fundamentals of computational swarm intelligence*. West Sussex: John Wiley & Sons, 2005.

[106] J. Kennedy, R. C. Eberhart, and Y. Shi, *Swarm intelligence*. San Diego, California: Morgan Kaufmann, 2001.

[107] J. L. Fernández-Martínez, T. Mukerji, E. García-Gonzalo, and A. Suman, 'Reservoir characterization and inversion uncertainty via a family of particle swarm optimizers', in *SEG Annual Meeting, SEG-2010-2334*, Denver, Colorado, 2010.

[108] L. Mohamed, M. A. Christie, and V. Demyanov, 'Comparison of stochastic sampling algorithms for uncertainty quantification', *SPE Journal, SPE-119139-PA*, vol. 15, no. 01, pp. 31–38, Mar. 2010.

[109] L. Mohamed, M. A. Christie, V. Demyanov, E. Robert, and D. Kachuma, 'Application of particle swarms for history matching in the Brugge reservoir', in *SPE Annual Technical Conference and Exhibition, SPE-135264-MS*, Florence, Italy, 2010.

[110] M. Kathrada and J. N. Carter, 'Case studies of successfully history matched reservoir simulation models using a powerful optimization algorithm being of limited predictive

value', in *Abu Dhabi International Petroleum Exhibition and Conference, SPE-136659-MS*, Abu Dhabi, UAE, 2010.

[111] R. W. Rwechungura, M. Dadashpour, and J. Kleppe, 'Application of particle swarm optimization for parameter estimation integrating production and time lapse seismic data', in *Offshore Europe, SPE-146199-MS*, Aberdeen, UK, 2011.

[112] E. Tolstukhin, B. Lyngnes, and H. H. Sudan, 'Ekofisk 4D seismic - Seismic history matching workflow', in *SPE Europec/EAGE Annual Conference, SPE-154347-MS*, Copenhagen, Denmark, 2012.

[113] O. Vazquez *et al.*, 'Produced water chemistry history matching in the Janice field', *SPE Reservoir Evaluation & Engineering, SPE-164903-PA*, vol. 18, no. 04, pp. 564–576, Nov. 2015.

[114] J. E. Onwunalu and L. J. Durlofsky, 'Application of a particle swarm optimization algorithm for determining optimum well location and type', *Computational Geosciences*, vol. 14, no. 1, pp. 183–198, Jan. 2010.

[115] M. Irgens and W. L. Lavenue, 'Use of advanced optimization techniques to manage a complex drilling schedule', in *SPE Annual Technical Conference and Exhibition, SPE-110805-MS*, Anaheim, California, 2007.

[116] R. V. Self, A. Atashnezhad, and G. Hareland, 'Use of a swarm algorithm to reduce the drilling time through measurable improvement in rate of penetration', in *50th U.S. Rock Mechanics/Geomechanics Symposium, ARMA-2016-456*, Houston, Texas, 2016.

[117] J. F. Schutte and A. A. Groenwold, 'A study of global optimization using particle swarms', *Journal of Global Optimization*, vol. 31, no. 1, pp. 93 – 108, 2005.

[118] Y. Shi and R. Eberhart, 'A modified particle swarm optimizer', in *Proceedings of the IEEE International Conference on Evolutionary Computation*, Anchorage, Alaska, 1998, pp. 69–73.

[119] J. Kennedy, 'The particle swarm: Social adaptation of knowledge', in *Proceedings of the IEEE International Conference on Evolutionary Computation*, Indianapolis, USA, 1997, pp. 303–308.

[120] M. Kathrada, 'Uncertainty evaluation of reservoir simulation models using particle swarms and hierarchical clustering', PhD Thesis, Heriot-Watt University, Edinburgh, 2009.

[121] A. Carlisle and G. Dozier, 'An off-the-shelf PSO', in *Proceedings of the Workshop on Particle Swarm Optimization*, Indianapolis, USA, 2001.

[122] N. A. Ab Aziz and Z. Ibrahim, 'Asynchronous particle swarm optimization for swarm robotics', *Procedia Engineering*, vol. 41, pp. 951–957, 2012.

[123] I. C. Trelea, 'The particle swarm optimization algorithm: Convergence analysis and parameter selection', *Information Processing Letters*, vol. 85, no. 6, pp. 317–325, Mar. 2003.

[124] T. Back, *Evolutionary algorithms in theory and practice: Evolution strategies, evolutionary programming, genetic algorithms*. Oxford, UK: Oxford University Press, 1996.

[125] J. H. Holland, *Adaptation in natural and artificial systems: an introductory analysis with applications to biology, control, and artificial intelligence*. Cambridge, MA, USA: MIT press, 1992.

[126] D. E. Goldberg, *Genetic algorithms in search, optimization, and machine learning*, 13th ed., vol. 1989. Boston, MA, USA: Addison-Wesley Publishing Company, Inc., 1989.

[127] I. Rechenberg, *Evolutionsstrategie optimierung technischer systeme nach prinzipien der biologishen evolution*, vol. 15. Chicago: Frommann-Holzboog, 1973.

[128] H.-P. Schwefel, *Numerical optimization of computer models*. New York, NY, USA: John Wiley & Sons, Inc., 1981.

[129] L. J. Fogel, A. J. Owens, and M. J. Walsh, *Artificial intelligence through simulated evolution*. Michigan, USA: John Wiley & Sons, 1966.

[130] D. B. Fogel, *Evolutionary computation: Toward a new philosophy of machine intelligence*, 3rd ed. Piscataway, NJ, USA: Wiley-IEEE Press, 2006.

[131] G. Jones, 'Genetic and evolutionary algorithms', in *Encyclopedia of Computational Chemistry*, vol. 2, John Wiley and Sons, Ltd, 2002.

[132] T. Bäck and H.-P. Schwefel, 'An overview of evolutionary algorithms for parameter optimization', *Journal Evolutionary Computation*, vol. 1, no. 1, pp. 1–23, 1993.

[133] A. Castellini, I. Gullapalli, V. T. Hoang, and P. J. Condon, 'Quantifying uncertainty in production forecast for fields with significant history: A West African case study',

in *International Petroleum Technology Conference, IPTC-10987-MS*, Doha, Qatar, 2005.

[134] A. A. Emerick *et al.*, 'Well placement optimization using a genetic algorithm with nonlinear constraints', in *SPE Reservoir Simulation Symposium, SPE-118808-MS*, The Woodlands, Texas, 2009.

[135] G. Montes, P. Bartolome, and A. L. Udias, 'The use of genetic algorithms in well placement optimization', in *SPE Latin American and Caribbean Petroleum Engineering Conference, SPE-69439-MS*, Buenos Aires, Argentina, 2001.

[136] M. Tavakkolian, F. Jalali F., and M. A. Emadi, 'Production optimization using genetic algorithm approach', in *Nigeria Annual International Conference and Exhibition, SPE-88901-MS*, Abuja, Nigeria, 2004.

[137] C. Carpenter, 'Optimal well-workover scheduling by use of genetic algorithms', *Journal of Petroleum Technology, SPE-0514-0120-JPT*, vol. 66, no. 05, pp. 120–123, May 2014.

[138] T. Bäck, D. Fogel, and Z. Michalewicz, *Handbook of evolutionary computation*, 1st ed. Bristol, UK: IOP Publishing Ltd. and Oxford University Press, 1997.

[139] P. J. Ballester and J. N. Carter, 'An effective real-parameter genetic algorithm with parent centric normal crossover for multimodal optimisation', in *Deb K. (eds) Genetic and Evolutionary Computation – GECCO 2004*, Seattle, Washington, USA, 2004, vol. 3102, pp. 901–913.

[140] D. E. Goldberg and K. Deb, 'A comparative analysis of selection schemes used in genetic algorithms', in *Foundations of genetic algorithms*, Morgan Kaufmann, 1991, pp. 69–93.

[141] T. Bäck and F. Hoffmeister, 'Extended selection mechanisms in genetic algorithms', in *Proceedings of the Fourth International Conference on Genetic Algorithms*, San Diego, California, 1991, pp. 92–99.

[142] M. de la Maza and B. Tidor, 'An analysis of selection procedures with particular attention paid to proportional and Boltzmann selection', in *Proceedings of the 5th International Conference on Genetic Algorithms*, San Francisco, CA, USA, 1993, pp. 124–131.

[143] P. J. Hancock, 'An empirical comparison of selection methods in evolutionary algorithms', in *Fogarty T.C. (eds) Evolutionary Computing. AISB EC*, Leeds, UK, 1994, vol. 865, pp. 80–94.

[144] K. Deb and R. B. Agrawal, 'Simulated binary crossover for continuous search space', *Complex Systems*, vol. 9, no. 2, pp. 115–148, 1995.

[145] K. Deb and M. Goyal, 'A combined genetic adaptive search (GeneAS) for engineering design', *Computer Science and Informatics*, vol. 26, pp. 30–45, 1996.

[146] I. C. Parmee, D. Cvetković, A. H. Watson, and C. R. Bonham, 'Multiobjective satisfaction within an interactive evolutionary design environment', *Evolutionary Computation*, vol. 8, no. 2, pp. 197–222, 2000.

[147] H.-Y. Park, A. Datta-Gupta, and M. J. King, 'Handling conflicting multiple objectives using Pareto-based evolutionary algorithm for history matching of reservoir performance', in *SPE Reservoir Simulation Symposium, SPE-163623-MS*, The Woodlands, Texas, USA, 2013.

[148] T. Stewart *et al.*, 'Real-world applications of multiobjective optimization', in *Branke J., Deb K., Miettinen K., Słowiński R. (eds) Multiobjective Optimization*, 2008, vol. 5252, pp. 285–327.

[149] A. Efstratiadis and D. Koutsoyiannis, 'One decade of multi-objective calibration approaches in hydrological modelling: A review', *Hydrological Sciences Journal–Journal Des Sciences Hydrologiques*, vol. 55, no. 1, pp. 58–78, 2010.

[150] J. Harlin, 'Development of a process oriented calibration scheme for the HBV hydrological model', *Hydrology Research*, vol. 22, no. 1, pp. 15–36, 1991.

[151] P. O. Yapo, H. V. Gupta, and S. Sorooshian, 'Multi-objective global optimization for hydrologic models', *Journal of Hydrology*, vol. 204, no. 1, pp. 83–97, 1998.

[152] B. J. Ritzel, J. W. Eheart, and S. Ranjithan, 'Using genetic algorithms to solve a multiple objective groundwater pollution containment problem', *Water Resources Research*, vol. 30, no. 5, pp. 1589–1603, 1994.

[153] S. E. Cieniawski, J. W. Eheart, and S. Ranjithan, 'Using genetic algorithms to solve a multiobjective groundwater monitoring problem', *Water Resources Research*, vol. 31, no. 2, pp. 399–409, 1995.

[154] D. Halhal, G. A. Walters, D. Ouazar, and D. Savic, 'Water network rehabilitation with structured messy genetic algorithm', *Journal of Water Resources Planning and Management*, vol. 123, no. 3, pp. 137–146, 1997.

[155] G. H. Harrison and J. A. Tweedie, 'A multi-objective economic analysis of oilfield production policy', in *SPE Annual Technical Conference and Exhibition, SPE-10327-MS*, San Antonio, Texas, 1981.

[156] L. Saputelli *et al.*, 'Integration of computer-aided high-intensity design with reservoir exploitation of remote and offshore locations', in *International Oil and Gas Conference and Exhibition, SPE-64621-MS*, Beijing, China, 2000.

[157] C. Michailides and D. C. Angelides, 'Multi objective optimization performance of a floating flexible system', in *The 22nd International Offshore and Polar Engineering Conference, ISOPE-I-12-200*, Rhodes, Greece, 2012.

[158] S. Dong, B. Feng, T. Shen, C. Zhan, and H. Chang, 'CFD-based hull form resistance and flow field multi-objective optimization research', in *The 24th International Ocean and Polar Engineering Conference, ISOPE-I-14-505*, Busan, Korea, 2014.

[159] Z.-H. Ji and D.-Y. Wang, 'Multi-objective optimization for ultimate strength and stiffness of ship hull', in *The 23rd International Offshore and Polar Engineering Conference, ISOPE-I-13-618*, Anchorage, Alaska, 2013.

[160] J. Jiang, H. Cai, C. Ma, and C. Ke, 'Multi-objective optimal design of ship propeller considering fluid - Structure interaction', in *The 26th International Ocean and Polar Engineering Conference, ISOPE-I-16-076*, Rhodes, Greece, 2016.

[161] J. Wu, X. Liu, and D. Wan, 'Multi-objective hydrodynamic optimization of ship hull based on approximation model', in *The 26th International Ocean and Polar Engineering Conference, ISOPE-I-16-028*, Rhodes, Greece, 2016.

[162] L. Zhang, J. N. Zhang, and Y. Zou, 'Multi-objective optimization method in the main dimensions of high performance ship based on current EEDI', in *The 26th International Ocean and Polar Engineering Conference, ISOPE-I-16-067*, Rhodes, Greece, 2016.

[163] J. S. Baioco, C. H. Albrech, B. P. Jacob, and D. M. Rocha, 'Multi-objective optimization of submarine pipeline routes considering on-bottom stability, VIV-induced fatigueand multiphase flow', in *The 25th International Ocean and Polar Engineering Conference, ISOPE-I-15-481*, Kona, Hawaii, USA, 2015.

[164] M. Mossolly, 'Techno-economic modeling & conceptual design optimization of CCS facilities using value engineering and multi-objective stochastic algorithm', in *Abu Dhabi International Petroleum Exhibition and Conference, SPE-138704-MS*, Abu Dhabi, UAE, 2010.

[165] C. Lu, Y. Lin, Z. Ji, and M. Chen, 'NURBS based ship form design using adaptive genetic algorithm', in *The 18th International Offshore and Polar Engineering Conference,, ISOPE-I-08-157*, Vancouver, Canada, 2008.

[166] R. Gao, Y. Xu, D. Wang, C. Zou, and C. Jin, 'Study on ship dynamic route planning in multi-bridges water area based on PSO-OPF algorithm', in *The 26th International Ocean and Polar Engineering Conference, ISOPE-I-16-291*, Rhodes, Greece, 2016.

[167] M. A. Q. Siddiqui, R. A. Khan, and M. S. Jamal, 'Multi-objective well placement optimization considering energy sustainability along with economical gains', in *SPE North Africa Technical Conference and Exhibition, SPE-175842-MS*, Cairo, Egypt, 2015.

[168] A. Hasan, B. Foss, S. Krogstad, V. Gunnerud, and A. F. Teixeira, 'Decision analysis for long-term and short-term production optimization applied to the Voador field', in *SPE Reservoir Characterization and Simulation Conference and Exhibition, SPE-166027-MS*, Abu Dhabi, UAE, 2013.

[169] R. Schulze-Riegert *et al.*, 'Well path design optimization under geological uncertainty: Application to a complex North Sea field', in *SPE Russian Oil and Gas Conference and Exhibition, SPE-136288-MS*, Moscow, Russia, 2010.

[170] M. A. Rajaieyamchee, R. B. Bratvold, and A. Badreddine, 'Bayesian decision networks for optimal placement of horizontal wells', in *SPE EUROPEC/EAGE Annual Conference and Exhibition, SPE-129984-MS*, Barcelona, Spain, 2010.

[171] M. Jesmani, M. C. Bellout, R. Hanea, and B. Foss, 'Particle swarm optimization algorithm for optimum well placement subject to realistic field development constraints', in *SPE Reservoir Characterisation and Simulation Conference and Exhibition, SPE-175590-MS*, Abu Dhabi, UAE, 2015.

[172] Z. M. Alghareeb, S. P. Walton, and J. R. Williams, 'Well placement optimization under constraints using modified cuckoo search', in *SPE Saudi Arabia Section Technical Symposium and Exhibition, SPE-172841-MS*, Al-Khobar, Saudi Arabia, 2014.

[173] A. A. Awotunde and N. Sibaweihi, 'Consideration of voidage-replacement ratio in well-placement optimization', *SPE Economics & Management, SPE-163354-PA*, vol. 6, no. 01, pp. 40–54, Jan. 2014.

[174] G. van Essen, P. Van den Hof, and J.-D. Jansen, 'Hierarchical long-term and short-term production optimization', *SPE Journal, SPE-124332-PA*, vol. 16, no. 01, pp. 191–199, Mar. 2011.

[175] K. Kostuik, A. A. Valdez, J. Bordovsky, Y. Mu, and C. Faig, 'Evaluation of multi-objective methods for portfolio tradeoff analysis', in *SPE Annual Technical Conference and Exhibition, SPE-166372-MS*, New Orleans, Louisiana, USA, 2013.

[176] M. M. Siraj, P. M. J. Van den Hof, and J. D. Jansen, 'Model and economic uncertainties in balancing short-term and long-term objectives in water-flooding optimization', in *SPE Reservoir Simulation Symposium, SPE-173285-MS*, Houston, Texas, USA, 2015.

[177] K. Kostuik, Y. Mu, R. Parma, J. Wearly, and K. Rooney, 'Optimizing unconventional asset development and reserves confidence with portfolio tradeoff analysis', in *SPE Annual Technical Conference and Exhibition, SPE-174845-MS*, Houston, Texas, USA, 2015.

[178] K. Kostuik, Y. Mu, M. El-Beltagy, and A. Naiem, 'Visualizing portfolio tradeoffs with perceptually accurate self-organizing maps', in *SPE Annual Technical Conference and Exhibition, SPE-181632-MS*, Dubai, UAE, 2016.

[179] C. B. Chung and C. Kravaris, 'Incorporation of a priori information in reservoir history matching by regularization', SPE e-library, 1990.

[180] R. W. Schulze-Riegert, M. Krosche, A. Fahimuddin, and S. G. Ghedan, 'Multi-objective optimization with application to model validation and uncertainty quantification', in *SPE Middle East Oil and Gas Show and Conference, SPE-105313-MS*, Manama, Bahrain, 2007.

[181] P. Ferraro and F. Verga, 'Use of evolutionary algorithms in single and multi-objective optimization techniques for assisted history matching', in *Offshore Mediterranean Conference and Exhibition, OMC-2009-079*, Ravenna, Italy, 2009.

[182] S. Watanabe, J. Han, A. Datta-Gupta, and M. J. King, 'Streamline-based time lapse seismic data integration incorporating pressure and saturation effects', in *SPE Annual Technical Conference and Exhibition, SPE-166395-MS*, New Orleans, Louisiana, USA, 2013.

[183] B. Min, J. M. Kang, S. Chung, C. Park, and I. Jang, 'Pareto-based multi-objective history matching with respect to individual production performance in a heterogeneous

reservoir', *Journal of Petroleum Science and Engineering*, vol. 122, pp. 551–566, Oct. 2014.

[184] F. Olalotiti-Lawal and A. Datta-Gupta, 'A multi-objective Markov chain Monte Carlo approach for history matching and uncertainty quantification', in *SPE Annual Technical Conference and Exhibition, SPE-175144-MS*, Houston, Texas, USA, 2015.

[185] F. Huguet, A. Lange, P. Egermann, and T. Schaaf, 'Automated history-matching of radial models using self organizing classification method for underground gas storage reservoirs characterization', in *SPE Europec featured at 78th EAGE Conference and Exhibition, SPE-180177-MS*, Vienna, Austria, 2016.

[186] Y. Han, C. Park, and J. M. Kang, 'Estimation of future production performance based on multi-objective history matching in a waterflooding project', in *SPE EUROPEC/EAGE Annual Conference and Exhibition, SPE-130500-MS*, Barcelona, Spain, 2010.

[187] M. Sayyafzadeh, M. Haghighi, and J. N. Carter, 'Regularization in history matching using multi-objective genetic algorithm and Bayesian framework', in *SPE Europec/EAGE Annual Conference, SPE-154544-MS*, Copenhagen, Denmark, 2012.

[188] F. Verga, M. Cancelliere, and D. Viberti, 'Improved application of assisted history matching techniques', *Journal of Petroleum Science and Engineering*, vol. 109, pp. 327–347, Sep. 2013.

[189] M. E. Niri and D. E. Lumley, 'A multi-objective optimization method for creating reservoir models that simultaneously match seismic and geologic data', in *SEG Annual Meeting, SEG-2014-0065*, Denver, Colorado, USA, 2014.

[190] D. Kam, J. Han, and A. Datta-Gupta, 'Streamline-based rapid history matching of bottomhole pressure and three-phase production data', in *SPE Improved Oil Recovery Conference, SPE-179549-MS*, Tulsa, Oklahoma, USA, 2016.

[191] M. S. Kanfar and C. R. Clarkson, 'Reconciling flowback and production data: A novel history matching approach for liquid rich shale wells', *Journal of Natural Gas Science and Engineering*, vol. 33, pp. 1134–1148, Jul. 2016.

[192] D. Schaffer, 'Some experiments in machine learning using vector evaluated genetic algorithms', PhD Thesis, Vanderbilt University, Nashville, TN, USA, 1984.

[193] C. M. Fonseca and P. J. Fleming, 'Genetic algorithms for multiobjective optimization: Formulation, discussion and generalization.', in *Proceedings of the 5th International Conference on Genetic Algorithms*, 1993, pp. 416–423.

[194] N. Srinivas and K. Deb, 'Multiobjective optimization using nondominated sorting in genetic algorithms', *Evolutionary Computation*, vol. 2, no. 3, pp. 221–248, 1994.

[195] J. Horn, N. Nafpliotis, and D. E. Goldberg, 'A niched Pareto genetic algorithm for multiobjective optimization', in *Proceedings of the 1st IEEE Conference on Evolutionary Computation.*, Orlando, FL, USA, 1994, pp. 82–87.

[196] E. Zitzler, M. Laumanns, and L. Thiele, 'SPEA2: Improving the strength Pareto evolutionary algorithm', in *Evolutionary Methods for Design Optimization and Control with Applications to Industrial Problems*, Athens, Greece, 2001, pp. 95–100.

[197] J. Knowles and D. Corne, 'The Pareto archived evolution strategy: A new baseline algorithm for Pareto multiobjective optimisation', in *Proceedings of the Congress on Evolutionary Computation, CEC.*, Washington D.C. USA, 1999, pp. 98–105.

[198] A. Osyczka and S. Kundu, 'A new method to solve generalized multicriteria optimization problems using the simple genetic algorithm', *Structural Optimization*, vol. 10, no. 2, pp. 94–99, 1995.

[199] H. Kita, Y. Yabumoto, N. Mori, and Y. Nishikawa, 'Multi-objective optimization by means of the thermodynamical genetic algorithm', in *Voigt HM., Ebeling W., Rechenberg I., Schwefel HP. (eds) Parallel Problem Solving from Nature — PPSN IV*, Berlin, Germany, 1996, vol. 1141, pp. 504–512.

[200] D. A. Van Veldhuizen, 'Multiobjective evolutionary algorithms: Classifications, analyses, and new innovations', PhD Thesis, Air Force Institute of Technology Air University, Ohio, 1999.

[201] K. Deb, A. Pratap, S. Agarwal, and T. Meyarivan, 'A fast and elitist multiobjective genetic algorithm: NSGA-II', *IEEE Transactions on Evolutionary Computation*, vol. 6, no. 2, pp. 182–197, 2002.

[202] A. Zhou, B.-Y. Qu, H. Li, S.-Z. Zhao, P. N. Suganthan, and Q. Zhang, 'Multiobjective evolutionary algorithms: A survey of the state of the art', *Swarm and Evolutionary Computation*, vol. 1, no. 1, pp. 32–49, 2011.

[203] K. E. Parsopoulos and M. N. Vrahatis, 'Particle swarm optimization method in multiobjective problems', in *Proceedings of the ACM Symposium on Applied Computing (SAC)*, Madrid, Spain, 2002, pp. 603–607.

[204] J. E. Fieldsend and S. Singh, 'A multi-objective algorithm based upon particle swarm optimisation, an efficient data structure and turbulence', in *UK Workshop on Computational Intelligence (UKCI)*, Birmingham, UK, 2002, pp. 37–44.

[205] X. Li, 'A non-dominated sorting particle swarm optimizer for multiobjective optimization', in *Cantú-Paz E. et al. (eds) Genetic and Evolutionary Computation — GECCO*, 2003, vol. 2723, pp. 37–48.

[206] C. A. C. Coello, G. T. Pulido, and M. S. Lechuga, 'Handling multiple objectives with particle swarm optimization', *IEEE Transactions on Evolutionary Computation*, vol. 8, no. 3, pp. 256–279, Jun. 2004.

[207] C. R. Raquel and P. C. Naval Jr, 'An effective use of crowding distance in multiobjective particle swarm optimization', in *Proceedings of the 7th Annual Conference on Genetic and Evolutionary Computation*, Washington, DC, USA, 2005, pp. 257–264.

[208] M. Reyes-Sierra and C. C. Coello, 'Multi-objective particle swarm optimizers: A survey of the state-of-the-art', *International Journal of Computational Intelligence Research*, vol. 2, no. 3, pp. 287–308, 2006.

[209] A. O'Sullivan, 'Modelling simulation error for improved reservoir prediction', PhD Thesis, Heriot-Watt University, Edinburgh, 2004.

[210] M. C. Baddeley, A. Curtis, and R. Wood, 'An introduction to prior information derived from probabilistic judgements: Elicitation of knowledge, cognitive bias and herding', *Geological Society, London, Special Publications*, vol. 239, pp. 15–27, 2004.

[211] A. H. El-Shaarawi and W. W. Piegorsch, *Encyclopedia of environmetrics*, 2nd ed., vol. 1, 6 vols. John Wiley & Sons, 2012.

[212] E. Manceau, M. Mezghani, I. Zabalza-Mezghani, and F. Roggero, 'Combination of experimental design and joint modeling methods for quantifying the risk associated with deterministic and stochastic uncertainties - An integrated test study', in *SPE Annual Technical Conference and Exhibition, SPE-71620-MS*, New Orleans, Louisiana, 2001.

[213] D. C. Montgomery, *Design and analysis of experiments*, 7th ed. Danvers: John Wiley & Sons, 2008.

[214] C. Robert and G. Casella, *Introducing Monte Carlo Methods with R*. London: Springer, 2009.

[215] M. Sambridge, 'Geophysical inversion with a neighbourhood algorithm—II. Appraising the ensemble', *Geophysical Journal International*, vol. 138, no. 3, pp. 727–746, 1999.

[216] S. Subbey, C. Mike, and M. Sambridge, 'A strategy for rapid quantification of uncertainty in reservoir performance prediction', in *SPE Reservoir Simulation Symposium, SPE-79678-MS*, Houston, Texas, 2003.

[217] K. Beven and A. Binley, 'The future of distributed models: Model calibration and uncertainty prediction', *Hydrological Processes*, vol. 6, no. 3, pp. 279–298, 1992.

[218] K. Beven, 'Prophecy, reality and uncertainty in distributed hydrological modelling', *Advances in Water Resources*, vol. 16, no. 1, pp. 41–51, 1993.

[219] M. Diskin and E. Simon, 'A procedure for the selection of objective functions for hydrologic simulation models', *Journal of Hydrology*, vol. 34, no. 1, pp. 129–149, 1977.

[220] S. Sorooshian, V. K. Gupta, and J. L. Fulton, 'Evaluation of maximum likelihood parameter estimation techniques for conceptual rainfall-runoff models: Influence of calibration data variability and length on model credibility', *Water Resources Research*, vol. 19, no. 1, pp. 251–259, 1983.

[221] H. V. Gupta, S. Sorooshian, and P. O. Yapo, 'Toward improved calibration of hydrologic models: Multiple and non-commensurable measures of information', *Water Resources Research*, vol. 34, no. 4, pp. 751–763, 1998.

[222] F. Roggero and L. Y. Hu, 'Gradual deformation of continuous geostatistical models for history matching', in *SPE Annual Technical Conference and Exhibition, SPE-49004-MS*, New Orleans, Louisiana, 1998.

[223] G. de Marsily, G. Lavedan, M. Boucher, and G. Fasanino, 'Interpretation of interference tests in a well field using geostatistical techniques to fit the permeability distribution in a reservoir model', *Geostatistics for Natural Resources Characterization, Proceedings of the NATO Advanced Study Institute*, vol. 2, pp. 831–849, 1984.

[224] M. Le Ravalec-Dupin and L. Hu, 'Combining the pilot point and gradual deformation methods for calibrating permeability models to dynamic data', *Oil & Gas Science and Technology-Revue de l'IFP*, vol. 62, no. 2, pp. 169–180, 2007.

[225] G. Enchery, F. Roggero, M. Le Ravalec, E. Tillier, and V. Gervais, 'A new parameterization technique for the calibration of facies proportions in history–matching processes', in *The 12th European Conference on the Mathematics of Oil Recovery (ECMOR XII)*, Oxford, UK, 2010.

[226] R. Potsepaev and C. Farmer, 'Application of stochastic partial differential equations to reservoir property modelling', in *The 12th European Conference on the Mathematics of Oil Recovery (ECMOR XII)*, Oxford, UK, 2010.

[227] P. Sarma, L. J. Durlofsky, and K. Aziz, 'Kernel principal component analysis for efficient, differentiable parameterization of multipoint geostatistics', *Mathematical Geosciences*, vol. 40, no. 1, pp. 3–32, 2008.

[228] V. Vapnik, S. E. Golowich, and A. Smola, 'Support vector method for function approximation, regression estimation, and signal processing', *Advances in Neural Information Processing Systems*, pp. 281–287, 1997.

[229] V. Demyanov, A. Pozdnoukhov, M. Kanevski, and M. Christie, 'Geomodelling of a fluvial system with semi-supervised support vector regression', in *Proceedings of the VII International Geostatistics Congress, GECAMIN*, Chile, 2008, pp. 627–636.

[230] V. Demyanov, L. Foresti, M. Kanevski, and M. Christie, 'Multiple kernel learning approach for reservoir modelling', in *The 12th European Conference on the Mathematics of Oil Recovery (ECMOR XII)*, Oxford, UK, 2010.

[231] V. Demyanov, L. Foresti, M. A. Christie, and M. Kanevski, 'Reservoir modelling with feature selection: Kernel learning approach', in *SPE Reservoir Simulation Symposium, SPE-141510-MS*, Woodlands, Texas, USA, 2011.

[232] J. Caers, *Petroleum geostatistics*. Texas: Society of Petroleum Engineers, 2005.

[233] O. Dubrule, *Geostatistics for seismic data integration in Earth models: 2003 distinguished instructor short course*. Tulsa, Oklahoma, USA: Society of Exploration Geophysicists, 2003.

[234] M. Le Ravalec-Dupin, *Inverse stochastic modeling of flow in porous media(applications to reservoir characterization)*. Paris: Editions Technip, 2005.

[235] F. Floris, M. Bush, M. Cuypers, F. Roggero, and A. R. Syversveen, 'Methods for quantifying the uncertainty of production forecasts: A comparative study', *Petroleum Geoscience*, vol. 7, pp. 87–97, 2001.

[236] R. W. Stallman, 'Numerical analysis of regional water levels to define aquifer hydrology', *Eos, Transactions American Geophysical Union*, vol. 37, no. 4, pp. 451–460, 1956.

[237] P. Jacquard, 'Permeability distribution from field pressure data', *SPE Journal, SPE-1307-PA*, vol. 5, no. 04, pp. 281–294, Dec. 1965.

[238] G. Pickup, M. Valjak, and M. Christie, 'Model complexity in reservoir simulation', in *The 11th European Conference on the Mathematics of Oil Recovery (ECMOR XI)*, Bergen, Norway, 2008.

[239] P. D. Grünwald, *The minimum description length principle*. Cambridge, MA, USA: MIT press, 2007.

[240] D. J. MacKay, *Information theory, inference and learning algorithms*. Cambridge, UK: Cambridge University Press, 2003.

[241] G. W. Brier, 'Verification of forecasts expressed in terms of probability', *Monthly Weather Review*, vol. 78, no. 1, pp. 1–3, Jan. 1950.

[242] C. Bos, 'Production forecasting with uncertainty quantification', *Final report of EC project, NITG-TNO report NITG*, pp. 99–255, 2000.

[243] J. N. Carter, 'Imperial College London, PUNQ-S3', *PUNQ-S3 Eclipse Dataset*. [Online]. Available: http://www.imperial.ac.uk/engineering/departments/earth-science/research/research-groups/perm/standard-models/eclipse-dataset/.

[244] J. W. Barker, M. Cuypers, and L. Holden, 'Quantifying uncertainty in production forecasts: Another look at the PUNQ-S3 problem', *SPE Journal, SPE-74707-PA*, vol. 6, no. 04, pp. 433–441, Dec. 2001.

[245] J. Crocker, 'New parameterisations for PUNQ-S3', MSc Thesis, Heriot-Watt University, Edinburgh, 2011.

[246] V. K. Gupta and S. Sorooshian, 'Uniqueness and observability of conceptual rainfall-runoff model parameters: The percolation process examined', *Water Resources Research*, vol. 19, no. 1, pp. 269–276, 1983.

[247] G. Hornberger, K. Beven, B. Cosby, and D. Sappington, 'Shenandoah watershed study: Calibration of a topography-based, variable contributing area hydrological model to a small forested catchment', *Water Resources Research*, vol. 21, no. 12, pp. 1841–1850, 1985.

[248] G. Kuczera and M. Mroczkowski, 'Assessment of hydrologic parameter uncertainty and the worth of multiresponse data', *Water Resources Research*, vol. 34, no. 6, pp. 1481–1489, 1998.

[249] T. Wagener, D. P. Boyle, M. J. Lees, H. S. Wheater, H. V. Gupta, and S. Sorooshian, 'A framework for development and application of hydrological models', *Hydrology and Earth System Sciences Discussions*, vol. 5, no. 1, pp. 13–26, 2001.

[250] N. G. Saleri and E. H. Bu-Hulaigah, 'Knowledge management in North Ghawar', in *17th World Petroleum Congress, WPC-32150*, Rio de Janeiro, Brazil, 2002.

[251] E. J. Hughes, 'Evolutionary many-objective optimisation: many once or one many?', in *Proceedings of The IEEE Congress on Evolutionary Computation*, Edinburgh, UK, 2005, vol. 1, pp. 222–227.

[252] E. J. Hughes, 'Multiple single objective Pareto sampling', in *Proceedings of The IEEE Congress on Evolutionary Computation*, Canberra, Australia, 2003, vol. 4, pp. 2678–2684.

[253] D. Brockhoff and E. Zitzler, 'On objective conflicts and objective reduction in multiple criteria optimization', Institut für Technische Informatik und Kommunikationsnetze, ETH Zürich, Zürich, Switzerland, TIK-Report No. 243, Feb. 2006.

[254] D. K. Saxena, J. A. Duro, A. Tiwari, K. Deb, and Q. Zhang, 'Objective reduction in many-objective optimization: Linear and nonlinear algorithms', *IEEE Transactions on Evolutionary Computation*, vol. 17, no. 1, pp. 77–99, Feb. 2013.

[255] X. Guo, Y. Wang, and X. Wang, 'Using objective clustering for solving many-objective optimization problems', *Mathematical Problems in Engineering*, vol. 2013, 2013.

[256] J. W. Kruisselbrink, M. T. Emmerich, T. Bäck, A. Bender, A. P. IJzerman, and E. van der Horst, 'Combining aggregation with Pareto optimization: A case study in evolutionary molecular design', in *Ehrgott M., Fonseca C.M., Gandibleux X., Hao JK., Sevaux M. (eds) Evolutionary Multi-Criterion Optimization (EMO)*, Nantes, France, 2009, vol. 5467, pp. 453–467.

[257] T. Murata and A. Taki, 'Many-objective optimization for knapsack problems using correlation-based weighted sum approach', in *Ehrgott M., Fonseca C.M., Gandibleux X., Hao JK., Sevaux M. (eds) Evolutionary Multi-Criterion Optimization (EMO)*, Nantes, France, 2009, vol. 5467, pp. 468–480.

[258] S. Otake, T. Yoshikawa, and T. Furuhashi, 'Basic study on aggregation of objective functions in many-objective optimization problems', in *Proceedings of the World Automation Congress (WAC), 2010*, Kobe, Japan, 2010, pp. 1–6.

[259] R. C. Purshouse and P. J. Fleming, 'Conflict, harmony, and independence: Relationships in evolutionary multi-criterion optimisation', in *Fonseca C.M., Fleming P.J., Zitzler E., Thiele L., Deb K. (eds) Evolutionary Multi-Criterion Optimization (EMO)*, Faro, Portugal, 2003, vol. 2632, pp. 16–30.

[260] W. S. Cleveland, *Visualizing data*. Summit, New Jersey: Hobart Press, 1993.

[261] A. R Freitas, P. J. Fleming, and F. Guimaraes, 'A non-parametric harmony-based objective reduction method for many-objective optimization', in *Proceedings of the IEEE International Conference on Systems, Man, and Cybernetics (SMC)*, Manchester, United Kingdom, 2013, pp. 651–656.

[262] A. Inselberg, 'The plane with parallel coordinates', *The Visual Computer*, vol. 1, no. 2, pp. 69–91, 1985.

[263] B. Efron and R. J. Tibshirani, *An introduction to the bootstrap*. Florida, USA: Chapman and Hall/CRC, 1994.

[264] M. J. Schervish, 'P values: What they are and what they are not', *The American Statistician*, vol. 50, no. 3, pp. 203–206, 1996.

[265] D. F. Bauer, 'Constructing confidence sets using rank statistics', *Journal of the American Statistical Association*, vol. 67, no. 339, pp. 687–690, 1972.

[266] J. Derrac, S. García, D. Molina, and F. Herrera, 'A practical tutorial on the use of nonparametric statistical tests as a methodology for comparing evolutionary and swarm intelligence algorithms', *Swarm and Evolutionary Computation*, vol. 1, no. 1, pp. 3–18, 2011.

[267] F. Sani and J. Todman, *Experimental design and statistics for psychology: a first course*. Garsington Road, Oxford: Blackwell Publishing, 2008.

[268] D. W. Corne and J. D. Knowles, 'Techniques for highly multiobjective optimisation: Some nondominated points are better than others', in *Proceedings of the 9th Annual Conference on Genetic and Evolutionary Computation (GECCO)*, London, UK, 2007, pp. 773–780.

[269] Z. He and G. G. Yen, 'Ranking many-objective evolutionary algorithms using performance metrics ensemble', in *Proceedings of the IEEE Congress on Evolutionary Computation (CEC)*, Cancun, Mexico, 2013, pp. 2480–2487.

[270] B. S. P. Mishra, S. Dehuri, and S.-B. Cho, 'Swarm intelligence in multiple and many objectives optimization: A survey and topical study on EEG signal analysis', in *Multi-objective Swarm Intelligence*, vol. 592, S. Dehuri, A. K. Jagadev, and M. Panda, Eds. Berlin, Heidelberg: Springer Berlin Heidelberg, 2015, pp. 27–73.

[271] M. Laumanns, L. Thiele, K. Deb, and E. Zitzler, 'Combining convergence and diversity in evolutionary multiobjective optimization', *Evolutionary Computation*, vol. 10, no. 3, pp. 263–282, 2002.

[272] F. di Pierro, S.-T. Khu, and D. A. Savic, 'An investigation on preference order ranking scheme for multiobjective evolutionary optimization', *IEEE Transactions on Evolutionary Computation*, vol. 11, no. 1, pp. 17–45, 2007.

[273] G. Wang and H. Jiang, 'Fuzzy-dominance and its application in evolutionary many objective optimization', in *Proceedings of the IEEE International Conference on Computational Intelligence and Security Workshops (CISW)*, Harbin, Heilongjiang, China, 2007, pp. 195–198.

[274] E. Zitzler and S. Künzli, 'Indicator-based selection in multiobjective search', in *Yao X. et al. (eds) Parallel Problem Solving from Nature - PPSN VIII*, Birmingham, UK, 2004, vol. 3242, pp. 832–842.

[275] X. Sun, Y. Chen, Y. Liu, and D. Gong, 'Indicator-based set evolution particle swarm optimization for many-objective problems', *Soft Computing*, vol. 20, no. 6, pp. 2219–2232, Jun. 2016.

[276] N. Beume, B. Naujoks, and M. Emmerich, 'SMS-EMOA: Multiobjective selection based on dominated hypervolume', *European Journal of Operational Research*, vol. 181, no. 3, pp. 1653–1669, 2007.

[277] J. Bader and E. Zitzler, 'HypE: An algorithm for fast hypervolume-based many-objective optimization', *Evolutionary Computation*, vol. 19, no. 1, pp. 45–76, 2011.

[278] L. While, P. Hingston, L. Barone, and S. Huband, 'A faster algorithm for calculating hypervolume', *IEEE Transactions on Evolutionary Computation*, vol. 10, no. 1, pp. 29–38, 2006.

[279] Q. Zhang and H. Li, 'MOEA/D: A multiobjective evolutionary algorithm based on decomposition', *IEEE Transactions on Evolutionary Computation*, vol. 11, no. 6, pp. 712–731, 2007.

[280] T. Murata, H. Ishibuchi, and M. Gen, 'Specification of genetic search directions in cellular multi-objective genetic algorithms', in *Proceedings of First International Conference on Evolutionary MultiCriterion Optimization*, Zurich, Switzerland, 2001, pp. 82–95.

[281] E. J. Hughes, 'MSOPS-II: A general-purpose many-objective optimiser', in *Proceedings of the IEEE Congress on Evolutionary Computation (CEC)*, Singapore, 2007, pp. 3944–3951.

[282] H.-L. Liu, F. Gu, and Q. Zhang, 'Decomposition of a multiobjective optimization problem into a number of simple multiobjective subproblems', *IEEE Transactions on Evolutionary Computation*, vol. 18, no. 3, pp. 450–455, 2014.

[283] R. Cheng, Y. Jin, M. Olhofer, and B. Sendhoff, 'A reference vector guided evolutionary algorithm for many-objective optimization', *IEEE Transactions on Evolutionary Computation*, vol. 20, no. 5, pp. 773–791, 2016.

[284] K. Deb and H. Jain, 'An evolutionary many-objective optimization algorithm using reference-point-based nondominated sorting approach, part I: Solving problems with box constraints', *IEEE Transactions on Evolutionary Computation*, vol. 18, no. 4, pp. 577–601, 2014.

[285] J. A. Cornell, *Experiments with mixtures: Designs, models, and the analysis of mixture data*, 3rd ed. Wiley, 2002.

[286] I. Giagkiozis, R. C. Purshouse, and P. J. Fleming, 'Towards understanding the cost of adaptation in decomposition-based optimization algorithms', in *Proceedings of the IEEE International Conference on Systems, Man, and Cybernetics*, Manchester, UK, 2013, pp. 615–620.

[287] K. Deb, L. Thiele, M. Laumanns, and E. Zitzler, 'Scalable test problems for evolutionary multiobjective optimization', in *Evolutionary multiobjective optimization*, Springer, 2005, pp. 105–145.

[288] S. Jiang, Y. S. Ong, J. Zhang, and L. Feng, 'Consistencies and contradictions of performance metrics in multiobjective optimization', *IEEE Transactions on Cybernetics*, vol. 44, no. 12, pp. 2391–2404, Dec. 2014.

[289] P. Hoffman, G. Grinstein, K. Marx, I. Grosse, and E. Stanley, 'DNA visual and analytic data mining', in *Proceedings of the IEEE Visualization'97*, Phoenix,, Arizona, 1997, pp. 437–441.

[290] Y. Jin and J. Branke, 'Evolutionary optimization in uncertain environments-A survey', *IEEE Transactions on Evolutionary Computation*, vol. 9, no. 3, pp. 303–317, 2005.

[291] F. Demirmen, 'Reserves estimation: The challenge for the industry', *Journal of Petroleum Technology, SPE-103434-JPT*, vol. 59, no. 05, pp. 80–89, May 2007.

[292] P. S. da Cruz, R. N. Horne, and C. V. Deutsch, 'The quality map: A tool for reservoir uncertainty quantification and decision making', in *SPE Annual Technical Conference and Exhibition, SPE-56578-MS*, Houston, Texas, 1999.

[293] O. Badru and C. S. Kabir, 'Well placement optimization in field development', in *SPE Annual Technical Conference and Exhibition, SPE-84191-MS*, Denver, Colorado, 2003.

[294] R. F. Martini, D. J. Schiozer, and L. Nakajima, 'Use of quality maps in reservoir management', *Journal of the Brazilian Society of Mechanical Sciences and Engineering*, vol. 27, no. 4, pp. 463–468, 2005.

[295] C. Wang, G. Li, and A. C. Reynolds, 'Optimal well placement for production optimization', in *Eastern Regional Meeting, SPE-111154-MS*, Lexington, Kentucky USA, 2007.

[296] P. Sarma and W. H. Chen, 'Efficient well placement optimization with gradient-based algorithms and adjoint models', in *Intelligent Energy Conference and Exhibition, SPE-112257-MS*, Amsterdam, The Netherlands, 2008.

[297] M. Zandvliet, M. Handels, G. van Essen, R. Brouwer, and J.-D. Jansen, 'Adjoint-based well-placement optimization under production constraints', *SPE Journal, SPE-105797-PA*, vol. 13, no. 04, pp. 392–399, Dec. 2008.

[298] F. Forouzanfar and A. Reynolds, 'Well-placement optimization using a derivative-free method', *Journal of Petroleum Science and Engineering*, vol. 109, pp. 96–116, 2013.

[299] A. C. Bittencourt and R. N. Horne, 'Reservoir development and design optimization', in *SPE Annual Technical Conference and Exhibition, SPE-38895-MS*, San Antonio, Texas, 1997.

[300] B. Yeten, L. J. Durlofsky, and K. Aziz, 'Optimization of nonconventional well type, location, and trajectory', *SPE Journal, SPE-86880-PA*, vol. 8, no. 03, pp. 200–210, Sep. 2003.

[301] V. Artus, L. J. Durlofsky, J. Onwunalu, and K. Aziz, 'Optimization of nonconventional wells under uncertainty using statistical proxies', *Computational Geosciences*, vol. 10, no. 4, pp. 389–404, Nov. 2006.

[302] W. Bangerth, H. Klie, M. F. Wheeler, P. L. Stoffa, and M. K. Sen, 'On optimization algorithms for the reservoir oil well placement problem', *Computational Geosciences*, vol. 10, no. 3, pp. 303–319, 2006.

[303] J. N. Carter and J. D. Matthews, 'Optimization of a reservoir development plan using a parallel genetic algorithm', *Petroleum Geoscience*, vol. 14, no. 1, pp. 85–90, 2008.

[304] F. Zarei, A. Daliri, and N. Alizadeh, 'The use of neuro-fuzzy proxy in well placement optimization', in *Intelligent Energy Conference and Exhibition, SPE-112214-MS*, Amsterdam, The Netherlands, 2008.

[305] J. E. Onwunalu and L. Durlofsky, 'A new well-pattern-optimization procedure for large-scale field development', *SPE Journal, SPE-124364-PA*, vol. 16, no. 03, pp. 594–607, Sep. 2011.

[306] C. Wang, G. Li, and A. C. Reynolds, 'Production optimization in closed-loop reservoir management', *SPE Journal, SPE-109805-PA*, vol. 14, no. 03, pp. 506–523, Sep. 2009.

[307] Y. Chen, D. S. Oliver, and D. Zhang, 'Efficient ensemble-based closed-loop production optimization', *SPE Journal, SPE-112873-PA*, vol. 14, no. 04, pp. 634–645, Dec. 2009.

[308] V. Bukshtynov, O. Volkov, L. J. Durlofsky, and K. Aziz, 'Comprehensive framework for gradient-based optimization in closed-loop reservoir management', *Computational Geosciences*, vol. 19, no. 4, pp. 877–897, Aug. 2015.

[309] X. Liu and A. C. Reynolds, 'Gradient-based multi-objective optimization with applications to waterflooding optimization', *Computational Geosciences*, Sep. 2015.

[310] X. Liu and A. C. Reynolds, 'A multiobjective steepest descent method with applications to optimal well control', *Computational Geosciences*, vol. 20, no. 2, pp. 355–374, Apr. 2016.

[311] Z. Bouzarkouna, D. Y. Ding, and A. Auger, 'Well placement optimization with the covariance matrix adaptation evolution strategy and meta-models', *Computational Geosciences*, vol. 16, no. 1, pp. 75–92, Jan. 2012.

[312] E. Nwankwor, A. K. Nagar, and D. C. Reid, 'Hybrid differential evolution and particle swarm optimization for optimal well placement', *Computational Geosciences*, vol. 17, no. 2, pp. 249–268, Apr. 2013.

[313] S. Ding, H. Jiang, J. Li, and G. Tang, 'Optimization of well placement by combination of a modified particle swarm optimization algorithm and quality map method', *Computational Geosciences*, vol. 18, no. 5, pp. 747–762, Oct. 2014.

[314] R. Schulze-riegert, M. Bagheri, M. Krosche, N. Kueck, and D. Ma, 'Multiple-objective optimization applied to well path design under geological uncertainty', in *SPE Reservoir Simulation Symposium, SPE-141712-MS*, The Woodlands, Texas, USA, 2011.

[315] Y. Chang, Z. Bouzarkouna, and D. Devegowda, 'Multi-objective optimization for rapid and robust optimal oilfield development under geological uncertainty', *Computational Geosciences*, vol. 19, no. 4, pp. 933–950, Aug. 2015.

[316] O. J. Isebor and L. J. Durlofsky, 'Biobjective optimization for general oil field development', *Journal of Petroleum Science and Engineering*, vol. 119, pp. 123–138, Jul. 2014.

[317] V. Demyanov, K. Gopa, D. Arnold, and M. A. Elfeel, 'Production optimisation under uncertainty in fractured reservoirs', in *The 14th European Conference on the Mathematics of Oil Recovery (ECMOR XIV)*, Catania, Sicily, Italy, 2014.

[318] J. J. Hutahaean, V. Demyanov, D. Arnold, and O. Vazquez, 'Optimization of well placement to minimize the risk of scale deposition in field development', in *Abu Dhabi International Petroleum Exhibition and Conference, SPE-171733-MS*, Abu Dhabi, UAE, 2014.

[319] Y. Chang, K. R. Petvipusit, and D. Devegowda, 'Multi-objective optimization coupled with dimension-wise polynomial-based approach in smart well placement under model

uncertainty', in *SPE Reservoir Simulation Symposium, SPE-173291-MS*, Houston, Texas, USA, 2015.

[320] U. Ozdogan and R. N. Horne, 'Optimization of well placement under time-dependent uncertainty', *SPE Reservoir Evaluation & Engineering, SPE-90091-PA*, vol. 9, no. 02, pp. 135–145, Apr. 2006.

[321] C. Scheidt and J. Caers, 'Representing spatial uncertainty using distances and kernels', *Mathematical Geosciences*, vol. 41, no. 4, pp. 397–419, 2009.

[322] H. Wang, D. Echeverría-Ciaurri, L. Durlofsky, and A. Cominelli, 'Optimal well placement under uncertainty using a retrospective optimization framework', *SPE Journal, SPE-141950-PA*, vol. 17, no. 01, pp. 112–121, Mar. 2012.

[323] C. Yang, C. Card, L. X. Nghiem, and E. Fedutenko, 'Robust optimization of SAGD operations under geological uncertainties', in *SPE Reservoir Simulation Symposium, SPE-141676-MS*, The Woodlands, Texas, USA, 2011.

[324] S. Salomon, G. Avigad, A. Goldvard, and O. Schütze, 'PSA–A new scalable space partition based selection algorithm for MOEAs', in *EVOLVE-A Bridge between Probability, Set Oriented Numerics, and Evolutionary Computation II*, London, UK: Springer, Berlin, Heidelberg, 2013, pp. 137–151.

[325] G. Schoups, C. L. Addams, and S. Gorelick, 'Multi-objective calibration of a surface water-groundwater flow model in an irrigated agricultural region: Yaqui Valley, Sonora, Mexico', *Hydrology and Earth System Sciences Discussions*, vol. 2, no. 5, pp. 2061–2109, 2005.

[326] G. Schoups, J. W. Hopmans, C. Young, J. Vrugt, and W. Wallender, 'Multi-criteria optimization of a regional spatially-distributed subsurface water flow model', *Journal of Hydrology*, vol. 311, no. 1, pp. 20–48, 2005.

[327] S.-T. Khu, H. Madsen, and F. Di Pierro, 'Incorporating multiple observations for distributed hydrologic model calibration: An approach using a multi-objective evolutionary algorithm and clustering', *Advances in Water Resources*, vol. 31, no. 10, pp. 1387–1398, 2008.

[328] R. L. Wasserstein and N. A. Lazar, 'The ASA's statement on *p*-values: Context, process, and purpose', *The American Statistician*, vol. 70, no. 2, pp. 129–133, Apr. 2016.

[329] J. K. Kruschke, 'Bayesian estimation supersedes the t test.', *Journal of Experimental Psychology: General*, vol. 142, no. 2, p. 573, 2013.

[330] R. Cheng and Y. Jin, 'A competitive swarm optimizer for large scale optimization', *IEEE Transactions on Cybernetics*, vol. 45, no. 2, pp. 191–204, 2015.

[331] R. Cheng and Y. Jin, 'A social learning particle swarm optimization algorithm for scalable optimization', *Information Sciences*, vol. 291, pp. 43–60, 2015.

[332] D. Corne, C. Dhaenens, and L. Jourdan, 'Synergies between operations research and data mining: The emerging use of multi-objective approaches', *European Journal of Operational Research*, vol. 221, no. 3, pp. 469–479, Sep. 2012.

§§§ • §§§